



Establishment of Best Practices for Construction and Design of Cement-Treated Materials

Technical Report 0-6949-1

August 2020; Published October 2020

CENTER FOR TRANSPORTATION INFRASTRUCTURE SYSTEMS
THE UNIVERSITY OF TEXAS AT EL PASO
EL PASO, TX 79968
[HTTPS://WWW.UTEP.EDU/ENGINEERING/CTIS/](https://www.utep.edu/engineering/ctis/)

in cooperation with the
Federal Highway Administration and the
Texas Department of Transportation

TECHNICAL REPORT STANDARD TITLE PAGE

1. Report No. FHWA/TX-21/0-6949-1	2. Government Accession No.	3. Recipient's Catalog No.	
4. Title and Subtitle Establishment of Best Practices for Construction and Design of Cement-Treated Materials		5. Report Date August 2020; Published October 2020	
		6. Performing Organization Code	
7. Author(s) Reza S. Ashtiani, Mohammad Rashidi, Edgar Rodriguez, Margarita Ordaz, Hector Cruz Lopez, German Garay, Sergio Rocha		8. Performing Organization Report No. TX 0-6949-1	
9. Performing Organization Name and Address Center for Transportation Infrastructure Systems The University of Texas at El Paso El Paso, Texas 79968-0516		10. Work Unit No.	
		11. Contract or Grant No. Project No. 0-6949	
12. Sponsoring Agency Name and Address Texas Department of Transportation Research and Technology Implementation Division P.O. Box 5080 Austin, Texas 78763-5080		13. Type of Report and Period Covered Technical Report Sept. 1, 2017 – Aug. 31, 2020	
		14. Sponsoring Agency Code	
15. Supplementary Notes Project performed in cooperation with Texas Department of Transportation and the Federal Highway Administration.			
16. Abstract <p>Cementitious stabilization of granular soils has been proven to be an economically viable option for sustainable construction and rehabilitation of pavement structures. The absence of a harmonized and rapid turnaround laboratory mixture design procedure, coupled with construction and inspection guidelines that need improvement have resulted in an ongoing challenge for TxDOT, contractors, and users of the transportation facilities. In addition, due to the lack of field data and practical laboratory tests in the past, the fatigue performance models in the Texas Mechanistic Empirical Flexible Pavement Design System (TxME) have never been verified nor calibrated. Therefore, the main objective of this study was twofold: provide an update to the current mixture design specification based on comprehensive laboratory testing and develop and calibrate a new generation of fatigue performance model that accounts for strength as well as shrinkage cracking potential of cement treated materials.</p> <p>To accomplish these objectives, current practices for mixture design and construction of cement treated base, subbase and subgrade soils were documented. This information then served as the basis for the selection of the type and sources of base aggregates and subgrade soils for inclusion in the experiment matrix of the project. Eight different aggregate base materials including multiple sources of limestone, siliceous gravel, reclaimed concrete aggregate, full depth reclamation materials, and reclaimed asphalt pavement, as well as seven different subgrade soils with unique characteristics were incorporated in this research effort. All permutations of the experimental design were prepared with different levels of stabilizer content to cover a wide spectrum of treatments from light stabilization to heavily stabilized systems. This research also provided two alternative moisture susceptibility procedures to quantify the loss of orthogonal strength properties of cement treated virgin and reclaimed materials due to moisture intrusion. More than 3,000 specimens, were prepared, and subjected to various mechanical and physio-chemical laboratory tests to characterize the strength, resilient properties, and permanent deformation potential, clay activity, moisture adsorption potential, as well as other properties of cement treated systems. Microstructural analysis of the cement treated specimen using X-ray computed tomography was instrumental to provide the basis for using the gyratory compactor in lieu of the traditional impact hammer for laboratory specimen preparation. The trend analysis of the laboratory results, statistical reliability and repeatability analysis, practicality of test methods, and operator friendliness were the contributing factors to draft the update to the cement treatment specification.</p> <p>In addition to the laboratory efforts, a new generation of fatigue performance models were developed and calibrated in this study. The model incorporated indirect diametrical tensile (IDT) strength and shrinkage strain to account for the cracking potential in the cement treated layer due to overly rigid matrices. A comprehensive database of pavement profiles and material properties were developed using field-based nondestructive testing such as Falling weight deflectometer, ground penetrating radar, and deployment of Portable WIN (P-WIM) for traffic characterization in this study. The database was instrumental for the calibration of a newly developed fatigue performance model for flexible pavement structures with cement treated layers.</p>			
17. Key Words		18. Distribution Statement No restrictions. This document is available to the public through the National Technical Service, 5285 Port Royal Road, Springfield, Virginia 22161, www.ntis.gov	
19. Security Classif. (of this report) Unclassified	20. Security Classif. (of this page) Unclassified	21. No. of Pages	22. Price



Establishment of Best Practices for Construction and Design of Cement-Treated Materials

Reza S. Ashtiani, Ph.D., P.E.

Mohammad Rashidi

Edgar Rodriguez

Margarita Ordaz

Hector Cruz Lopez

German Garay

Sergio Rocha

Jose Garibay

Project 0-6949; Report 0-6949-1

August 2020; Published October 2020

Conducted for

Texas Department of Transportation

P.O. Box 5080

Austin, Texas 78763

Center for Transportation Infrastructure Systems

The University of Texas at El Paso

El Paso, TX 79968

DISCLAIMERS

The contents of this report reflect the view of the authors who are responsible for the facts and the accuracy of the data presented herein. The contents do not necessarily reflect the official views or policies of the Texas Department of Transportation or the Federal Highway Administration. This report does not constitute a standard, a specification, or a regulation.

The material contained in this report is experimental in nature and is published for informational purposes only. Any discrepancies with official views or policies of the Texas Department of Transportation or the Federal Highway Administration should be discussed with the appropriate Austin Division prior to implementation of the procedures or results.

NOT INTENDED FOR CONSTRUCTION, BIDDING, OR PERMIT PURPOSES

Reza S. Ashtiani, Ph.D., P.E.

Mohammad Rashidi, MSCE

Edgar Rodriguez, MSCE

Margarita Ordaz, BSCE

Hector Cruz Lopez, BSCE

German Garay, BSCE

Sergio Rocha, BS

Jose Garibay, MSCE

Executive Summary

TxDOT have extensive experience with the use of calcium-based treatment agents such as cement, lime, fly ash, etc., in road construction. Improved orthogonal load bearing capacity and enhanced durability of cement treated layers are the primary motivations for pavement engineers to include stabilization strategies in their toolbox for the design of new roads and the rehabilitation of existing pavement structures. However, the absence of a rapid turn-around and harmonized laboratory mixture design protocol that accounts for compressive strength, tensile strength, and long-term durability due to moisture intrusion have resulted in an ongoing challenge for Districts across Texas. The primary goal of this project was to update the existing mixture design specification to account for the diversity of soils and aggregates, blend ratios of reclaimed and virgin materials, and environmental factors.

In addition to the laboratory efforts, the secondary focus of this project was to develop and calibrate new generation of fatigue performance models for the estimation of service life of pavements with cement treated base and subbase layers. The new model accounts for the shrinkage cracking potential due to excessive cement content in the mix, as well as a modified Indirect Diametrical Tensile (IDT) strength in lieu of modulus of rupture for the cement treated materials. The new models can be potentially incorporated in the TxME pavement design system.

To achieve the objectives of the project, the research team developed and distributed a survey questionnaire among the TxDOT Districts to compile districts experiences using cement treatment for subgrade soils and base layers, and to document the challenges of using calcium-based stabilizers across TxDOT. This information then served as the basis for the refinement of laboratory testing procedures, and the selection of the type and sources of aggregates and subgrade soils for inclusion in the experiment matrix. The final lithological selection was based on the frequency of use, geographical diversification to cover the diverse climate of Texas, and aggregate type variations based on the survey results.

Eight different aggregate base materials, namely limestone sourced from El Paso and Houston, FDR sourced from Atlanta, siliceous gravel sourced from Pharr, RAP materials from Atlanta and El Paso, RCA sourced from Houston and El Paso were incorporated in this research study. In addition, seven different subgrade soils, namely sandy soils sourced from Corpus Christi, Atlanta and El Paso, clay soils sourced from Sierra Blanca, Houston, Bryan and El Paso were used in this effort. All permutations of the experiment design were prepared at different levels of stabilizer content to cover a wide spectrum of treatments from light stabilization to heavily stabilized systems. Different quantities of calcium-based treatment agents such as cement, lime, and fly ash in combination with polypropylene fibers were also incorporated in the experimental design to investigate the effectiveness of fiber reinforcement along with chemical additives on the strength properties and volumetric stability of expansive plastic soils with high sulfate contents.

In this project, alternative approaches for the laboratory evaluation of moisture susceptibility of cement treated materials were explored. Several systematic shortcomings were identified associated with the characterization of the moisture susceptibility of granular bases in using the traditional TST test. The research team developed alternative moisture susceptibility protocols including submergence and backpressure saturation tests with special heat treatment provisions for expedited curing, in conjunction with routine mechanical tests to underscore the significance of including moisture susceptibility tests in the mixture design process. This information can potentially serve coastal districts prone to flooding and extreme weather conditions. These newly developed procedures were then incorporated in the updated mixture design specification in lieu of traditional TST test.

This study also focused on providing updates to sample fabrication in the laboratory to ensure the uniformity of compaction and distribution of the treatment agent in the mixture. The cement treated specimens were prepared in the laboratory using four compaction methods, namely Texas Gyrotory Compactor (TGC), impact hammer, vibratory hammer, and SuperPave gyrotory compactor to evaluate the potential benefits and shortcomings of using gyrotory and vibratory compactors on the engineering properties of the cement treated materials. Subsequently, X-ray Computed Tomography (CT) imaging technique was used to identify the porosity distribution and void structure to analyze the uniformity of compaction using different compaction methods in this study. The results revealed that gyrotory compactor yielded more uniform specimens. The superiority of the gyrotory compacted specimens were also evident in 1-D swell tests due to the absence of “lifts” in this method. The particle crushing analysis also showed that reclaimed materials, such as RCA, are more prone to disintegrate and generate fines when the traditional impact hammer is used for the compaction of cement treated RCA systems.

More than 3,000 specimens, considering replicates, were fabricated, and subjected to various laboratory tests to provide the basis for the update the to the mixture design specification. The Unconfined Compressive Strength (UCS) test, modified IDT strength test with outside strain measurements, submaximal modulus tests at different strength ratios, and Free-Free Resonant Column (FFRC) tests were incorporated in the laboratory experimental design to characterize compressive and tensile strength, resilient properties, and permanent deformation potential of cement treated systems. Aggregate Image Measurement Systems (AIMS) was also incorporated in this study to analyze the geometry of aggregates and its relevance to strength and stiffness properties of cement treated materials. The results revealed angular aggregate with more equi-dimensional particles provide better interlocking effect, and exhibited improved mechanical properties compared to aggregate systems with more rounded and flat and elongated particles.

One dimensional swell and swell pressure tests were used in this project to study the volumetric stability and expansion characteristics of subgrade soils in presence of cementitious materials. The swell pressure, and rate of expansion for permutations consisted of various percentages of cement, lime, fly ash, combinations of lime and cement, and polypropylene fibers were determined in this study. The results showed the superiority of dual-stabilization techniques, such as combination of

cement and polypropylene fibers to mitigate the volumetric expansion of laboratory prepared specimens. The dual stabilization results for problematic subgrade soils in this study with high plasticity and high sulfate content showed the potential of this strategy to significantly reduce the uplift pressure and reduce the moisture adsorption capacity of treated subgrade soils. The point of caution however, is to ensure the uniformity of the small fiber content during field construction. Adherence to the developed mixture design procedure can serve as a guide for pavement design engineers for the proper selection of the type and the amount of the calcium-based stabilizers to ensure the strength and durability of pavement foundations.

Reflective cracking in pavements with cement treated layers is an ongoing challenge for Districts in Texas and across the nation. This is primarily due to formation of cracks in overly rigid treated layers, and subsequent propagation of cracks to surface layers. To better understand the shrinkage cracking behavior, the research team conducted a series of coefficient of thermal expansion (COTE) tests on prismatic beams to examine the influence of various cement contents on shrinkage characteristics of treated specimens. The shrinkage strain from the COTE test was an input to the newly developed fatigue performance model.

The research team developed and calibrated a new fatigue performance model for flexible pavements with cement treated pavement foundations. The primary divergence from the existing model is the departure from using modulus of rupture and incorporation of shrinkage strain for the estimation of fatigue life of pavement with cement treated base layers. A comprehensive catalogue of pavement features based on non-destructive field testing, such as field distress measurements, Falling Weight Deflectometer (FWD), and Ground Penetrating Radar (GPR) in combination with available databases from previous TxDOT projects were developed for calibration of the fatigue performance model. Subsequent to development of the model, the performance equation was calibrated for 62 pavement sections across Texas with material properties and climatic conditions to improve the generalization of the model.

This study also provided a succinct description of the inverted pavement design concept. The primary focus was on providing a sensitivity analysis on the influencing parameters that contribute to the longevity and performance of inverted pavements. The results for numerical analysis of an inverted pavement section constructed on State Highway SH-123 in Corpus Christi was compared to an existing conventional flexible pavement design in the vicinity of the inverted section.

The research team also developed a series of statistically robust relationships among the laboratory testing parameters and properties to provide an estimate for Level II analysis in TxME. Due to time and budgetary constraints, sometimes the design engineers opt out of performing full laboratory characterization, and primarily rely on past experience and engineering judgment to assign design input parameters. Such an approach compromises the reliability of the pavement life predictions and can potentially incur unforeseen costs to the traveling public. Therefore, the material models developed in this study can serve as a starting point for the pavement design engineers to provide an estimate of tensile strength, resilient modulus, and shrinkage cracking

potential of cement treated materials for the analysis and design of pavement structures. The developed relationships are a valuable means in the hierarchical pavement design approach for incorporation in the level II pavement design and analysis.

The laboratory testing, numerical simulations, and field-testing efforts were synthesized to draft an update to the existing mixture design specification for an implementable deliverable of the project. Based on the laboratory testing of various virgin and reclaimed aggregate sources, as well as trend analysis of the results, the traditional unconfined compressive strength value is necessary but not sufficient to identify the optimum cement content in the mix. This is more pronounced when reclaimed materials with high blend ratios are considered in the mixture. Therefore, in the updated protocol, we incorporated the modified IDT strength, two alternative moisture susceptibility tests, and the retained strength concept to provide an all-inclusive view of the influence of cement to improve the orthogonal strength properties and reduce the moisture susceptibility of treated systems. Other noteworthy departures from existing mixture design protocols pertain to the specimen fabrication in the laboratory. Based on the micro-structure analysis of the specimens using X-ray CT, the SuperPave gyratory compactor is recommended to replace the traditional impact hammer. In addition, slurry mixing, in lieu of dry powder mixing, is incorporated in the updated specification to alleviate the concerns with cement distribution uniformity in lightly cement treated specimens.

Table of Contents

Chapter 1. Introduction	1
1.1 Background	1
1.2 Project Objectives	1
1.3 Value of Research	1
1.3.1 Environmental Sustainability	1
1.3.2 Materials and Pavement	2
1.3.3 Reduced Construction, Operations, and Maintenance Cost	2
1.3.4 Increasing Service Life.....	2
1.4 Research Tasks	5
1.5 Report Contents and Organization	5
Chapter 2. Literature Review	6
2.1 Performance Issues of Pavements with Cement Stabilized Materials	6
2.1.1 Rutting	6
2.1.2 Block and Transverse Cracking.....	8
2.1.3 Bottom-Up Cracking (Alligator Cracking)	8
2.1.4 Top-down Cracking (Longitudinal Cracking).....	9
2.1.5 Inverted Pavement as a Crack Mitigation System.....	10
2.1.6 Expansive Soils	11
2.2 Laboratory Characterization of Cement Stabilized Materials	12
2.2.1 Strength Properties	12
2.2.2 Stiffness Properties	14
2.2.3 Durability.....	16
2.2.4 Strength Requirements	17
2.3 Summary of the Literature Review	18
Chapter 3. Survey of Texas Districts.....	21
3.1 Subgrade Treatment	21
3.1.1 Predominant Subgrade Soil Type	21
3.1.2 Typical Issues with the Subgrade Soils	22
3.1.3 Type of Stabilizing Agent used for Subgrade Treatment.....	22
3.1.4 Typical Laboratory Mix Design Requirements for Cement Treated Subgrade Soils	22
3.1.5 Typical Field Acceptance Requirements for Cement Treated Subgrade Soils	23
3.1.6 Laboratory Tests and Protocols for Subgrade Treatment.....	23

3.1.7 Rationale for the Selection of the Stabilizer Content and the Type of Stabilizer for Subgrade Treatment	24
3.2 Base Treatment.....	25
3.2.1 UCS Requirement for the Mixture Design of Cement Treated Base and Subbase Layers	25
3.3 Reclaimed Material Treatment.....	25
3.3.1 Incorporation of Reclaimed Materials in Cement Treated Layers	25
3.3.2 Design Requirements for the Cement Treated Base Layers with Reclaimed Materials	26
3.3.3 Acceptance Requirements for the Treated Base Layers with Reclaimed Asphalt or Reclaimed Concrete Materials	27
3.4 General Aspects for the Base and Subgrade Treatment.....	28
3.4.1 Main Challenges for Using Calcium-Based Stabilizers	28
3.4.2 Typical Range of Cement Content Used for the Treatment of Subgrade Soils and Base Materials.....	28
3.4.3 Predominant Distresses Associated with Cement Treated Subgrade and Base Layers.....	30
3.4.4 Using Inverted Pavement Design to Mitigate the Issues Associated with Reflective Cracking	31
Chapter 4. Experimental Design for Comprehensive Laboratory Tests	32
4.1 Strength and Stiffness Properties	41
4.1.1 Unconfined Compressive Strength (UCS) Test	41
4.1.2 Indirect Diametrical Tensile (IDT) Test.....	41
4.1.3 Submaximal Modulus Test.....	42
4.1.4 Dynamic IDT Test.....	43
4.1.5 Free-Free Resonant Column Test.....	44
4.2 Moisture Susceptibility	44
4.2.1 Tube Suction Test.....	45
4.2.2 Backpressure Saturation Test	46
4.2.3 Submergence Test	47
4.2.4 Hot Water Submergence Test.....	48
4.3 Particle Geometry Analysis.....	49
4.4 Volumetric Stability of Fine-Grained Soils	51
4.4.1 One Dimensional Swell Test	51
4.4.2 Swell Pressure Test.....	52

4.4.3 Characterization of Activity and Plasticity of Clay Materials with Methylene Blue Test	53
4.5 Cementitious Materials Coefficient of Thermal Expansion.....	54
4.6 Compaction Characterization	56
Chapter 5. Laboratory Test Results.....	58
5.1 Aggregate and Soil Properties.....	58
5.2 Strength and Stiffness Properties	61
5.2.1 Unconfined Compressive Strength (UCS)	61
5.2.2 Indirect Diametrical Tensile (IDT) Test.....	63
5.2.3 Submaximal Modulus Test.....	64
5.3 Particle Geometry Analysis.....	69
5.3.1 Angularity Index.....	70
5.3.2 Texture Index.....	71
5.3.3 Form Index	72
5.4 Dry Powder Mixing versus Slurry	74
5.5 Shrinkage in Cement Stabilized Materials	77
5.6 Flexural Strength Test	80
5.7 Micro-Structural Analysis with X-Ray Computed Tomography Imaging.....	84
Chapter 6. Alternative Approaches for the Laboratory Evaluation of Moisture Susceptibility for Cement Stabilized Materials	88
6.1 Introduction	88
6.2 Methodology	88
6.3 Assessment of Moisture Susceptibility Protocols	89
6.3.1 Effect of Temperature on the Strength Development.....	90
6.3.2 Analysis of Accelerated Moisture Susceptibility Protocols	91
6.3.3 Feasibility and Relevance of the Tube Suction Test	98
6.4 Retained Unconfined Compressive Strength and Retained Inverse Diametrical Tensile Strength.....	101
6.5 Summary of the Major Points	104
Chapter 7. Analysis of the Variability of the Laboratory Data.....	106
7.1 Layout of the Experimental Procedure.....	106
7.1.1 Precision Assessment between Experimental Procedures.....	107
7.2 Assessing Variability of Gyrotory Compactor and Impact Hammer	111
7.3 Assessing Variability of Moisture Susceptibility Protocols.....	112
Chapter 8. Compaction Characterization	114

8.1 Impact Hammer.....	114
8.2 Vibratory Hammer	115
8.3 Gyratory Compactor.....	116
8.3.1 Factorial Analysis for Gyratory Compactor Parameters	117
8.4 Compaction Energy.....	121
8.4.1 Moisture-Density Evaluation.....	122
8.5 Aggregate Breakdown in Impact Hammer.....	132
Chapter 9. Strategies to Improve Orthogonal Strength Capacity and Volumetric Stability of Expansive Soils.....	135
9.1 Introduction	135
9.2 Methodology	135
9.3 Atterberg Limits and Methylene Blue Value Test Results	137
9.4 Swell Behavior of Expansive Soils	141
9.5 Statistical Modelling	144
9.6 Unconfined Compressive Strength Test Results	147
9.7 Summary of the Major Points	155
Chapter 10. Development of Material Models	157
10.1 Relationship between the UCS and IDT	157
10.1.1 Genetic Expression Programming.....	163
10.2 Resilient Modulus of Cement Stabilized Materials.....	166
10.2.1 Regression Analysis	167
10.3 Practical Estimation for Shrinkage Strain of Stabilized Materials.....	171
10.4 Summary of the Major Points	174
Chapter 11. Field Testing Database	175
11.1 Ground Penetrating Radar.....	175
11.2 Falling Weight Deflectometer	176
11.3 Field Testing Results	177
11.4 Data Collection.....	184
Chapter 12. Field Calibration of the Fatigue Performance Model	187
12.1 Introduction	187
12.2 Fatigue Performance Model in the TxME.....	187
12.3 Development and Calibration of the Fatigue Performance Model	190
12.3.1 Step 1: Determination of Strain Ratio	192
12.3.2 Step 2: Development of the Fatigue Performance Model	193
12.3.3 Step 3: Field Data Collection	197

12.3.4 Step 4: Filed Simulation by Finite Element Method	197
12.3.5 Step 5: Determination of Strain Values in the Field.....	199
12.3.6 Step 6: Model Calibration	202
12.4 Summary of the Major Points	206
Chapter 13. Analysis and Design of Inverted Pavements	207
13.1 Inverted Pavement Structure	207
13.2 Mechanical Behavior.....	209
13.2.1 Unbound Granular Base Layer.....	209
13.2.2 Asphalt Concrete Layer	209
13.2.3 Cement Stabilized Granular Subbase Layer.....	210
13.3 Construction Considerations	210
13.4 Advantages and Shortcomings	212
13.5 Numerical Analysis	213
13.6 Summary of the Major Points	219
Chapter 14. Development of Draft Laboratory Test Procedure	222
14.1 Comparison Between the Proposed and Current Specification	222
14.2 Proposed Test Procedure for Cement Treated Materials Testing	223
14.3 Summary of the Major Points	223
Chapter 15. Conclusions.....	225
15.1 Key Findings and Conclusions.....	226
References	230
Appendix A. Draft Laboratory Test Procedure.....	249

List of Tables

Table 1-1: The Cost Benefit for Different Functional Areas	3
Table 1-2: Estimation of Value of Research.....	3
Table 1-3: Estimation of Value of Research for 10 Years.....	4
Table 2-1: Comparison of Three Moduli Test Methods (Scullion et al., 2008).	15
Table 2-2: U.S. Army Corps of Engineers Unconfined Compressive Strength Criteria.	17
Table 2-3: Comparison of Laboratory Test Methods for Strength and Modulus Characterization.	19
Table 2-4: Comparison of Laboratory Test Methods for Characterization of Moisture Susceptibility.....	20
Table 2-5: Comparison of Materials Used for Cement Stabilized Base Layers.	20
Table 4-1: Laboratory Experiment Design for Aggregate Base Materials (640 specimens).....	33
Table 4-2: Laboratory Experiment Design for Aggregate Base Materials (440 specimens).....	34
Table 4-3: Laboratory Experiment Design for Subgrade Soils (421 specimens)	34
Table 4-4: Laboratory Experiment Design for High Sulfate Clay Soils sourced from Bryan (280 specimens).....	35
Table 4-5: Laboratory Experiment Design for High Plasticity Clay Soils Sourced from Sierra Blanca (280 specimens).....	35
Table 4-6: Laboratory Experiment Design for Initial Assessment of Moisture Susceptibility Tests (144 specimens).	36
Table 4-7: Laboratory Experiment Design for the Evaluation of Different Mixing Procedures (136 specimens).....	36
Table 4-8: Laboratory Experiment Design for Evaluation of Blend Ratio in Stabilized Reclaimed Materials (320 specimens).	36
Table 4-9: Laboratory Experiment Design for Investigating the Effect of High Fines Content (160 specimens).....	37
Table 4-10: Laboratory Experiment Design for Influence of Subgrade Fraction on Performance of FDR Materials (96 specimens).....	37
Table 4-11: Laboratory Experiment Design for High Plasticity Clay Soils Sourced from Houston (55 specimens).	38
Table 4-12: Laboratory Experiment Design for Poor Sandy Materials Sourced from Corpus Christi (80 specimens).	38
Table 5-1: Material Properties for Base Aggregates.....	61
Table 5-2: Material Properties for Subgrade Soils.	61
Table 5-3: Calculated Porosities from Different Compaction Methods	87
Table 7-1: UCS, IDT, and Submaximal Tests Results.	107

Table 7-2: Average, Standard Deviation and Coefficient of Variation For Different Test Methods at Two Levels of Lightly and Heavily Stabilized Materials.	109
Table 7-3: F-Static for Different Test Methods at Two Levels Of Lightly and Heavily Stabilized Materials.	110
Table 7-4: Cut-Off Value of F in the F-Distribution Table for the Confidence Level of 95% ($\alpha=0.05$).	111
Table 8-1: Main Variables of Gyrotory Compactor in Previous Studies.	117
Table 8-2: Main Variables of Gyrotory Compactor in Previous Studies.	121
Table 8-3: Calculation of Compaction Energy for Different Compaction Procedures.	122
Table 9-1: Atterberg Limits and Moisture-Density Test Results.	137
Table 10-1: Available Relationships for IDT Strength and UCS.	158
Table 10-2: Statistical Measures for the Performance of the Models.	165
Table 10-3: Available Relationships for IDT Strength and UCS.	170
Table 10-4: Regression Parameter (K) in Shrinkage Prediction Model for Different Materials.	172
Table 11-1: FWD Data of SH-123 in Corpus Christi.	181
Table 11-2: General Overview of the Database Compiled from NDT in Texas.	185
Table 12-1: Laboratory Regression Factors of Fatigue Performance Models.	196
Table 12-2: Most Frequent Truck Classes and Tire Pressures in Texas (TxDOT 6965)	199
Table 12-3: Local Field Calibration Factors and Laboratory Regression Factors of Fatigue Performance Models	205
Table 13-1: Material Requirements for South African G1 Base Layers. Adapted from TRH (1985), Buchanan (2010), Tutumluer (2013), and Boudreau et al. (2016).	211
Table 13-2: Pavement Layers Configuration and Material Properties.	214
Table 14-1: Comparison of Current and Modified Laboratory Specifications for Mixture Design of Cement Treated Materials.	224

List of Figures

Figure 2-1: Rutting of the HMA Layers without Deformation of the Cemented Base Layer (Austroads, 2008).....	7
Figure 2-2: Compression Fatigue of Cement Stabilized Materials (De Beer 1990).....	7
Figure 2-3: (a) Block Cracking and (b) Transverse Cracking in HMA with Stabilized Base Materials (Sebesta and Scullion 2004).	8
Figure 2-4: Separation between Asphalt and Cement Stabilized Base (Thogersen et al., 2004).....	9
Figure 2-5: Fatigue Cracking from the Bottom of the Cemented Layer (Austroads, 2008).....	9
Figure 2-6: Top-Down Cracking in HMA Layer on Stabilized Base (Button et al., 2001).....	10
Figure 2-7: Inverted Pavement Section.....	11
Figure 2-8: Nature of Stress Distributions in Traditional Tension Tests: (a) Third Point Bending Beam Test, and (b) Indirect Diametrical Tensile (IDT) Test (Ashtiani et al., 2016).....	14
Figure 2-9: Summary of State DOTs for Design of 7-Day Compressive Strength of Cement Treated Aggregate Base Layers.	18
Figure 3-1: Texas Districts Responded to the Survey.	21
Figure 3-2: Distribution of Subgrade Types in Texas.	22
Figure 3-3: Distribution of Issues Types in the Subgrade Soils reported by Texas Districts.	22
Figure 3-4: Typical Stabilizers used for Subgrade Treatment in Texas Districts.....	22
Figure 3-5: Typical Laboratory Mix Design Requirements for Subgrade Treatment.	23
Figure 3-6: Typical Field Acceptance Requirements for Subgrade Treatment.	23
Figure 3-7: Laboratory Tests Performed for the Mix Design and Acceptance of Subgrade Treatment in Texas Districts.	24
Figure 3-8: Rationale for the Selection of the Stabilizer Content for Subgrade Treatment.	24
Figure 3-9: Threshold for the Unconfined Compressive Strength for the Mixture Design of Cement Treated Base and Subbase Layers.	25
Figure 3-10: Incorporating Reclaimed Materials in Cement Treated Layers.....	26
Figure 3-11: Design Requirements for the Treated Base Layers with Reclaimed Asphalt or Reclaimed Concrete Materials.	26
Figure 3-12: UCS (psi) Requirement for Laboratory Mixture Design with Reclaimed Asphalt or Reclaimed Concrete Materials.	27
Figure 3-13: Typical Cement Content Used for Base Layers with Reclaimed Materials.	27
Figure 3-14: Acceptance Criteria for the Treated Base Layers with Reclaimed Asphalt or Reclaimed Concrete Materials.	28

Figure 3-15: Main Challenges for using Calcium-based Stabilizers.	28
Figure 3-16: Percentage of Cement Content Typically used for Treatment of Base Layers and Subgrades.	29
Figure 3-17: Typical Cement Content Used for the Treatment of Subgrade Soils and Base Materials in Texas.	30
Figure 3-18: Predominant Distresses Associated with the Cement Treated Subgrade and Base Layers.	31
Figure 3-19: Using Inverted Pavement Design in Texas Districts.	31
Figure 4-1: Flow Chart for the Execution of the Laboratory Tests.	39
Figure 4-2: Geographical Distribution of Selected Material Source.	40
Figure 4-3: Unconfined Compressive Strength Test Setup and Different Measures of Modulus in the UCS Stress-Strain Curve.	41
Figure 4-4: Schematic Representation of Test Setup and Fractured Specimen in the IDT Test.	42
Figure 4-5: Submaximal Modulus Test Setup.	43
Figure 4-6: Dynamic IDT Test Fixture and Specimen.	44
Figure 4-7: FFRC Test Setup.	44
Figure 4-8: 10-Days Capillary Soak Procedure.	46
Figure 4-9: Backpressure Saturation Test Setup and Schematic.	47
Figure 4-10: Submergence Test.	48
Figure 4-11: Hot Water Submergence Test.	49
Figure 4-12: Components of an Aggregate Shape: Form, Angularity, and Texture.	49
Figure 4-13: Aggregate Image Measurement Systems (AIMS).	50
Figure 4-14: One Dimensional Swell Test Setup and Schematic.	52
Figure 4-15: Swell Pressure Test Setup and Schematic.	53
Figure 4-16: Methylene Blue Absorption Test.	53
Figure 4-17: Methylene Blue Value Test Procedure (Test Steps are Numbered Sequentially).	54
Figure 4-18: COTE Test Setup.	56
Figure 4-19: Impact Hammer, Texas Gyrotory Compactor (TGC), Gyrotory Compactor, and Vibratory Hammer.	57
Figure 4-20: Differences between the Mechanism of Gyrotory Compactor and Impact Hammer.	57
Figure 5-1: Sieve Analysis for Base Materials.	58
Figure 5-2: Moisture Density Test Results for Base Aggregates.	59

Figure 5-3: Moisture Density Test Results for Subgrade Soils.	60
Figure 5-4: Unconfined Compressive Strengths Results for 7-Day Moist Cured Samples - Sample Size 6 in (d) ×12 in (h).	62
Figure 5-5: Unconfined Compressive Strengths Results for Sandy Subgrade Materials sourced from El Paso compacted with Impact Hammer - Sample Size 4 in (d) × 6 in (h).	63
Figure 5-6: Unconfined Compressive Strengths Results for Clay Subgrade Soils sourced from El Paso compacted with Impact Hammer - Sample Size 4 in (d) × 6in (h).	63
Figure 5-7: Indirect Diametrical Tensile Strength Results for Samples compacted with Impact Hammer.	64
Figure 5-8: Submaximal Modulus Test Set Up and Fractured Specimens.	65
Figure 5-9: Resilient Modulus for 7-Day Moist Cured Samples (Stress Ratio = 50%).	66
Figure 5-10: Resilient Modulus for 7-Day Moist Cured Samples (Stress Ratio = 25%).	66
Figure 5-11: Normalized Permanent Deformation for 7-Day Moist Cured Samples (Stress Ratio = 50%).	67
Figure 5-12: Normalized Permanent Deformation for 7-Day Moist Cured Samples (Stress Ratio = 25%).	67
Figure 5-13: Unconfined Compressive Strength of Stabilized Siliceous Gravel Materials Sourced from Pharr after 5,000 Load Applications at Stress Ratios of 25% and 50%.	68
Figure 5-14: Unconfined Compressive Strength of Stabilized RCA Materials Sourced from Houston after 5,000 Load Applications at Stress Ratios of 25% and 50%.	68
Figure 5-15: Unconfined Compressive Strength of Stabilized Limestone Materials Sourced from El Paso after 5,000 Load Applications at Stress Ratios of 25% and 50%.	69
Figure 5-16: Aggregate Image Measurement System (AIMS).	69
Figure 5-17: Angularity Distribution of Siliceous Gravel from Pharr.	70
Figure 5-18: Variations of Angularity Index for Different Base Aggregates.	71
Figure 5-19: Surface Texture Index for Different Base Aggregates.	72
Figure 5-20: Variations of Sphericity Distributions Based on Different Coarse Aggregates.	73
Figure 5-21: Relationship between Tensile and Compressive Strengths Stabilized Materials with Sphericity of Aggregates.	73
Figure 5-22: (a) Slurry Mixing and (b) Dry Powder Mixing in the Field.	74
Figure 5-23: (a) Cement Loss by Wind, (b) Uneven Distribution of Stabilizer on Road Surface (Caltrans, 2012).	74
Figure 5-24: Slurry and Dry Powder Mixing Procedures in the Laboratory	75
Figure 5-25: Unconfined Compressive Strength for Stabilized Granular Materials with Different Mixing Procedures.	76

Figure 5-26: Indirect Tensile Strength for Stabilized Granular Materials with Different Mixing Procedures.	76
Figure 5-27: Compressive and Tensile Strengths Improvement for Stabilized Base and Subgrade Materials using Dry Powder Mixing In lieu of Slurry Mixing in the Laboratory.	77
Figure 5-28: Shrinkage Strain versus Time for the Stabilized Base Materials with 4% Cement Content.	78
Figure 5-29: Shrinkage Strain versus Time for the Stabilized Crushed Limestone Aggregates (El Paso) with Different Cement Content.	79
Figure 5-30: Shrinkage Strain versus Time for the Stabilized RCA Materials (Houston) with Different Cement Content.	79
Figure 5-31: Shrinkage Strain versus Time for the Stabilized FDR Materials (Atlanta) with Different Cement Content.	80
Figure 5-32: Shrinkage Strain versus Time for the Stabilized Siliceous Gravel Materials (Pharr) with Different Cement Content.	80
Figure 5-33: Flexural Beam Test Setup.	81
Figure 5-34: Modulus of Rupture for different Stabilized Base Materials (Beam Size: 4×4×20 in.).	82
Figure 5-35: Relationship between Indirect Diametrical Tensile Strength and Modulus of Rupture for Cement Stabilized Base Materials (Compaction Method: Vibratory Hammer).	83
Figure 5-36: Relationship between Unconfined Compressive Strength and Modulus of Rupture for Cement Stabilized Base Materials (Compaction Method: Vibratory Hammer).	84
Figure 5-37: Equipment Components for X-ray Computer Tomography (CT) Test.	85
Figure 5-38: Example of Slice Image and Calculation of Porosity by Metallographic Image-Processing Software using ImageJ.	85
Figure 5-39: Porosity Distribution for Specimens Compacted with (a) Vibratory Hammer, (b) Impact Hammer, (c) Gyratory Compactor, and (d) Porosity Comparison of Different Compaction Methods.	86
Figure 5-40: X-Ray CT Scan of Limestone Aggregates with Different Compaction Procedures.	87
Figure 6-1: Mechanisms of Moisture Intrusion into Pavement.	88
Figure 6-2: Flow Chart for the Execution of the Laboratory Tests.	89
Figure 6-3: Unconfined Compressive Strength of Stabilized Limestone Aggregate over a Range of Curing Temperature and Time with Different Cement Content.	91
Figure 6-4: Comparison of the Unconfined Compressive Strength for Different Cement Stabilized Materials System for 7-Day Moist Cured Samples.	92

Figure 6-5: Unconfined Compressive Strength Results for Cement Stabilized Limestone Aggregates Sourced from El Paso with different Curing/Conditioning Procedures.....	93
Figure 6-6: Unconfined Compressive Strength Results for Stabilized Recycled Materials with Different Curing Conditioning Procedures.	94
Figure 6-7: Unconfined Compressive Strength Results for 5% Cement Stabilized Subgrade Soils with Different Curing/Conditioning Procedures.....	95
Figure 6-8: Stabilized (A) Clayey and (B) Sandy Subgrade Specimens with and without Membrane after Submergence Test.....	95
Figure 6-9: Unconfined Compressive Strength Results for Cement Stabilized Siliceous Gravel Sourced from Pharr with Different Curing/Conditioning Procedures.....	96
Figure 6-10: Unconfined Compressive Strength Results for Cement Stabilized RCA Materials Sourced from Houston with Different Curing/Conditioning Procedures.....	97
Figure 6-11: Unconfined Compressive Strength Results for Cement Stabilized FDR Materials Sourced from Atlanta with Different Curing/Conditioning Procedures.	97
Figure 6-12: Average Dielectric Values after 10 Days of Capillary Soak for Limestone (LS). Aggregates, Reclaimed Concrete Aggregate (RCA), Reclaimed Asphalt Pavement (RAP), Sandy and Clayey Subgrade Materials.	98
Figure 6-13: Variation of Degree of Saturation and Dielectric Values with Time for RCA Materials.....	99
Figure 6-14: Capillary Rise in The Tube Suction Test.....	100
Figure 6-15: Degree of Saturation after Completion of Different Curing Conditioning Procedures.	100
Figure 6-16: Retained UCS Values of Base Materials.	102
Figure 6-17: Retained IDT Strength Values of Base Materials.....	103
Figure 6-18: Comparison of Retained UCS and IDT Strength Values of Base Materials Subjected to 2-Day Backpressure Saturation Test.	103
Figure 6-19: Comparison of Retained UCS and IDT Strength Values of Base Materials Subjected to 1-Day Submergence Test.	104
Figure 7-1: Variation within Samples with Low and High Variability.	108
Figure 7-2: Distribution of the F-values.	110
Figure 7-3: Coefficient Variations of Unconfined Compressive Strength Tests for Stabilized Specimens Compacted with Different Compactions Procedures.....	112
Figure 7-4: Coefficient Variations of Various Moisture Susceptibility Protocols for Stabilized Base Materials.....	113
Figure 8-1: Impact Hammer, Texas Gyratory Compactor (TGC), Gyratory Compactor, and Vibratory Hammer.....	114
Figure 8-2: Impact Hammer Setup and Circular Steel Tamping Plate and Metal Shaft.....	115

Figure 8-3: Schematic Cross-section and View of Gyratory Compactor.	116
Figure 8-4: Variation of Density Versus Number of Gyration for Different Compaction Pressures (a) Angle of Rotation = 1.25° (b) Angle of Rotation = 1.16°	118
Figure 8-5: Variation of Height of Specimen Versus Number of Gyration for Different Compaction Pressures – (a) Angle of Rotation = 1.25° (b) Angle of Rotation = 1.16°.	118
Figure 8-6: Variation of Height of Specimen Versus Number of Gyration for Different Angle of Rotations – (a) Compaction Pressure = 116 psi (b) Compaction Pressure = 87 psi.	119
Figure 8-7: Unconfined Compressive Strength Test Results for Stabilized Materials with Different Angle of Rotations and Compaction Pressure.	120
Figure 8-8: Density of Stabilized Materials Compacted by Gyratory Compactor with Different Angle of Rotations and Compaction Pressure.	120
Figure 8-9: Moisture-Density Curves for (a) RCA Materials Sourced from Houston, (b) FDR Materials Sourced from Atlanta, (c) Siliceous Gravel Materials Sourced from Pharr, (d) Limestone Aggregates Sourced from El Paso, (e) Limestone Aggregates Sourced from Houston, and (f) RAP materials Sourced from Atlanta.	123
Figure 8-10: Moisture-Density Curves for (a) Clayey Materials Sourced from Sierra Blanca, (b) Sandy Soils Sourced from El Paso, and (c) Sandy Soils Sourced from Corpus Christi.	124
Figure 8-11: Optimum Moisture Content for Different Types of Stabilized Base Aggregates with Different Compaction Procedures.	125
Figure 8-12: Optimum Moisture Content for Different Types of Stabilized Subgrade Soils with Different Compaction Procedures.	125
Figure 8-13: Maximum Dry Density for different Types of Stabilized Base Aggregates with Different Compaction Procedures.	126
Figure 8-14: Maximum Dry Density for Different Types of Stabilized Subgrade Soils with Different Compaction Procedures.	127
Figure 8-15: Maximum Dry Density for Different Types of Stabilized Base Aggregates Compacted with Impact Hammer and Gyratory Compactor.	127
Figure 8-16: Unconfined Compressive Strengths Results for Samples Stabilized with (a) 2%, (b) 3%, and (c) 4% Cement Contents and Compacted with Different Compaction Procedures.	129
Figure 8-17: Unconfined Compressive Strengths Results for Samples Stabilized with (a) 2%, (b) 3%, and (c) 4% Cement Contents and Compacted with Different Compaction Procedures – (L/D ratio =2).	130
Figure 8-18: Indirect Tensile Strength Results for Samples Stabilized with (a) 2%, (b) 3%, and (c) 4% Cement Content and Compacted with different Compaction Procedures.	131
Figure 8-19: Aggregate Breakage during the Impact Hammer Compaction.	132

Figure 8-20: Schematic Diagrams of Aggregate Breakage after Impact Hammer Compaction for Different Base Materials.	133
Figure 8-21: Schematic Diagrams of Aggregate Breakage after Impact Hammer Compaction for all Base Materials.	133
Figure 9-1: Expansive Subgrade Soils sourced from (a and b) Sierra Blanca, and (c) Bryan.	136
Figure 9-2: Testing Program for Expansive Subgrade Soils.	137
Figure 9-3: Plasticity Index for (a) the HP Soil, (b) the HS Soil, and (c) the LS Soil at Different Stabilizer Types and Contents.	139
Figure 9-4: Methylene Blue Value for (a) the HP Soil, (b) the HS Soil, and (c) the LS Soil with Different Stabilizer Types and Contents.	140
Figure 9-5: pH Test Results.	141
Figure 9-6: Swell Pressure for (a) the HP Soil, (b) the HS Soil, and (c) the LS Soil with Different Stabilizer Types and Contents.	142
Figure 9-7: Swell Index and Swell Pressure for (a) the HS Soil and (b) the HP Soil with Different Stabilizer Types and Contents.	143
Figure 9-8: Swell Index for (a) the HS Soil and (b) the HP Soil with Different Stabilizer Types and Contents.	144
Figure 9-9: Relationship between Methylene Blue Value and Plasticity Index.	145
Figure 9-10: Relationship between Methylene Blue Value and Swell Index.	145
Figure 9-11: Relationship between Methylene Blue Value and Swell Pressure.	145
Figure 9-12: Relationship between Plasticity Index and Swell Index.	146
Figure 9-13: Relationship between Plasticity Index and Swell Pressure.	146
Figure 9-14: Relationship between Swell Index and Swell Pressure.	147
Figure 9-15: Unconfined Compressive Strength of HS Soils with Different Stabilizer Types and Contents.	148
Figure 9-16: Unconfined Compressive Strength of (a) HS Soils and (b) HP soils with Different Stabilizer Types and Contents.	149
Figure 9-17: Stabilized Clay Soils Sourced from Bryan District after 7 Days of Curing.	150
Figure 9-18: Unconfined Compressive Strength of HS Soils Stabilized with 5% Cement, 5% Lime, 5% Fly Ash, and the Combinations of the Cement and Fly Ash (5% Cement+5%Fly Ash) versus Curing Time.	152
Figure 9-19: Unconfined Compressive Strength of HP Soils Stabilized with 5% Cement, 5% Lime, 5% Fly Ash, the Combinations of the Cement and Fly Ash (5% Cement+5%Fly Ash) and the Combinations of the Cement and Lime (5% Cement+5%Lime) versus Curing Time.	153

Figure 9-20: Unconfined Compressive Strength of Stabilized Expansive Soils Sourced from Bryan with Different Stabilizers Type and Content After 7-Day and 28-Day Curing.....	154
Figure 9-21: Stabilized Clay Soils with 5% Fly Ash and 5% Cement after 7-day, 14-day, and 28-day Curing.	155
Figure 10-1: Relationship between UCS and IDT Strength for Cement Stabilized Base Materials in the Laboratory.	158
Figure 10-2: Relationship between UCS and IDT Strength for Cement Stabilized Base Materials Categorized Based on the Cement Content.....	159
Figure 10-3: Comparisons of Tensile and Compressive Strengths for Heavily Cement Stabilized Materials and Conventional Concrete Models.	160
Figure 10-4: Relationships between the UCS and IDT Categorized by Aggregate Type.	161
Figure 10-5: Relationships between the UCS and IDT Categorized by Compaction Methods.	162
Figure 10-6: Relationships between the UCS and IDT Categorized by Specimen Dimension.	163
Figure 10-7: Measured Versus Predicted IDT Strength for Specimens Compacted with Impact Hammer Using Genetic Programming Models for (a) Equation 10-3 and (b) Equation 10-4.	165
Figure 10-8: Measured Versus Predicted IDT Strength for Specimens Compacted with (a) Gyrotory Compactor, (b) Vibratory Hammer, and (c) TGC Using Genetic Programming Models.	166
Figure 10-9: Relationship between Resilient Modulus and Unconfined Compressive Strength Categorized by Aggregate Type.	168
Figure 10-10: Relationship between Resilient Modulus and Unconfined Compressive Strength at 25% and 50% Strength Ratios.	169
Figure 10-11: Relationship between Resilient Modulus and Unconfined Compressive Strength.	170
Figure 10-12: Measured Versus Predicted Resilient Modulus for Cement Stabilized Materials.....	171
Figure 10-13: Relationship between Shrinkage Strain and Unconfined Compressive Strength for Different Cement Stabilized Materials.	172
Figure 10-14: Relationship between Shrinkage Strain and Unconfined Compressive Strength for Cement Stabilized Materials with Different Cement Percentages.....	173
Figure 10-15: Measured Versus Predicted Shrinkage Strain for Cement Stabilized Materials.....	174
Figure 11-1: Typical GPR Reflections from a Pavement System.	176
Figure 11-2: Pavement Deflection Basin resulted from FWD Device.	177

Figure 11-3: Location of SH-123 and SH-72 in Texas.....	178
Figure 11-4: Pavement Construction Section and View of SH-123 in Corpus Christi.	179
Figure 11-5: GPR Data of SH-123 in Corpus Christi.....	180
Figure 11-6: Pavement Construction Section and View of SH-72 in Corpus Christi.	182
Figure 11-7: GPR Data of SH-72 in Corpus Christi.....	183
Figure 11-8: FWD Data of SH-72 in Corpus Christi.....	184
Figure 12-1: Nature of Stress Distributions in Traditional Tension Tests: (a) Third Point Bending Beam Test, and (b) Indirect Diametrical Tensile (IDT) Test (Ashtiani et al., 2016).....	189
Figure 12-2: Calibration of the Fatigue Performance Model.....	191
Figure 12-3: Calculation of Strain Ratio.....	192
Figure 12-4: Number of Load Application to Failure (Nf) for Different Types of Stabilized Base Materials and Typical Damage Evolution.....	194
Figure 12-5: Relationship between Number of Load Applications to Failure and Strain Ratio for Cement Stabilized Base Materials in the Laboratory.....	195
Figure 12-6: Relationship between Number of Load Applications to Failure and Strain Ratio for Stabilized Virgin Aggregates and Reclaimed Materials.....	196
Figure 12-7: Compiling Pavement Section Parameters and Material Properties from NDT (SH-123 – San Antonio).....	197
Figure 12-8: Meshing and Pavement Layers Simulations in ABAQUS.	198
Figure 12-9: Pavement Responses Contours for Horizontal Tensile Strain (ϵ_t).....	199
Figure 12-10: Measured Versus Predicted Shrinkage Strain for Cement Stabilized Materials.....	200
Figure 12-11: Relationship between Tensile Strain at Failure and Tensile Strength.	201
Figure 12-12: Tensile Strain at Failure for Different Cement Stabilized Materials.	201
Figure 12-13: Relationship between Shrinkage Strain and Time.	202
Figure 12-14: Improvement of Bias and Precision through Field Calibration.	203
Figure 12-15: Predicted (Model) Versus Measured (Field) Strain Ratio before Local Calibration for (a) Stabilized Virgin Base Layers and for (b) Stabilized Reclaimed Base Layers.....	204
Figure 12-16: Predicted (Model) Versus Measured (Field) Strain Ratio After Local Calibration for (a) Stabilized Virgin Base Layers and for (b) Stabilized Reclaimed Base Layers.....	205
Figure 13-1: Side by Side Comparison of Conventional and Inverted Pavement Structure.	208

Figure 13-2: Schematic of the Different Stiffness Values per Layer in Conventional and Inverted Pavement Structures. Adapted from Papadopoulos (2014) and Boudreau et al. (2016).	208
Figure 13-3: Gradation Limits for TxDOT Base Layers and South African G1 Base Layers with 37.5 mm NMS (top) and 26.5 mm NMS (bottom).....	212
Figure 13-4: Portable WIM Equipment Setup for Traffic In-Situ Measurements.....	215
Figure 13-5: Tire Pressure Estimation. A: Painting of Vehicle Tires. B: Print of Painted Tires on Papers. C: Axle Weight Measurements.	215
Figure 13-6: Tridem Axle Tire Contact Area of Analysis.....	216
Figure 13-7: Tensile Strains at the Bottom of the Asphalt Concrete Layer for the Three Pavement Structures. (a) Summer Season. (b) Winter Season.	217
Figure 13-8: Compressive Strains at the Top of the Subgrade for the Three Pavement Structures. (a) Summer Season. (b) Winter Season.	218
Figure 13-9: Vertical Stresses at the Top of the Subgrade for the Three Pavement Structures. (a) Summer Season. (b) Winter Season.	219

Chapter 1. Introduction

1.1 Background

Cementitious stabilization has been widely used to improve the strength and durability of granular materials for the construction and rehabilitation of pavement structures. Improved mechanical properties and durability of the stabilized materials combined with relatively low cost makes it an attractive method for design engineers. Although this technique appears simple and straightforward, engineering properties of individual soils and aggregates may alter widely due to the heterogeneity in soil composition, difference in microstructure among soils, heterogeneity of geologic deposits and differences in chemical interactions of water with soil particles. These differences need to be comprehensively studied to provide the best design framework and specific treatment options for stabilization of base layers and subgrade soils in pavement foundations.

1.2 Project Objectives

The main objective of this study was to develop a new protocol for the design of cement treated base and subgrade soil mixtures and calibrate field performance models for stabilized virgin aggregates and reclaimed materials. This research also provides the development of a series of statistically robust relationships between the laboratory measured data for pavement design and the development of new moisture susceptibility procedures to quantify the loss of orthogonal strength properties due to moisture intrusion.

1.3 Value of Research

The value of this research study was assessed by a series of metrics that includes environmental sustainability, materials and pavement, reduced construction, operations, and maintenance costs, and estimated increases in service life. These metrics were quantified in the following sections.

1.3.1 Environmental Sustainability

Texas uses more than 4 million tons of reclaimed materials for road construction projects annually (Snyder, 2016). By making modest changes to pavement design guidelines, greenhouse gas emissions can be reduced by incorporating reclaimed materials (including recycled asphalt pavement or RAP, recycled concrete aggregate or RCA, and full depth reclamation or FDR). Lee et al. (2010) revealed that by using reclaimed materials in the base and subbase layers of a pavement could result in CO₂ reductions of around 40,000 tons in Wisconsin out of a total annual tonnage of reclaimed materials of about 2 million tons. Thus, the annual reduction in CO₂ by using 4 million tons of reclaimed materials in Texas can be estimated at around 80,000 tons. According to recent studies conducted by Climate Discovery (2018), the cost of CO₂ reduction has been estimated \$20 per ton. As one of the objectives of this project was to update the existing mixture

design specification for reclaimed materials, this would represent a societal cost avoidance of approximately \$1.6 million in Texas annually.

1.3.2 Materials and Pavement

Ponte et al. (2017) conducted an economic impact analysis by comparing the unit prices of virgin and reclaimed materials in six states, Georgia, Illinois, Minnesota, Pennsylvania, Virginia, and Wisconsin. The authors reported that total system-wide economic savings from the use of reclaimed materials in these states was estimated to be \$62.5 million based on a total use of approximately 7.4 million tons of reclaimed materials. Successful implementation of developed specifications from this study and adherence to the design and analysis procedures can potentially save \$34 million in Texas.

1.3.3 Reduced Construction, Operations, and Maintenance Cost

Recent research efforts showed that the stabilization of base or subgrade layers can potentially reduce the price of construction and rehabilitation by reducing the amount of materials imported to the job site (Robinette and Epps, 2010). Robinette and Epps (2010) revealed that using stabilization techniques in the high-traffic volume facilities (20,000,000 ESALs) in lieu of conventional aggregate base could save \$11 for each ton of aggregate. If 10 million tons of cement treated aggregate materials is used annually in Texas, \$110 million saving each year can be saved by the elimination of excavation, reduced purchase and haul of natural aggregate, and reduced pavement thickness over the stiffer base.

In addition, in the current marketplace, the price of materials necessary for reconstruction, rehabilitation, and maintenance of state's aging transportation infrastructure is increasing at rates exceeding the ability to provide funding. Many highway agencies find that a dollar does not go as far as before; as a result, the level of service of the roadway network is suffering. Robinette and Epps (2010) indicated that the rehabilitation price per square yard is around \$18. Using 80 million square yards of cement stabilized aggregate in Texas annually could contribute to savings of \$1,440 million due to reduction of the rehabilitation activities after 10 years. Therefore, up to \$144 million per year could be saved by reducing maintenance costs by using cement treated aggregates.

1.3.4 Increasing Service Life

Puppala et al. (2016) showed that the stabilization solutions could prolong the life of pavements in Texas by 30% to 40% when built on high sulfate soils with minimal distress. The effectiveness of polypropylene fiber along with chemical additives on the strength properties and volumetric stability of high sulfate soils was investigated in this project. Therefore, considering a \$100 million worth of pavement construction projects built on high sulfate soils across Texas districts, these savings could amount to \$100 million or more (100% of original construction costs) as there will be no need for complete rehabilitation of the pavements.

Table 1-1 demonstrates the cost benefits for functional areas based on these assumptions considering 5% project impact. Conservative assessment of the values of these areas indicates that this project can potentially save \$19.48 million annually by successful implementation of developed the laboratory mixture design specification for cement treated base and subgrade soils (Table 1-2). The net present value after 10 years would be around \$170 million, which represent significant statewide benefit of this project (Table 1-3).

Table 1-1: The Cost Benefit for Different Functional Areas

Benefit Area	Benefit Amounts	Project Impact	Total Savings
Environmental Sustainability	\$1.6 million	5%	\$0.08 million
Materials and Pavements	\$34 million	5%	\$1.7 million
Reduced Construction Cost	\$110 million	5%	\$5.5 million
Reduced Operations and Maintenance Cost	\$144 million	5%	\$7.2 million
Increased Service Life	\$100 million	5%	\$5 million

Table 1-2: Estimation of Value of Research.



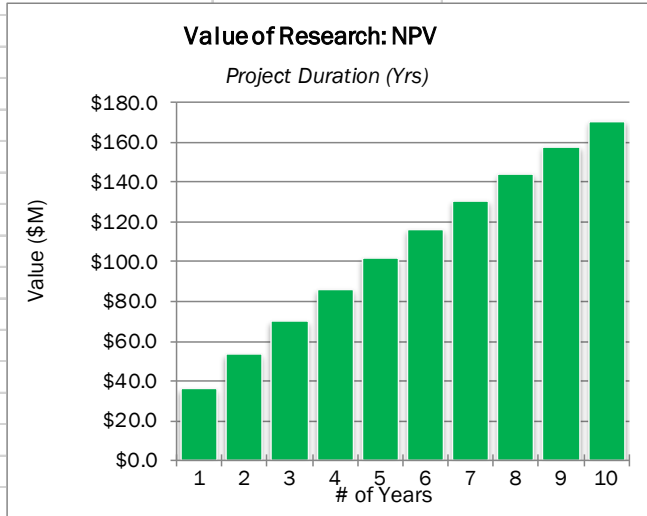
	Project # 0-6949					
	Project Name: Establishing Best Practice for construction and Design of Cement Treated Materials					
	Agency: University of Texas at El Paso					
	Variable Amounts					
Benefit Area	#1	#2	#3	#4	#5	Totals
System Reliability						\$ -
Increased Service Life	\$ 5,000,000.00					\$ 5,000,000.00
Improved Productivity and Work Efficiency						\$ -
Expedited Project Delivery						\$ -
Environmental Sustainability	\$ 80,000.00					\$ 80,000.00
Traffic and Congestion Reduction						\$ -
Reduced User Cost						\$ -
Reduced Construction, Operations, and Maintenance Cost	\$ 5,500,000.00	\$ 7,200,000.00				\$ 12,700,000.00
Materials and Pavements	\$ 1,700,000.00					\$ 1,700,000.00
Infrastructure Condition						\$ -
Freight movement and Economic Vitality						\$ -
Intelligent Transportation Systems						\$ -
Engineering Design Improvement						\$ -
Safety						\$ -
						Total \$ 19,480,000.00

Table 1-3: Estimation of Value of Research for 10 Years.

	Project #	0-6949		
	Project Name:	Establishing Best Practice for construction and Design of Cement Treated Materials		
	Agency:	UTEP	Project Budget	\$ 404,202
	Project Duration (Yrs)	3.0	Exp. Value (per Yr)	\$ 19,480,000
Expected Value Duration (Yrs)		10	Discount Rate	4%

Economic Value			
Total Savings:	\$ 194,395,798	Net Present Value (NPV):	\$ 170,265,431
Payback Period (Yrs):	0.020750	Cost Benefit Ratio (CBR, \$1 : \$ ___):	\$ 421

Years	Expected Value
0	\$19,075,798
1	\$19,480,000
2	\$19,480,000
3	\$19,480,000
4	\$19,480,000
5	\$19,480,000
6	\$19,480,000
7	\$19,480,000
8	\$19,480,000
9	\$19,480,000
10	\$19,480,000



Years	Expected Value	Expected Value	Expected Value	NPV
0	\$19,075,798	\$19,075,798	\$19.08	\$18.34
1	\$19,480,000	\$38,555,798	\$38.56	\$36.35
2	\$19,480,000	\$58,035,798	\$58.04	\$53.67
3	\$19,480,000	\$77,515,798	\$77.52	\$70.32
4	\$19,480,000	\$96,995,798	\$97.00	\$86.33
5	\$19,480,000	\$116,475,798	\$116.48	\$101.73
6	\$19,480,000	\$135,955,798	\$135.96	\$116.53
7	\$19,480,000	\$155,435,798	\$155.44	\$130.77
8	\$19,480,000	\$174,915,798	\$174.92	\$144.45
9	\$19,480,000	\$194,395,798	\$194.40	\$157.61
10	\$19,480,000	\$213,875,798	\$213.88	\$170.27

Notes:

Amounts on Value of Research are estimates.

Project cost should be expensed at a rate of no more than the expected value per year.

This electronic form contains formulas that may be corrupted when adding or deleting rows, by variables within the spreadsheet, or by conversion of the spreadsheet. The university is responsible for the accuracy of the Value of Research submitted.

1.4 Research Tasks

To address the research objectives of this project, ten Tasks were identified and incorporated in this study. The main components of this study were laboratory characterization of cement treated base, sub-base, and subgrade soils, development of new moisture susceptibility procedures with special heat treatment, development of material models, development of new fatigue performance models based on strength and shrinkage potential of cement treated specimens, and synthesis of the laboratory achieved data to draft updated mixture laboratory design specification. To optimize the project deliverables considering the time and funding constraints, a three-year comprehensive study was conducted during fiscal year (FY) 2018, (FY) 2019 and (FY) 2020.

1.5 Report Contents and Organization

The general organization of this report is provided in this section. Subsequent to the introductory chapter detailing the project objectives and the envisioned tasks to meet the objective of the project, the following information was presented in succinct yet detailed manner:

- Chapter 2: Literature Review
- Chapter 3: Survey of Texas Districts
- Chapter 4: Experimental Design for Comprehensive Laboratory Tests
- Chapter 5: Laboratory Test Results
- Chapter 6: Alternative Approaches for the Laboratory Evaluation of Moisture Susceptibility for Cement Stabilized Materials
- Chapter 7: Analysis of the Variability of the Laboratory Data
- Chapter 8: Compaction Characterizations.
- Chapter 9: Strategies to Improve Orthogonal Strength Capacity and Volumetric Stability of Expansive Soils
- Chapter 10: Development of Material Models
- Chapter 11: Field Testing Database
- Chapter 12: Field Calibration of the Fatigue Performance Model
- Chapter 13: Analysis and Design of Inverted Pavements
- Chapter 14: Development of the Draft Laboratory Test Procedure
- Chapter 15: Conclusions

Chapter 2. Literature Review

For utilization in accomplishing the research objective, an extensive literature review that documented strengths and shortcomings of available procedures, construction guidelines and field quality control protocols of cement treated granular materials is incorporated in this chapter. A comprehensive review of performance issues of pavements with cement stabilized materials is initially introduced, followed by the compilation of previous experiences on laboratory characterization of the cement treated soils and base layers in the pavement industry. A thorough investigation of the nationally and internationally available moisture susceptibility tests for the characterization of the moisture induced damage of cement treated materials is also described. Then, the previous laboratory and field experiences with cement treated reclaimed concrete and reclaimed asphalt systems are summarized and tabulated with their potential challenges such as moisture susceptibility and durability issues. Finally, the available pavement performance models for the characterization of the deformation and fatigue characteristics of cement treated layers are compiled and presented.

2.1 Performance Issues of Pavements with Cement Stabilized Materials

The cement stabilized layer may significantly affect the performance of the Hot Mix Asphalt (HMA) layer, especially when the former is located directly underneath the HMA layer. Performance issues related to pavements with cement stabilized materials include rutting, block, and transverse cracking, top-down cracking, and bottom-up fatigue cracking. Moreover, high sulfate content soils and expansive soils lead to swelling or shrinkage of cement stabilized layers, greatly impacting the success of cement treatment projects. These issues as main challenges of using calcium-based stabilizers are identified and described in detail in the following sections.

2.1.1 Rutting

The cement stabilized material has the ability to substantially reduce rutting in the subgrade and bound base layers in comparison with unbound materials due to the high stiffness of these materials. Using the cement stabilized base materials significantly changes the stress/strain distribution and results in higher shear strain in the HMA layer. Austroads (2008) reported that due to an increase in shear stress distribution in HMA, the high stiffness of cement stabilized materials can lead to deep rutting in HMA as well as top-down cracking as shown in Figure 2-1.



Figure 2-1: Rutting of the HMA Layers without Deformation of the Cemented Base Layer (Austroads, 2008).

In addition to rutting induced by high shear stresses in the HMA layer, repeated compressive loads at the top of the cement stabilized layer lead to top crushing by fatigue that will ultimately generate rutting in cement stabilized materials. De Beer (1990) indicated that thick lightly cemented layers may fail by crushing or compression at the top 2 or 3 inches, in which crushed materials will lead to rutting as observed in Figure 2-2. However, the author concluded that the tensile strain beneath this thick layer is extremely small, and thus tensile fatigue is not an important issue in this case. In a follow-up study, Theyse and De Beer (1996) found that increasing the unconfined compressive strength of cement stabilized materials reduces the compression strain, and thus increases the compression fatigue life.

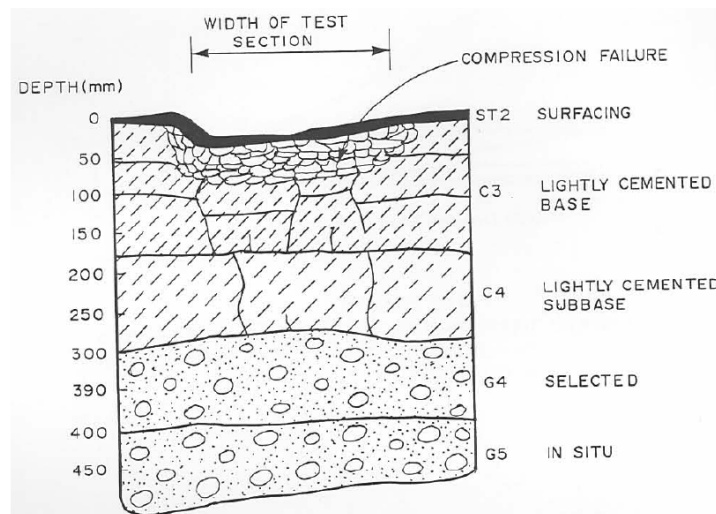


Figure 2-2: Compression Fatigue of Cement Stabilized Materials (De Beer 1990).

2.1.2 Block and Transverse Cracking

Roads and highways in many parts of the world that use cement stabilized base materials as a platform for HMA layers have encountered block or transverse cracking (Austroads, 2008). Zube et al. (1969) reported that these types of cracking stem from shrinkage of the underlying stabilized base and often occurs when the HMA layer is thin, as for local roads. They also indicated that high unconfined compressive strength results in block cracking, which is likely due to the high shrinkage of cement stabilized materials with high stabilizer content. Sebesta and Scullion (2004) reported that transverse and block cracking results from shrinkage of the stabilized base, starting from the bottom of the surface layer and propagating through the surface layer, as observed in Figure 2-3. This propagation is due to the bond between the HMA and stabilized base materials. In a relevant study, George (2002) revealed that heavily stabilized base materials are more prone to shrinkage cracking according to Long-Term Pavement Performance (LTPP). The author concluded that no shrinkage cracking happens when the unconfined compressive strength subjected to seven-day moist cured is lower than 300 psi.



Figure 2-3: (a) Block Cracking and (b) Transverse Cracking in HMA with Stabilized Base Materials (Sebesta and Scullion 2004).

2.1.3 Bottom-Up Cracking (Alligator Cracking)

Bottom-up cracking is divided in two groups including bottom-up cracking due to cement stabilized layer surface raveling and bottom-up tension cracking due to fatigue of stabilized base. Thogersen et al. (2004) showed that the surface of a stabilized base layer can ravel, and then generate a layer of loose material between the HMA layer and the cement stabilized base layer as shown in Figure 2-4. The authors revealed that alligator cracking can be created by raveling of the base that increases the strain level at the bottom of the HMA layer. According to studies conducted in South Africa (De Beer, 1985), bottom-up cracking due to Cement Treated Base (CTB) surface raveling probably is linked to the erodibility of stabilized materials, which usually occurs when relatively fine raw materials are stabilized.



Figure 2-4: Separation between Asphalt and Cement Stabilized Base (Thogersen et al., 2004).

The second type of bottom-up cracking (fatigue cracking) occurs as results of tensile strain at the bottom of the cement stabilized base layer due to repeated traffic loads. According to studies conducted by Austroads (2008), micro cracking is initiated at the bottom of cement stabilized base layer due to tensile stresses or strains and propagates upwards under repeated traffic as it is shown in Figure 2-5. De Beer (1990) found that bottom-up cracking typically occurs in relatively thin cement stabilized base layers in which tensile strain could cause fatigue damage.



Figure 2-5: Fatigue Cracking from the Bottom of the Cemented Layer (Austroads, 2008).

Little et al. (1995) found out that heavily stabilized base materials often fail by fatigue because of tension in the relatively thin cement stabilized layer. They recommended a minimum thickness of 8 inches for fatigue crack resistance. The fatigue of a cement stabilized layer is related directly to the strength of the cement stabilized materials. Yeo et al. (2008) reported that a longer fatigue life of the cement stabilized layer can be obtained by the higher flexural strength. Ashtiani et al. (2016) investigated the indirect tensile strength (IDT) of lightly and heavily cement stabilized materials and found that increasing IDT strength increases fatigue resistance. Theyse et al. (1996) reported that the tensile fatigue life of a cement stabilized layer can be improved by increasing the break strain of cement stabilized materials.

2.1.4 Top-down Cracking (Longitudinal Cracking)

As discussed in previous sections, cement stabilized base layers provide a very strong platform for surface layer such as HMA. This support reduces the fatigue of surface layers that can happen as a result of tension at the bottom of the HMA layer. Thus, cement stabilized materials mitigate alligator cracking in the surface layer. However, it was concluded in the literature that high

stiffness and strength values of cement stabilized materials induce top-down cracking in asphalt pavement as observed in Figure 2-6 (Button et al., 2001). A stabilized base layer with high modulus due to an excessive amount of stabilizer leads to longitudinal cracking in the wheel path. In this regard, Syed and Scullion (2001) recommended a maximum 7-day UCS of 200 psi for cement stabilized layers. In a follow-up study, Scullion et al. (2003) revealed that cement stabilized full-depth recycled base with high stiffness values are more prone to top-down cracking in the wheel path. George et al. (2002) reported that top-down cracking in the wheel path is most of the major distresses for roads built with cement stabilized layers.



Figure 2-6: Top-Down Cracking in HMA Layer on Stabilized Base (Button et al., 2001).

2.1.5 Inverted Pavement as a Crack Mitigation System

An inverted pavement as a crack mitigation system is an innovative pavement technology developed in South Africa in the 1970s. This system is being investigated for various roadway applications in the U.S. since the 1980s. The materials used in an inverted pavement design are similar to a conventional flexible pavement, while the material layers are rearranged and the unbound layer is sandwiched between the asphalt layer and the stabilized layer as depicted in Figure 2-7. The switching of the order of layers proved to be a successful approach to mitigate reflective cracking (Cortes & Santamarina, 2013). In such an inverted pavement design, the unbound layer acts as a crack-arrest medium that can potentially eliminate the reflective cracking initiated in the cement treated layer and propagated to the asphalt layer (Adaska & Luhr, 2004). Therefore, this innovative and practical design results in significant improvements in the service life of pavements. Additionally, the presence of the treated layer below the unbound layer allows for a robust platform and therefore better compaction of the aggregate base is achieved in inverted pavements.

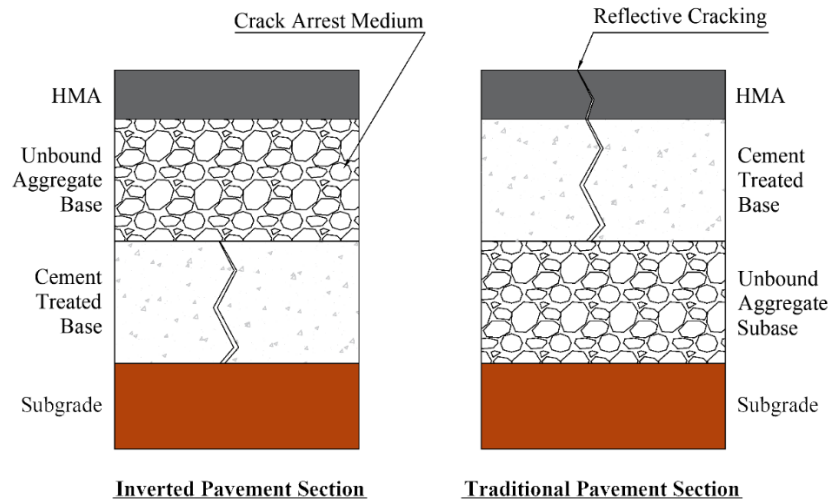


Figure 2-7: Inverted Pavement Section.

2.1.6 Expansive Soils

Construction of pavement foundations on soft subgrade soils such as expansive clays is a particular challenge to engineers as these typical soils are highly susceptible to permanent deformation due to its poor shear strength and high compressibility. Shrinking and swelling of expansive clays due to seasonal moisture variation also results in detrimental cracking, uneven pavement surface, and ultimately, instability of the pavement structures. Improvement of certain desired properties such as bearing capacity, volumetric stability, strength, and stiffness of soils can be undertaken by a variety of ground improvement techniques such as pre-wetting, soil replacement with compaction control and surcharge loading (Punthutaecha et al., 2006). All these methods have the disadvantage of being expensive and ineffective.

Stabilizing clays with calcium-based stabilizers such as cement, lime, and fly ash is a proven technique for improving the performance at lower cost than either replacing material or increasing the base thickness to reduce subgrade stresses (Prusinski & Bhattacharja, 1999). However, these chemical additives occasionally result in a high stiffness and brittle behavior, which is not favorable for the structures with dynamic loading conditions, such as pavement foundations (Basha et al., 2005). Additionally, chemical stabilization cannot adequately compromise the swelling tendency of stabilized clayey soils (Stavridakis et al., 2005). Cokca (2001) reported that using independently calcium-based stabilizers such as lime, cement, and class C fly ash is not capable to substantially mitigate the swelling potential of expansive soils. Moreover, the majority of these stabilizers do not provide effective treatment for expansive soils containing large amounts of soluble sulfates (Si & Herrera, 2007; Harris, 2002). Sulfate minerals attack on cementitious materials leads to the conversion of the hydration products of cement to ettringite and gypsum, which ultimately leads to the destabilization of the cement-soil matrix (Santhanam et al., 2002). Vasudev (2007) showed that sulfate-bearing soils stabilized with combination of cement and fly ash exhibit the best field performance in terms of heaving resistance. Comparatively, Si (2008)

strongly recommended the soil with the higher sulfate content not be stabilized using traditional calcium-based stabilizers alone due to the high potential for swelling and low retained unconfined compressive strength. The author revealed that the combination of lime and fly ash appears to be the most suitable stabilizer for higher sulfate bearing soils. Hence, new solutions are still required to reduce volumetric strain of expansive soils with high sulfate contents in pavement foundations.

The use of polypropylene fibers for the reinforcement and stabilization of clayey soils is a major focus of several research studies. Polypropylene fibers as cost-competitive materials can be manufactured with desired properties, do not create leaching problems, and are unaffected by chemical and biological degradation (Puppala et al., 2000; Gilazghi et al., 2016; Bin-Shafique et al., 2017). Mirzababaei (2017) evaluated the effect of fiber reinforcement on the shear strength of soft and stiff clayey soils. The author found that soft clays reinforced with polypropylene fibers did not perform well in terms of mechanical properties. Ayeldeen and Kitazume (2017) revealed that polypropylene fibers with the combination of calcium based stabilizers has significant potential to enhance the compressive strength of soft clays. Therefore, an experimental program should be carried out to investigate the effects of polypropylene fiber along with chemical additives on the swelling and mechanical behavior of soft subgrade soils.

2.2 Laboratory Characterization of Cement Stabilized Materials

The strength and modulus values of cement stabilized materials are important in pavement analysis and directly affect overall pavement performance. These values are typically characterized by unconfined compressive strength, indirect tensile strength, flexural strength, resilient modulus, modulus of elasticity, and seismic modulus. A thorough investigation of the nationally and internationally available strength and stiffness characterization tests for cement treated materials is extensively discussed in the following section.

2.2.1 Strength Properties

Several researchers reported inconsistencies with the flexural beam test and explored alternative testing methods to estimate the tensile behavior of stabilized materials. Gnanendran and Piratheepan (2009) used the Indirect Diametrical Tensile (IDT) test as an alternative to the flexural beam test for the characterization of strength properties of lightly stabilized materials. The authors determined the Static Stiffness Modulus (SSM) from monotonic loading with an imposed vertical deformation rate of 1mm/min. They also calculated a measure of Dynamic Stiffness Modulus (DSM) based on a series of repeated sinusoidal loading with 3Hz frequency. The authors reported that SSM and DSM were not affected by the moisture content but did increase with stabilizer content in the mixes. Yan et al. (2011) reported high variability in the fatigue life of cement stabilized specimens subjected to similar stress states and cement contents. The researchers attributed the high variability of the results to low cement content, disintegration of external granules, variability in strength of specimens, and loss of moisture during testing. Sobhan and Das (2007) assessed the durability of soil-cements against fatigue fracture. The researchers performed

flexural fatigue tests with third point loading at a frequency of 2 Hz on 6×6×20 in. prismatic specimens using a sinusoidal load shape function. They reported that the upper bound limit for the endurance threshold of a cement stabilized specimen was approximately 53% of its maximum unconfined compressive strength. Additionally, the authors developed a criterion based on the dissipated energy to characterize the fatigue performance of cementitious materials. They also postulated that the rehabilitation strategy of the pavement structure can be determined using such criteria in the laboratory.

Arnold (2012) developed a laboratory protocol for the estimation of the flexural strength, modulus, and fatigue properties of stabilized materials using the three-point loading test. The authors used a vibrating hammer for the compaction of prismatic beams in the laboratory. The researchers recommended at least one million load cycles to be incorporated in the laboratory testing protocol. In a relevant study, Majumder et al. (1999) carried out flexural fatigue tests on 4×4×20 in. beam specimens using a three-point loading system. The on-load and the off-load durations were 0.27 seconds each. Load was applied until sudden and brittle failure was observed. The relations developed using fatigue life versus stress ratio was used as an input for the design of pavements. They also found that cement treated materials with laterite aggregates exhibit higher fatigue lives when compared to mixes with gravel and dolerite aggregate types.

Midgley and Yeo (2008) explored the use of indirect tensile test as an alternative means to characterize the fatigue behavior of the cement treated materials. They reported that gyratory compactor was suitable for the preparation of laboratory indirect tensile samples. They also found out that indirect tensile test is more appropriate for testing materials of lower stiffness. Flintsch et al. (2008) found that deflections in a pavement structure are significantly reduced as the stiffness of the base layer was increased. They also found that fatigue cracking in asphalt layers was greatly minimized due to the use of stabilized layers. However, findings were based on pavement design models and not from a laboratory characterization of fatigue crack resistance.

Ashtiani et al. (2016) performed several Finite Element (FE) analysis considering different material properties and stress paths to investigate the systematic error associated with the bending beam test for stabilized materials in the laboratory. As evidenced in Figure 2-8a, due to the pure bending mechanism in the bending beam test, the top portion of the beam is in compression, while the bottom fibers experience tension. They concluded that approximately 60% of the beam is still in compression due to the pure bending loading in the third point test based on the parameters selected for the finite element analysis. Additionally, the distributions of the stress follow a highly nonlinear pattern in the mid-span cross section of the prismatic beam. They also showed the capability of the IDT test to induce a relatively uniform tension along the axis of loading in the specimen as observed in Figure 2-8b. The exaggerated deformed meshes showed small compression zones immediately beneath the loading platform and adjacent to the support at the bottom of the specimen, however the majority of the specimen stays in tension upon the application of the axial load. The authors finally concluded that the theoretical issues and practical aspects of the third point beam test underscore the necessity of developing an alternative test method to

estimate, in an effective and efficient manner, the tensile behavior of cementitious materials in the laboratory.

2.2.2 Stiffness Properties

Stiffness of cement treated base varied significantly from laboratory to field cored specimens. These variations were manifested due to the difference in the environmental conditions between laboratory and field sections. The elastic layer analyses of pavement structures with cement treated bases showed reduced stresses and strains at the bottom of asphalt layer and top of subgrade when compared to pavement structures with traditional bases and asphalt treated base layers. Therefore, the life of pavements with cement treated base layers was substantially longer when compared to traditional pavements (Mahasantipiya, 2000).

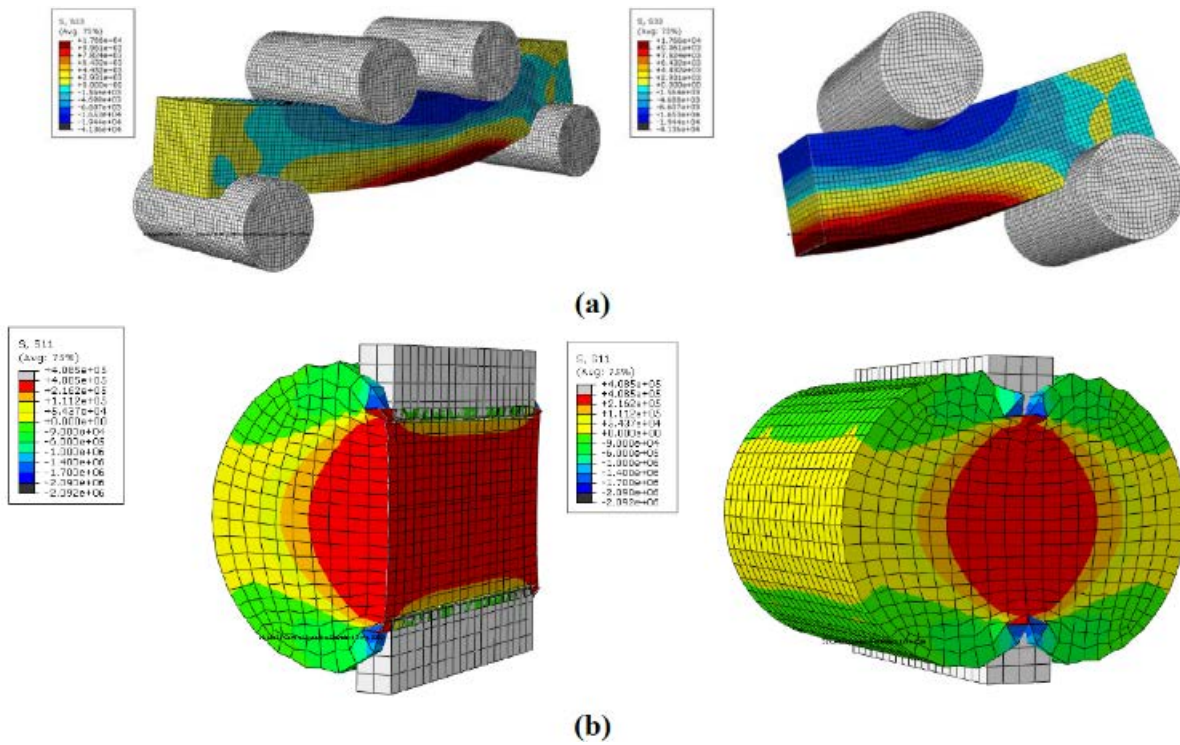


Figure 2-8: Nature of Stress Distributions in Traditional Tension Tests: (a) Third Point Bending Beam Test, and (b) Indirect Diametrical Tensile (IDT) Test (Ashtiani et al., 2016).

Scullion et al. (2008) characterized material properties of cement treated soil bases to determine input values for a mechanistic-empirical pavement design analysis. The material properties used for design were the resilient modulus, modulus of rupture, and Poisson's ratio. Results showed resilient modulus as half of the value of modulus measured using seismic based devices. They used three different methods to measure the resilient modulus in the laboratory; these include the seismic modulus test, dynamic modulus test, and the resilient modulus test. The authors reported that the frequency of loading has no significant effect on the modulus, therefore they concluded that the soil cement acted as an elastic material. For this reason, they rationalized that the dynamic

modulus is the same as the resilient modulus and can be used as an input. Table 2-1 shows the comparison of the three test methods. The seismic modulus test is the least expensive and fastest test to obtain a measure of the resilient modulus. The authors performed a case study on two different materials. The authors concluded that the seismic modulus can be considered as a reliable and repeatable alternative to traditional test procedures. The authors also developed a relationship between the unconfined compressive strength and the resilient modulus as well as with the modulus of rupture though this relationship was based on very limited data.

Table 2-1: Comparison of Three Moduli Test Methods (Scullion et al., 2008).

Comparison Criteria	Seismic Modulus Test	Dynamic Modulus Test	Resilient Modulus Test
Equipment Cost	\$5,000	\$40,000	\$350,000
Testing Time	3 minutes	40 minutes	30 minutes
Sample Capping	No capping	Capping	Capping
Coefficient of Variation	7%	7%	10%

In a relevant study, Puppala et al. (2011) reported that the resilient modulus estimations were less sensitive to the change in confining pressure for the cement treated materials. He rationalized that this is due to the influence of stiffening in the process of stabilization of materials fabricated in the laboratory.

Papacostas and Alderson (2013) tested different cementitious materials to determine flexural strength, breaking strength, and flexural modulus. They concluded that cement content was most significantly correlated with flexural strength followed by moisture content and fine aggregate content. The materials tested included general purpose Portland cement, lateritic gravel, weathered granite, calcrete, ferricrete, and met greywacke. The test methods included the flexural test method, the flexural strength testing, and the flexural modulus testing. It can be noted that for the flexural beam test, a beam with dimensions of 4×4×16 in. was used for easier handling. The researchers developed a model based on the laboratory collected data to relate the material characteristics to the flexural strength and the breaking strength of the beams. This model concluded that cement content was the most significant feature and no significant relationship between the breaking strain and material characteristic was found. They also reported that there is enough evidence to conclude that a meaningful relationship exists between the unconfined compressive strength and the flexural modulus.

Burns and Tillman (2006) researched the influence of fines content, cement content, mineralogy, and freeze-thaw cycles on the strength properties of the mixes characterized by the unconfined compressive strength tests for the Virginia Department of Transportation. The aggregates incorporated in the experiment design were mica, limestone, diabase, and granite. These aggregates were tested at 3, 4, 5, and 6% cement content by weight. The authors reported that the mineralogy of the aggregate materials significantly influenced the strength of the cement treated specimen. As expected, an increase in unconfined compressive strength was measured in the

aggregates with greater cement content. Based on the laboratory results the authors recommend a minimum of 250 psi for 7-day unconfined compressive strength of cement treated aggregates.

Paul and Gnanendran (2012) studied the characterization of lightly stabilized granular base materials by the flexural beam test and the effect of the rate of loading on the results. In this study, a monotonic load/displacement flexural beam test with an improved deflection measurement setup was used. The two types of aggregates used under the Unified Soil Classification System (USCS) were classified as well-graded sandy gravel with some fines. The binders chosen were general blend cement and fly ash because of their low shrinkage/cracking potential and for economic reasons. The aggregates were stabilized with 1% to 3% stabilizer content. The dimensions of the specimen in this study were 3×3×12 in. It was shown that two of the samples containing 1% stabilizer content were damaged in the process of removal from the mold. A second attempt also resulted in failure. The test began with a displacement rate of 1.2 mm/min as per ASTM D1635 (ASTM, 2019) but the specimens failed within seconds, which suggested that such guidelines are not suitable for lightly stabilized materials. The specimens were then tested at different rates. The results showed that rate significantly influences the load deflection behavior of lightly stabilized material. Failure load and slope of load deformation curve increased with the increase in the imposed displacement rate. The authors noted that because of unavailability of equipment and required training of the operator, the test may not be very practical and therefore a relationship between the flexural strength and the stiffness modulus was created.

2.2.3 Durability

Khoury and Zaman (2007) studied the influence of different stabilizing materials on the durability of the mixes. Cement kiln dust, fly ash, and bed ash were selected as stabilizing binders. They found that resilient modulus decreases with increased number of freeze-thaw cycles. Distortion of composites during freezing and increased moisture content due to thawing was explained as the reason for decrease in resilient modulus with freeze-thaw cycles.

Ashtiani et al. (2014) presented a mechanistic procedure for performance characterization of recycled aggregate systems for use as aggregate base layers. They selected twelve recycled aggregate systems with different lithology and known field performance histories. A shear strength test at different confinement levels and the Canadian freeze-thaw test, Micro-Deval test, and tube suction test were performed on the samples. They found out that several recycled systems performed equally or better compared to control systems consisting of virgin aggregates in terms of higher shear strength and higher hardening index. The authors also concluded that recycled concrete materials typically had superior mechanical properties such as a higher resilient modulus and hardening index compared to recycled asphalt systems; however, recycled concrete systems showed higher frost susceptibility. In a relevant study, Kim et al. (2013) evaluated resilient modulus and moisture susceptibility of unbound aggregate base composed of recycled concrete materials to establish comparison plots with control systems. The authors concluded that the recycled system had equal or better performance in terms of resilient properties compared to virgin

aggregate systems. However, the recycled system showed more affinity for moisture retention that is associated with loss of stiffness due to freezing and thawing in service. Although the dielectric value of unbound aggregate base composed of recycled concrete materials was within the marginal range, the value was close to the poor aggregate quality limit. Therefore, authors recommended further study to characterize the moisture susceptibility of recycled systems in conjunction with the resilient modulus for the design of pavement structures with recycled concrete aggregate layer.

2.2.4 Strength Requirements

U.S. Army Corps of Engineers and the American Concrete Institute (ACI) recommends the strength criteria presented in Table 2-2. The lowest cement content in the mixture design that meets the requirements in Table 2-2 should be used as the design content. If the selected samples do not comply with the recommendations, then higher cement contents may be added to the soil and strength and durability tests may be repeated until the strength values conform the requirements.

Table 2-2: U.S. Army Corps of Engineers Unconfined Compressive Strength Criteria.

Purpose of Stabilized Layer	Minimum 7 Days UCS (psi)	
	Flexible Pavement	Rigid Pavement
Base Course	750	500
Subbase, selected material, or subgrade	250	200

In addition, the Virginia Department of Transportation (VDOT) currently evaluated the mechanical properties for cement treated aggregate base (Hossain et al. 2017). As part of the literature review of this study, several state DOTs were contacted regarding their Cement Treated Aggregate (CTA) specification and range of design for 7-day compressive strength. Figure 2-9 shows a summary of the findings.

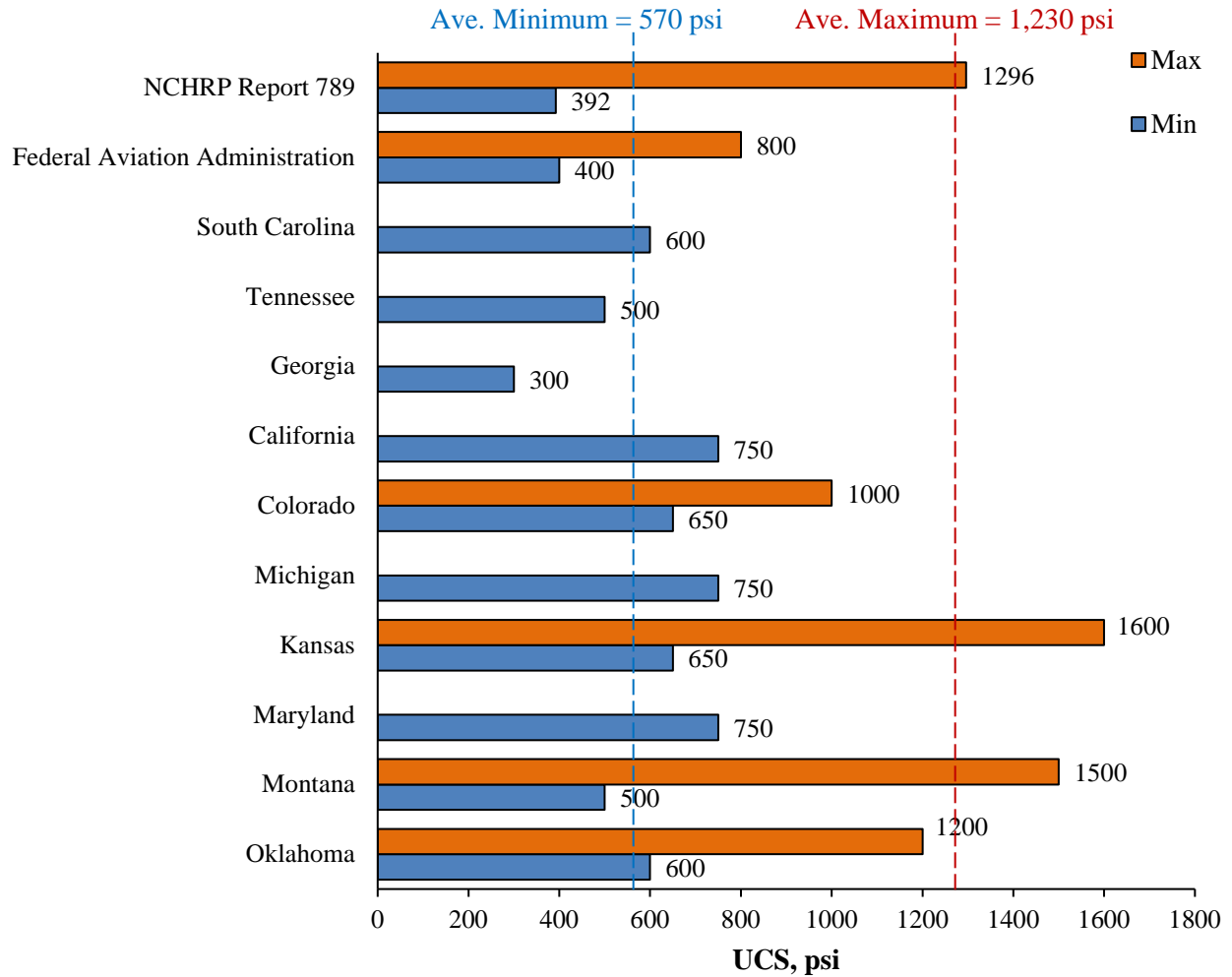


Figure 2-9: Summary of State DOTs for Design of 7-Day Compressive Strength of Cement Treated Aggregate Base Layers.

2.3 Summary of the Literature Review

An extensive literature review that documents strengths and shortcomings of available procedures, construction guidelines, and field quality control protocols of cement treated materials was carried out in this study. Tables 2-3 and 2-4 summarize various testing protocols found in the literature with their advantages and limitations for the characterization of strength, modulus, and moisture susceptibility. Table 2-5 also shows the comparison of different reclaimed materials and virgin aggregates used for cement stabilized base layers.

Table 2-3: Comparison of Laboratory Test Methods for Strength and Modulus Characterization.

Tests	Purpose	Specimen Size (in.)	Test Time	Advantages	Disadvantages
UCS	Compressive Strength	6(d) x 12 (h)	20 min	Widely accepted, practical and user-friendly test	Localized plastic behavior and higher strain below the load platens due to high stress in those region
IDT	Indirect Tensile Strength	6(d) x 4.5 (h)	12 min	Failure is initiated in a region of relatively uniform tensile stress.	Loading conditions do not resemble those in the field
Flexural Beam	Modulus of Rupture	4 x 4 x 15.75	> 100 min	Simulating pavement field conditions	non-uniform and undefined stress distribution
Submaximal Modulus	Resilient Modulus / Permanent Deformation	6(d) x 12 (h)	> 100 min	Obtaining accurately resilient modulus and permanent deformation	Not applicable for routine use
Seismic Modulus	Modulus	No restrictions	2 min	Very rapid and inexpensive	Estimating only the linear-elastic (low-strain) modulus

Table 2-4: Comparison of Laboratory Test Methods for Characterization of Moisture Susceptibility.

Tests	Specimen Size (in.)	Test Time	Advantages	Disadvantages
Tube Suction	No restrictions	10 Days	Cost-effective	Time consuming test, non-uniform distribution of moisture in sample, and dropping the dielectric value of cement stabilized materials after long-term curing due to the effect of chemical reactions
Back Pressure	4(d) x 6 (h)	24 hours	A simple and applicable test, uniform distribution of moisture in sample, ability to measure other information such as permeability and pH	Generating excessive hydraulic gradient which may damage the specimen during conditioning.
Submergence	No restrictions	28 hours	Very simple and inexpensive	Not reliable test, and disintegrating of specimen during moisture conditioning
Vacuum Saturation	4(d) x 6 (h)	12 hours	Quickest moisture susceptibility test, uniform distribution of moisture in sample	Expensive due to control of vacuum suction more than 1 atmosphere

Table 2-5: Comparison of Materials Used for Cement Stabilized Base Layers.

Material	Advantages	Disadvantages
Reclaimed Asphalt Pavement (RAP)	Higher resilient modulus, Reduction of greenhouse gas emissions, cost effective material	Lower shear strength, higher permanent deformation, lower hardening index
Reclaimed Concrete Aggregate (RCA)	Higher resilient modulus, Lower permanent deformation, cost effective material	Relatively moisture susceptible materials, lower shear strength,
Virgin aggregate Materials	Higher quality materials and shear strength, relatively non-moisture susceptible materials	Higher cost, and higher emission of greenhouse gas emissions

Chapter 3. Survey of Texas Districts

A questionnaire was developed to compile Texas district experiences using cement treatment for subgrade soils and base layers, and document ongoing and future cement treatment projects. The main objective of this chapter was to document the challenges of using calcium-based stabilizers and compile information on the rationale behind the stabilizer selection across TxDOT districts.

Survey responses were received from the following 16 districts: Tyler, Waco, Fort Worth, Austin, Abilene, Corpus Christi, Bryan, Paris, Atlanta, El Paso, Dallas, San Angelo, Houston, Pharr, San Antonio, and Lufkin, as highlighted in Figure 3-1. This chapter summarizes the districts responses to the online survey distributed among the districts. The research team will further utilize this information for the refinement of laboratory testing procedures, and site selection for non-destructive testing of representative pavement sections.

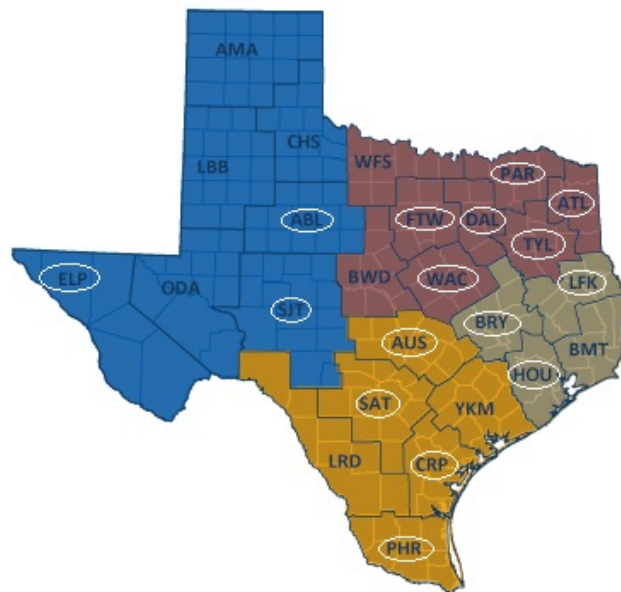


Figure 3-1: Texas Districts Responded to the Survey.

3.1 Subgrade Treatment

3.1.1 Predominant Subgrade Soil Type

Sixteen districts responded to the subgrade soil type identification question in the online survey. As shown in Figure 3-2, 94% of the districts identified the subgrade soil as clay, and the remaining 38% as sand. The respondents were allowed to select one or more options, therefore the total percentages exceeds 100%.

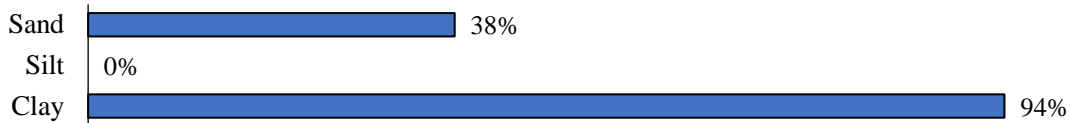


Figure 3-2: Distribution of Subgrade Types in Texas.

3.1.2 Typical Issues with the Subgrade Soils

One of the main objectives of the survey was to document the typical issues associated with the subgrade soils in each district. Presence of deleterious materials such as soil contaminants, organic and high sulfate soils, expansive soils, etc. greatly influence the success of the cement treatment projects. As evidenced in Figure 3-3, the majority of districts (88%) reported concerns pertaining to the presence of expansive soils in their projects. Additionally, 50% of districts reported concerns pertaining to the presence of sulfate or organic matter in their subgrade soils.

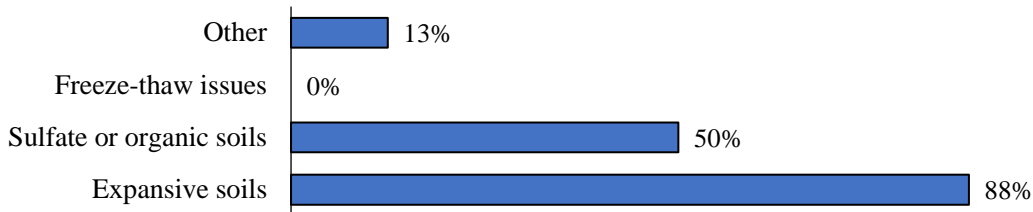


Figure 3-3: Distribution of Issues Types in the Subgrade Soils reported by Texas Districts.

3.1.3 Type of Stabilizing Agent used for Subgrade Treatment

The purpose of incorporating this question in the survey was to identify the type of the stabilizers that districts use for subgrade treatment. As expected, it is shown in Figure 3-4 that most districts use cement and lime as the predominant stabilizer types for the modification and treatment of subgrade soils. El Paso was the only district that reported the use of fly ash for subgrade treatment.

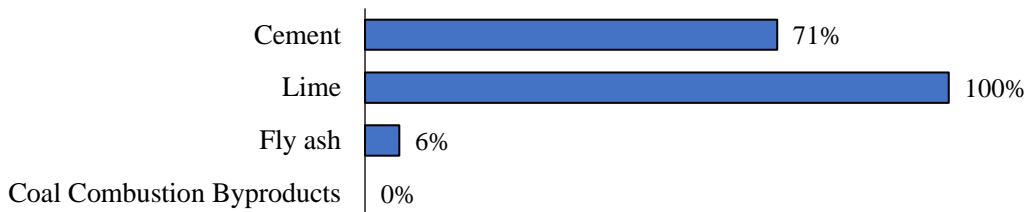


Figure 3-4: Typical Stabilizers used for Subgrade Treatment in Texas Districts.

3.1.4 Typical Laboratory Mix Design Requirements for Cement Treated Subgrade Soils

The majority of the districts identified the Tex-120-E specification (Soil-Cement Compressive Strength Testing) as the basis for the selection of the cement content for the treatment of subgrade

soils, as evidenced in Figure 3-5. Austin and San Antonio specify a strength requirement of 50 psi for the UCS, whereas Fort Worth and Waco have a requirement of 175 and 250 psi strength on UCS as criteria. In addition, 31% of districts experimentally select the stabilizer content for the treatment of the subgrade soils. For instance, Atlanta, Paris, and Fort Worth typically use 4% cement by weight as the cement content for the modification and treatment of subgrade soils. Corpus Christi reported using the highest percent of cement (8%) for subgrade treatment among the respondents. Some districts, namely San Antonio, Fort Worth, and Corpus Christi have both requirements in laboratory mix design.

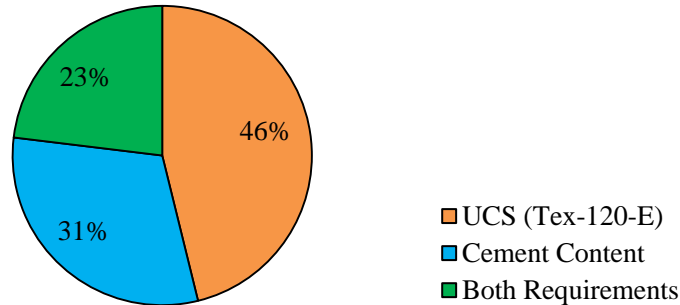


Figure 3-5: Typical Laboratory Mix Design Requirements for Subgrade Treatment.

3.1.5 Typical Field Acceptance Requirements for Cement Treated Subgrade Soils

The majority of the districts reported the density and moisture control as the field acceptance requirement for cement treated subgrade soils (Figure 3-6). 23% of districts such as Atlanta, Houston, and Corpus Christi also responded that they followed Items 275 (Road-Mixed) and 276 (Plant-Mixed) as the acceptance criteria for their projects. Strength requirement (23%), verification of cement content (15%), FWD (8%), and gradation (8%) were also reported as typical field acceptance requirements for cement treated subgrade soils.

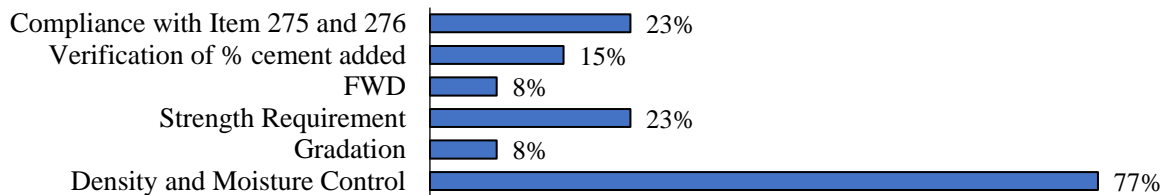


Figure 3-6: Typical Field Acceptance Requirements for Subgrade Treatment.

3.1.6 Laboratory Tests and Protocols for Subgrade Treatment

As shown in Figure 3-7, Tex-120-E (Soil-Cement Compressive Strength Testing) and Tex-121-E (Soil-Lime Compressive Strength Testing) are the predominant laboratory tests employed by the districts for the mixture design of cement treated subgrade soils. Several districts also incorporate Tex-128-E (Soil pH Test) as a requirement to identify deleterious materials in the subgrade soil. The survey responses also indicate that Tex-106-E (Plasticity Index), Tex-113-E (Moisture-

Density Relationship of Base), Tex-114-E (Moisture-Density Relationship of Subgrade), Tex-115-E (Field Density), Tex-117-E (Triaxial Compression), Tex-124-E (Potential Vertical Rise (PVR) of Subgrade), Tex-200-F (Sieve Analysis), and Tex-620-J (Determining Sulfate) are other laboratory tests for the mix design in Texas districts. It is important to point out that 21% of the districts such as Lufkin, Paris, and Dallas experimentally select the stabilizer content for subgrade treatment without laboratory tests.

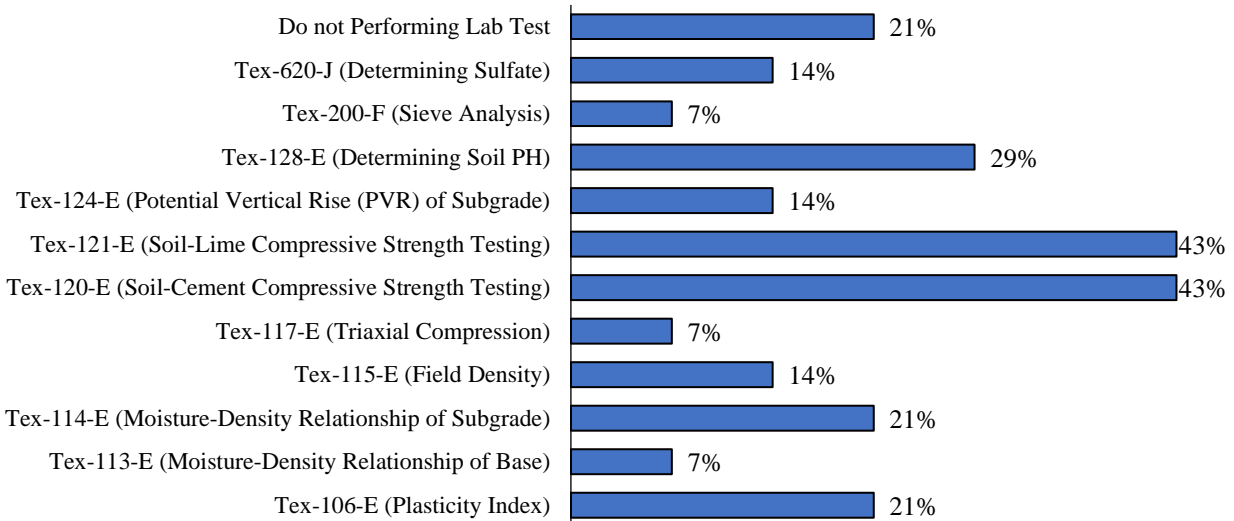


Figure 3-7: Laboratory Tests Performed for the Mix Design and Acceptance of Subgrade Treatment in Texas Districts.

3.1.7 Rationale for the Selection of the Stabilizer Content and the Type of Stabilizer for Subgrade Treatment

As it is shown in Figure 3-8, over 40% of respondents indicated that the decision for the selection of the type and percentage of stabilizing agents is primarily based on the plasticity index of the subgrade soils. For instance, Austin district responded that for subgrade soils with PI value of smaller than 25%, cement will be the choice of treatment agent, while for subgrades with PI values larger than 25%, lime must be chosen in lieu of cement for subgrade treatment. This PI threshold is 20% and 11% for San Antonio and Pharr districts, respectively.

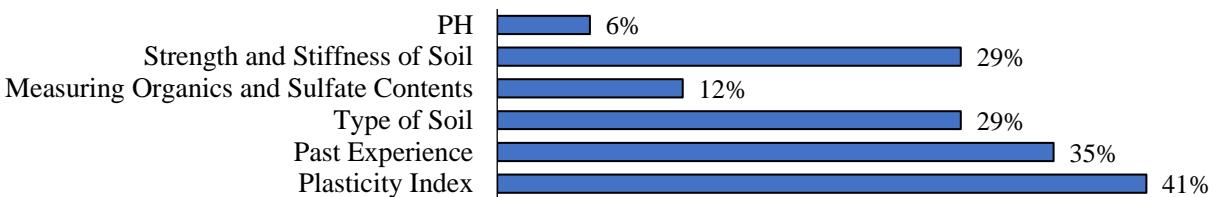


Figure 3-8: Rationale for the Selection of the Stabilizer Content for Subgrade Treatment.

In addition, 35% of districts reported that the rationale for the selection of the type and stabilizer content is based on their past experience in their districts. Other parameters and properties such as soil type, UCS, organic content, sulfate content, and soil pH were also reported as supplementary determining factors for the selection of stabilizer type and content for subgrade treatment.

3.2 Base Treatment

3.2.1 UCS Requirement for the Mixture Design of Cement Treated Base and Subbase Layers

Figure 3-9 shows the typical unconfined compressive strength requirement for the mixture design of cement treated base and subbase layers across districts. Due to distresses associated with the reflective cracking, districts tend to follow an upper bound limit for the unconfined compressive strength, to ensure the cement treated matrix is not overly rigid and prone to cracking. The UCS threshold for the base layer ranges between 150 psi to 400 psi across districts. The respondents reported lower ranges of 40 to 250 psi for the subbase layers as summarized in Figure 3-9.

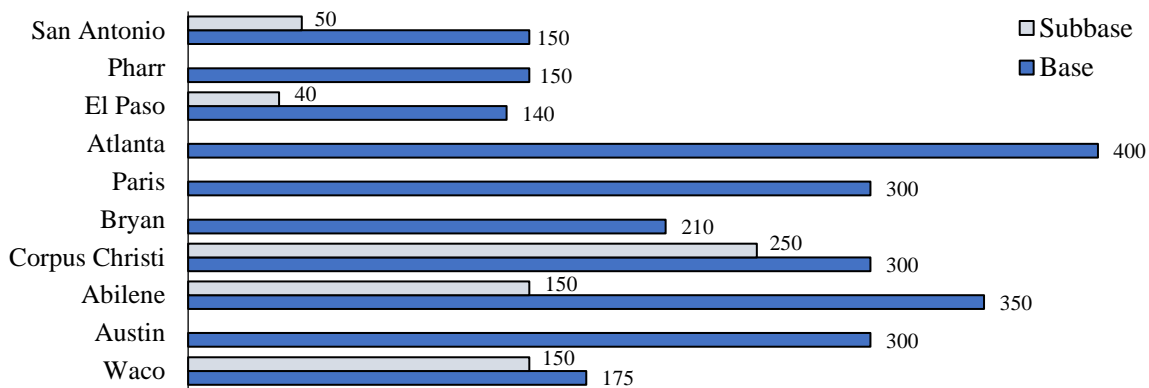


Figure 3-9: Threshold for the Unconfined Compressive Strength for the Mixture Design of Cement Treated Base and Subbase Layers.

3.3 Reclaimed Material Treatment

3.3.1 Incorporation of Reclaimed Materials in Cement Treated Layers

The majority of Texas districts reported that they use reclaimed materials in the cement treated base layers (Figure 3-10). 80% of districts responded that they used RAP (Recycled Asphalt Pavement) materials in their project, while only 33% of districts such as Austin, Atlanta, Houston, and Lufkin have used RCA (Recycled Concrete Aggregates) in the cement treated base layers. In addition, more than 70% of districts considered various blends of reclaimed and virgin materials for the construction of the cement treated base layers.

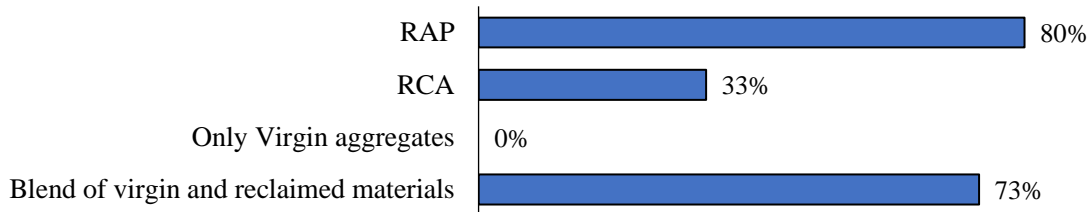


Figure 3-10: Incorporating Reclaimed Materials in Cement Treated Layers

3.3.2 Design Requirements for the Cement Treated Base Layers with Reclaimed Materials

The majority of the districts reported the unconfined compressive strength test as the primary laboratory test for the mixture design of cement treated systems with reclaimed materials. The UCS requirement reported by the districts are provided in Figure 3-11. San Antonio, Pharr, and Austin districts consider strength requirement of 150 psi for the treated reclaimed materials. However, Atlanta, Corpus Christi, and Waco allow for higher UCS strength in their laboratory mixture design (Figure 3-12). Based on the collected information, some districts experimentally selected the cement content for reclaimed mixes. Dallas and Pharr reported that they use 2% cement as a design requirement when treated reclaimed materials incorporated in their projects, while Paris, El Paso, San Angelo, and Houston consider 4% cement content for the treated RAP and RCA (Figure 3-13).

Based on the collected responses, 23% of districts use a blend of virgin and reclaimed materials in the cement treated layers. For instance, Dallas and Bryan districts use 50% or less reclaimed materials combined with virgin aggregates in their mix design. Paris district also reported that they used 4% cement for base and subbase treatment for mixtures with less than 25% reclaimed materials. However, if the mixture contains more than 25% RAP materials, they usually consider 5% cement for the treatment process.

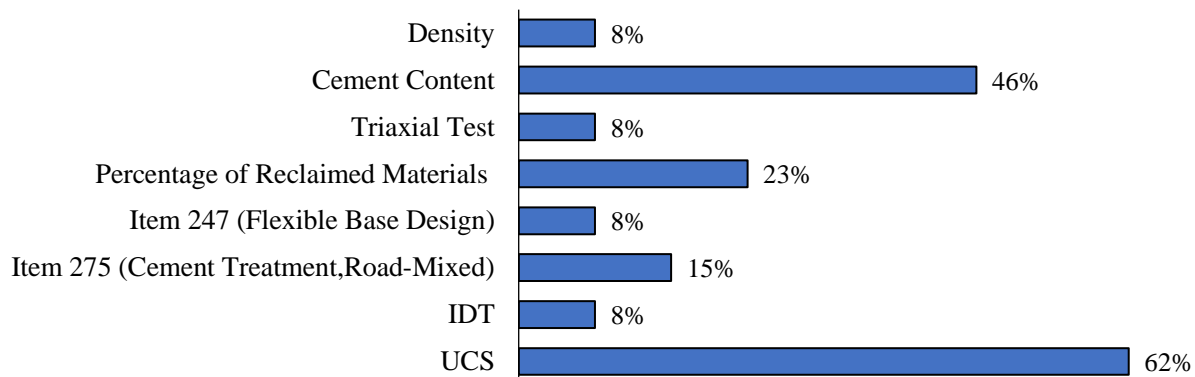


Figure 3-11: Design Requirements for the Treated Base Layers with Reclaimed Asphalt or Reclaimed Concrete Materials.

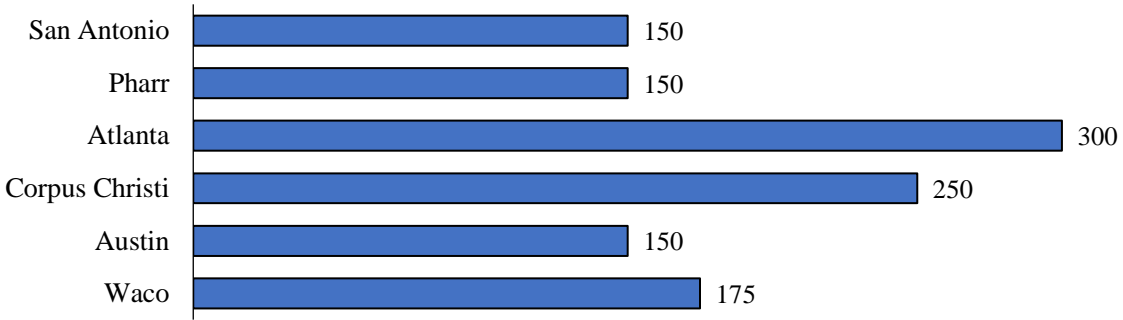


Figure 3-12: UCS (psi) Requirement for Laboratory Mixture Design with Reclaimed Asphalt or Reclaimed Concrete Materials.

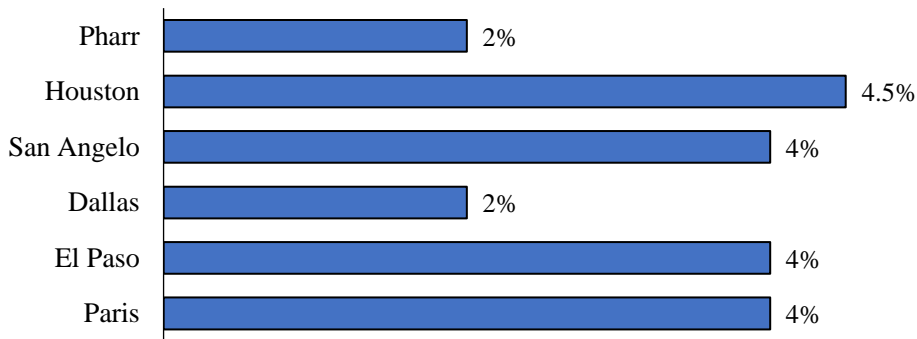


Figure 3-13: Typical Cement Content Used for Base Layers with Reclaimed Materials.

3.3.3 Acceptance Requirements for the Treated Base Layers with Reclaimed Asphalt or Reclaimed Concrete Materials

The majority of the districts reported the density, based on Tex-115-E Density Control, as the acceptance criteria for cement treated base layers (Figure 3-14). 23% of districts also responded that they followed all standard specifications including moisture, density, and strength requirements. Cement content (8%) and UCS test (15%) were also reported as typical acceptance criteria for cement treated reclaimed materials.

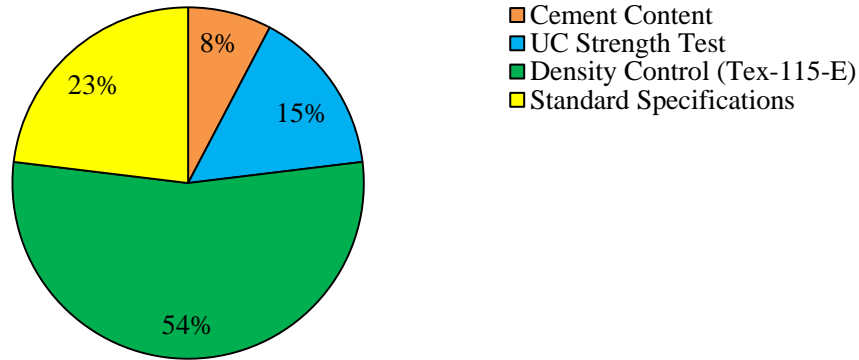


Figure 3-14: Acceptance Criteria for the Treated Base Layers with Reclaimed Asphalt or Reclaimed Concrete Materials.

3.4 General Aspects for the Base and Subgrade Treatment

3.4.1 Main Challenges for Using Calcium-Based Stabilizers

Figure 3-15 shows the reported main challenges for using calcium based stabilizers based on local experience from previous projects across Texas. 70% of the respondents namely, Dallas, Waco, Fort Worth, Austin, Paris, and El Paso identified high sulfate issues as the primary concern for the cement treatment of subgrade soils. However, Atlanta, and San Antonio districts identified issues pertaining to the uniformity of construction as well as to the mixing to correct depth as the primary concern in their cement treatment projects. Bryan, Dallas and San Antonio districts specified presence of silt and curing issues as the main challenges for using calcium based stabilizers in their projects.

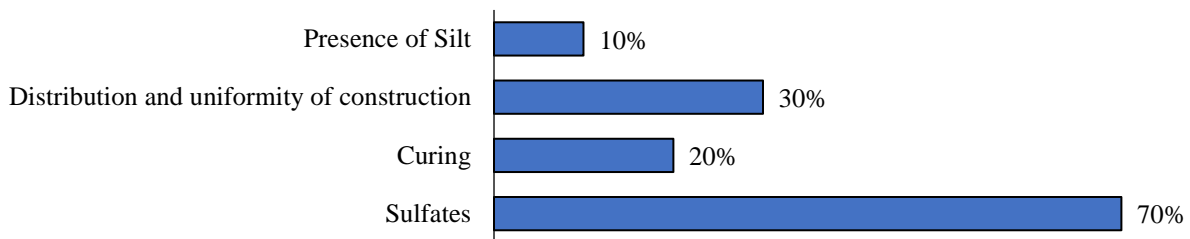


Figure 3-15: Main Challenges for using Calcium-based Stabilizers.

3.4.2 Typical Range of Cement Content Used for the Treatment of Subgrade Soils and Base Materials

Figure 3-16 demonstrates the cement content used for the treatment of base layers and subgrades. Based on the collected information from the districts, the cement content for base layer application ranges from 2-5%, while for the subgrade soils the reported range is 3-8%. The survey results showed that 3% and 5% are the most common percentage of cement used for base layer and subgrade treatment, respectively. Figure 3-17 outlines the mixture cement contents reported by the districts.

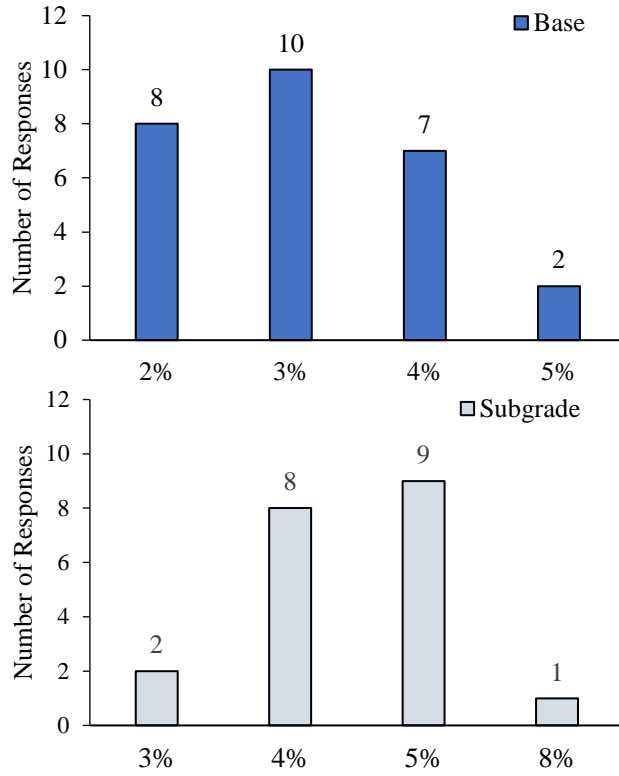


Figure 3-16: Percentage of Cement Content Typically used for Treatment of Base Layers and Subgrades.

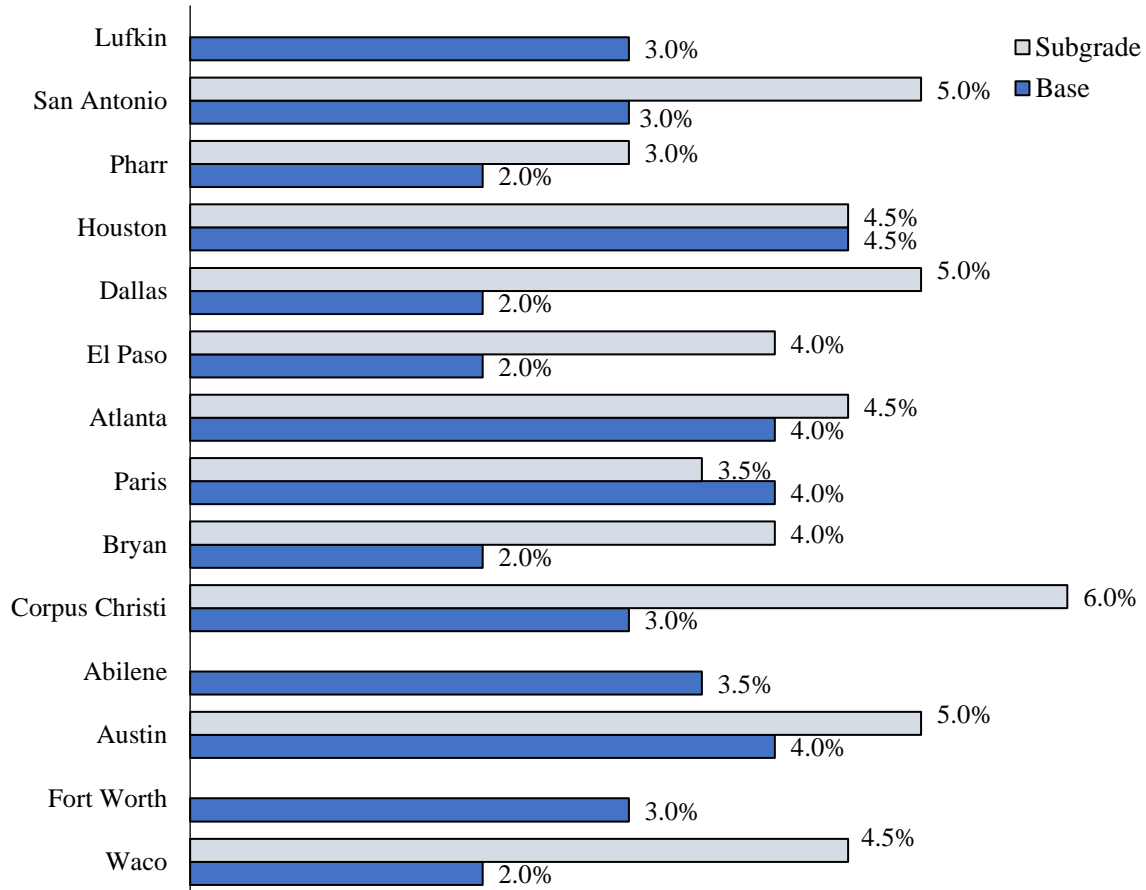


Figure 3-17: Typical Cement Content Used for the Treatment of Subgrade Soils and Base Materials in Texas.

3.4.3 Predominant Distresses Associated with Cement Treated Subgrade and Base Layers

Based on the survey results, the majority of the respondents (72%) identified reflective cracking as the predominant distress type associated with the pavement sections with cement treated layers (Figure 3-18). Two of the survey districts reported rutting issues with cement treated sections. The response provided by the San Antonio district associated the rutting with the curing of treated layers under traffic. Another plausible explanation for the rutting of the section was provided by Waco district. They attributed the permanent deformation in the wheel path to the inadequate depth of subgrade treatment. Atlanta and El Paso districts reported that their cement treated projects generally performed well in service.

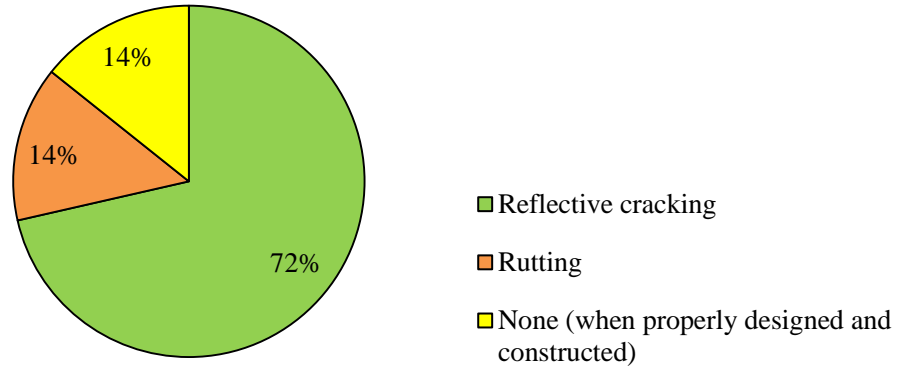


Figure 3-18: Predominant Distresses Associated with the Cement Treated Subgrade and Base Layers.

3.4.4 Using Inverted Pavement Design to Mitigate the Issues Associated with Reflective Cracking

An inverted pavement design consists of an asphalt layer, then an unbound base layer supported by stabilized base layer as previously discussed in Chapter 2. More than 70% of the respondents indicated that they have benefitted from this design concept. Tyler, Waco, Corpus Christi, Bryan, Paris, Atlanta, Dallas, and San Antonio reported that this design concept has served very well to mitigate issues associated with reflective cracking in their projects (Figure 3-19). 27% of districts, namely El Paso, Houston, and San Angelo have not tried this design concept.

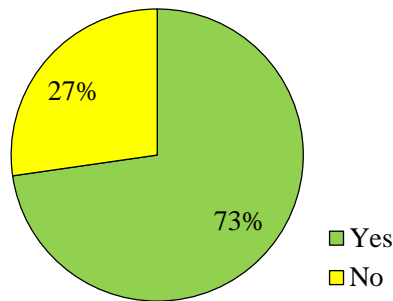


Figure 3-19: Using Inverted Pavement Design in Texas Districts.

Chapter 4. Experimental Design for Comprehensive Laboratory Tests

The main objective of this task was to develop a logical full factorial experiment design to address the objectives of this study. As previously outlined in Chapter 3, a survey was conducted to gather the existing knowledge of the materials used, and tests performed to characterize the cement treated materials in each district. This information then served as the basis for the selection of the type and sources of virgin aggregate types, gradations, subgrade soils and recycled materials for inclusion in the experiment matrix. The final lithological selection was based on the frequency of use, geographical diversification to cover the diverse climate of Texas, and aggregate type diversification based on the survey results. The gradation was also selected based on the predominant type used across the districts.

Tables 4-1 to 4-12 represent the experiment matrix developed in this research effort. Eight different aggregate base materials, namely limestone sourced from El Paso and Quintana Roo (Mexico), RCA sourced from Houston and El Paso, FDR sourced from Atlanta, and siliceous gravel aggregates sourced from Pharr, and RAP materials sourced from Atlanta and El Paso were incorporated in this research study. In addition, seven different subgrade soils, namely sandy subgrade sourced from Corpus Christi, Atlanta and El Paso, clay sourced from Sierra Blanca, Houston, Bryan, and El Paso were used in this effort. All permutations of the experiment design were prepared in three levels of cement content. Moreover, four curing conditioning procedures were incorporated to study the influence of moisture ingress on the mechanical performance of the stabilized materials. More than 3,000 specimens, considering the replicates, were prepared, and subjected to various laboratory tests as shown in the following tables. Additionally, around 500 nondestructive laboratory tests, such as free-free resonant column and dielectric value tests, were performed before the running mechanical tests. Figure 4-1 presents the flowchart for the execution of the laboratory tests in this study.

Table 4-1: Laboratory Experiment Design for Aggregate Base Materials (640 specimens).

Compaction Type	Curing Conditioning Procedure	Test Type	Dimension	Aggregate Base Materials											
				Limestone			FDR			RCA			Gravel		
				<i>El Paso</i>			<i>Atlanta</i>			<i>Houston</i>			<i>Pharr</i>		
				2%	3%	4%	2%	3%	4%	2%	3%	4%	2%	3%	4%
Impact Hammer	7 Day	UCS	6x12"	*✓	*✓	*✓	*✓	*✓	*✓	*✓	*✓	*✓	*✓	*✓	*✓
		UCS	4x6"	✓	✓	✓	✓	✓	✓	✓	✓	✓	✓	✓	✓
		UCS	4x4"	✓	✓	✓	✓	✓	✓	✓	✓	✓	✓	✓	✓
		IDT	4x4"	✓	✓	✓	✓	✓	✓	✓	✓	✓	✓	✓	✓
		Submaximal Test 25%	6x12"	*✓	*✓	*✓	*✓	*✓	*✓	*✓	*✓	*✓	*✓	*✓	*✓
		Submaximal Test 50%	6x12"	*✓	*✓	*✓	*✓	*✓	*✓	*✓	*✓	*✓	*✓	*✓	*✓
	TST	UCS	4x6"	#✓	#✓	#✓	#✓	#✓	#✓	#✓	#✓	#✓	#✓	#✓	#✓
		UCS	4x4"	#✓	#✓	#✓	#✓	#✓	#✓	#✓	#✓	#✓	#✓	#✓	#✓
		IDT	4x4"	#✓	#✓	#✓	#✓	#✓	#✓	#✓	#✓	#✓	#✓	#✓	#✓
		Submaximal Test 25%	6x12"	*#✓	*#✓	*#✓	*#✓	*#✓	*#✓	*#✓	*#✓	*#✓	*#✓	*#✓	*#✓
		Submaximal Test 50%	6x12"	*#✓	*#✓	*#✓	*#✓	*#✓	*#✓	*#✓	*#✓	*#✓	*#✓	*#✓	*#✓
	Back Pressure	UCS	4x6"	#✓	#✓	#✓	#✓	#✓	#✓	#✓	#✓	#✓	#✓	#✓	#✓
Submergence	UCS	4x6"	#✓	#✓	#✓	#✓	#✓	#✓	#✓	#✓	#✓	#✓	#✓	#✓	
TGC	7 Day	UCS	4x4"	✓	✓	✓	✓	✓	✓	✓	✓	✓	✓	✓	
		IDT	4x4"	✓	✓	✓	✓	✓	✓	✓	✓	✓	✓	✓	
	TST	UCS	4x4"	#✓	#✓	#✓	#✓	#✓	#✓	#✓	#✓	#✓	#✓	#✓	
		IDT	4x4"	#✓	#✓	#✓	#✓	#✓	#✓	#✓	#✓	#✓	#✓	#✓	
Vibratory Hammer ¹	UCS	6x12"	✓	✓	✓	✓	✓	✓	✓	✓	✓	✓	✓		
	IDT	4x4"	✓	✓	✓	✓	✓	✓	✓	✓	✓	✓	✓		
	Moisture-Density			✓		✓		✓		✓		✓			
Gyratory Comactor ²	UCS	6x12"	✓	✓	✓	✓	✓	✓	✓	✓	✓	✓	✓		
	IDT	4x4"	✓	✓	✓	✓	✓	✓	✓	✓	✓	✓	✓		
	Moisture-Density			✓		✓		✓		✓		✓			
Shrinkage Test			4x4x12	✓	✓	✓	✓	✓	✓	✓	✓	✓	✓		
	Sulfate Content Test			✓		✓		✓		✓		✓			
	AIMS			✓		✓		✓		✓		✓			
	Moisture-Density Test			✓		✓		✓		✓		✓			
	Atterberg Limits Test			✓	✓	✓	✓	✓	✓	✓	✓	✓	✓		
^{1&2} Curing Conditioning Procedure is 7-Day				* Free-Free Resonant Column (FFRC)											
				# Dielectric Value Test											

Table 4-2: Laboratory Experiment Design for Aggregate Base Materials (440 specimens).

Compaction Type	Curing Conditioning Procedure	Test Type	Dimension	Aggregate Base Materials														
				Limestone <i>Houston</i>			RAP <i>El Paso</i>			RCA <i>El Paso</i>			RAP <i>Austin</i>					
				2%	3%	4%	2%	3%	4%	2%	3%	4%	2%	3%	4%			
Impact Hammer	7 Day	UCS	6x12"	*✓	*✓	*✓	*✓	*✓	*✓	*✓	*✓	*✓	*✓	*✓	*✓	*✓	*✓	
		UCS	4x6"	✓	✓	✓	✓	✓	✓	✓	✓	✓	✓	✓	✓	✓	✓	
		IDT	4x4"	✓	✓	✓	✓	✓	✓	✓	✓	✓	✓	✓	✓	✓	✓	
		Submaximal Test 25%	6x12"	*✓	*✓	*✓	*✓	*✓	*✓	*✓	*✓	*✓	*✓	*✓	*✓	*✓	*✓	*✓
		Submaximal Test 50%	6x12"	*✓	*✓	*✓	*✓	*✓	*✓	*✓	*✓	*✓	*✓	*✓	*✓	*✓	*✓	*✓
	TST	UCS	6x12"	#✓	#✓	#✓	#✓	#✓	#✓	#✓	#✓	#✓	#✓	#✓	#✓	#✓	#✓	#✓
		UCS	4x6"	#✓	#✓	#✓	#✓	#✓	#✓	#✓	#✓	#✓	#✓	#✓	#✓	#✓	#✓	#✓
		IDT	4x4"	#✓	#✓	#✓	#✓	#✓	#✓	#✓	#✓	#✓	#✓	#✓	#✓	#✓	#✓	#✓
		Submaximal Test 25%	6x12"	*#✓	*#✓	*#✓	*#✓	*#✓	*#✓	*#✓	*#✓	*#✓	*#✓	*#✓	*#✓	*#✓	*#✓	*#✓
		Submaximal Test 50%	6x12"	*#✓	*#✓	*#✓	*#✓	*#✓	*#✓	*#✓	*#✓	*#✓	*#✓	*#✓	*#✓	*#✓	*#✓	*#✓
		Moisture-Density Test		✓			✓			✓			✓					
Vibratory Hammer ¹	UCS	6x12"	✓	✓	✓	✓	✓	✓	✓	✓	✓	✓	✓	✓	✓	✓	✓	
	IDT	4x4"	✓	✓	✓	✓	✓	✓	✓	✓	✓	✓	✓	✓	✓	✓	✓	
			Moisture-Density		✓			✓			✓			✓				
Gyratory Comactor ²	UCS	6x12"	✓	✓	✓	✓	✓	✓	✓	✓	✓	✓	✓	✓	✓	✓	✓	
	IDT	4x4"	✓	✓	✓	✓	✓	✓	✓	✓	✓	✓	✓	✓	✓	✓	✓	
			Moisture-Density		✓			✓			✓			✓				
		AIMS		✓			✓			✓			✓					
		Atterberg Limits Test		✓	✓	✓	✓	✓	✓	✓	✓	✓	✓	✓	✓	✓	✓	
^{1&2} Curing Conditioning Procedure is 7-Day				* Free-Free Resonant Column (FFRC)														
				# Dilectric Value Test														

Table 4-3: Laboratory Experiment Design for Subgrade Soils (421 specimens)

Compaction Type	Curing Conditioning Procedure	Test Type	Dimension	Subgrade Soils																	
				Sand <i>Corpus Christi</i>					Sand <i>El Paso</i>					Clay <i>El Paso</i>							
				3%	5%	7%	10%	12%	3%	5%	7%	8%	10%	12%	3%	5%	7%	8%	10%	12%	
Impact Hammer	7 Day	UCS	4x8"	✓	✓	✓	✓	✓	✓	✓	✓	✓	✓	✓	✓	✓	✓	✓	✓	✓	
		UCS	4x6"	✓	✓	✓	✓	✓	✓	✓	✓	✓	✓	✓	✓	✓	✓	✓	✓	✓	✓
		Submaximal Test 25%	4x8"	✓	✓	✓	✓	✓	✓	✓	✓	✓	✓	✓	✓	✓	✓	✓	✓	✓	✓
		Submaximal Test 50%	4x8"	✓	✓	✓	✓	✓	✓	✓	✓	✓	✓	✓	✓	✓	✓	✓	✓	✓	✓
	TST	UCS	4x8"	✓	✓	✓	✓	✓	✓	✓	✓	✓	✓	✓	✓	✓	✓	✓	✓	✓	✓
		UCS	4x6"	✓	✓	✓	✓	✓	✓	✓	✓	✓	✓	✓	✓	✓	✓	✓	✓	✓	✓
		Submaximal Test 25%	4x8"	✓	✓	✓	✓	✓	✓	✓	✓	✓	✓	✓	✓	✓	✓	✓	✓	✓	✓
		Submaximal Test 50%	4x8"	✓	✓	✓	✓	✓	✓	✓	✓	✓	✓	✓	✓	✓	✓	✓	✓	✓	✓
	Back Pressure Submergence	UCS	4x6"	✓	✓	✓	✓	✓	✓	✓	✓	✓	✓	✓	✓	✓	✓	✓	✓	✓	✓
		UCS	4x6"	✓	✓	✓	✓	✓	✓	✓	✓	✓	✓	✓	✓	✓	✓	✓	✓	✓	✓
Vibratory Hammer ¹	UCS	4x6"	✓	✓	✓	✓	✓														
			Moisture-Density	4x4"	✓																
Gyratory Comactor ²	UCS	4x6"	✓	✓	✓	✓	✓														
			Moisture-Density	4x4"	✓																
		Sulfate Content Test		✓					✓					✓							
		Moisture-Density Test		✓					✓					✓							
		Atterberg Limits Test		✓	✓	✓	✓	✓	✓						✓						
		Swell Test		✓	✓	✓	✓	✓													
		Methylene Blue Value		✓	✓	✓	✓	✓													

Table 4-4: Laboratory Experiment Design for High Sulfate Clay Soils sourced from Bryan (280 specimens).

Compaction Type	Curing Conditioning Procedure	Test Type	Specimen Size	Subgrade Soils																							
				High Sulfate Clay																							
				Bryan																							
				Cement			Lime			Fly Ash			Fly Ash with Cement			Lime with Cement			Polypropylene with cement								
				5% Cement			5% Cement			5% Cement			5% Cement			0.2% pp		0.4% pp									
3%	5%	7%	3%	5%	7%	3%	5%	7%	3%	5%	7%	3%	5%	7%	3%	5%	7%	3%	5%	7%	3%	5%	7%				
Impact Hammer	7-Day	UCS	4x6"	✓	✓	✓	✓	✓	✓	✓	✓	✓	✓	✓	✓	✓	✓	✓	✓	✓	✓	✓	✓	✓			
	14-Day	UCS	4x6"	✓	✓	✓	✓	✓	✓	✓	✓	✓	✓	✓	✓	✓	✓	✓	✓	✓	✓	✓	✓	✓			
	28-Day	UCS	4x6"	✓	✓	✓	✓	✓	✓	✓	✓	✓	✓	✓	✓	✓	✓	✓	✓	✓	✓	✓	✓	✓			
	-	Moisture-Density Test		✓																							
Gyratory Compactor	7-Day	UCS	4x6"	✓	✓	✓	✓	✓	✓	✓	✓	✓	✓	✓	✓	✓	✓	✓	✓	✓	✓	✓	✓	✓			
	-	Moisture-Density Test		✓																							
		Sulfate Content Test		✓																							
		Atterberg Limits Test		✓	✓	✓	✓	✓	✓	✓	✓	✓	✓	✓	✓	✓	✓	✓	✓	✓	✓	✓	✓	✓			
		One Dimensional Swell		✓	✓	✓	✓	✓	✓	✓	✓	✓	✓	✓	✓	✓	✓	✓	✓	✓	✓	✓	✓	✓			
		Swell Pressure Test		✓	✓	✓	✓	✓	✓	✓	✓	✓	✓	✓	✓	✓	✓	✓	✓	✓	✓	✓	✓	✓			
		Methylene Blue Value		✓	✓	✓	✓	✓	✓	✓	✓	✓	✓	✓	✓	✓	✓	✓	✓	✓	✓	✓	✓	✓			

Table 4-5: Laboratory Experiment Design for High Plasticity Clay Soils Sourced from Sierra Blanca (280 specimens).

Compaction Type	Curing Conditioning Procedure	Test Type	Specimen Size	Subgrade Soils																							
				High Plasticity Clay																							
				Sierra Blanca																							
				Cement			Lime			Fly Ash			Fly Ash with Cement			Lime with Cement			Polypropylene with cement								
				5% Cement			5% Cement			5% Cement			5% Cement			0.2% pp		0.4% pp									
3%	5%	7%	3%	5%	7%	3%	5%	7%	3%	5%	7%	3%	5%	7%	3%	5%	7%	3%	5%	7%	3%	5%	7%				
Impact Hammer	7-Day	UCS	4x6"	✓	✓	✓	✓	✓	✓	✓	✓	✓	✓	✓	✓	✓	✓	✓	✓	✓	✓	✓	✓	✓			
	14-Day	UCS	4x6"	✓	✓	✓	✓	✓	✓	✓	✓	✓	✓	✓	✓	✓	✓	✓	✓	✓	✓	✓	✓	✓			
	28-Day	UCS	4x6"	✓	✓	✓	✓	✓	✓	✓	✓	✓	✓	✓	✓	✓	✓	✓	✓	✓	✓	✓	✓	✓			
	-	Moisture-Density Test		✓																							
Gyratory Compactor	7-Day	UCS	4x6"	✓	✓	✓	✓	✓	✓	✓	✓	✓	✓	✓	✓	✓	✓	✓	✓	✓	✓	✓	✓	✓			
	-	Moisture-Density Test		✓																							
		Sulfate Content Test		✓																							
		Atterberg Limits Test		✓	✓	✓	✓	✓	✓	✓	✓	✓	✓	✓	✓	✓	✓	✓	✓	✓	✓	✓	✓	✓			
		One Dimensional Swell		✓	✓	✓	✓	✓	✓	✓	✓	✓	✓	✓	✓	✓	✓	✓	✓	✓	✓	✓	✓	✓			
		Swell Pressure Test		✓	✓	✓	✓	✓	✓	✓	✓	✓	✓	✓	✓	✓	✓	✓	✓	✓	✓	✓	✓	✓			
		Methylene Blue Value		✓	✓	✓	✓	✓	✓	✓	✓	✓	✓	✓	✓	✓	✓	✓	✓	✓	✓	✓	✓	✓			

Table 4-6: Laboratory Experiment Design for Initial Assessment of Moisture Susceptibility Tests (144 specimens).

Compaction Type	Curing Conditioning Procedures	Dimension	Aggregate Base Materials							Subgrade	
			Limestone		RAP	RCA	RAP&LS	RCA&LS	Sand	Clay	
			<i>El Paso</i>							<i>El Paso</i>	
			Cement Content							Cement Content	
2%	3%	4%	3%	3%	3%	3%	5%	5%			
Impact Hammer	7-Day Moist Cured	4x6"	✓	✓	✓	✓	✓	✓	✓	✓	✓
	TST	4x6"	✓	✓	✓	✓	✓	✓	✓	✓	✓
	Cured in the Oven	4x6"	✓	✓	✓	✓	✓	✓	✓	✓	✓
	Submergecne Hot Water	4x6"	✓	✓	✓	✓	✓	✓	✓	✓	✓
	Submergence	4x6"	✓	✓	✓	✓	✓	✓	✓	✓	✓
	1-Day Back Presssre	4x6"	✓	✓	✓	✓	✓	✓	✓	✓	✓
	2-Day Back Presssre	4x6"	✓	✓	✓	✓	✓	✓	✓	✓	✓
	3-Day Back Pressure	4x6"	✓	✓	✓	✓	✓	✓	✓	✓	✓

Table 4-7: Laboratory Experiment Design for the Evaluation of Different Mixing Procedures (136 specimens).

Compaction Type	Curing Conditioning Procedure	Mixing	Test Type	Dimension	Aggregate Base Materials										Subgrade Soils					
					Limestone		FDR		RCA		Marginal		RAP		Limestone	Sand	Sand	Clay	Clay	Clay
					<i>El Paso</i>		<i>Atlanta</i>		<i>Houston</i>		<i>Pharr</i>		<i>Atlanta</i>		<i>Houston</i>	<i>Corpus</i>	<i>El Paso</i>	<i>Sierra Blanca</i>	<i>Brayan</i>	<i>El Paso</i>
					Cement Content															
2%	3%	2%	3%	2%	3%	2%	3%	2%	3%	2%	3%	2%	3%	5%	5%	5%	5%	5%		
Impact Hammer	7-Day	Slurry	UCS	4x6"	✓	✓	✓	✓	✓	✓	✓	✓	✓	✓	✓	✓	✓	✓	✓	
			IDT	4x4"	✓	✓	✓	✓	✓	✓	✓	✓	✓	✓	✓	✓	✓	✓	✓	✓
		Powder	UCS	4x6"	✓	✓	✓	✓	✓	✓	✓	✓	✓	✓	✓	✓	✓	✓	✓	✓
			IDT	4x4"	✓	✓	✓	✓	✓	✓	✓	✓	✓	✓	✓	✓	✓	✓	✓	✓

Table 4-8: Laboratory Experiment Design for Evaluation of Blend Ratio in Stabilized Reclaimed Materials (320 specimens).

Compaction Type	Curing Conditioning Procedure	Test	Ratio of Recycled Materials	RCA Houston				RCA El Paso				RAP Atlanta				RAP El Paso			
				Cement Content				Cement Content				Cement Content				Cement Content			
				2%	3%	4%	5%	2%	3%	4%	5%	2%	3%	4%	5%	2%	3%	4%	5%
				2%	3%	4%	5%	2%	3%	4%	5%	2%	3%	4%	5%	2%	3%	4%	5%
Impact Hammer	7-Day	UCS	0%	✓	✓	✓	✓	✓	✓	✓	✓	✓	✓	✓	✓	✓	✓	✓	
			25%	✓	✓	✓	✓	✓	✓	✓	✓	✓	✓	✓	✓	✓	✓	✓	
			50%	✓	✓	✓	✓	✓	✓	✓	✓	✓	✓	✓	✓	✓	✓	✓	
			75%	✓	✓	✓	✓	✓	✓	✓	✓	✓	✓	✓	✓	✓	✓	✓	
			100%	✓	✓	✓	✓	✓	✓	✓	✓	✓	✓	✓	✓	✓	✓	✓	
		IDT	0%	✓	✓	✓	✓	✓	✓	✓	✓	✓	✓	✓	✓	✓	✓	✓	
			25%	✓	✓	✓	✓	✓	✓	✓	✓	✓	✓	✓	✓	✓	✓	✓	
			50%	✓	✓	✓	✓	✓	✓	✓	✓	✓	✓	✓	✓	✓	✓	✓	
			75%	✓	✓	✓	✓	✓	✓	✓	✓	✓	✓	✓	✓	✓	✓	✓	
			100%	✓	✓	✓	✓	✓	✓	✓	✓	✓	✓	✓	✓	✓	✓	✓	

Table 4-9: Laboratory Experiment Design for Investigating the Effect of High Fines Content (160 specimens).

Compaction Type	Test	Curing Conditioning	Fines Content	RAP	RAP	RAP	Limestone	Limestone
				<i>El Paso</i>	<i>Atlanta</i>	<i>Austin</i>	<i>El Paso</i>	<i>Houston</i>
				<i>Cement Content</i>				
3%					3%	3%	3%	3%
Impact Hammer	UCS	7-Day	0%	✓	✓	✓	✓	✓
			5%	✓	✓	✓	✓	✓
			10%	✓	✓	✓	✓	✓
			15%	✓	✓	✓	✓	✓
	IDT		0%	✓	✓	✓	✓	✓
			5%	✓	✓	✓	✓	✓
			10%	✓	✓	✓	✓	✓
			15%	✓	✓	✓	✓	✓
	UCS	10-Day Capillary Soak	0%	✓	✓	✓	✓	✓
			5%	✓	✓	✓	✓	✓
			10%	✓	✓	✓	✓	✓
			15%	✓	✓	✓	✓	✓
	IDT		0%	✓	✓	✓	✓	✓
			5%	✓	✓	✓	✓	✓
			10%	✓	✓	✓	✓	✓
			15%	✓	✓	✓	✓	✓

Table 4-10: Laboratory Experiment Design for Influence of Subgrade Fraction on Performance of FDR Materials (96 specimens).

Compaction Type	Curing Conditioning	Subgrade Percentage	FDR			
			<i>Atlanta</i>			
			UCS		IDT	
			<i>Cement Content</i>		<i>Cement Content</i>	
2%		4%				
Impact Hammer	7-Day Curing	0%	✓	✓	✓	✓
		10%	✓	✓	✓	✓
		20%	✓	✓	✓	✓
		30%	✓	✓	✓	✓
		40%	✓	✓	✓	✓
		50%	✓	✓	✓	✓
	10-Day Capillary Soak	0%	✓	✓	✓	✓
		10%	✓	✓	✓	✓
		20%	✓	✓	✓	✓
		30%	✓	✓	✓	✓
		40%	✓	✓	✓	✓
		50%	✓	✓	✓	✓

Table 4-11: Laboratory Experiment Design for High Plasticity Clay Soils Sourced from Houston (55 specimens).

Test Type	Subgrade Soils											
	High Plasticity Clay											
	Houston											
	Cement			Lime			Fly Ash			Fly Ash with Cement		
	5% Cement									7%		
	3%	5%	7%	3%	5%	7%	3%	5%	7%	3%	5%	7%
Moisture-Density Test	✓											
Sulfate Content Test	✓											
Atterberg Limits Test	✓	✓	✓	✓	✓	✓	✓	✓	✓	✓	✓	✓
One Dimensional Swell	✓	✓	✓	✓	✓	✓	✓	✓	✓	✓	✓	✓
Swell Pressure Test	✓	✓	✓	✓	✓	✓	✓	✓	✓	✓	✓	✓
Methylene Blue Value	✓	✓	✓	✓	✓	✓	✓	✓	✓	✓	✓	✓

Table 4-12: Laboratory Experiment Design for Poor Sandy Materials Sourced from Corpus Christi (80 specimens).

Compaction	Test	Curing Conditioning	Problematic Sand					
			Corpus Christi					
			Fly Ash	Cement				
3%	5%	7%		10%	12%			
Impact Hammer	UCS	7-Day	0%	✓	✓	✓	✓	✓
		28-Day	0%	✓	✓	✓	✓	✓
			3%	✓	✓	✓	✓	✓
			5%	✓	✓	✓	✓	✓
			7%	✓	✓	✓	✓	✓
		7-Day	Poly Propylene	Cement				
			3%	5%	7%	10%	12%	
			0%	✓	✓	✓	✓	✓
			0.4%	✓	✓	✓	✓	✓
				0.8%	✓	✓	✓	✓

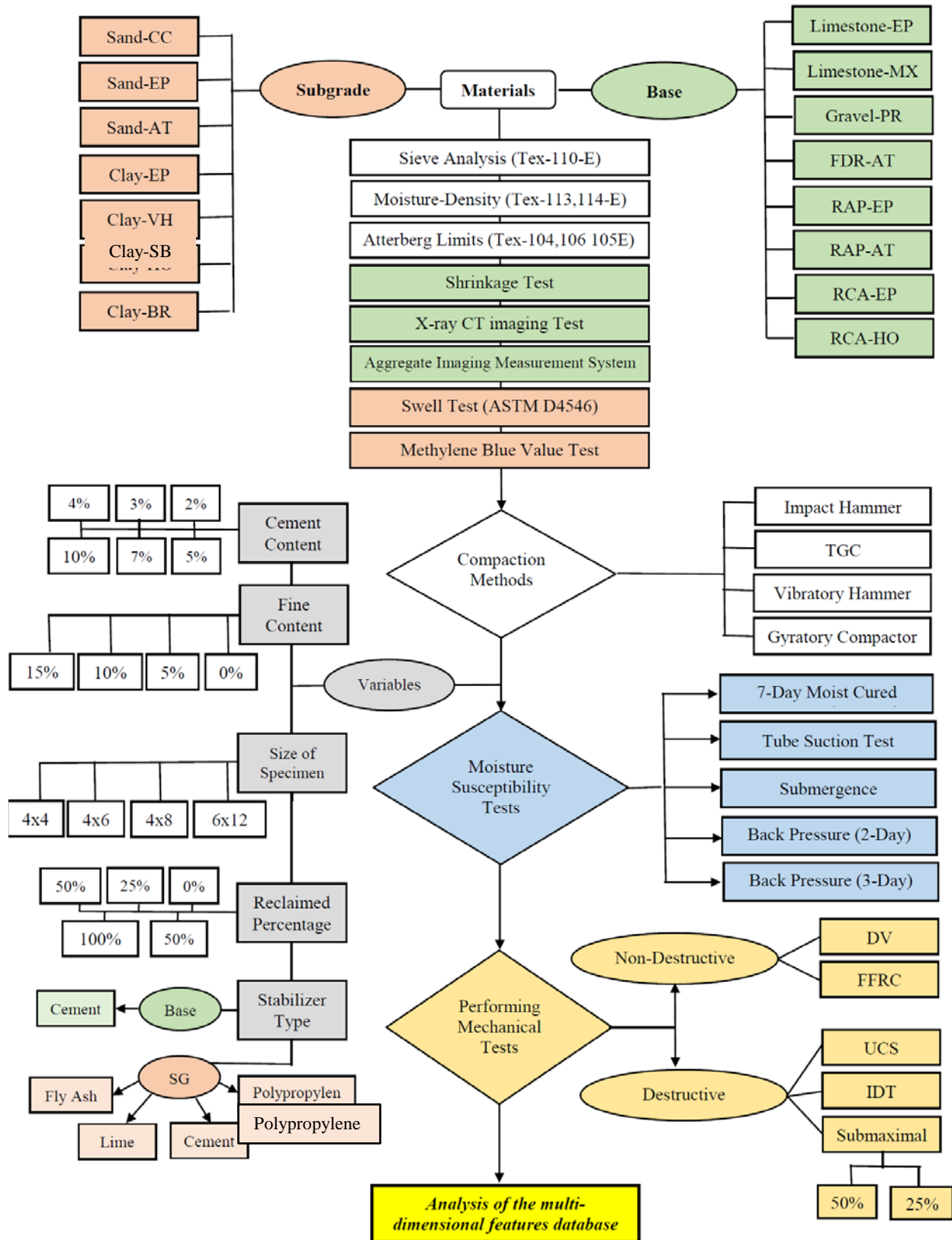


Figure 4-1: Flow Chart for the Execution of the Laboratory Tests.

The geographical distribution of the districts was also considered as a supplementary decision parameter for the selection of the aggregate types/sources. This criterion was considered to account for the diversity of the lithological properties and environmental conditions across the state of Texas. As indicated in Figure 4-2, materials from Paris and Atlanta districts in north side, Houston and Bryan districts in central/east side, Corpus Christi and Pharr districts in south side, and El Paso and Sierra Blanca in west side of Texas were incorporated in the experiment design. In addition, limestone aggregate sourced from Quintana Roo in western Mexico which has been widely using in Houston for the construction of the pavement foundation were added to the list of materials.



Figure 4-2: Geographical Distribution of Selected Material Source.

In Tables 4-1 to 4-12, a comprehensive experiment design was outlined in order to identify the mechanical behavior of cement treated materials in tension, compression, permanent deformation potential, and the role of moisture to compromise the performance of the treated mixes. The features database will contain the following laboratory testing program to characterize the mechanical performance of the cement treated soils and base materials:

4.1 Strength and Stiffness Properties

The strength and stiffness are the primary input parameters for the design of pavements with cement treated layers. In this study, the Unconfined Compressive Strength (UCS) test, Indirect Diametrical Tensile (IDT) strength test, and submaximal modulus tests, and Free-Free Resonant Column (FFRC) tests are incorporated in the laboratory mixture design protocols to characterize the strength, resilient properties, and permanent deformation potential of cement treated systems.

4.1.1 Unconfined Compressive Strength (UCS) Test

The UCS test was performed on all permutations of the experiment design to determine the compressive strength of the stabilized materials at different cement contents. UCS is a strain-controlled test at an imposed strain rate of 2% strain/min. This test involves a cylindrical sample being loaded in a direction that is parallel to its long axis until failure as shown in Figure 4-3. The results were used to identify the unconfined compressive strength, nature of stress-strain curves, variation of the degree of nonlinearity of stabilized materials with increase of cement, and ultimately different measures of modulus such as tangent modulus and secant modulus at peak strength. This information was incorporated in the aggregate database for further post processing and trend analysis of the data.

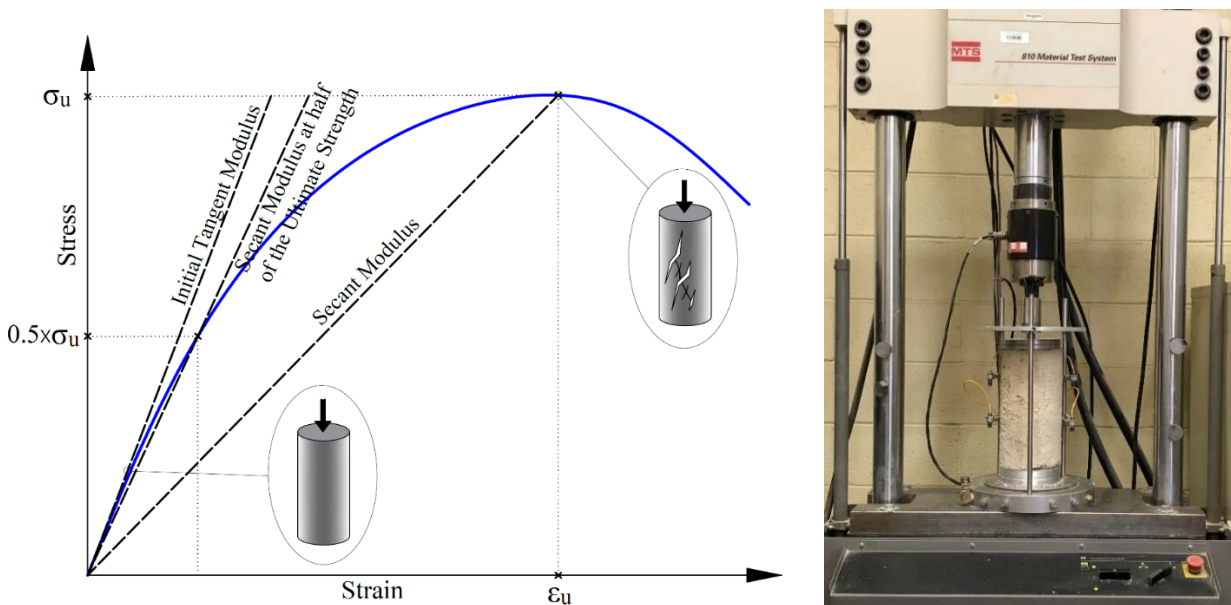


Figure 4-3: Unconfined Compressive Strength Test Setup and Different Measures of Modulus in the UCS Stress-Strain Curve.

4.1.2 Indirect Diametrical Tensile (IDT) Test

The IDT test is a common method to characterize the tensile strength properties of cement stabilized materials in the laboratory. In the IDT test, 4-inch diameter by 4-inch thick cement treated specimen is subjected to a strain-controlled loading scheme until mid-span fracture is

induced along the vertical diameter of the specimen as shown in Figure 4-4. The load is applied monotonically at a constant rate of 1 mm/min to induce in a relatively uniform transverse tensile stress along the vertical diameter. The load is distributed by two bearing strips to prevent multiple cracks and crushing at the point of loading. This test provides an indication of the tensile strength of the specimen subjected to strain-controlled stress path tests in the laboratory. The IDT is computed in this test from Equation 4-1 as:

$$IDT = \frac{2 \times P}{\pi \times h \times d} \quad \text{Equation 4-1}$$

Where P is the peak load, h is the height of the specimen, and d is the diameter of the specimen.

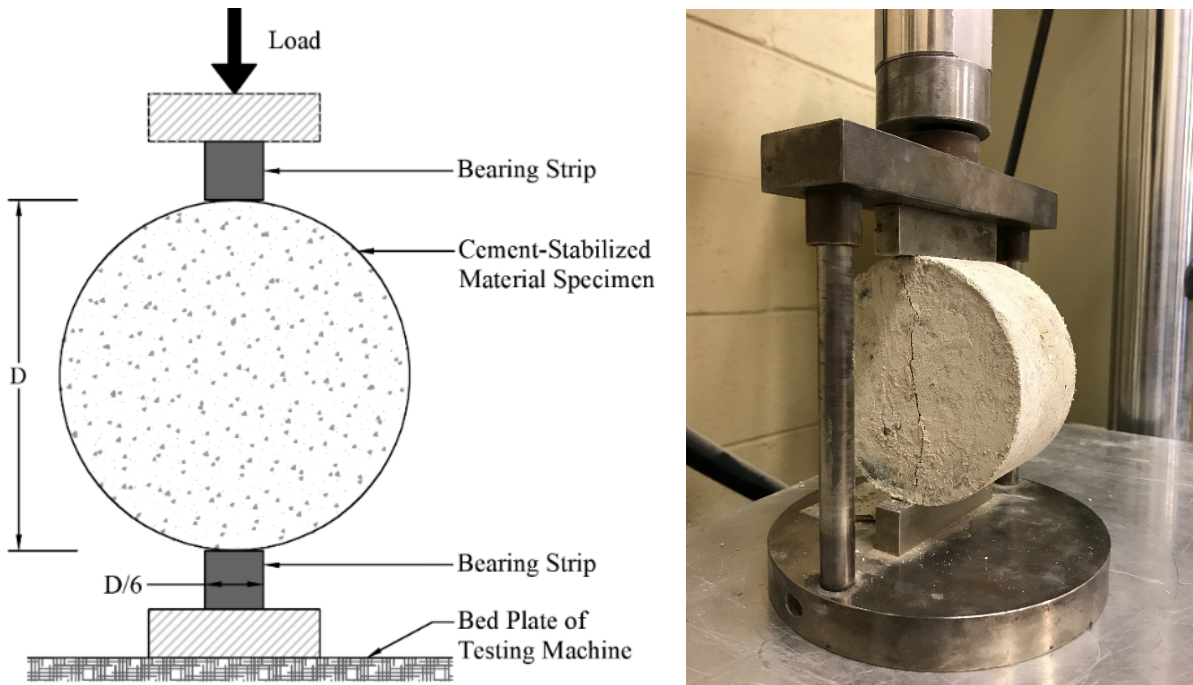


Figure 4-4: Schematic Representation of Test Setup and Fractured Specimen in the IDT Test.

4.1.3 Submaximal Modulus Test

The submaximal modulus test was used for the characterization of the resilient behavior of the stabilized subgrade and base materials subjected to traffic loading. This test provides the permanent deformation properties and energy dissipation mechanism due to repeated traffic loads in stabilized pavement foundations. The strength values obtained from the UCS test were the basis for the selection of the stress amplitudes applied to the specimens. Pre-determined fractions of the UCS-value at two levels of 25% and 50% were applied for 5,000 load cycles under axial compressive loads to a 6-inch diameter by 12-inch height specimen. Subsequently, the vertical deformations were recorded using four internal proximeters attached to the specimens and external LVDTs as shown in Figure 4-5.

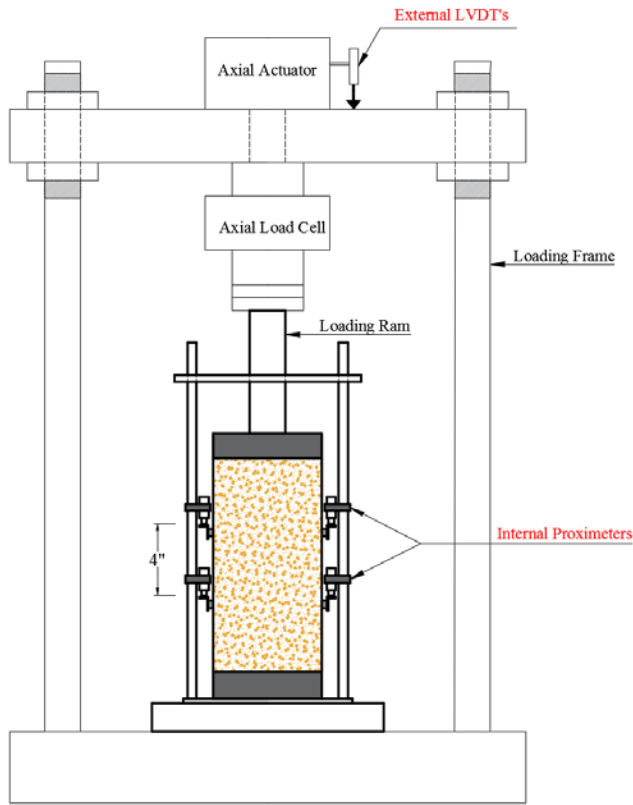


Figure 4-5: Submaximal Modulus Test Setup.

4.1.4 Dynamic IDT Test

The dynamic IDT test was performed in this study to evaluate the performance of cement stabilized materials subjected to repeated load in tension. Similar to the concept presented in the submaximal modulus test, the static IDT test results were used as a benchmark to determine the loading protocol in the dynamic IDT test. For conducting this test, initially the IDT strength of each permutation of the experiment design was determined using the static IDT test. Subsequently a percentage of the static IDT strength was applied for a certain number of load cycles where tensile failure occurred in the specimen as shown in Figure 4-6. The selected levels of the cyclic loads were 25% and 50% of the static IDT strength in this study. Figure 4-6 shows the test setup, brackets arrangements, and the locations of the LVDTs for the accurate evaluation of cyclic behavior of cement stabilized materials.



Figure 4-6: Dynamic IDT Test Fixture and Specimen.

4.1.5 Free-Free Resonant Column Test

The Free-Free Resonant Column (FFRC) tests were performed on specimens prepared for submaximal modulus tests. FFRC is a laboratory test for determining the seismic modulus of pavement materials (see Figure 4-7). The periodic measurement of the seismic modulus values during a 10-day period can provide valuable information on the rate and the magnitude of strength gain due to hydration reactions as a function of time and available moisture.

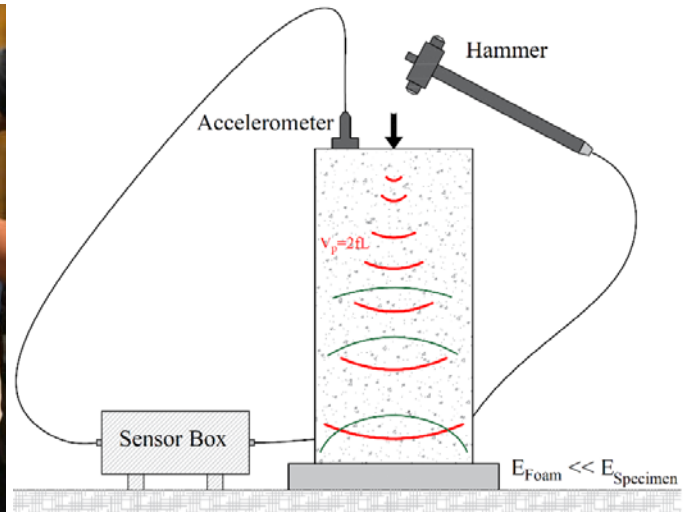


Figure 4-7: FFRC Test Setup.

4.2 Moisture Susceptibility

Several moisture susceptibility tests such as tube suction test, backpressure saturation test at different durations, and multiple submergence protocols were incorporated in this study to evaluate

the influence of moisture ingress on the mechanical properties of the stabilized materials. The main motivation for the inclusion of these approaches in the experiment was to study the relationship between the moisture intrusion mechanism and the loss of adhesive bonds in cement stabilized systems. The assumption is that unreacted moisture trapped in the pore structure can potentially degrade the stiffness properties of the stabilized layers and consequently jeopardize the longevity of the pavement structure. After the completion of the moisture susceptibility procedures, the specimen was subjected to the compressive strength tests. The variations in the strength properties of the mixes were further studied to quantify the deleterious effect of moisture on the resilient and strength properties of the cement treated base and subgrade materials.

4.2.1 Tube Suction Test

The Tube Suction Test (TST) has been used extensively to characterize the affinity of unbound and stabilized aggregate systems to hold and transport moisture. In the process of TST, the stabilized specimens were molded at optimum moisture content and then placed in the oven, with porous stones at the top and at the bottom. After 2 days of drying at 104°F (40°C), the specimens were removed from the oven, cooled at room temperature, and capped with porous stones. Subsequently, the specimens were subjected to capillary soak for ten days prior to mechanical tests. The TST results were used as the benchmark for comparative analysis and further post processing of various durability protocols.

The dielectric values of the TST specimen were measured every day for 10 consecutive days at five different points at the top of the specimen, as shown in Figure 4-8. The average values of the five measurements were calculated and reported as the representative dielectric value for each variant of the experiment design.

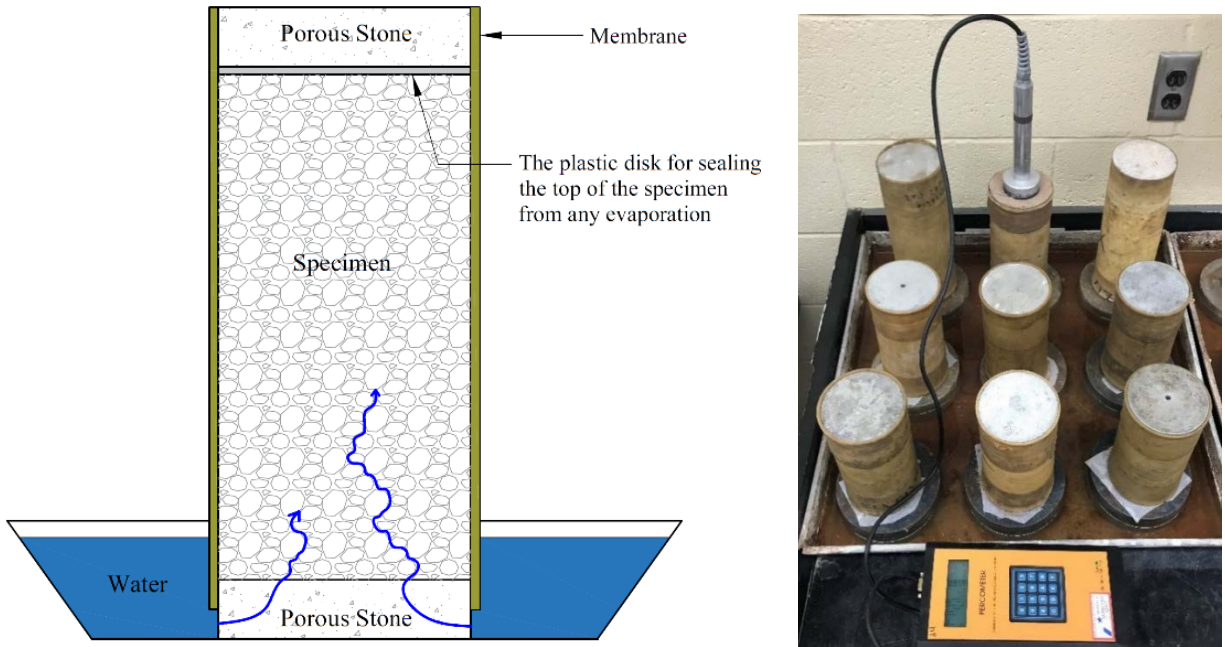


Figure 4-8: 10-Days Capillary Soak Procedure.

4.2.2 Backpressure Saturation Test

The backpressure saturation test was incorporated in the experiment design to simulate the full saturation conditions, such as inundation of pavement structures during natural disasters. In this procedure, water is forced through the specimen by the application of an all-around confining pressure in a triaxial setup as shown in Figure 4-9. Immediately after compaction, the 4-inch diameter by 6-inch tall stabilized specimens were placed in the 140 °F (60 °C) oven to expedite the strength-gain reactions. After 24 hours of oven drying, the specimens were capped with porous stones and placed in a rubber membrane sleeve for subsequent installation in the backpressure test equipment.

Evidently, the full saturation of the stabilized soils is a function of the internal microstructure, interconnected void structure, and the magnitude of the confining pressure applied to the perimeter of the specimen in the backpressure test. The confinement in the backpressure test was selected as such that it will not disrupt the internal structure of the cement treated specimen. Additionally, excessive confinement can potentially cause unwarranted hydraulic gradients within the specimen and cause unrepresentative flow around the outside perimeter of the specimen and the membrane. Based on the trial laboratory experiments, 10 psi was selected as the confinement level in the backpressure saturation tests in this study. For most cement treated base materials, full saturation can be achieved in less than 7 hours with 10 psi confinement in the backpressure saturation test. This was cross-validated by the calculations of the volume of water required to completely fill the voids using traditional phase relationship equations. In order to simulate prolong inundation periods in the field, several backpressure durations were incorporated in the experiment matrix. The heat-treated specimens were subjected to fully saturated states for 24 hours, 48 hours, and 72

hours prior to mechanical tests. This will allow for mechanistic characterization of the strength loss and degradation of the stiffness properties of the cement treated pavement foundations due to moisture infiltrations during natural disasters, such as flooding and heavy rainfall.

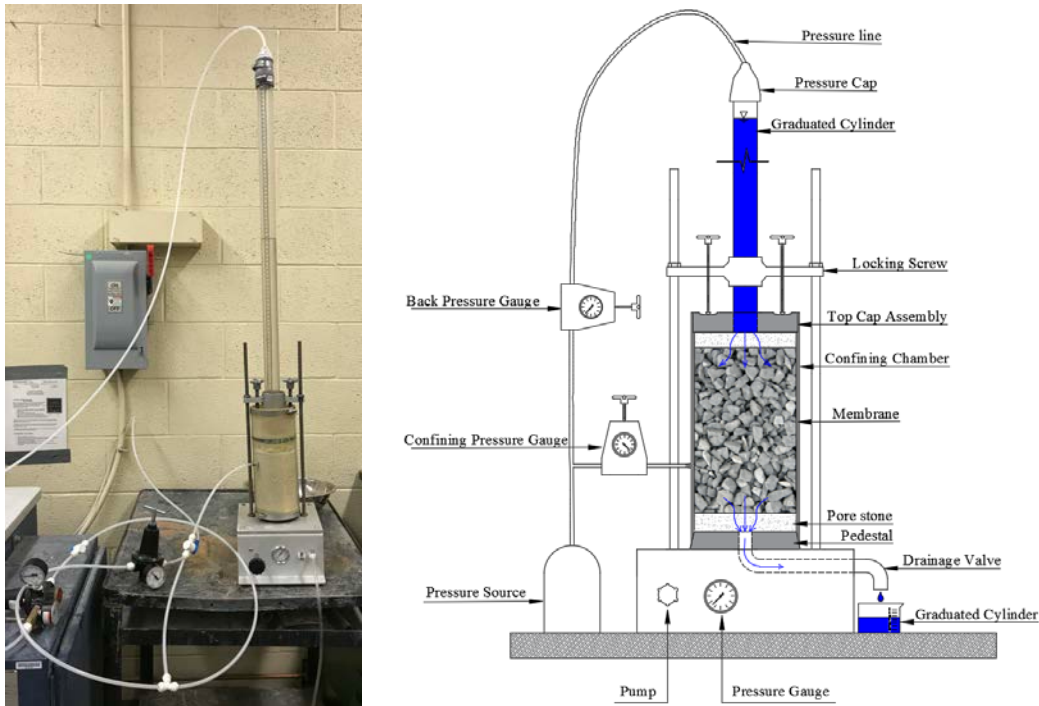


Figure 4-9: Backpressure Saturation Test Setup and Schematic.

4.2.3 Submergence Test

The submergence test was conducted on 4-inch diameter by 6-inch tall stabilized specimen prepared at optimum moisture content. In the submergence test, the stabilized specimens were placed in the 140 °F (60 °C) oven to expedite the strength-gain reactions. After 24 hours of oven drying, the specimens were capped with porous stones and placed in a rubber sleeve to prevent disintegration during the submergence process, as shown in Figure 4-10. Following this, the specimen was submerged in a 70 °F water bath for 24 hours. The test was conducted using a 5-gallon bucket filled with distilled water to 2 inches above the porous stone, as shown in Figure 4-10.

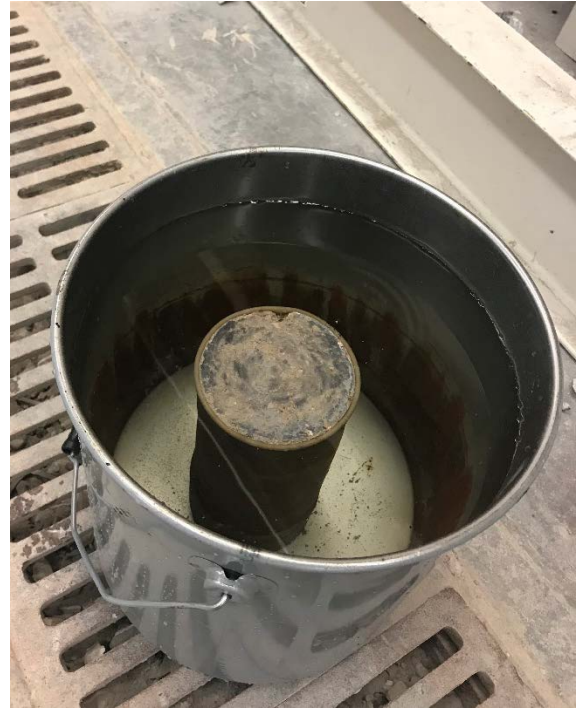
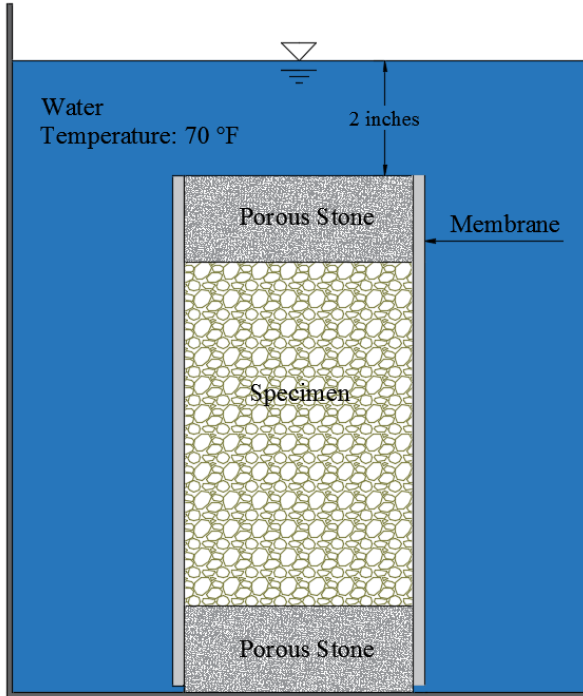


Figure 4-10: Submergence Test.

4.2.4 Hot Water Submergence Test

Hot Water Submergence (HWS) test was proposed in this study as an additional accelerated moisture susceptibility test for the cement stabilized materials. In this procedure, the stabilized specimens were prepared at optimum moisture content and capped with porous stones and placed in a rubber sleeve similar to the submergence test. Subsequently, the specimens were fully immersed in the 140 °F (60 °C) water bath kept in an oven set at 140 °F (60 °C) to maintain the temperature, for 24 hours (Figure 4-11). Upon completion of the submergence period, a cooling regime was proposed in this study to avoid a sudden drop in specimen temperature and possible damage to the specimen. In the cooling regime, the specimens were immediately transferred into a sealed plastic container after the 24-hr period in the 60 °C water bath. After cooling procedure for nearly 4 hours, the samples were subjected to mechanical tests.

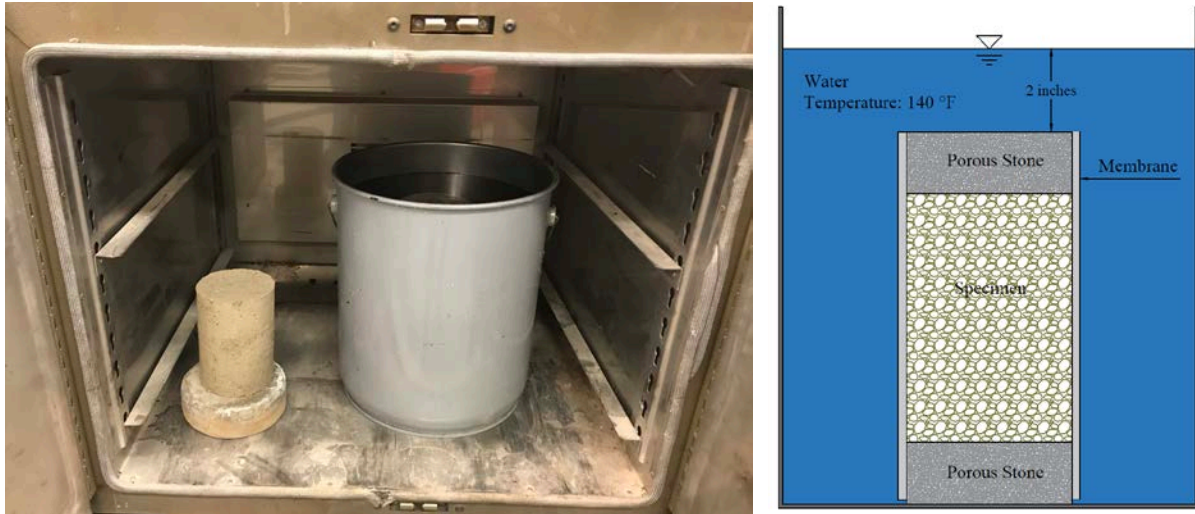


Figure 4-11: Hot Water Submergence Test.

4.3 Particle Geometry Analysis

Particle geometry can be fully expressed in terms of three independent properties: form, angularity, and surface texture. Figure 4-12 shows a schematic that illustrates the differences between these properties. Form, the first order property, reflects variations in the proportions of a particle. Angularity, the second order property, reflects variations at the corners, that is, variations superimposed on shape. Surface texture is used to describe the surface irregularity at a scale that is too small to affect the overall shape.

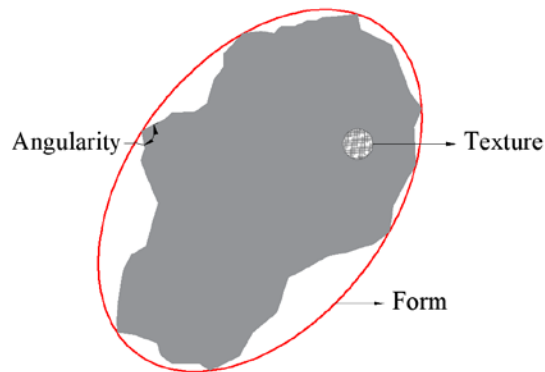


Figure 4-12: Components of an Aggregate Shape: Form, Angularity, and Texture.

Analysis using an Aggregate Image Measurement Systems (AIMS) is an effective method for the particle geometry analysis of aggregates and soils in the laboratory (Figure 4-13). AIMS is designed to analyze the form, angularity, and texture of coarse aggregates and the angularity and form of fine aggregates.

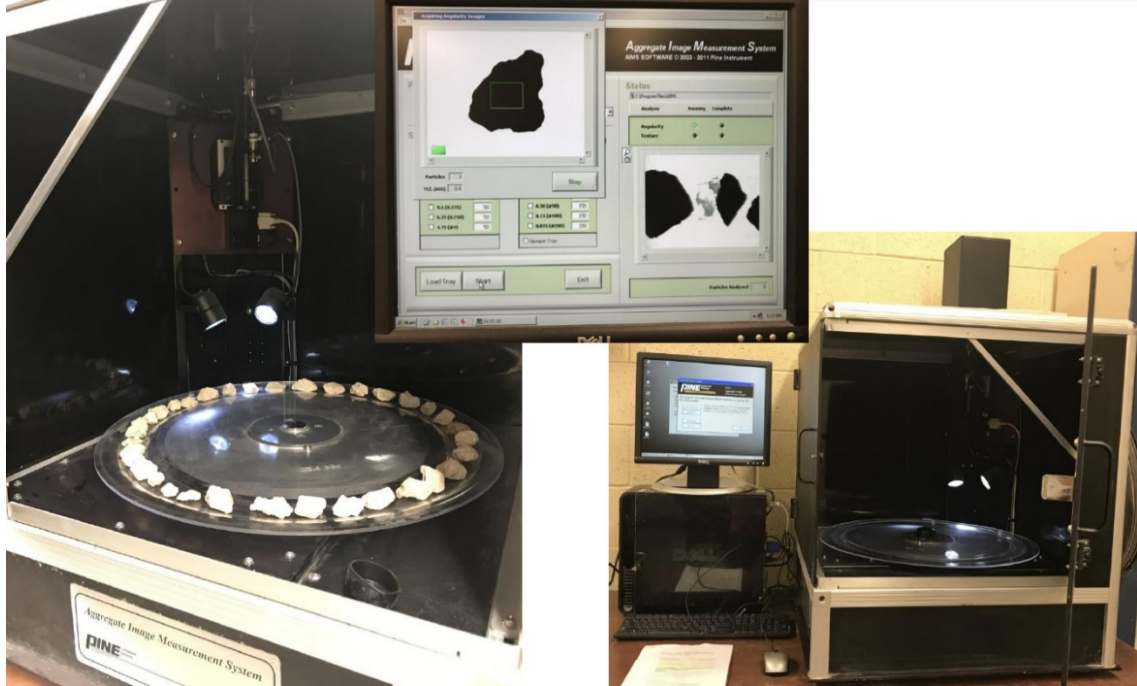


Figure 4-13: Aggregate Image Measurement Systems (AIMS).

In AIMS, the shape properties of coarse aggregates are defined by sphericity (Equation 4-2), flatness ratio (Equation 4-3), elongation ratio (Equation 4-4), and flatness-and-elongation (FE) ratio (Equation 4-5) as given in the following equations:

$$\text{Sphericity} = \sqrt[3]{\frac{D_s D_m}{D_l^2}} \quad \text{Equation 4-2}$$

$$\text{Flatness Ratio} = \frac{D_s}{D_m} \quad \text{Equation 4-3}$$

$$\text{Elongation Ratio} = \frac{D_m}{D_l} \quad \text{Equation 4-4}$$

$$\text{FE Ratio} = \frac{D_m}{D_s} \quad \text{Equation 4-5}$$

where D_s is shortest dimension of aggregate particle, D_l is longest dimension of aggregate particle, and D_m is dimension of aggregate particle perpendicular to both D_s and D_l .

The angularity index is calculated by the sum of angularity values for all the boundary points accumulated around the edge of the aggregate particle. The angularity is mathematically represented as indicated in Equation 4-6.

$$\text{Angularity Index} = \sum_{i=1}^{N-3} |\theta_i - \theta_{i+3}| \quad \text{Equation 4-6}$$

where N is the total number of points on the edge of the particle with the subscript i denoting the i th point on the edge of the particle.

AIMS was incorporated in this study to analyze the particle geometry of aggregates and its relationship with strength and stiffness properties of cement stabilized materials.

4.4 Volumetric Stability of Fine-Grained Soils

Expansive soils and high sulfate content soils in any layer of a pavement system are detrimental to its performance, creating problems such as cracking. Typically, highly plastic soils are prone to adsorb significant amounts of moisture and expand upon moisture intrusion. During dry conditions, the subgrade soils tend to shrink due to evaporation and moisture transport. Cementitious stabilization often is used to mitigate the swell tendencies of expansive soil and sulfate-induced heave.

For determination of the rate of swell pressures change in clay subgrade materials, two different tests, the One Dimensional Swell and Swell Pressure tests were incorporated in this study. These swell tests will characterize the shrinking and swelling potential of subgrade soils upon addition of cement, lime, fly ash, and polypropylene in the mix in the presence of moisture.

4.4.1 One Dimensional Swell Test

The One Dimensional Swell test setup, shown in Figure 4-14, was used to determine one dimensional swell strains in the vertical direction. The vertical deformation was measured using strain gauges positioned on top of the soil sample. In this test, soil specimens were compacted in molds having a 6-inch diameter and 8-inch height. Height and diameter were measured at three different locations along the specimen, and the averages will be recorded. The specimen was then carefully placed in a bucket of water. A thin and light porous stone was then placed on top of the sample. The porous stone eliminates the point load effect caused by the tip of the dial gauge. Dial gauges with 25-mm travel were used and were adjusted to zero readings. The specimen was then inundated with water from both ends. Water access to the specimen was maintained at both the top and the bottom. One dimensional swell (vertical rise) readings were recorded against the actual time and elapsed time. The readings were taken at suitable and regular time intervals. The one dimensional swell rate is higher initially, and this rate subsides slowly with time. Therefore, more readings were taken at the beginning of the test. The normal soaking period for most clays ranges from 2 to 3 days. In this study, this test was considered complete when the readings were the same over an 8-h interval.

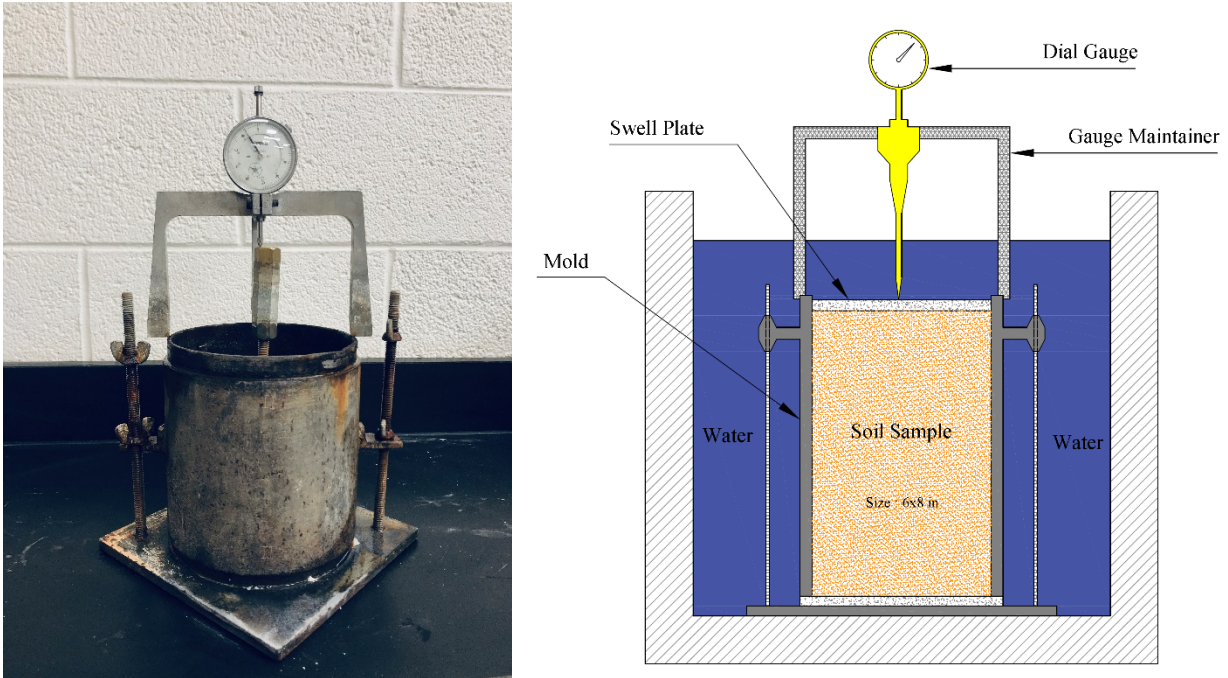


Figure 4-14: One Dimensional Swell Test Setup and Schematic.

4.4.2 Swell Pressure Test

The swell pressure was characterized by constraining the clay to maintain its original volume. This test was similar to the one dimensional swell test. In this test, the stabilized specimen is compacted into the consolidation ring. Initially, the ring is placed in the mold, and the desired amount of mixture is placed in the ring. The stabilized specimen was then compressed by a loading plate until the top of the plate came in contact with the ring as shown in Figure 4-15.

Subsequently, the ring was placed into the oedometer after placing dry filter papers and air-dry porous stones on top and bottom of the specimen. After the oedometer was mounted on the loading device, the deflection dial was adjusted to a zero reading. Upon completion of the sample setup, the specimen was fully submerged by adding water from the top and bottom. This resulted in the swelling of the specimen as the moisture seeped into the soils structure and participated in the hydration reactions. The reading from the dial gauge was recorded until the swell-readings reached an asymptotic behavior with respect to time. The nature of the swell-time curve and the reduced rate of change at the end of the test was used for the characterization of the volumetric expansion behavior, and swelling pressure of cement treated materials.

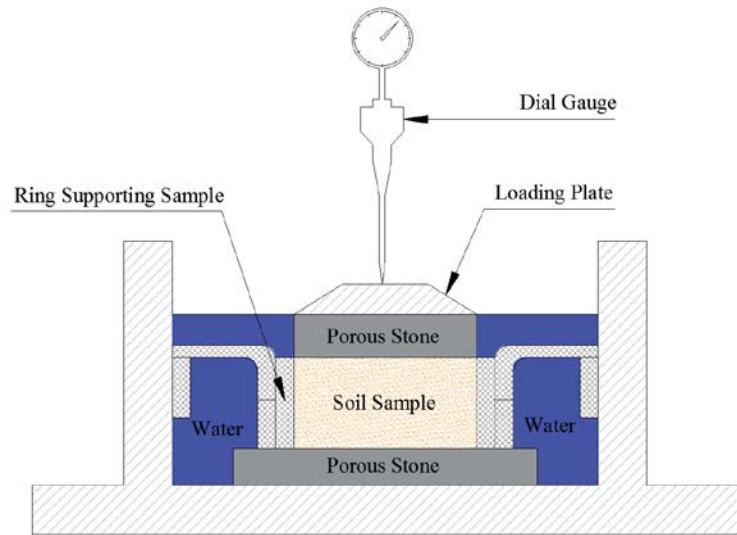


Figure 4-15: Swell Pressure Test Setup and Schematic.

4.4.3 Characterization of Activity and Plasticity of Clay Materials with Methylene Blue Test

The activity of the plastic clays were identified using the Methylene Blue test. This test provides an indication of the moisture adsorption potential, and therefore the swelling behavior of fine grained soils. According to the ASTM C832 (ASTM, 2015), 20 g of material passing the #200 sieve is titrated with Methylene blue dye and a spot is tested on a filter paper. The addition of more dye to the solution continues until the spot of material is no longer able to adsorb additional dye. This is evidenced by a lighter blue ring around the test spot. Figure 4-16 shows a schematic representation of dye absorption by fine particles. The Methylene Blue test was incorporated as a simple and practical measure to characterize the moisture adsorption potential of subgrade soils, and to explore correlations with volumetric swell potential and plasticity of clay subgrade soils.

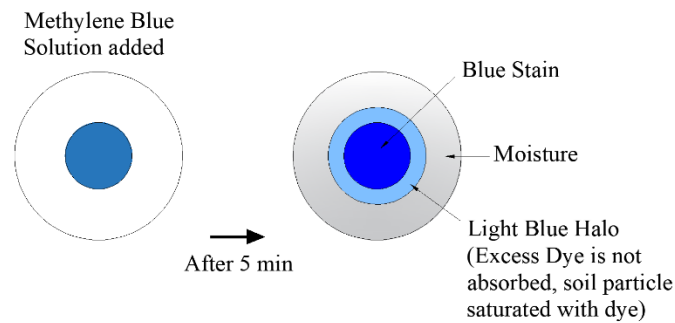


Figure 4-16: Methylene Blue Absorption Test.

This test examines the activity of the fines and allows for the detection of both non-plastic and plastic fines in the mixture. The fines are classified as non-plastic and plastic materials according to their different specific surface area. The methylene blue separates these two types of fines at the critical value of 7.0 mg/g. The methylene blue test method uses a 20.0 g sample of fine aggregates that pass the No. 4 sieve. The 20.0 g sample is added to 30.0 mL of calibrated methylene blue solution in a plastic tube. The mixture is agitated for 1 min, allowed to rest for 3 min, and agitated again for 1 more min. Next, the solution is filtered through a 2.0 μm filter using a syringe. The sample passing the filter is used for the rest of the experiment.

Subsequently, 130.0 mL of the filtered solution is added to a plastic tube and filled with distilled water until a total of 45.0 g is collected. The newly mixed solution is placed in a small glass tube that is placed in the colorimeter. The Methylene Blue Value (MBV) is determined by the colorimeter device. If the MBV reading is smaller than 7.0 mg/g, it is considered as a valid reading; hence, 20.0 g is a valid sample size. The total test time for a measurement is less than 10 min. Figure 4-17 shows the procedure for the methylene blue value test.

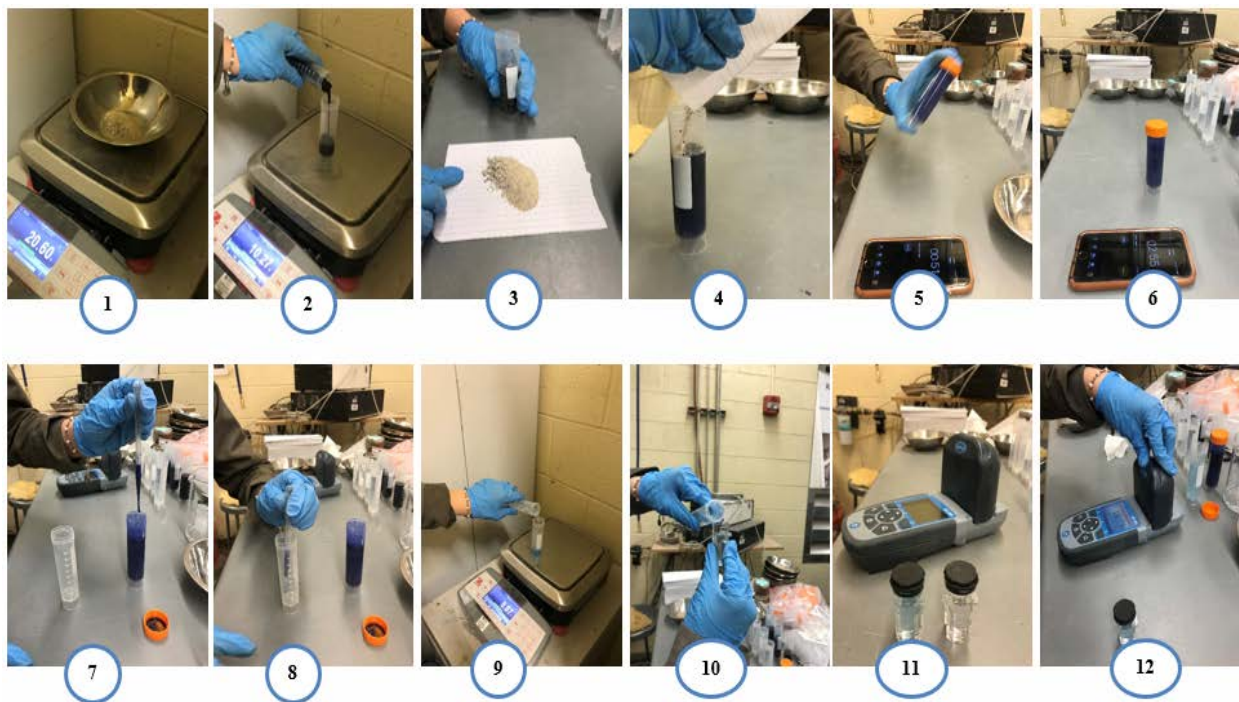


Figure 4-17: Methylene Blue Value Test Procedure (Test Steps are Numbered Sequentially).

4.5 Cementitious Materials Coefficient of Thermal Expansion

The consumption of the available moisture in the cement treated mixes will result in the formation of new compounds that contribute to the strength of the treated layers. The time and temperature dependent cement hydration process influences the shrinking and expansion behavior of the treated layers. Such volumetric change, if restricted, can manifest itself in the form of shrinkage cracks in the cement treated base layers. These cracks can propagate to the asphalt surface layers and

jeopardize the longevity of pavement structures. Therefore, it is imperative to properly characterize the volumetric characteristics of the cement treated materials.

The coefficient of thermal expansion (COTE) is a key parameter that can describe the shrinkage cracking behavior of stabilized materials. The originally proposed test method for the COTE of concrete, based on AASHTO TP60, Standard Method of Test for Coefficient of Thermal Expansion of Concrete, is not suitable for measuring the COTE of lightly or heavily cement stabilized materials. The saturation method recommended in AASHTO TP60 would severely damage the stabilized materials (Cusson & Hoogeveen, 2006). Therefore, this study modified the AASHTO TP60 procedure to accommodate both lightly and conventional cement treated aggregate soils.

The modified COTE test was performed in this study for characterization of shrinkage cracking of cementitious stabilized materials. In this test, prismatic specimens with dimensions of 4 in. × 4 in. × 20 in. were prepared and placed in an environmental chamber with relative humidity of 50% and at an initial ambient temperature of 77°F as shown in Figure 4-18. The chamber cycled the temperature between 77°F and 86°F using a saw-tooth pattern while the RH was kept constant. After the target temperature in the chamber was reached, which takes about 20 minutes, the temperature was kept constant for 12 hours. One full cycle can be completed in one day. The constant temperature period is long enough to ensure a stable and uniformly distributed temperature in the prismatic sample. The developed COTE test, which is based on temperature cycling, was capable of measuring the COTE of both lightly and heavily stabilized materials.



Figure 4-18: COTE Test Setup.

4.6 Compaction Characterization

Uniform specimen preparation is important to properly characterize the mechanical behavior of cement treated materials in the laboratory. Traditionally, the impact hammer method is used to compact specimens in the laboratory to establish the moisture-density curve, perform strength tests, and to characterize the deformation potential of cement treated systems (Figure 4-19). Based on experience, due to the nature of the application of compaction energy, specimens prepared using the impact method exhibit high levels of non-uniformity, resulting in a less reliable performance assessment in the laboratory. Additionally, the methods of compaction energy in the field, such as static pressure, vibration, kneading and etc. are vastly different from the impact hammer in the laboratory. This would ultimately result in significant differences in the void structure and preferred orientation of the aggregate particles. High variability of strength test results and presence of a layer interface between lifts can be other limiting factors in this compaction technique. Figure 4-19 shows additional methods to fabricate cement-treated specimens in the laboratory.



Figure 4-19: Impact Hammer, Texas Gyrotory Compactor (TGC), Gyrotory Compactor, and Vibratory Hammer.

Gyrotory compactors have been commonly used in recent years for the compaction of asphalt mixtures (Figure 4-20). In this compactor, material is compacted through simultaneous action of compressive pressure and shearing forces generated as a result of mold gyration about its vertical axis as shown in Figure 4-20. Literature is sparse regarding the compaction of soil and granular materials with the gyrotory compactor. In some of these few research studies, satisfactory results such as leading to a better simulation of field compaction were observed using gyrotory compaction (Arabali et al., 2018). Therefore, the cement treated specimen using four compaction methods, namely Texas gyrotory compactor, impact hammer, vibratory hammer, and gyrotory compactor were prepared to investigate the potential benefits and effects of using gyrotory and vibratory compactors on the engineering properties of the cement treated base and subgrade materials (Figure 4-20).

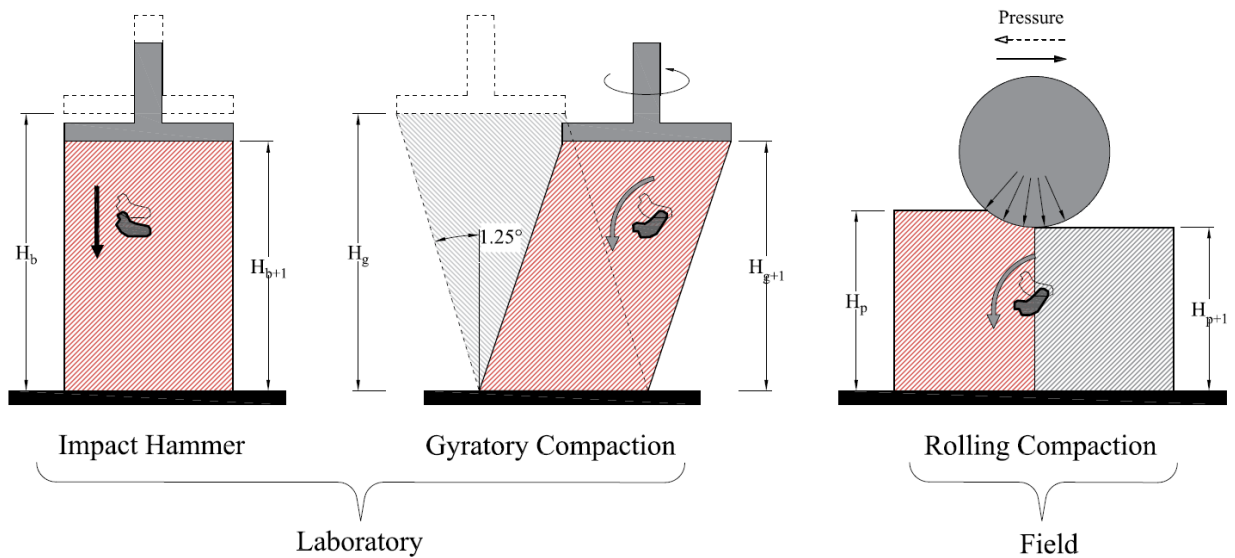


Figure 4-20: Differences between the Mechanism of Gyrotory Compactor and Impact Hammer.

Chapter 5. Laboratory Test Results

This chapter focuses on presenting the results and analysis of the data from the laboratory experiment. Also, the determination of the material parameters and material properties for all the permutations of the experiment design for inclusion in the aggregate feature database is included. The features database is discussed in the following sections.

5.1 Aggregate and Soil Properties

Nine aggregate sources with distinct lithologies were incorporated in this research to account for the impact of mineralogy and surface properties on the compressive, tensile, and resilient behavior of cement treated aggregates. Sieve analysis tests were performed on these aggregate sources to identify the particle size distribution of aggregates according to Tex-110-E (2016). The particle size distributions for selected materials in this study is presented in Figure 5-1. The selection of the particle size distributions was based on Item 247 of TxDOT standard construction specifications for Grade 2 materials. The particle-size distributions indicate that the RAP and FDR have considerably more medium and fine particles than the RCA and virgin aggregates. The presence of excess fines can be attributed to the crumbling of the materials during milling and crushing operations.

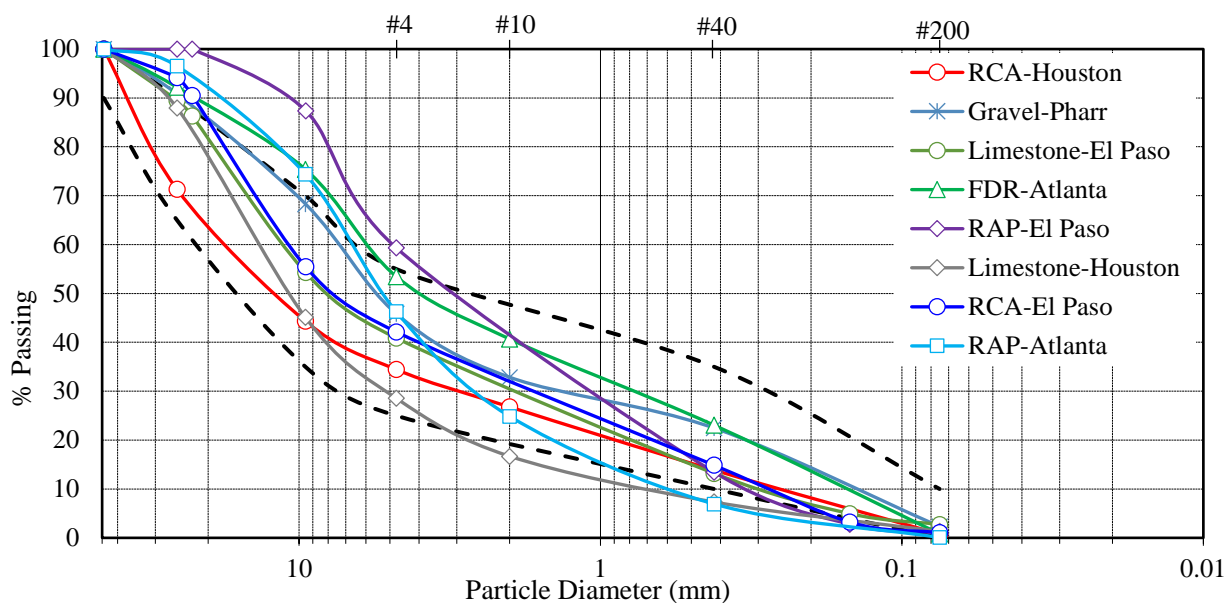


Figure 5-1: Sieve Analysis for Base Materials.

Depending on the crushing methods, the particle size distribution of an RCA can have a wide variability, with a lower particle density and greater angularity than would normally be found in more traditional virgin base course aggregates. Residual mortar and cement paste are typically found on the surface of the RCA, as well as contaminants associated with construction and

demolition debris. The presence of this mortar contributes to a rougher surface texture, lower specific gravity, and higher water absorption than typical aggregates.

The moisture-density tests were also performed on untreated materials to identify the Optimum Moisture Content (OMC) and Maximum Dry Density (MDD) following Tex-113-E (2016) and Tex-114-E (2016) test methods. Figures 5-2 and 5-3 also provide the Moisture-Density test results for base aggregates and subgrade soils, respectively. Results revealed that marginal base and reclaimed materials exhibited significantly lower maximum dry density in comparison with good quality crushed limestone aggregate materials sourced from El Paso.

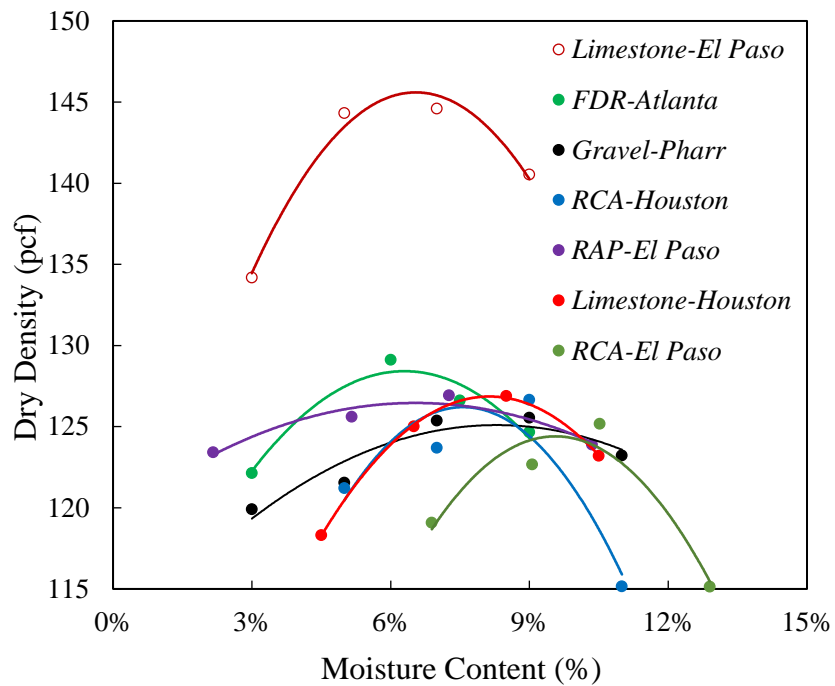


Figure 5-2: Moisture Density Test Results for Base Aggregates.

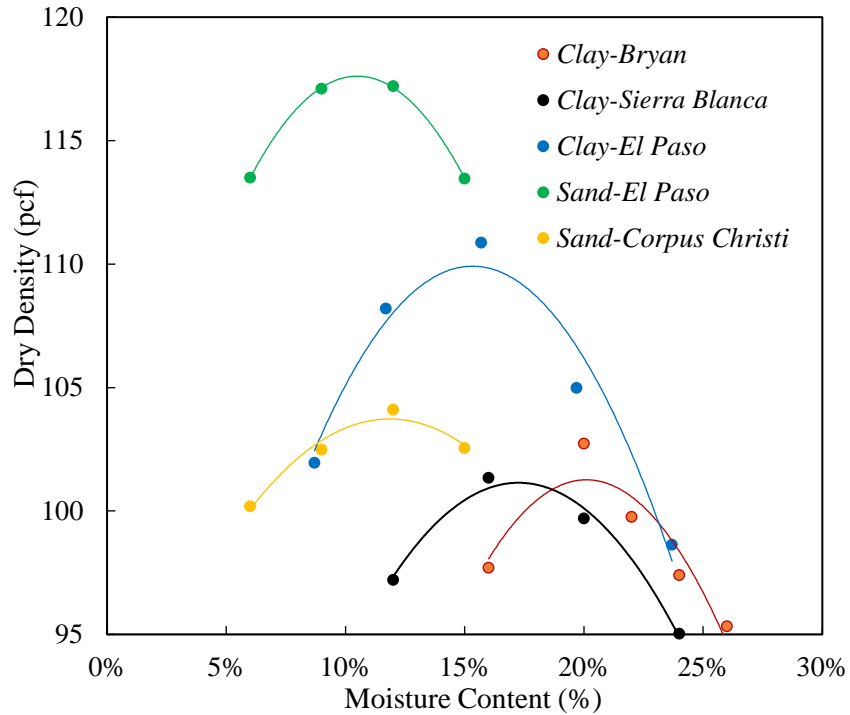


Figure 5-3: Moisture Density Test Results for Subgrade Soils.

Subsequently, the Atterberg limits tests were performed to determine the Plastic Limit (PL), Liquid Limit (LL), and the Plasticity Index (PI) of the subgrade materials following Tex-104-E, Tex-105-E, and Tex-106-E specifications, respectively. Additionally, soluble sulfate content of soils was calculated by using the colorimetric method according to Tex-145-E specification. Tables 5-1 and 5-2 present parameters pertaining to the sieve analysis, Atterberg limits, moisture-density, and sulfate content tests for the base aggregates and subgrade soils. Table 5-2 indicates that clayey materials sourced from Sierra Blanca and Bryan with sulfate concentration of 24,320 ppm and 13,093 ppm were referred as high sulfate soils. This value for clay sourced from Houston was 480 ppm, which is referred to as the low sulfate soil.

Table 5-1: Material Properties for Base Aggregates.

Material Properties	Virgin Aggregates		Marginal Aggregates	Recycled Aggregates				
	Limestone	Limestone	Siliceous Gravel	RAP	RAP	RCA	RCA	FDR
	El Paso	Houston	Pharr	Atlanta	El Paso	Houston	El Paso	Atlanta
% Gravel	59.1	71.4	54.1	53.7	40.7	65.6	55.4	46.5
% Sand	38.2	27.2	43.5	46.2	58.3	33.7	41.1	52.6
% Fine	2.7	1.3	2.3	0.1	1	0.8	1	0.8
D ₁₀	0.2	0.8	0.16	0.6	0.34	0.28	0.28	0.17
D ₃₀	2	4	1.6	2.8	1.1	3	1.8	0.8
D ₆₀	10.2	10.4	7.5	6.8	5	10.8	12	6
C _u	51	13	46.875	11.33	14.7	38.57	42.86	35.3
C _c	1.96	1.93	2.13	1.92	0.71	2.97	0.96	0.63
MMD (pcf)	145.8	127	125.4	121.7	126.5	126.2	124.2	128.8
OMC	6.50%	8.20%	8.40%	7.00%	6.50%	7.60%	9.60%	6.30%

Table 5-2: Material Properties for Subgrade Soils.

Soil Properties	Sand	Sand	Clay	Clay	Clay	Clay
	El Paso	Corpus Christi	El Paso	Sierra Blanca	Houston	Bryan
LL	17	8	34.5	48	53	63
PI	5	-	27	37	36	45
Sulfate Content	140	320	280	24,320	480	13,093
MMD (pcf)	120.2	103.7	110	101.1	103	102
OMC	10.00%	11.80%	15.40%	17.20%	18.50%	20.10%

5.2 Strength and Stiffness Properties

The strength and stiffness are the primary input parameters for the design of pavements with cement treated layers. In this study, the Unconfined Compressive Strength (UCS) test, Indirect Diametrical Tensile (IDT) strength test, and submaximal modulus tests, and Free-Free Resonant Column (FFRC) tests are incorporated in the laboratory mixture design protocols to characterize the strength, resilient properties, and permanent deformation potential of cement treated systems.

5.2.1 Unconfined Compressive Strength (UCS)

As previously stated in this project, cement content ranging from 2% to 4% were added to each permutation of the experiment design to cover a wide spectrum of cement treatment from light stabilization to heavily stabilized systems. Figure 5-4 demonstrates the unconfined compressive

strength results for base aggregate types with different stabilizer contents and with different mold size. The plots show the beneficial role of the increase of cement content on the compressive strength of base aggregates. This favorable influence is more pronounced for crushed limestone aggregates sourced from El Paso. For instance, compressive strength of specimens treated with 4% cement content were up to four times greater than FDR specimens treated with 4% cement content.

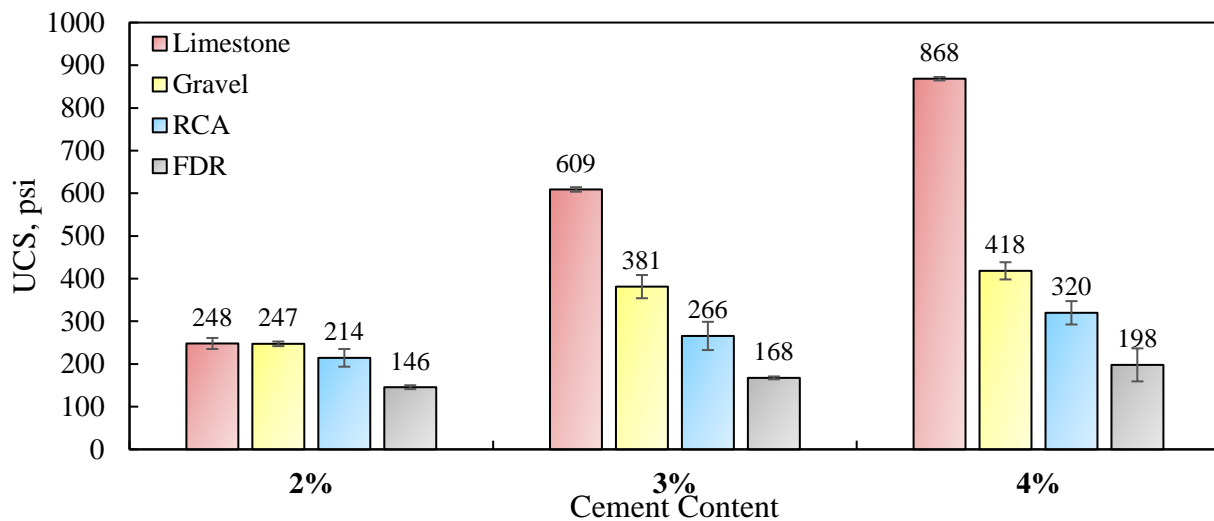


Figure 5-4: Unconfined Compressive Strengths Results for 7-Day Moist Cured Samples - Sample Size 6 in (d) × 12 in (h).

Figures 5-5 and 5-6 show the laboratory results of the unconfined compressive strength test for sandy and clayey subgrade soils sourced from El Paso. The ascending nature of the trend lines is an indication of the favorable impact of increasing cement contents on the unconfined compressive strength of sandy and clayey subgrade soils. The slope of the trend lines, which represents the rate of improvements in the compressive strength can provide valuable insight on the impact of the soil mineralogy and surface properties on the rate of the strength gain in presence of pozzolanic materials. As indicated in this plot, UCS tests on El Paso sandy soils resulted in sharper slopes which are an indication of the favorable influence of increasing cement contents to improve the strength of the stabilized materials. Comparatively, the UCS results on low plastic clay sourced from El Paso district exhibited flatter slope, which is an indication of lower influence of increasing cement content to improve the strength properties of the cement stabilized clayey materials. This information can be utilized for selection of the optimum cement content for the stabilization of pavement foundations. The UCS test results clearly indicate that sand benefited more from the increase of cement in terms of improvements in strength properties of the soils as illustrated in the plots.

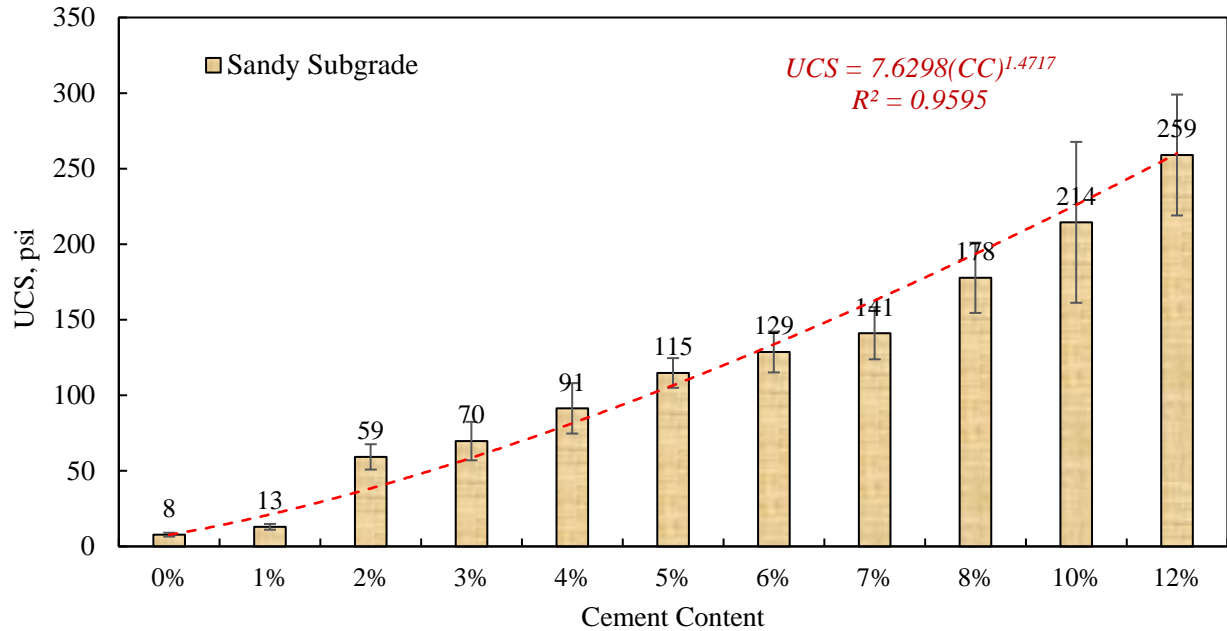


Figure 5-5: Unconfined Compressive Strengths Results for Sandy Subgrade Materials sourced from El Paso compacted with Impact Hammer - Sample Size 4 in (d) × 6 in (h).

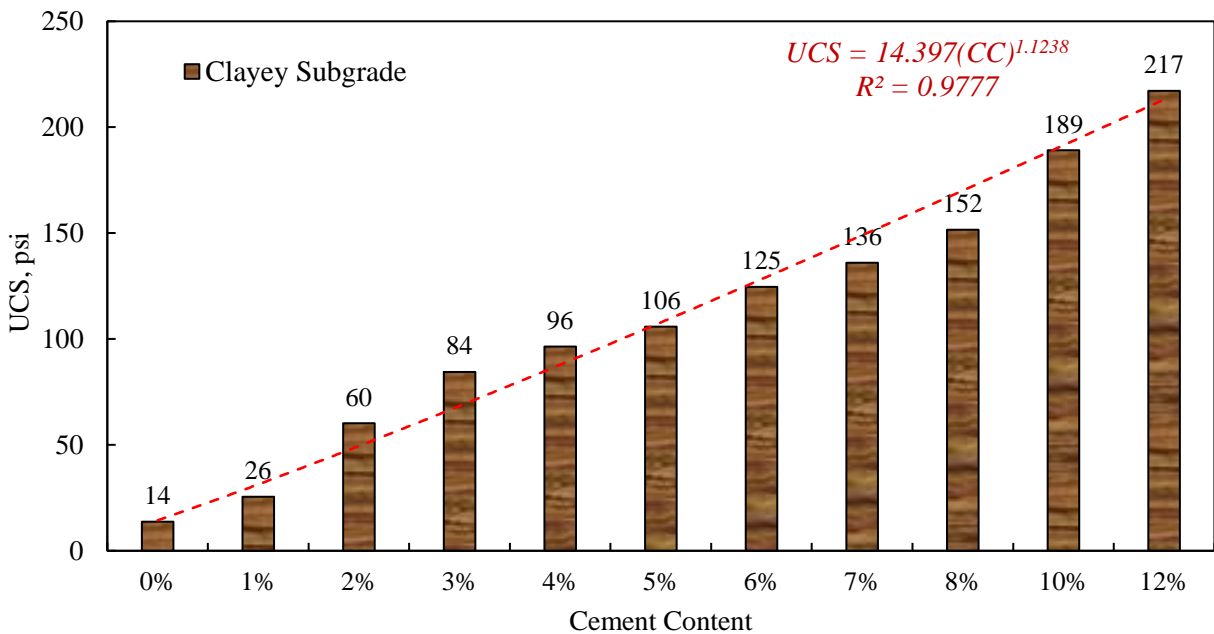


Figure 5-6: Unconfined Compressive Strengths Results for Clay Subgrade Soils sourced from El Paso compacted with Impact Hammer - Sample Size 4 in (d) × 6 in (h).

5.2.2 Indirect Diametrical Tensile (IDT) Test

This section presents the laboratory results of the IDT test for 7-day moist cure specimens to characterize the tensile strength properties of cement stabilized materials in the laboratory. Strain controlled static Indirect Diametrical Tests (IDT) were performed on 4×4 in stabilized specimens.

Similar to the UCS tests results, incremental addition of the stabilizer content improved the mechanical properties of the tested specimen. All permutations exhibited increase in the tensile strength with increasing stabilizer contents. However, the rate and the magnitude of improvements were highly impacted by the lithology of aggregates as indicated in Figure 5-7. The IDT test results indicated that limestone and gravel aggregates have benefited most from the increase in cement content. Conversely, the rate of the improvements in the tensile strength of reclaimed materials such as FDR and RCA with increasing cement contents has been considerably lower.

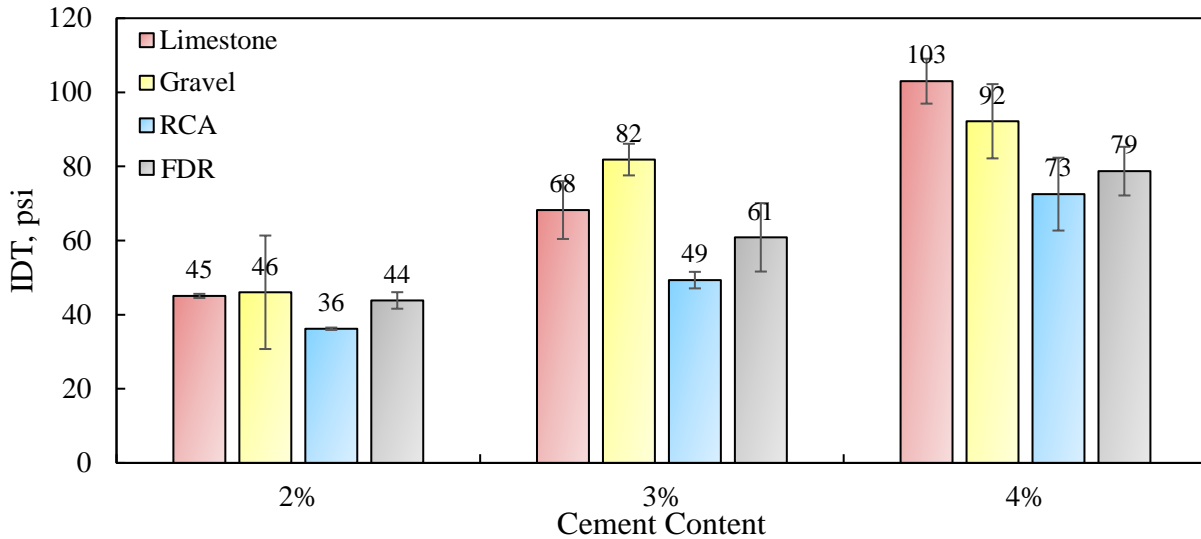


Figure 5-7: Indirect Diametrical Tensile Strength Results for Samples compacted with Impact Hammer.

5.2.3 Submaximal Modulus Test

The new Mechanistic-Empirical Pavement Design Guide (MEPDG) requires a measure of the resilient modulus for the analysis and design of pavements. This information is required for the calculation of the responses of pavements subjected to traffic loads. Therefore, the submaximal modulus test was used for the characterization of the resilient behavior of stabilized subgrade and base materials subjected to traffic loading. This test provides valuable information on the permanent deformation properties and energy dissipation mechanism due to repeated traffic loads in stabilized pavement foundations. The strength values obtained from the UCS test will be the basis for the selection of the stress amplitudes applied to the specimens. Pre-determined fractions of the UCS-value at two levels of 25% and 50% will be applied for 5,000 load cycles under axial compressive loads to 6 inches diameter and 12 inches height specimens. Subsequently, the vertical deformations are recorded using four internal proximeters attached to the specimens and external LVDTs as shown in Figure 5-8.

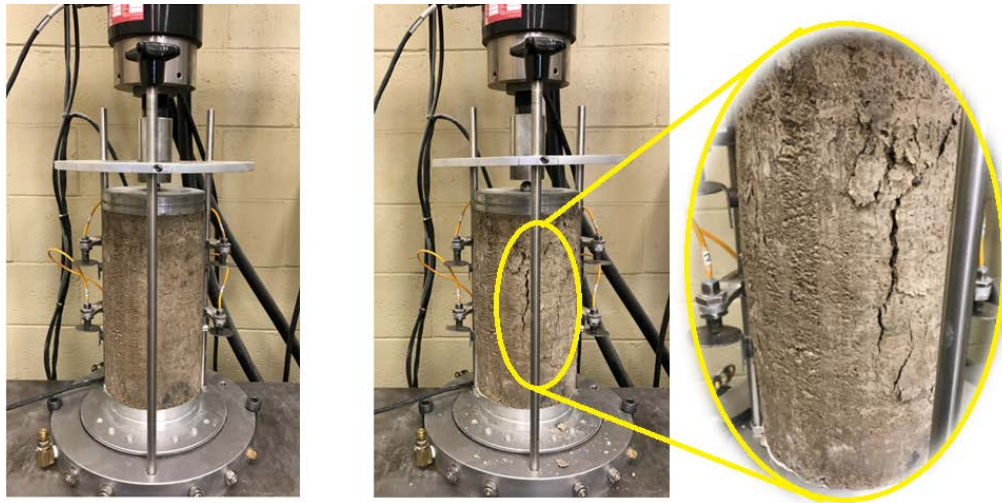


Figure 5-8: Submaximal Modulus Test Set Up and Fractured Specimens.

Figures 5-9 and 5-10 provide the resilient modulus tests results for 7-day moist-cured specimens at two levels of 25% and 50% stress ratios, respectively. This plot is primarily based on the averages of two replicates subjected to 5,000 load cycles for all aggregate types in the experiment design. As illustrated in the plots, stabilized reclaimed materials had lower resilient modulus compared to the crushed limestone and gravel aggregates. For instance, the 3% cement stabilized gravel materials had approximately 150% higher resilient modulus compared to the stabilized RCA materials at both stress ratios. This underscores the role of the mineralogy and aggregate source with regard to stiffness behavior during service life of stabilized pavement foundations.

Figures 5-9 and 5-10 also underscore the influence of the stress path protocol on the resilient modulus of stabilized materials. As previously indicated, 25% and 50% of the unconfined compressive strength were cycled for 5,000 repetitions to characterize the resilient properties of the cement treated materials. The plots indicate that the variants subjected to less taxing stress paths had higher resilient modulus values. These results from the low-stress excitation levels and, therefore, low induced strains of 25% were considered at the loading protocol. Conversely, a strain ratio (SR) equals to 50% stress path protocol induce higher strain and the net effect will be lower modulus values. Therefore, it deems necessary to consider the strain levels imposed by traffic loads on pavement layers for realistic selection of resilient modulus for design and analysis of pavements.

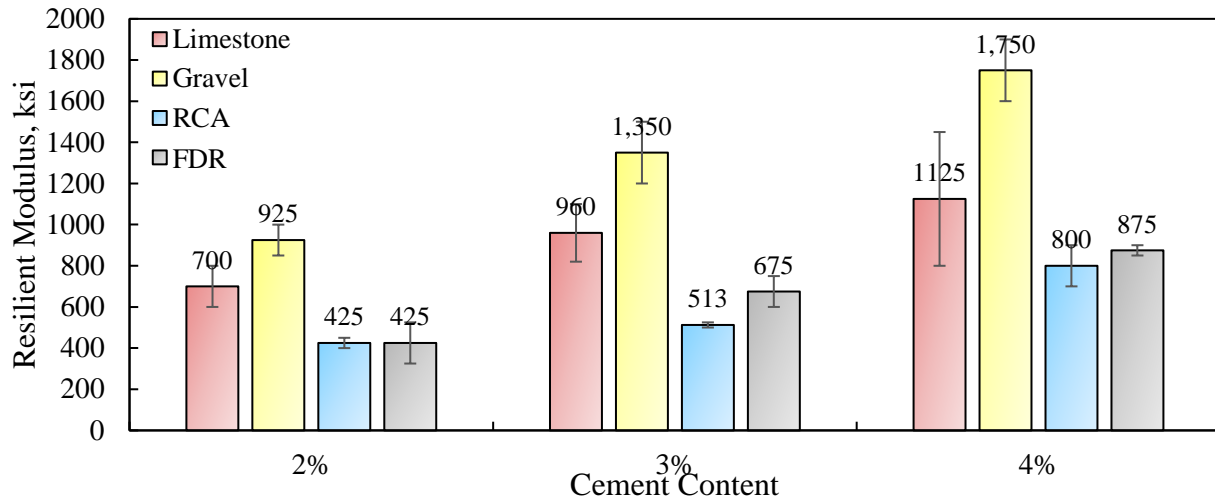


Figure 5-9: Resilient Modulus for 7-Day Moist Cured Samples (Stress Ratio = 50%).

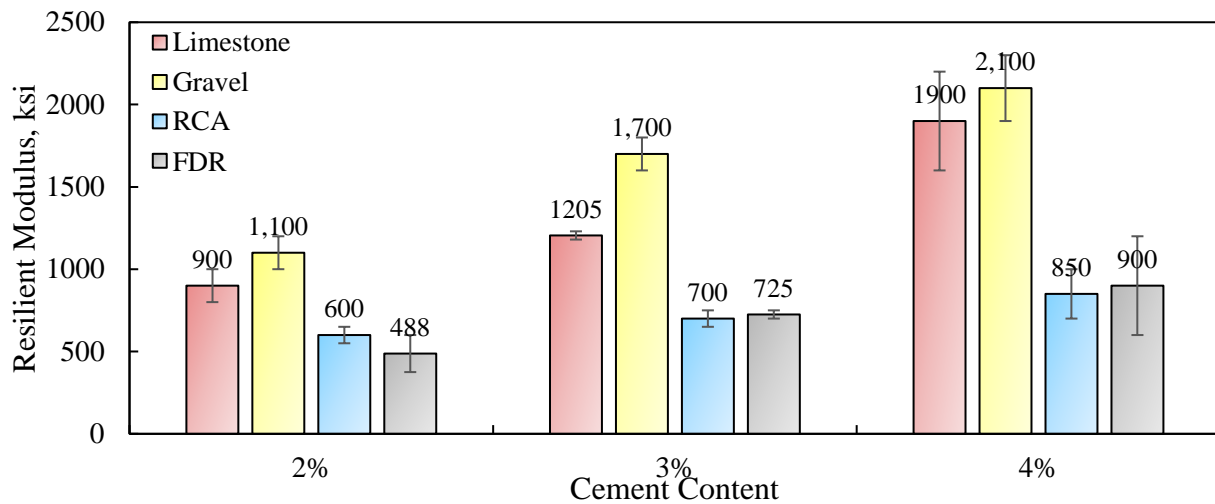


Figure 5-10: Resilient Modulus for 7-Day Moist Cured Samples (Stress Ratio = 25%).

Other important information that can be extracted from the submaximal test is the permanent deformation of the specimens. Figures 5-11 and 5-12 illustrate normalized permanent deformation of cement stabilized materials after 5,000 load application at 50% and 25% of strength ratios, respectively. Since the percentage of strength is constant, it is imperative to normalize the measured deformations by strength values (or stress amplitudes) for proper comparison of deformations. This is simply due to the fact that 20% UCS of a stabilized material X with w% cement content is significantly different compared to a material Y with w% cement content; therefore, the selected stress amplitude in the two tests are different. For instance, 20% of the UCS for limestone specimens is significantly higher than 20% strength for FDR specimens.

The results from the high-stress excitation levels (SR=50%) clearly indicate that the RCA materials sourced from Houston significantly underperformed in terms of higher permanent strain after 5,000 load cycles for 7 day moist cured specimens. In contrast, limestone aggregates and gravel

materials showed superior performance in terms of lower permanent strain compared to the other materials in the experiment design. Another interesting observation that can be clearly visualized from this figure is the significant reduction of permanent deformation for RCA materials in low stress path protocol (SR=25%). This could be attributed to the initiation of micro-cracks in stabilized RCA materials at the high-stress excitation levels imposed by traffic loads.

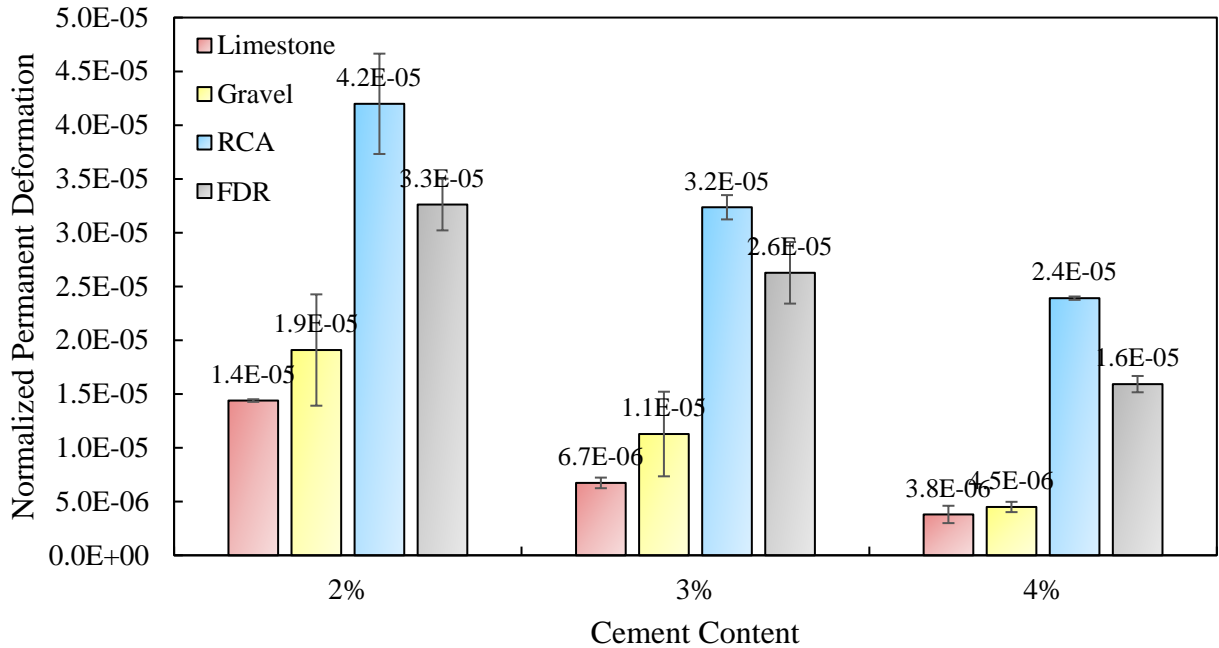


Figure 5-11: Normalized Permanent Deformation for 7-Day Moist Cured Samples (Stress Ratio = 50%).

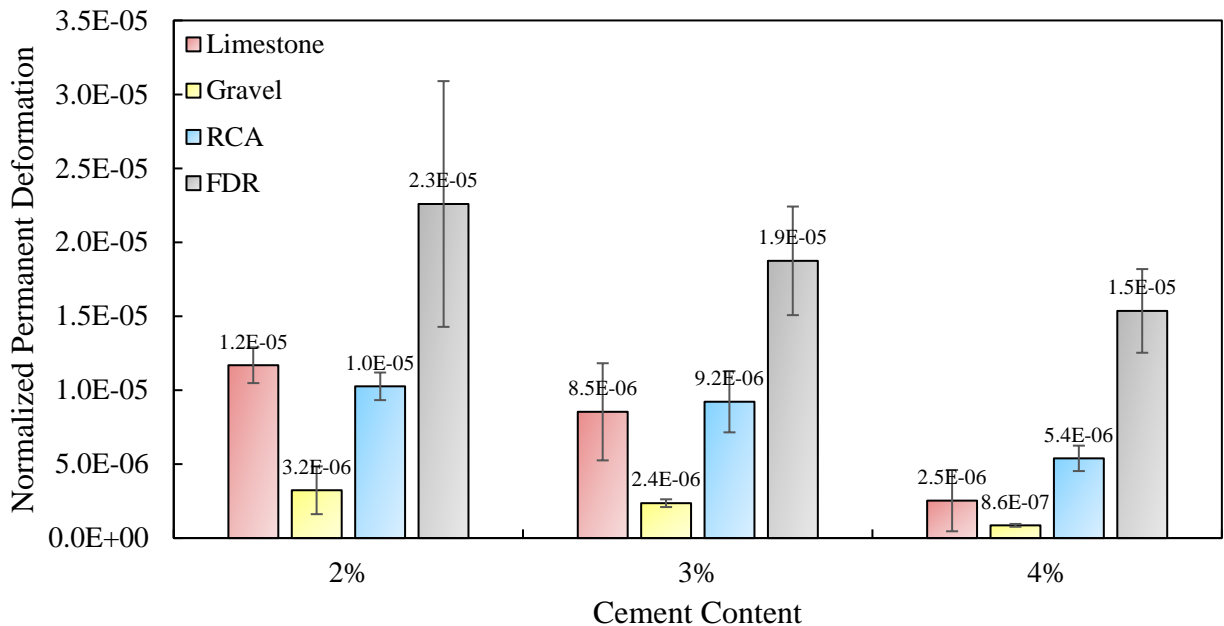


Figure 5-12: Normalized Permanent Deformation for 7-Day Moist Cured Samples (Stress Ratio = 25%).

Figures 5-13, 5-14, and 5-15 show the unconfined compressive strength of stabilized base materials before and after subjecting the specimens to repeated loads in permanent deformation tests at 25% and 50% strength ratio for siliceous gravel, RCA, and crushed limestone aggregates, respectively. The primary motivation for these test was to investigate the potential damage imparted on the stabilized specimen after 5,000 load cycles. The results clearly show that the compressive strength for RCA and siliceous gravel after 5,000 load application at both strength ratios was lower than UCS test results. This is more pronounced for materials stabilized with 4% cement content. This can be attributed to the spread of micro-cracks in overly rigid stabilized mixes. Comparatively, virgin aggregates specimens after 5,000 load cycles had the same compressive strength compared to specimens before subjecting them to repeated loads. This is an indication of lower influence of traffic loads on the strength properties of virgin aggregate materials in comparison with marginal aggregates and reclaimed materials.

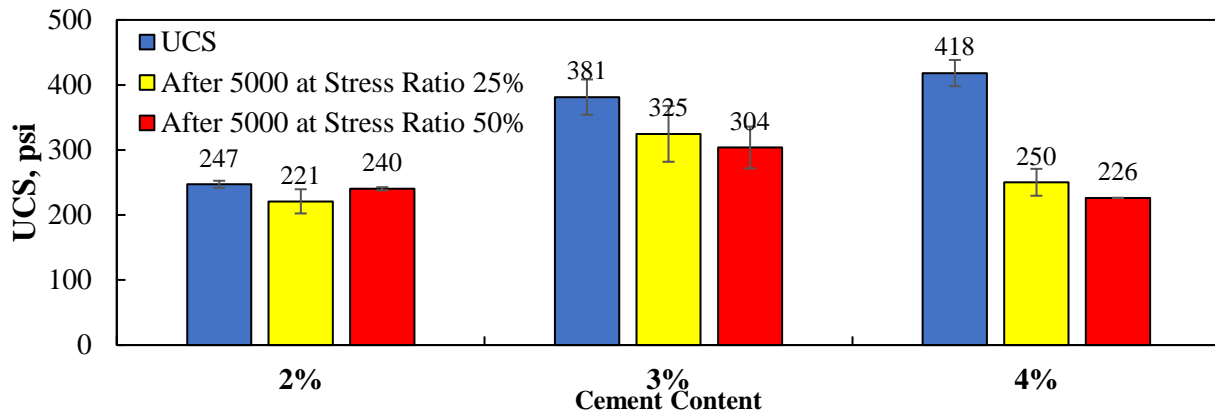


Figure 5-13: Unconfined Compressive Strength of Stabilized Siliceous Gravel Materials Sourced from Pharr after 5,000 Load Applications at Stress Ratios of 25% and 50%.

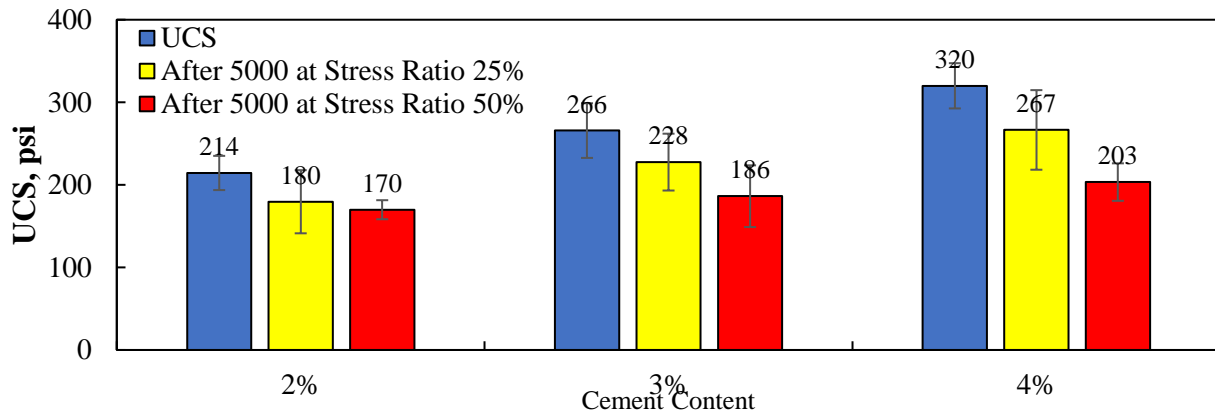


Figure 5-14: Unconfined Compressive Strength of Stabilized RCA Materials Sourced from Houston after 5,000 Load Applications at Stress Ratios of 25% and 50%.

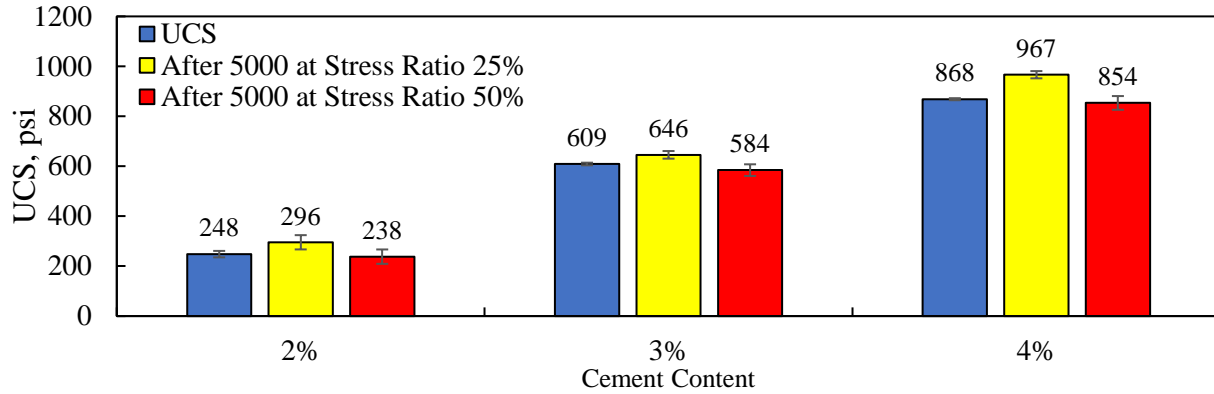


Figure 5-15: Unconfined Compressive Strength of Stabilized Limestone Materials Sourced from El Paso after 5,000 Load Applications at Stress Ratios of 25% and 50%.

5.3 Particle Geometry Analysis

Particle geometry can be fully expressed in terms of three independent properties: form, angularity, and surface texture. Form reflects variations in the proportions of a particle. Angularity reflects variations at the corners, that is, variations superimposed on shape. Surface texture is used to describe the surface irregularity at a scale that is too small to affect the overall shape. In this study, Aggregate Image Measurement Systems (AIMS) was used as an effective method for the particle geometry analysis of aggregates and soils in the laboratory. AIMS is capable of capturing the aggregate characteristics over a range of aggregates sizes from 37.5 mm to 0.075 mm. Figure 5-16 shows an illustration of the AIMS system.

Aggregate Image Measurement System (AIMS)

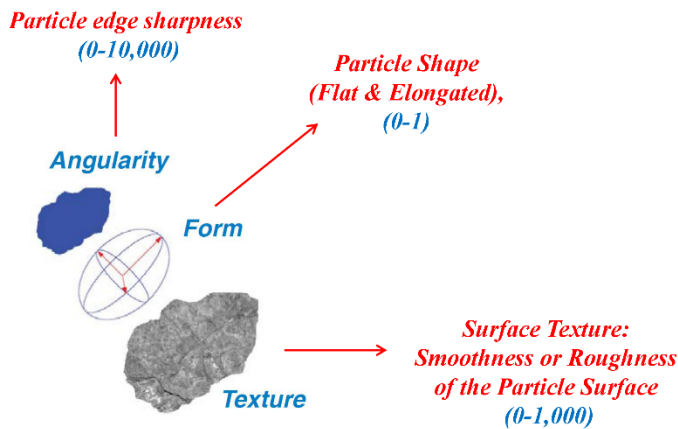


Figure 5-16: Aggregate Image Measurement System (AIMS).

5.3.1 Angularity Index

Angularity index applies to base materials sizes and quantifies variations at the particle boundary that influence the overall shape. The angularity of aggregates is evaluated by quantifying the change in the gradient on a particle boundary and is related to the sharpness of the corners of 2-dimensional images of aggregate particles as illustrated in Equation 5-1.

$$\text{Angularity Index} = \frac{1}{\left(\frac{n}{3}\right)^{-1}} \times \sum_{i=1}^{n-3} |\theta_i - \theta_{i+3}| \quad \text{Equation 5-1}$$

Where θ is the angle of orientation of the edge points; n is the total number of points; and i denotes the i th point on the edge of particle.

Figure 5-17 presents the angularity distribution of siliceous gravel sourced from Pharr based on the characterization of the aggregate edges. AIMS characterizes the particle edge sharpness on a scale of 0-10,000 and categorizes the angularity of aggregates in four different classifications, namely low (0-2,100), moderate (2,101-3,975), high (3,976-5,400), and extreme (5,401-10,000) angularity. As observed in the plot, this material contained particles pertaining to three different classifications. The average value has been used in this study to determine the level of angularity of the materials. Siliceous gravel materials exhibited a moderate angularity with the average value of 2,589.

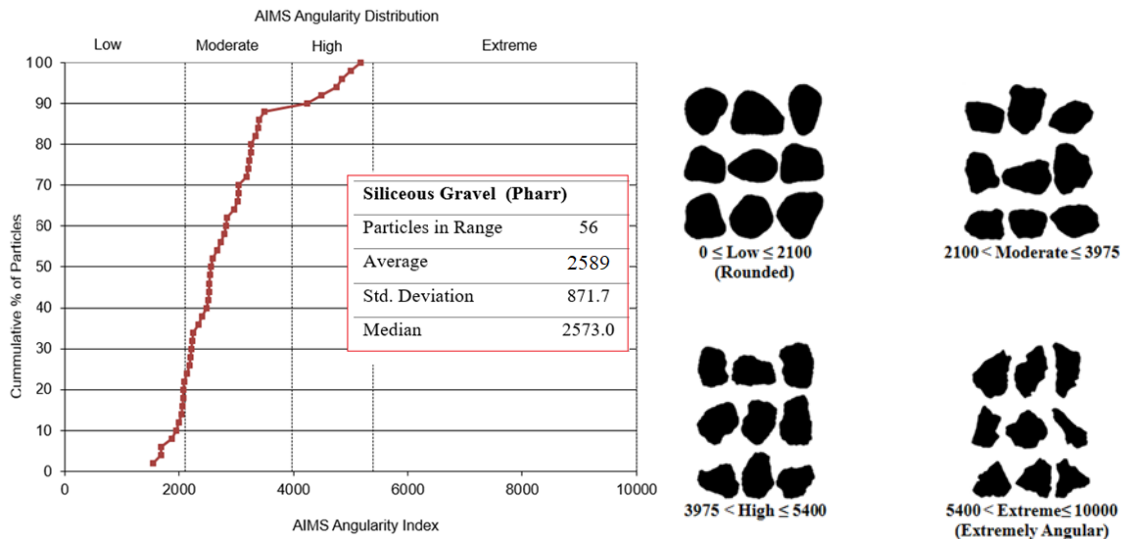


Figure 5-17: Angularity Distribution of Siliceous Gravel from Pharr.

Figure 5-18 represents the average of angularity values for all aggregate base presented in the experiment design. As exhibited in the plot, siliceous gravel and crushed limestone aggregates sourced from Houston had the lowest and highest angularity indexes, respectively. This indicates that siliceous gravel sourced from Pharr mainly contains rounded particles, while crushed limestone aggregates had more angular particles.

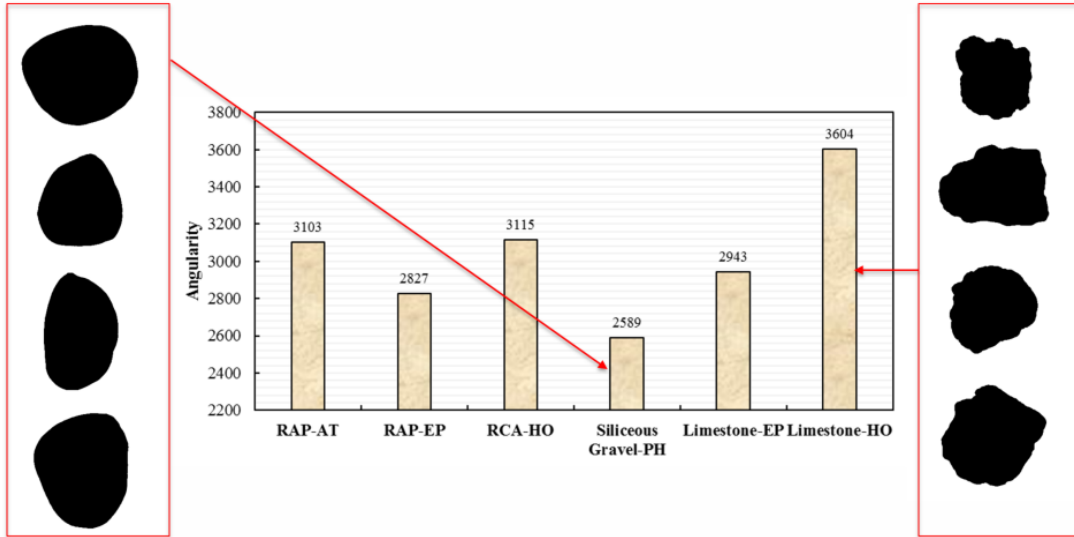


Figure 5-18: Variations of Angularity Index for Different Base Aggregates.

5.3.2 Texture Index

Texture index describes the relative smoothness or roughness of aggregate particle surfaces. Figure 5-19 presents the surface texture images of base aggregates obtained from the AIMS image-based analysis. With the top light on, the video microscope moves up on a vertical direction in order to focus on the aggregate surface. Through this method, the video microscope is able to capture the level of roughness of the aggregates and characterizes their surface texture on a scale of 0-1,000 where a value of zero is a polish surface and a value of 1000 is an extremely rough surface. The AIMS analysis demonstrates that reclaimed materials including RAP and RCA contain particles with high roughness surface texture, while virgin aggregates consist of smoother aggregate particles. For instance, RAP materials sourced from El Paso with roughness particle surface and crushed limestone aggregates sourced from Houston with smoothness particle surface had texture indexes of 641 and 207, respectively.

Smoothness or Roughness of the Particle Surfaces

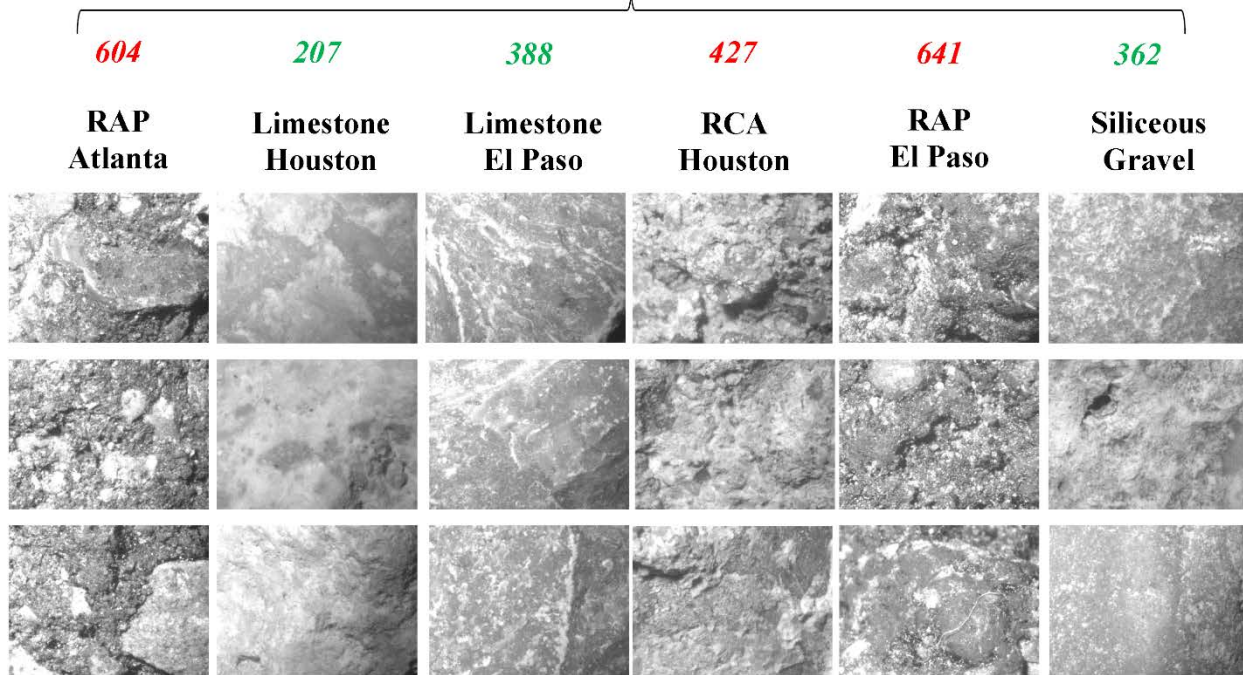


Figure 5-19: Surface Texture Index for Different Base Aggregates.

5.3.3 Form Index

Form index describes the overall three dimensional shape of aggregate particles such as round, elliptical, and flat. The AIMS equipment calculates the sphericity of aggregates by sorting the three dimensions of particles based on the length as shown in the following equation:

$$Sphericity = \sqrt[3]{\frac{D_s D_m}{D_l^2}} \tag{Equation 5-2}$$

where D_s is shortest dimension of aggregate particle, D_l is longest dimension of aggregate particle, and D_m is dimension of aggregate particle perpendicular to both D_s and D_l .

The comparative results of sphericity for the different course materials are presented in Figure 5-20. This graph provides valuable insight for comparative analysis for the sphericity and elongation of the particle. The results showed that crushed limestone aggregates sourced from El Paso exhibited relatively lower sphericity index (0.688) compared to other permutation of experiment design, while crushed limestone aggregates sourced from Houston was the most spherical material with a value of 0.734. This indicates that limestone aggregates specimens sourced from El Paso should have relatively higher amounts of flat and elongated aggregates in comparison with other mixture.

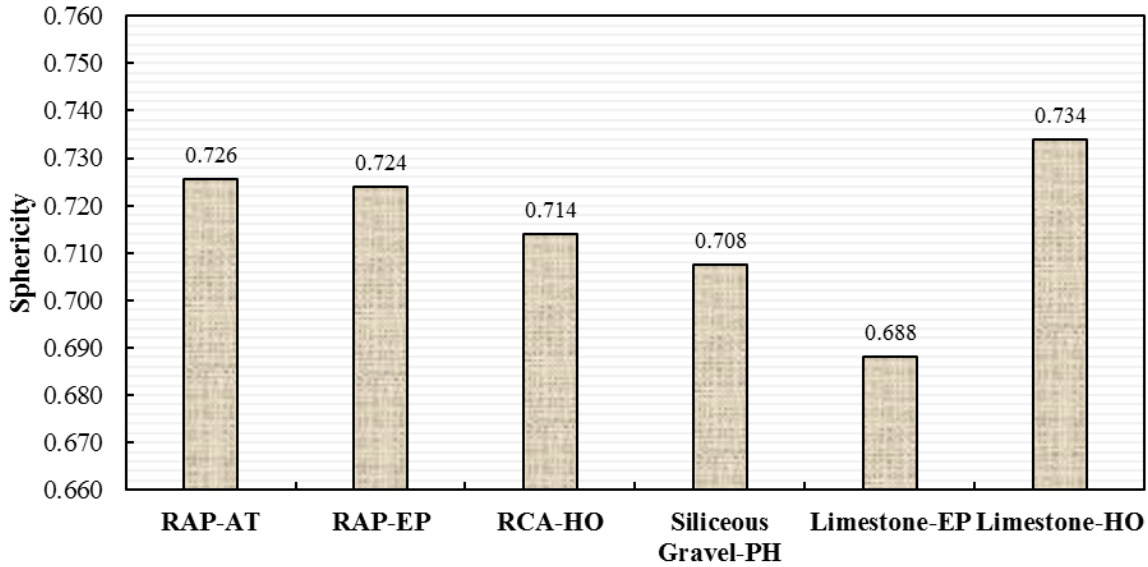


Figure 5-20: Variations of Sphericity Distributions Based on Different Coarse Aggregates.

To examine the effect of aggregate size on the strength properties of cement treated base materials, UCS and IDT test results were compared to the aggregate size obtained from AIMS analysis. Figure 5-21 present the relationships between strength properties of the cement treated base with sphericity of aggregates. The descending nature of the trend lines suggests a direct correlation between the compressive and tensile behavior of the cement stabilized materials with sphericity of aggregates. In other words, permutations with lower sphericity exhibited higher compressive and tensile strengths compared to other counterparts in the experiment matrix. Therefore, it can be concluded that elongated and flat particles such as crushed limestone aggregates sourced from El Paso perform better under compression and tension in the cement treated base layers of pavement structures.

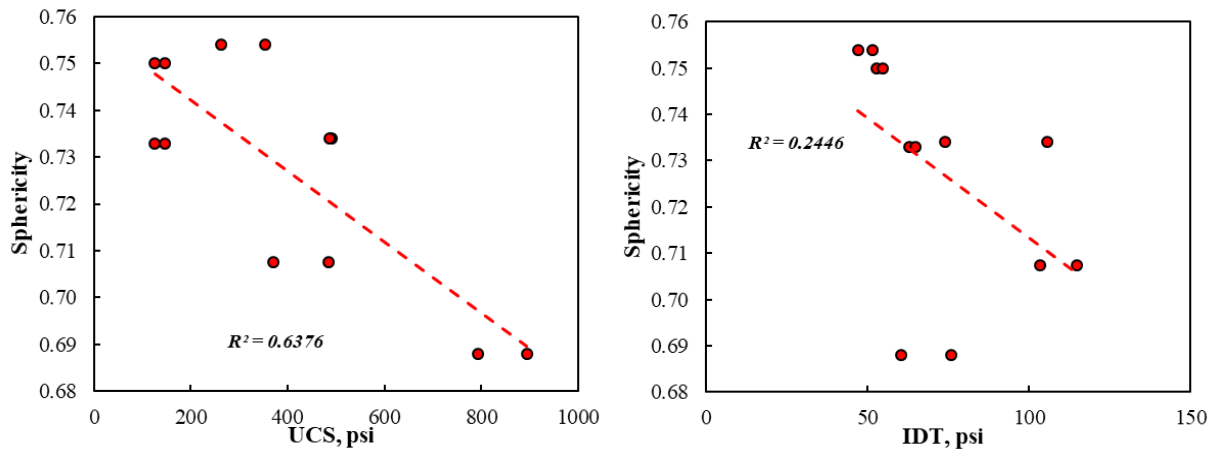


Figure 5-21: Relationship between Tensile and Compressive Strengths Stabilized Materials with Sphericity of Aggregates.

5.4 Dry Powder Mixing versus Slurry

The stabilizer is allowable to spread onto the road in the dry or slurry form based on the existing protocols as shown in Figure 5-22. Stabilization guidelines just recommends that adding the stabilizer as a slurry may increase the fluid content of the soil beyond optimum levels, and it should not be used if soil moisture contents are already high. California Department of Transportation (Caltrans) also considered the application of powdered stabilizers such as lime, cement, fly ash as a slurry instead of as a dry powder to prevent loss by wind and to limit uneven distribution, which could lead to areas of over and under stabilization and consequent weak spots or spots with excessive shrinkage (Figure 5-23). Therefore, parameters pertaining to the uniform distribution of the stabilizer in the mix such as dry powder mixing versus slurry mixing need to be properly identified and incorporated in this study to better guide construction practitioners. Figure 5-24 shows the slurry and dry powder mixing procedures in the laboratory that simulate field condition.



Figure 5-22: (a) Slurry Mixing and (b) Dry Powder Mixing in the Field.

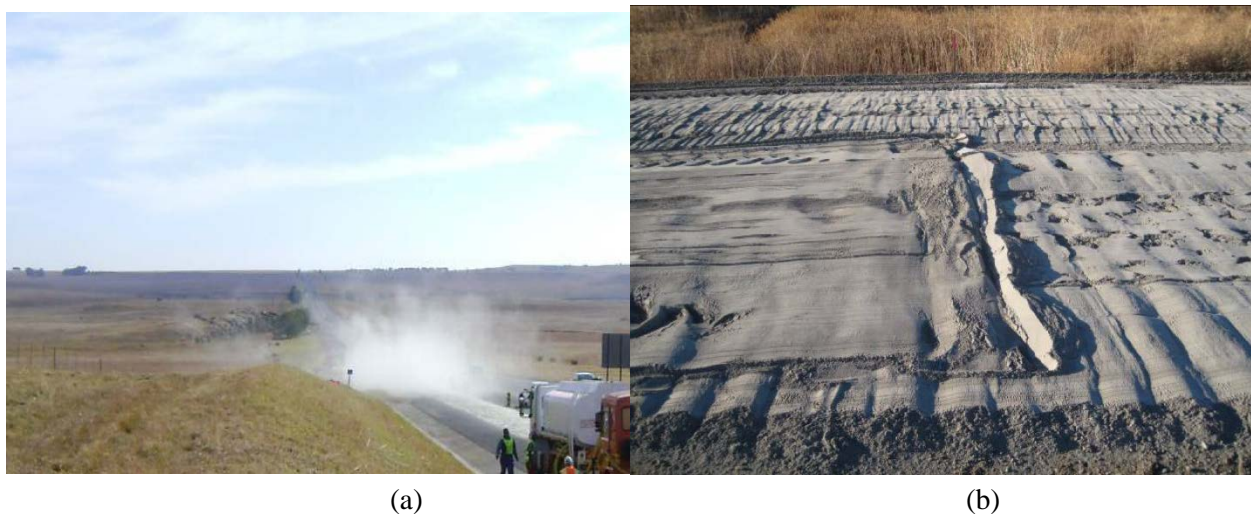


Figure 5-23: (a) Cement Loss by Wind, (b) Uneven Distribution of Stabilizer on Road Surface (Caltrans, 2012).



Figure 5-24: Slurry and Dry Powder Mixing Procedures in the Laboratory

Figures 5-25 and 5-26 provide the unconfined compressive strength and indirect tensile strength tests results for stabilized granular materials with different mixing procedures. These plots are primarily based on the results of two replicates prepared considering slurry and powder mixing in the laboratory. No significant differences in the compressive strength was found between cement treated base mixes prepared with slurry mixing and powder mixing. Comparatively, cylindrical specimens prepared with cement powder mixing had significantly high tensile strength compared to the slurry mixing procedure. This underperformance of specimen preparation with slurry mixing is more pronounced for the virgin aggregates. For instance, the tensile strength of samples of crushed limestone aggregates sourced from El Paso and Houston improved by 166% and 53%, by using cement powder mixing in lieu of slurry mixing. This underscores the role of mixing procedure on the strength properties and uniformity of the cement treated mix.

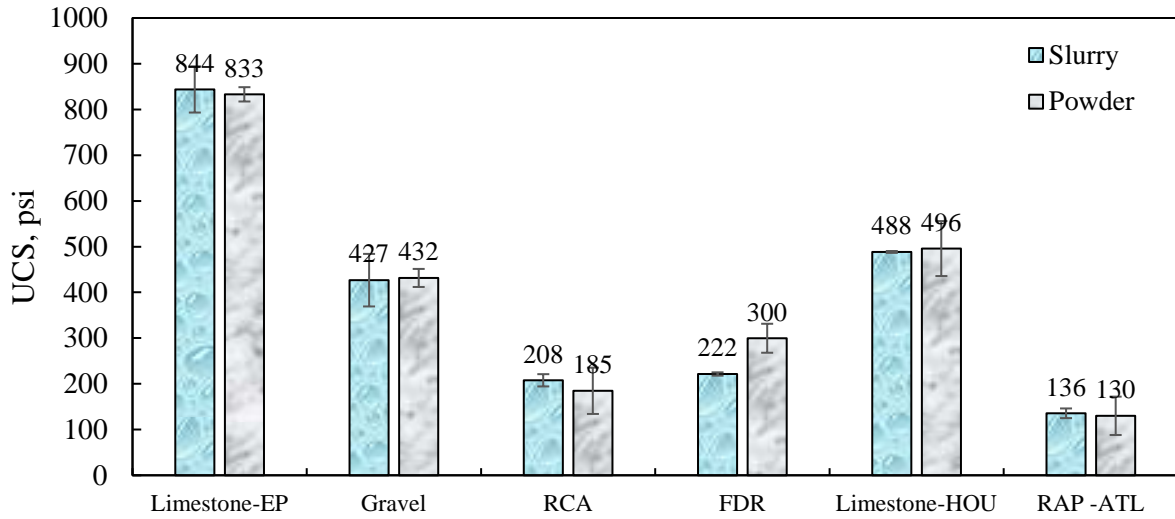


Figure 5-25: Unconfined Compressive Strength for Stabilized Granular Materials with Different Mixing Procedures.

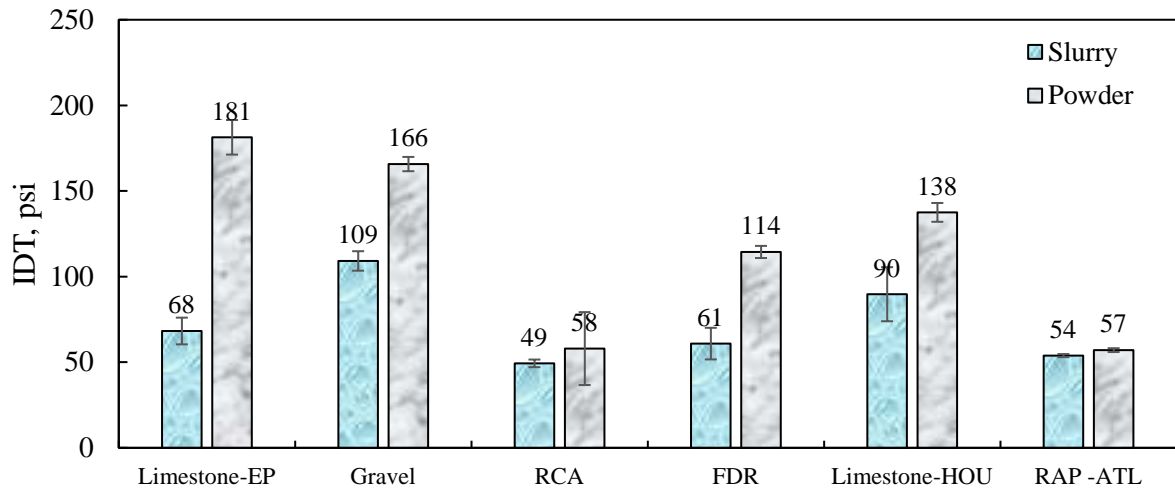


Figure 5-26: Indirect Tensile Strength for Stabilized Granular Materials with Different Mixing Procedures.

Figure 5-27 represent the comparison between tensile and compressive strengths improvements for each stabilized materials. The radar chart revealed that tensile strength of stabilized materials is more influenced by the mixing procedure than by the compressive behavior. This information can provide valuable insight on the selection of mixing procedures in the field to better guide practitioners in the construction part.

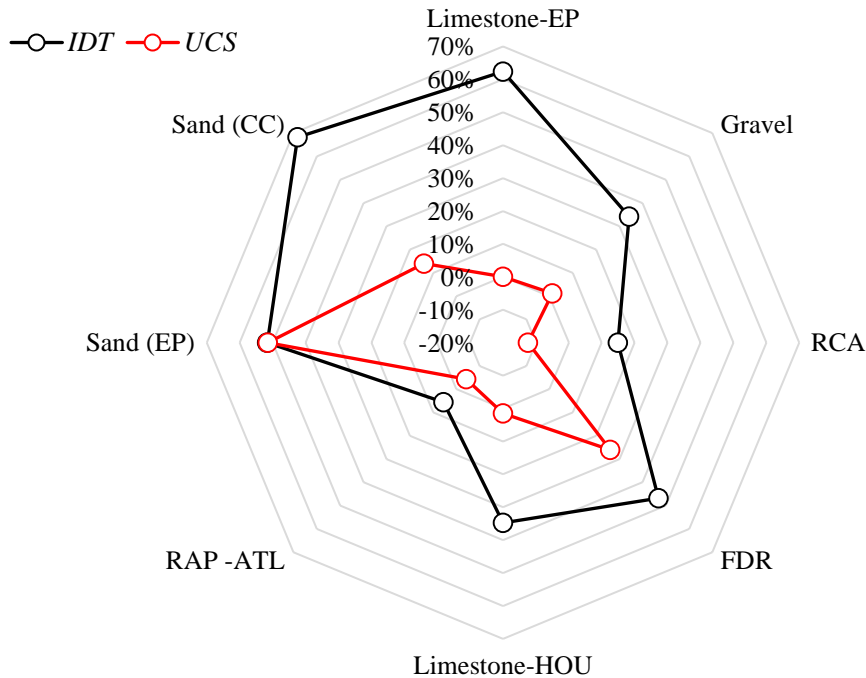


Figure 5-27: Compressive and Tensile Strengths Improvement for Stabilized Base and Subgrade Materials using Dry Powder Mixing In lieu of Slurry Mixing in the Laboratory.

5.5 Shrinkage in Cement Stabilized Materials

Shrinkage test was incorporated in the experiment design for characterization of shrinkage cracking of cement stabilized materials. In this test, prismatic specimens with dimensions of 4 in. × 4 in. × 20 in. were prepared and placed in a control environmental chamber with relative humidity of 50% and at an initial ambient temperature of 77°F. The chamber cycled the temperature between 77°F and 86°F using a saw-tooth pattern while the relative humidity is kept constant. After the target temperature in the chamber is reached, which takes about 20 minutes, the temperature is kept constant for 12 hours, in one full cycle (or two steps) per day. The constant temperature period is long enough to ensure a stable and uniformly distributed temperature in the prismatic sample. The amplitude of the temperature cycle (9°F) is selected to be small enough to maximize the number of cycles per day and obtain more shrinkage strain values at early ages. Overall, this test, which is based on temperature cycling, is capable of measuring the shrinkage strain of both lightly and heavily stabilized materials.

Figure 5-28 shows the relation between the time and shrinkage strain of cement stabilized base materials. As evidenced in the plot, the shrinkage rate increases as the time increases, then it tends to be stable after few days for majority of materials in the experiment design. Several researchers revealed the direct relationships between water loss in cementitious materials and shrinkage rate (Li et al., 2017; Kurda et al., 2019). They showed that the increasing rate of shrinkage is an indication of water loss in the cement stabilized systems. Therefore, shrinkage-time plots provide valuable information for the efficient selection of curing time needed for a specific aggregate type. For instance, the curing conditions are very important for the first 5 days after construction for

cement stabilized limestone aggregates in pavement foundations. Another noteworthy observation in the plot is the role of aggregate mineralogy in the process of shrinkage test. Measured values of shrinkage strain for crushed limestone aggregates and RCA materials at the completion of the test were lower than 0.04%. However, this value increased drastically to 0.20% after 7 days for the FDR materials. It can be inferred that the FDR materials had higher affinity for shrinkage cracking and therefore is more prone to performance degradation due to cracking damage in service.

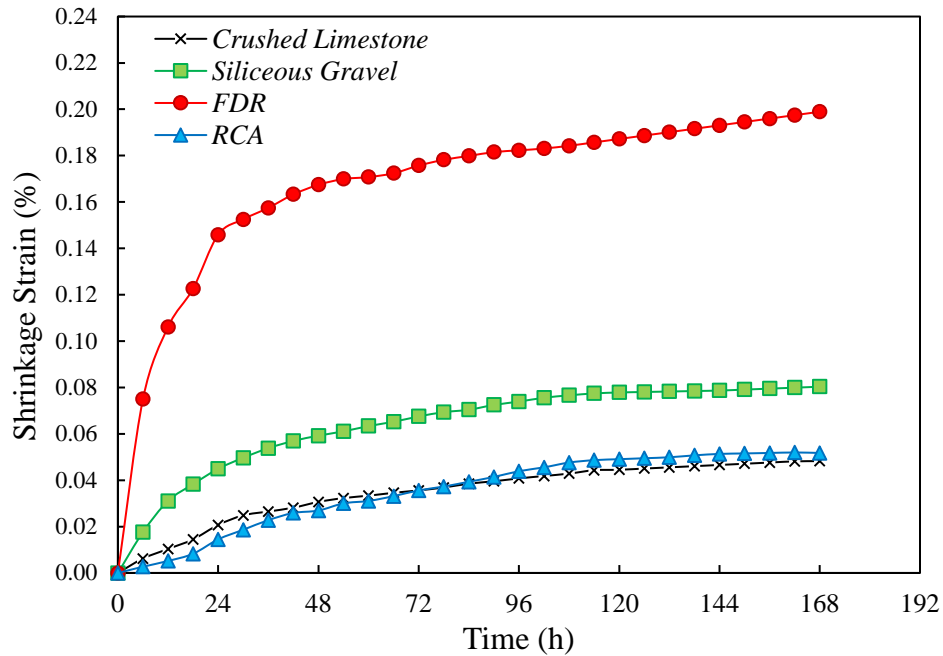


Figure 5-28: Shrinkage Strain versus Time for the Stabilized Base Materials with 4% Cement Content.

Figures 5-29 to 5-32 illustrates the variations of the shrinkage strain for limestone, RCA, FDR, and gravel materials stabilized with different cement contents ranging from 2% to 4%. The results showed the increase of shrinkage strain with the addition of cement content to the mixture. For instance, increasing the cement content from 2% to 4% for FDR materials resulted in more than 200% increase in the shrinkage strain while the same increase of stabilizer content for the crushed limestone aggregates resulted in approximately 25% improvements in shrinkage strain. This underscores the influence of the lithology and surface properties of the geomaterials as potential candidates for stabilized layers. Additionally, this indicates that cement treatment greatly alter the shrinkage rate of stabilized layers in pavement structures.

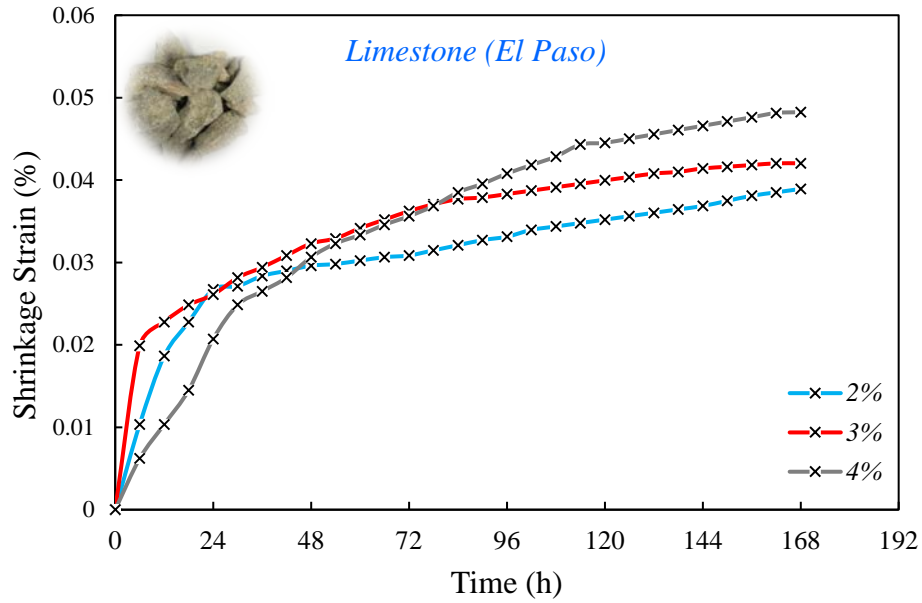


Figure 5-29: Shrinkage Strain versus Time for the Stabilized Crushed Limestone Aggregates (El Paso) with Different Cement Content.

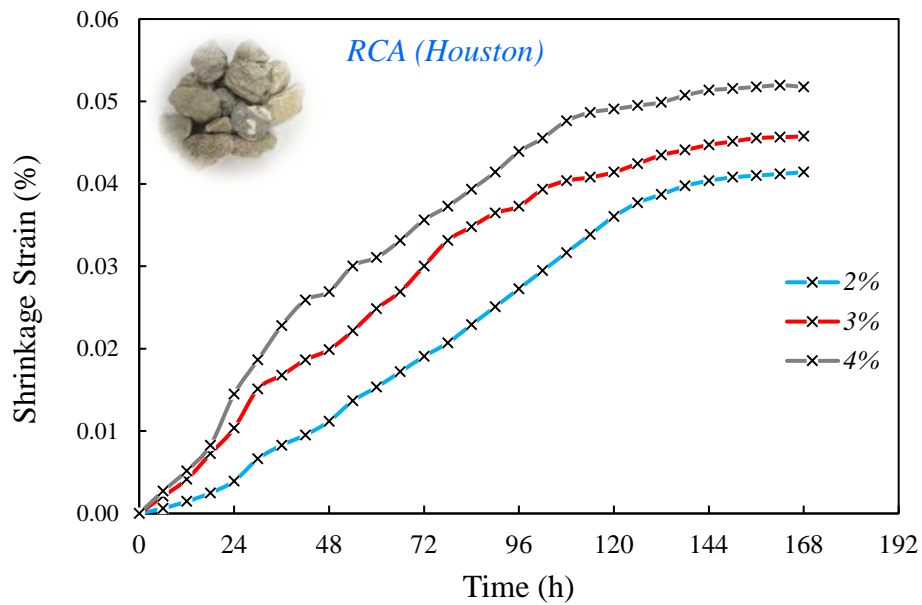


Figure 5-30: Shrinkage Strain versus Time for the Stabilized RCA Materials (Houston) with Different Cement Content.

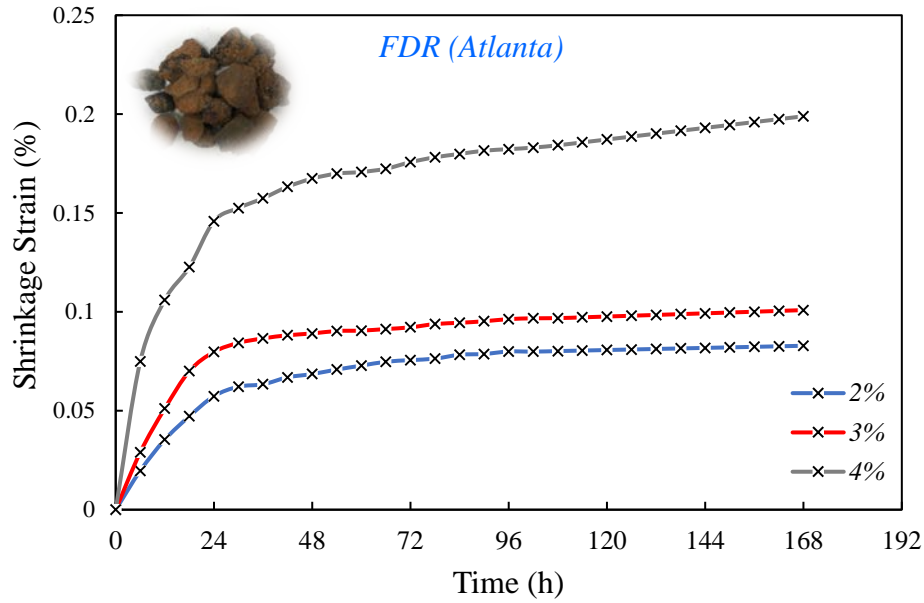


Figure 5-31: Shrinkage Strain versus Time for the Stabilized FDR Materials (Atlanta) with Different Cement Content.

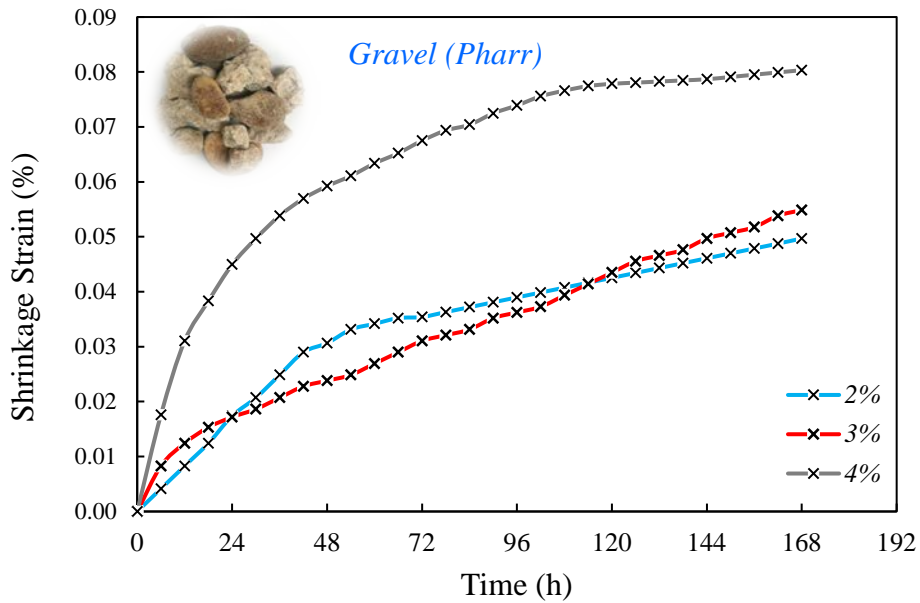


Figure 5-32: Shrinkage Strain versus Time for the Stabilized Siliceous Gravel Materials (Pharr) with Different Cement Content.

5.6 Flexural Strength Test

The flexural beam test is a direct measurement of modulus of rupture of cement stabilized materials and the resistance of these materials to bending and cracking. In this study, beam specimens for the flexural beam test with two dimension sizes, $4 \times 4 \times 20$ in. and $6 \times 6 \times 20$ in., were subjected

to a bending load at constant stress rate until failure as observed in Figure 5-33. The modulus of rupture from a third-point beam was determined by Equation 5-3:

$$MOR = \frac{P \times L}{b \times d^2} \quad \text{Equation 5-3}$$

Where MOR is the modulus of rupture (psi); P is the maximum applied load (lb.), L is the span length (in.); b is the average width of specimen (in). and d is the average depth of specimen (in.). Equation 5-6 is valid only if the fracture in the tension surface is within the middle third of the span length. If the fracture is outside by not more than 5% of the span length, the modified relationship presented in Equation 5-4 should be used:

$$MOR = \frac{3 \times P \times a}{b \times d^2} \quad \text{Equation 5-4}$$

Where a is equal to the average distance between the line of fracture and the nearest support measured on the tension surface of the beam. It is important to point out that the results of the test should be rejected if the fracture is outside by more than 5 percent of the span length.

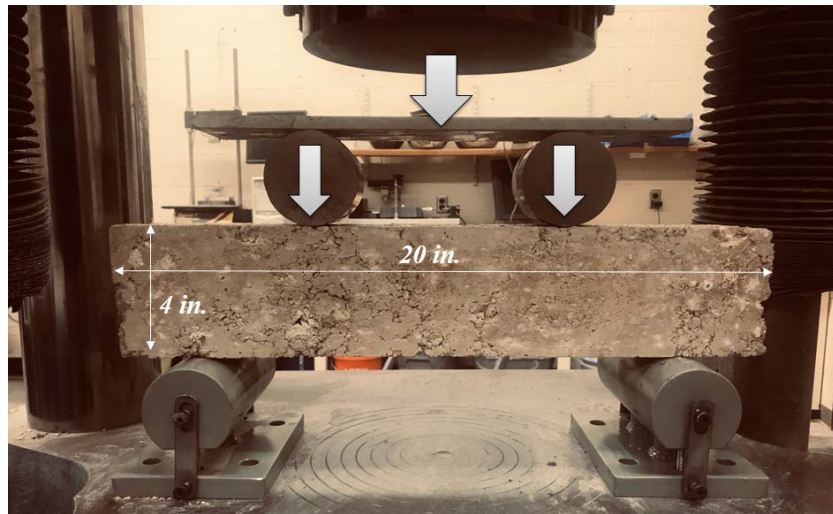


Figure 5-33: Flexural Beam Test Setup.

Figure 5-34 presents the modulus of rupture for different stabilized base materials with the beam size of 4 × 4 × 20 inches. The results clearly demonstrate improvement in flexural strength for all materials tested due to the increase of cement content in the mixes. This positive influence is more pronounced for crushed limestone aggregates. Another interesting observation depicted in this graph is the underperformance of stabilized siliceous gravel aggregates, and reclaimed materials in the flexural strength test. For example, the modulus of rupture for FDR and siliceous gravel materials stabilized with 3% cement content were 84 psi and 75 psi, while this value for limestone aggregates were 211 psi, respectively.

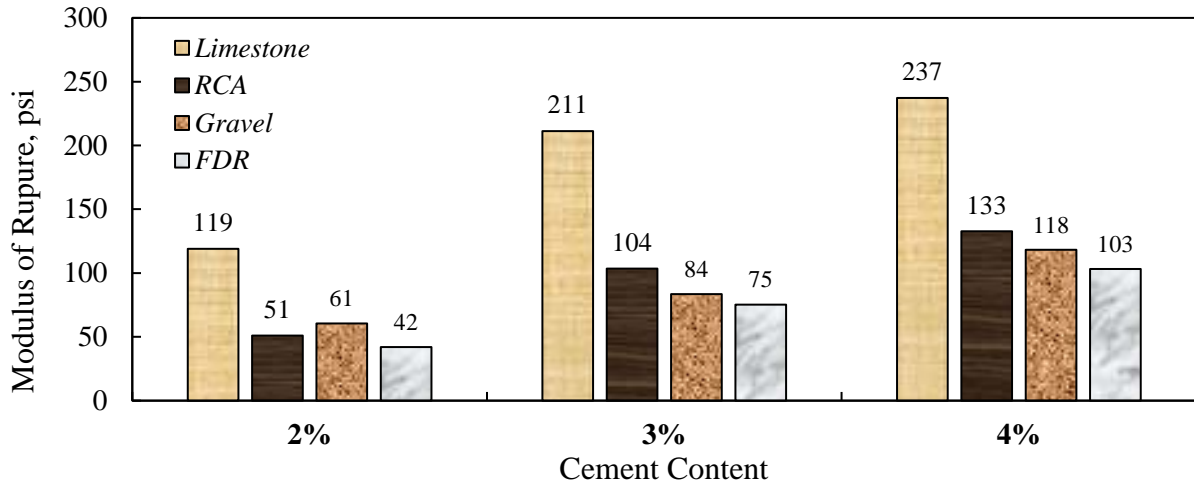


Figure 5-34: Modulus of Rupture for different Stabilized Base Materials (Beam Size: 4×4×20 in.).

For level 1 input in the MEPDG for flexible pavement design, the modulus of rupture can be determined from ASTM D1635 (ASTM, 2019), standard test method for flexural strength of soil cement using simple beam with third point loading. At input level 2, modulus of rupture can be also estimated from the unconfined compressive strength testing of the cured chemically stabilized samples. This value can be conservatively estimated as being 20% of the UCS (MEPDG). At input level 3, modulus of rupture is estimated from experience or historical records based on the types of materials, for instance this value is 200 psi and 100 psi for cement stabilized aggregate and soil cement, respectively. Execution of the full spectrum of the flexural strength test is a costly and time-consuming undertaking for small projects, therefore, a series of relationships between the UCS and IDT with the modulus of rupture were developed in this study. Such models can serve as a starting point to provide an estimate of the modulus of rupture for stabilized reclaimed materials for practitioners and pavement design engineers.

Figure 5-35 provides the relationship between the indirect tensile strength and modulus of ruptures for cement stabilized base materials. The ascending nature of the trend line suggest a direct correlation between the tensile and flexural behaviors of the cement stabilized materials. In other words, permutations with higher tensile strength exhibited higher modulus of rupture compared to other counterparts in the experiment matrix.

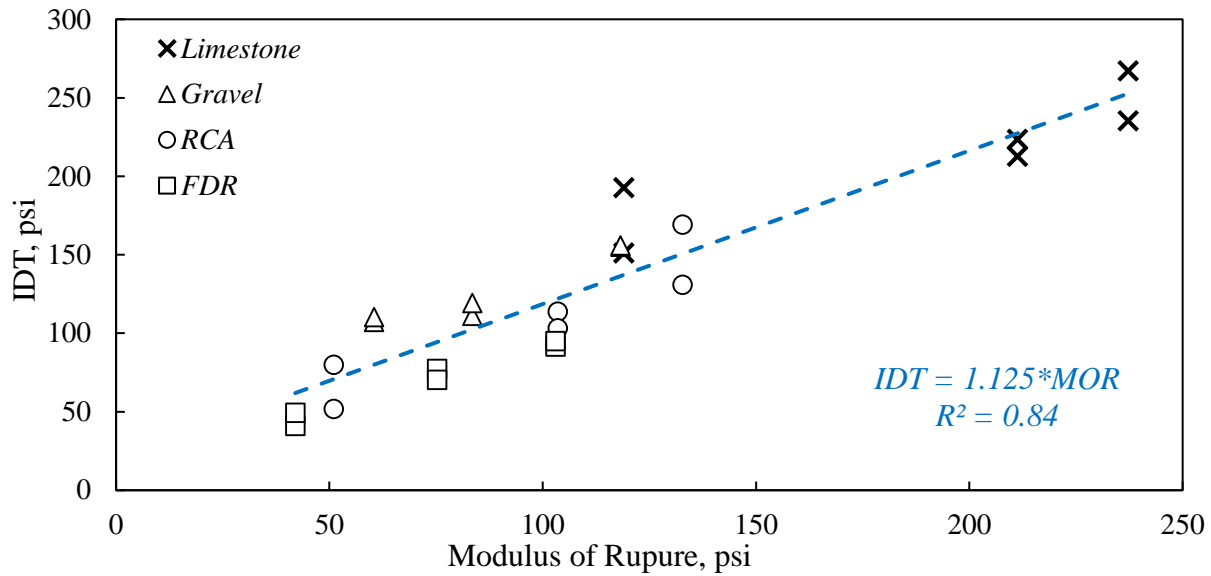


Figure 5-35: Relationship between Indirect Diametrical Tensile Strength and Modulus of Rupture for Cement Stabilized Base Materials (Compaction Method: Vibratory Hammer).

Equation 5-5 presents the relationship between the modulus of rupture and tensile strength of the cement stabilized systems. The model is based on the IDT and third point beam testing of 24 permutations in the laboratory.

$$IDT = 1.125 \times MOR \quad (R^2=0.84) \quad \text{Equation 5-5}$$

Figure 5-36 presents the relationship between modulus of rupture and unconfined compressive strength. This relationship suggests that the modulus of rupture from the third point beam test is approximately 30% of the unconfined compressive strength of the cement stabilized materials. The results were relatively different with models developed by MEPDG. This could be due to incorporation of different types of aggregates such as RCA, FDR, marginal and virgin aggregates in the developed model. The relationship developed between the compressive strength and the modulus of rupture is presented in Equation 5-6.

$$UCS = 3.12 \times MOR \quad (R^2=0.85) \quad \text{Equation 5-6}$$

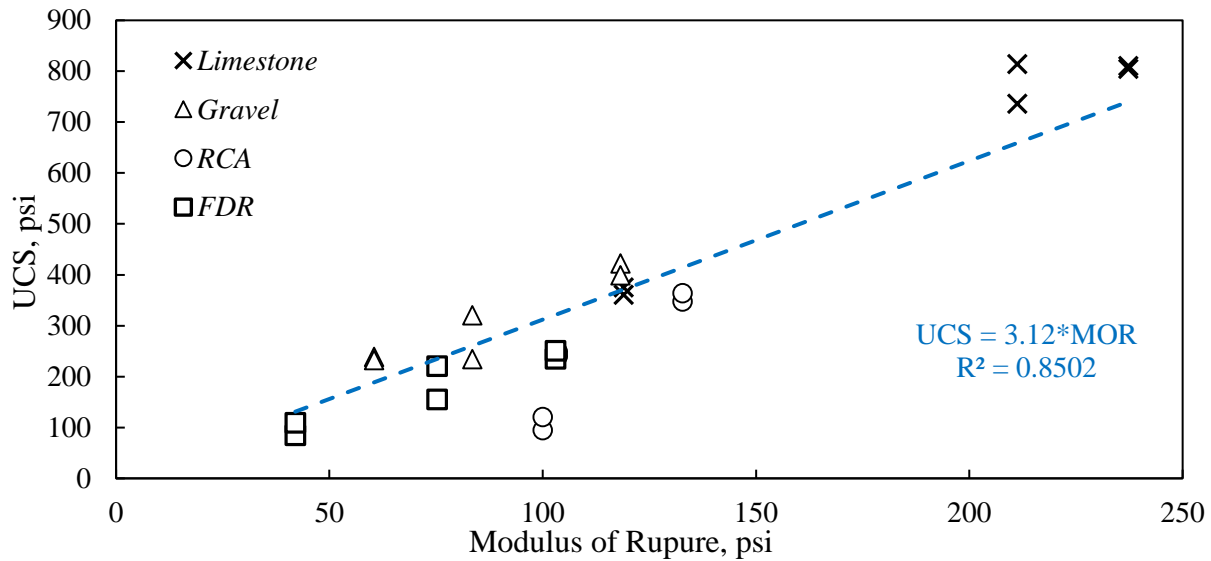


Figure 5-36: Relationship between Unconfined Compressive Strength and Modulus of Rupture for Cement Stabilized Base Materials (Compaction Method: Vibratory Hammer).

5.7 Micro-Structural Analysis with X-Ray Computed Tomography Imaging

This section describes the use of X-ray computed tomography imaging technique toward the nondestructive characterization of internal structure of stabilized base aggregates. This technique was used to identify the porosity distribution with depth and analyze the non-uniformity of specimen compacted with different compaction procedures. This test consists of an X-ray source, detector, and specimen, which is located between the source and the detector as observed in Figure 5-37. X-rays of known intensities are emitted by the source, and then the intensities after the X-rays pass through a rotating sample is recorded by the detector. Once a full rotation is completed, the sample is shifted vertically by a fixed amount, which defines the slice thickness, until the end of the specimen is reached. The intensity values are used to measure the distribution of the linear attenuation coefficients within the sample in order to map into grayscale CT scan images. The density of the sample in each point can be showed by the grayscale intensity of each pixel ranging from 0 for black color to 255 for white color in the image. 1,830 horizontal image slices were taken for each specimen to visualize the internal macro-structure of the cement stabilized materials. The X-ray CT scan image files were then processed using the “ImageJ” software package (Ferreira & Rasband, 2012). The software has been developed for medical imaging purposes. The objective of the image processing was to partition the image content into solids and voids and measure the porosity (Figure 5-38). The post processed images were ultimately used to study the void structure difference between specimens compacted with impact hammer, gyratory compactor, vibratory hammer.

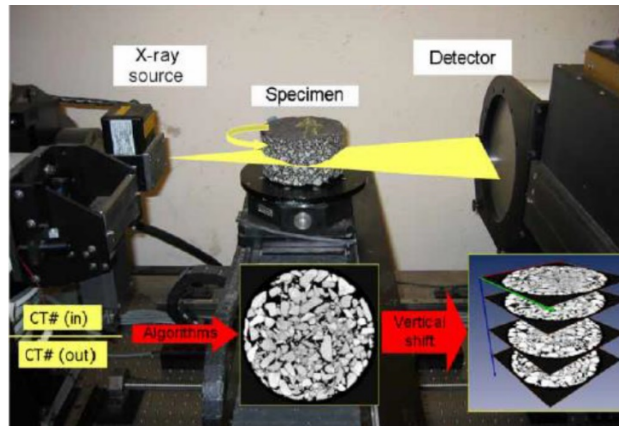


Figure 5-37: Equipment Components for X-ray Computer Tomography (CT) Test.

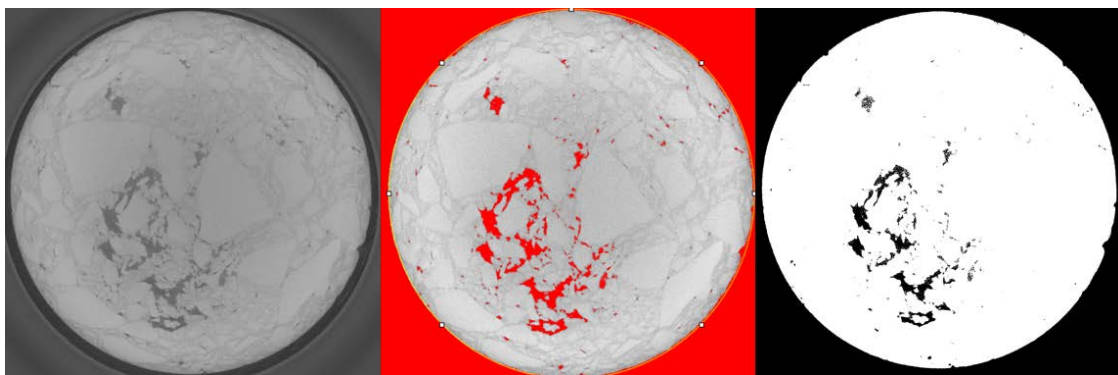


Figure 5-38: Example of Slice Image and Calculation of Porosity by Metallographic Image-Processing Software using ImageJ.

Figure 5-39 shows the porosity distributions over specimen depth (porosity gradient) for three specimens compacted with different compaction procedures. As depicted in the plot, the specimen compacted with impact and vibratory hammers shows clear interfaces between lifts and air void gradients within each lift. The interface lift area has relatively higher porosity, namely lower density, while the middle of each lift has lower porosity. On the other hand, the air void distribution of the gyratory compacted specimen indicates considerably more uniformity as compared to the vibratory and impact hammer specimens. The porosity gradient probably relates to the observed lower precision and repeatability of UCS and IDT test results on the stabilized aggregates compacted with the vibratory and impact hammers.

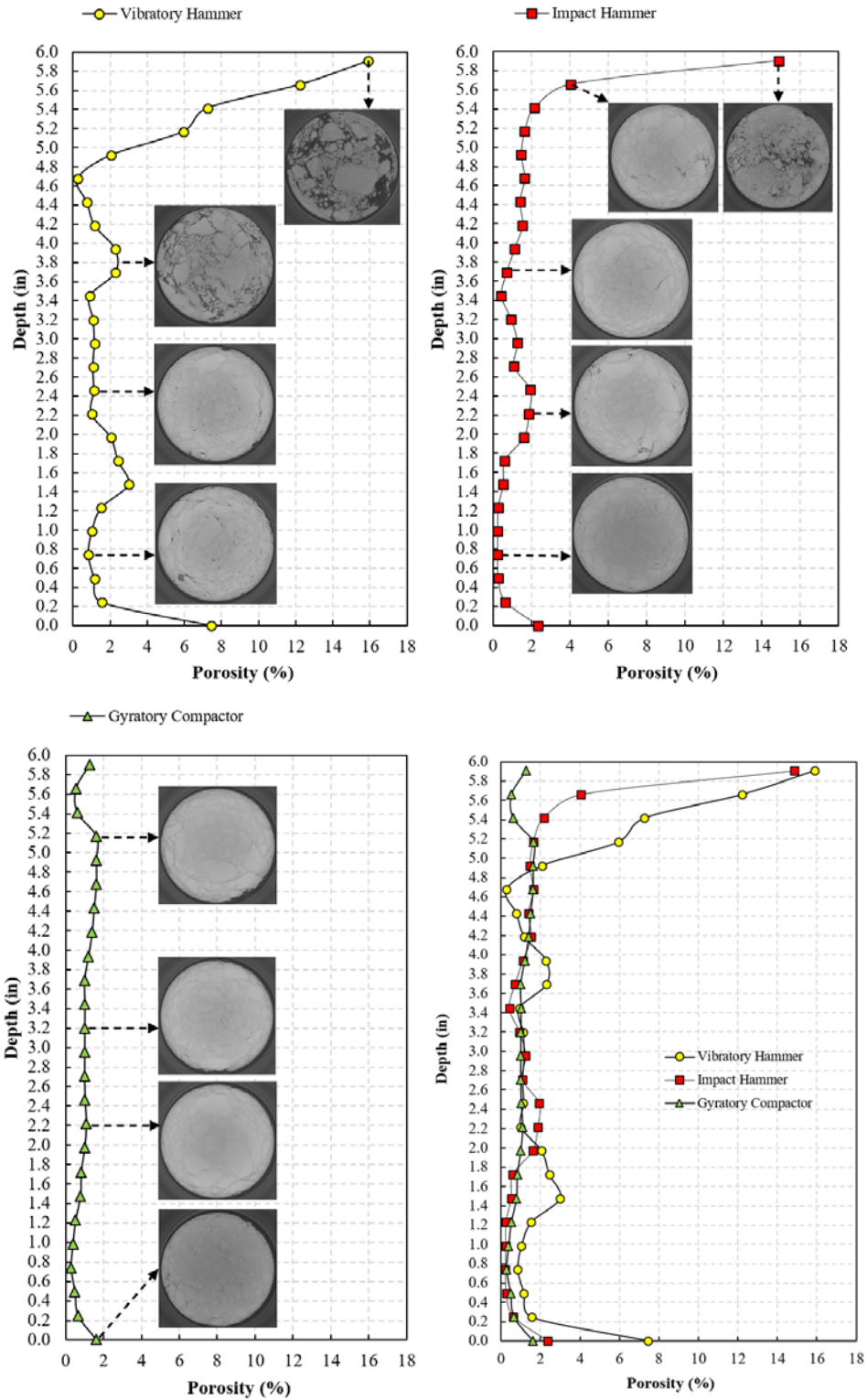


Figure 5-39: Porosity Distribution for Specimens Compacted with (a) Vibratory Hammer, (b) Impact Hammer, (c) Gyrotory Compactor, and (d) Porosity Comparison of Different Compaction Methods.

Figure 5-40 represents X-ray CT scanning images of stabilized base materials sourced from El Paso with different compaction methods. The plot shows non-uniformity and weak planes in specimen compacted with the vibratory and impact hammers while the specimen compacted with gyratory compactor shows relatively uniform structure throughout the height. Accordingly, the vibratory and impact hammer specimens exhibit porosity gradients even within each lift while the porosity of gyratory compactor specimen is fairly uniform.

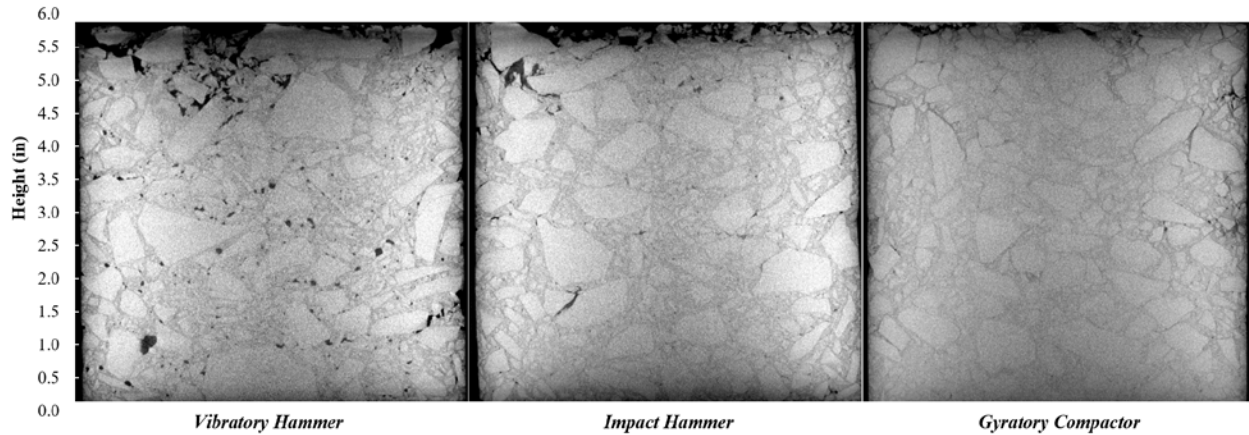


Figure 5-40: X-Ray CT Scan of Limestone Aggregates with Different Compaction Procedures.

Table 5-3 summarizes the calculated porosity parameters for specimens compacted with compaction methods. As demonstrated in the Table, the average porosity was 3.10, 1.79, and 1.00 for specimen compacted with vibratory hammer, impact hammer, and gyratory compactor, respectively. The maximum porosity for impact and vibratory hammers was ten times higher than gyratory compactor. The low variability of porosity and the lack of layer interface barrier between lifts can be main superior factors of gyratory compaction technique compared to the impact and vibratory hammers.

Table 5-3: Calculated Porosities from Different Compaction Methods

Compaction Method		Vibratory Hammer	Impact Hammer	Gyratory Compactor
Porosity (%)	Average	3.10	1.79	1.00
	Maximum	15.90	14.86	1.63
	Minimum	0.26	0.22	0.28
	STD	3.85	2.86	0.41

Chapter 6. Alternative Approaches for the Laboratory Evaluation of Moisture Susceptibility for Cement Stabilized Materials

6.1 Introduction

Moisture ingress significantly impacts on the serviceability and longevity of the transportation infrastructure facilities. Moisture enters pavement structures through various mechanisms such as infiltration through cracks and shoulders, vapour transport, and capillary action as shown in Figure 6-1. Moisture intrusion can give rise to the early development of distresses by creating pumping in pavement layers, reduced effective strength of pavement foundations, and erosion of the subgrade soils. Traditionally, the Tube Suction Test (TST) has been used to characterize the affinity of the unbound and stabilized aggregate bases to hold and transport moisture. There are several systematic shortcomings associated with the characterization of the moisture susceptibility of granular bases in using the TST test. This was the motivation to explore alternative approaches to mitigate such anomalies and refine the laboratory mixture design process of cement stabilized granular bases. Therefore, several alternative moisture susceptibility tests including submergence and backpressure saturation tests in conjunction with routine mechanical tests were incorporated in this study to determine the degradation of mechanical properties at elevated saturation states. To better characterize the influence of aggregate type and mineralogy upon moisture intrusion, several aggregate bases and subgrade materials were incorporated in this study.

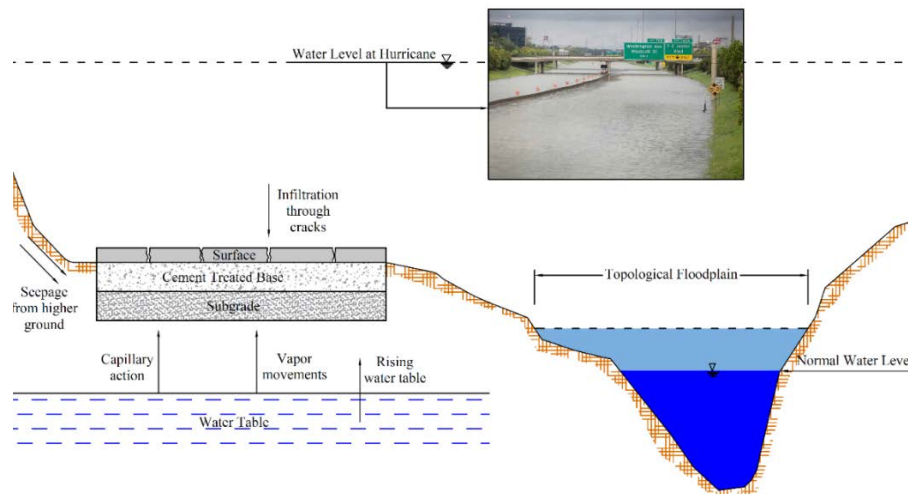


Figure 6-1: Mechanisms of Moisture Intrusion into Pavement.

6.2 Methodology

Five granular materials sources, namely limestone aggregate, Reclaimed Asphalt pavement (RAP), and Recycled Concrete Aggregate (RCA) as aggregate base, and two different subgrade materials from sandy and clayey soils sourced from El Paso were incorporated. Different ratios of reclaimed to virgin aggregates, namely 0/100, 50/50, 100/0, were incorporated in the experiment

design to study the strength and durability characteristics of various blends of reclaimed and virgin aggregate sources. Figure 6-2 presents the comprehensive experiment design for the initial assessment of moisture susceptibility protocols.

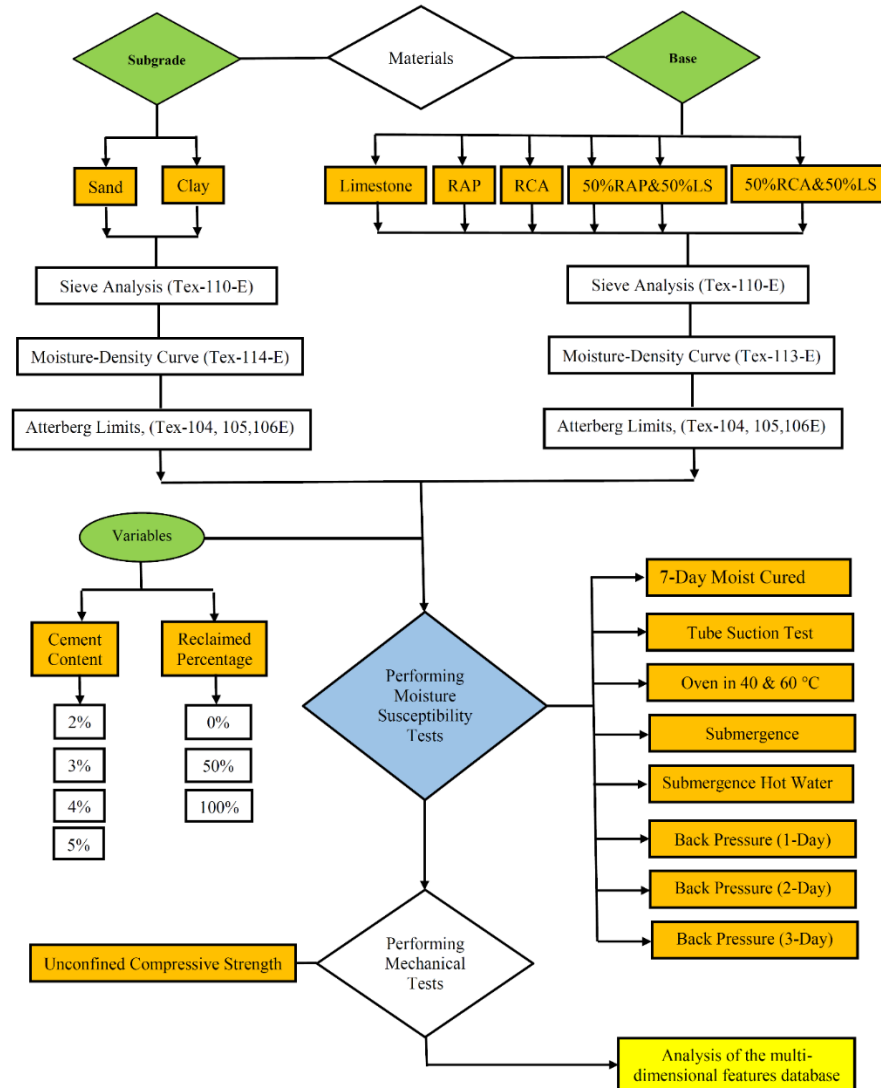


Figure 6-2: Flow Chart for the Execution of the Laboratory Tests.

6.3 Assessment of Moisture Susceptibility Protocols

Several moisture susceptibility tests such as tube suction test, backpressure saturation test at different durations, and multiple submergence protocols were incorporated in this study to evaluate the influence of moisture ingress on the mechanical properties of the stabilized materials. The main motivation for the inclusion of these approaches in the experiment was to study the relationship between the moisture intrusion mechanism and the loss of adhesive bonds in cement stabilized systems. The primary rationale for this test is that unreacted moisture trapped in the pore structure

can potentially degrade the stiffness properties of the stabilized layers and consequently jeopardize the longevity of the pavement structure. After the completion of the moisture susceptibility procedures, the specimens were subjected to unconfined compressive strength tests. The variations in the strength properties of the mixes were further studied to quantify the deleterious effect of moisture on the strength properties of the cement treated base and subgrade materials.

6.3.1 Effect of Temperature on the Strength Development

As stated earlier in this paper, the rationale for the heat treatment of the cement treated base and subgrade specimen is to accelerate the process of strength gain reactions prior to moisture susceptibility tests. Several researchers studied the role of heat treatment to replicate early stage strength; 7-day compressive strength; in less than 30 hours at elevated temperatures (Rao and Shivananda, 2005; Lu et al. 2012). However, excessive heat has the potential to adversely impact on the integrity of cementitiously stabilized materials (Wang et al. 2016). Mindess et al. (1981) indicated that higher rate of hydration at elevated temperatures (above 80°C) will lead to a lower ultimate strength. Therefore, it is imperative to select proper temperature range for the heat treatment of samples without compromising the strength properties of the stabilized mixes. For this reason, the research team devised a separate experiment to characterize the role of temperature and the duration of the heat treatment on the compressive strength of cement stabilized materials. The results were further compared with the traditional 7-day moist-cured specimen as the control system. Figure 6-3 shows the synergistic influence of temperature and heat treatment duration on the compressive strength of limestone materials stabilized with 2, 3, and 4% cement in the mix. The control system, 7-day moist-cured, were placed in the moisture chamber at 73 °F (23 °C) and 95% relative humidity for 7 days prior to compressive strength test. For the heat treated systems, shorter durations were selected for higher temperatures. In other words, two variations of 1-day at 60°C and 2-days at 40 °C were incorporated in the study. The compressive strength results of 18 stabilized specimen, summarized in Figure 6-3, clearly shows the role of the temperature and heat treatment duration on the compressive strength of laboratory tested samples. The results show comparable compressive strength properties of 1-day at 60°C and 2-days at 40°C with the benchmark 7-day moist-cured for 2% and 3% cement stabilized systems. For 4% cement stabilized systems, the compressive strength values tend to diverge. One plausible explanation for this behavior could be attributed to the time-dependency of hydration reactions. The abundance of hydration products in 4% cement stabilized systems, coupled with provided moisture for the duration of 7 days in the control systems could be the culprit for higher strength properties compared to specimen cured for 1-day and 2-days. Therefore, the compressive strength of 2-day 4% cement stabilized systems were approximately 6% lower than the control system cured for 7 days at 23°C in the moisture chamber. Another possible explanation for lower strength values of 4% cement treated specimen can be attributed to the initiation of the micro-cracks in heavily stabilized systems, and therefore lower strength properties due to shrinkage cracking potential in overly rigid stabilized materials.

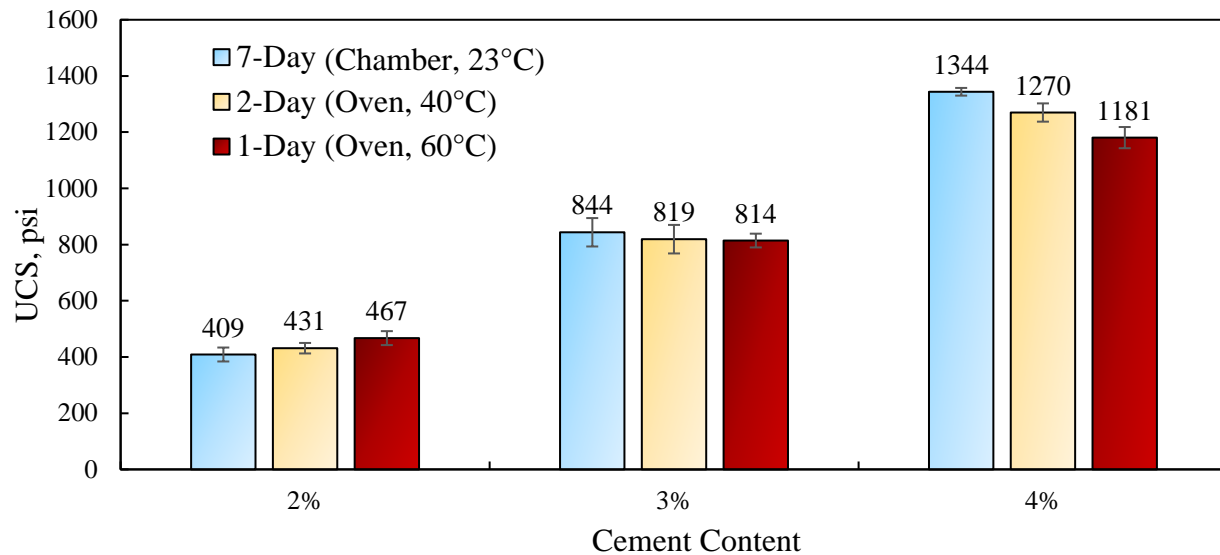


Figure 6-3: Unconfined Compressive Strength of Stabilized Limestone Aggregate over a Range of Curing Temperature and Time with Different Cement Content.

6.3.2 Analysis of Accelerated Moisture Susceptibility Protocols

The compressive strength results presented in this section was the basis for the selection of the temperatures and durations of heat treated submergence protocols. This information was further utilized to develop accelerated moisture susceptibility protocols in lieu of traditional 10-day TST test. Figure 6-4 provides the unconfined compressive strength test results for virgin and blends of reclaimed specimen cured for 7 days at 95% relative humidity at 23°C. This plot is primarily based on the averages of two replicates of stabilized specimens with 3% cement content for base materials and 5% cement content for subgrade soils. The results illustrate that the recycled materials significantly underperformed in terms of compressive strength compared to the virgin aggregates. The compressive strength for RAP and RCA materials were less than 15% and 40% of good quality crushed limestone base materials, respectively. Another noteworthy observation was the significant improvement of compressive strength of recycled materials by blending with virgin aggregate materials. As observed in the plot, the compressive strength for blends of RAP and limestone base materials at 50% blend ratio was over twice the stabilized mixture with 100% of RAP materials. In other words, the strength properties significantly improved by replacing half of the mixture with good quality crushed limestone base materials. Such blending techniques can be a useful means to utilize reclaimed and marginal materials that do not pass traditional requirements for incorporation in treated pavement layers.

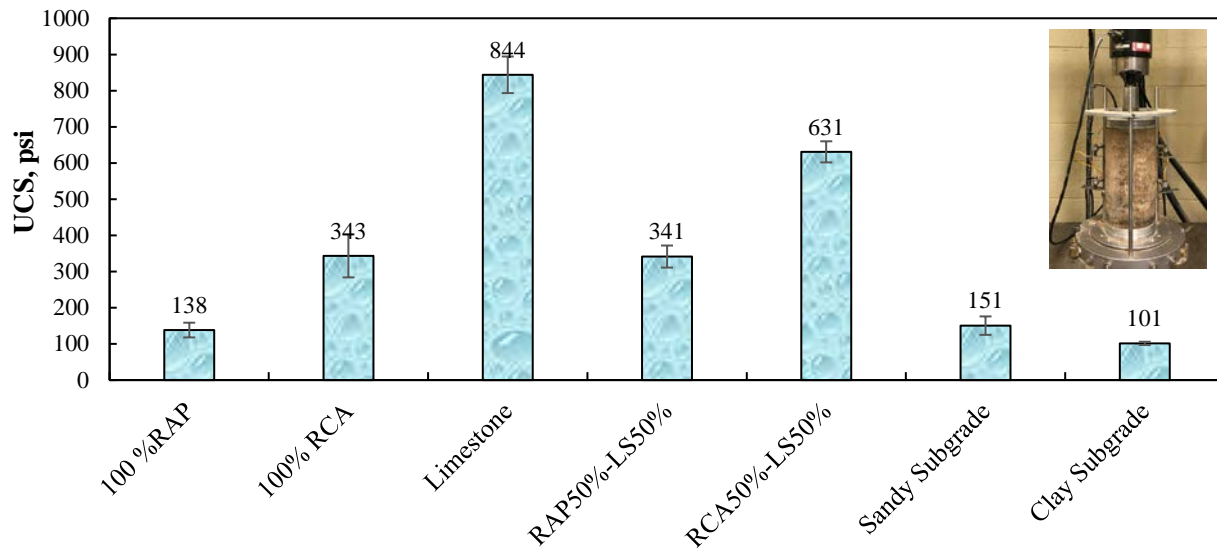


Figure 6-4: Comparison of the Unconfined Compressive Strength for Different Cement Stabilized Materials System for 7-Day Moist Cured Samples.

As stated earlier, six different moisture susceptibility approaches, namely Tube Suction Test (TST), backpressure saturation tests for 1, 2, and 3 days (BP1, BP2, and BP3), Submergence (S) test, and Hot Water Submergence (HWS) procedures were incorporated in the experiment design to evaluate the influence of moisture ingress on the compressive strength of the stabilized systems. The UCS results for the 7-day (7D) moist cured specimen were used as the benchmark for comparative purposes. Figure 6-5 provides the compressive strength results for the cement stabilized crushed limestone base materials subjected to various moisture susceptibility tests. As evidenced in the plot, stabilized specimens subjected to TST had the highest compressive strength, while the 3-Day backpressure saturation protocol resulted in the specimen with lowest compressive strength. The backpressure saturation results showed that the saturation period had negligible effect on the compressive strength properties of stabilized systems with good quality crushed limestone base materials. Another noteworthy observation from the plot pertains the compressive strength results of the TST procedure; capillary saturation; compared to inundation protocols. The compressive strength of the cement stabilized limestone materials subjected to 10-capillary soak turned out 20% higher compared to the 7-day moist-cured specimen. The improvements in strength properties could be attributed to the provided moisture through capillary action in the TST procedure that partakes in the time-dependent hydration reactions. This underscores the limitations of the TST procedure to capture the deleterious effect of moisture on degradation of the strength properties of cementitiously stabilized systems with good quality aggregates in the mix.

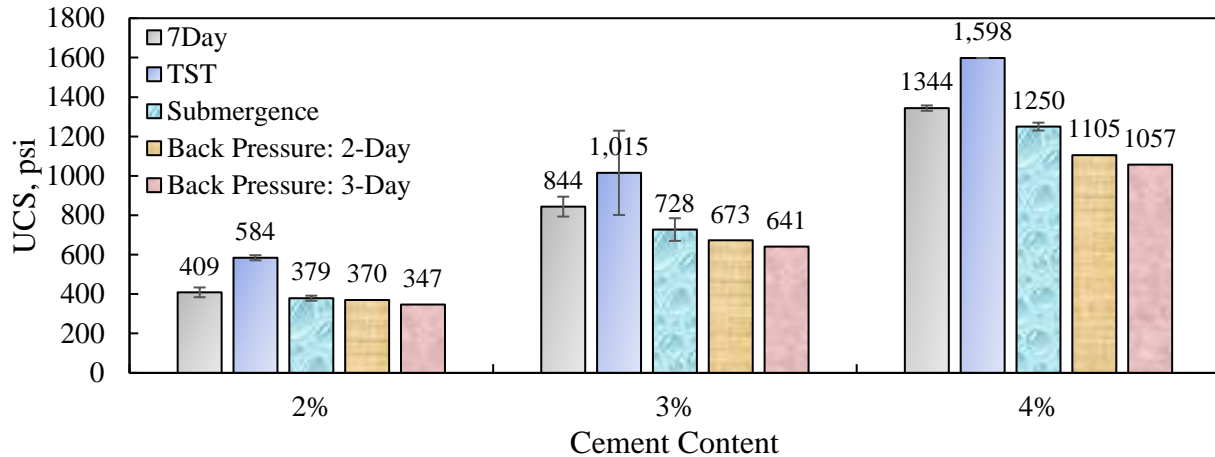


Figure 6-5: Unconfined Compressive Strength Results for Cement Stabilized Limestone Aggregates Sourced from El Paso with different Curing/Conditioning Procedures.

Figure 6-6 present the unconfined compressive strength results for 56 stabilized specimen subjected to different curing and moisture susceptibility tests in this study. The results are sub-categorized for stabilized RAP, RCA, blends of RCA and limestone (RCA50%-LS50%), and blends of RAP and limestone (RAP50%-LS50%). All permutations were stabilized with 3% cement. This plot clearly shows the degradation of the compressive strength properties when specimens were subjected to protocols that simulate prolonged inundation of stabilized systems. As evidenced in the plots, the loss of strength properties of the stabilized specimen was greatly influenced by aggregate types and the adopted moisture susceptibility protocols. For instance, the 3% cement stabilized specimen consisted of 100% RAP showed significant reduction in compressive strength from 138 psi for benchmark 7-day moist cured to 35 psi when subjected to the backpressure saturation procedure for 3 days. Similarly, the stabilized specimen consisted of 100% RCA materials showed approximately 60% loss of strength when subjected to 3-day backpressure saturation protocol. The traditional TST moisture susceptibility test however, resulted in merely 2% reduction in the compressive strength compared to the benchmark. This underscores the significance of the moisture susceptibility protocol to realistically simulate field conditions during flooding and natural disasters for the resilient design of transportation infrastructure facilities. Evidently, the type of reclaimed materials as well as the blend ratios greatly influence the moisture susceptibility of the mixes as observed in the plots. The comparisons between the 100% reclaimed materials and 50% blends of reclaimed materials with good quality crushed limestone base shows the significance of aggregate type and mineralogy on the moisture susceptibility of the mixes. For instance, the unconfined compressive strength of RAP materials for all moisture susceptibility protocols significantly improved by 3 to 4 times when half of reclaimed materials was replaced by limestone. This information can provide valuable guidelines for the incorporation of reclaimed materials in pavement foundations in coastal areas prone to flooding and natural disasters.

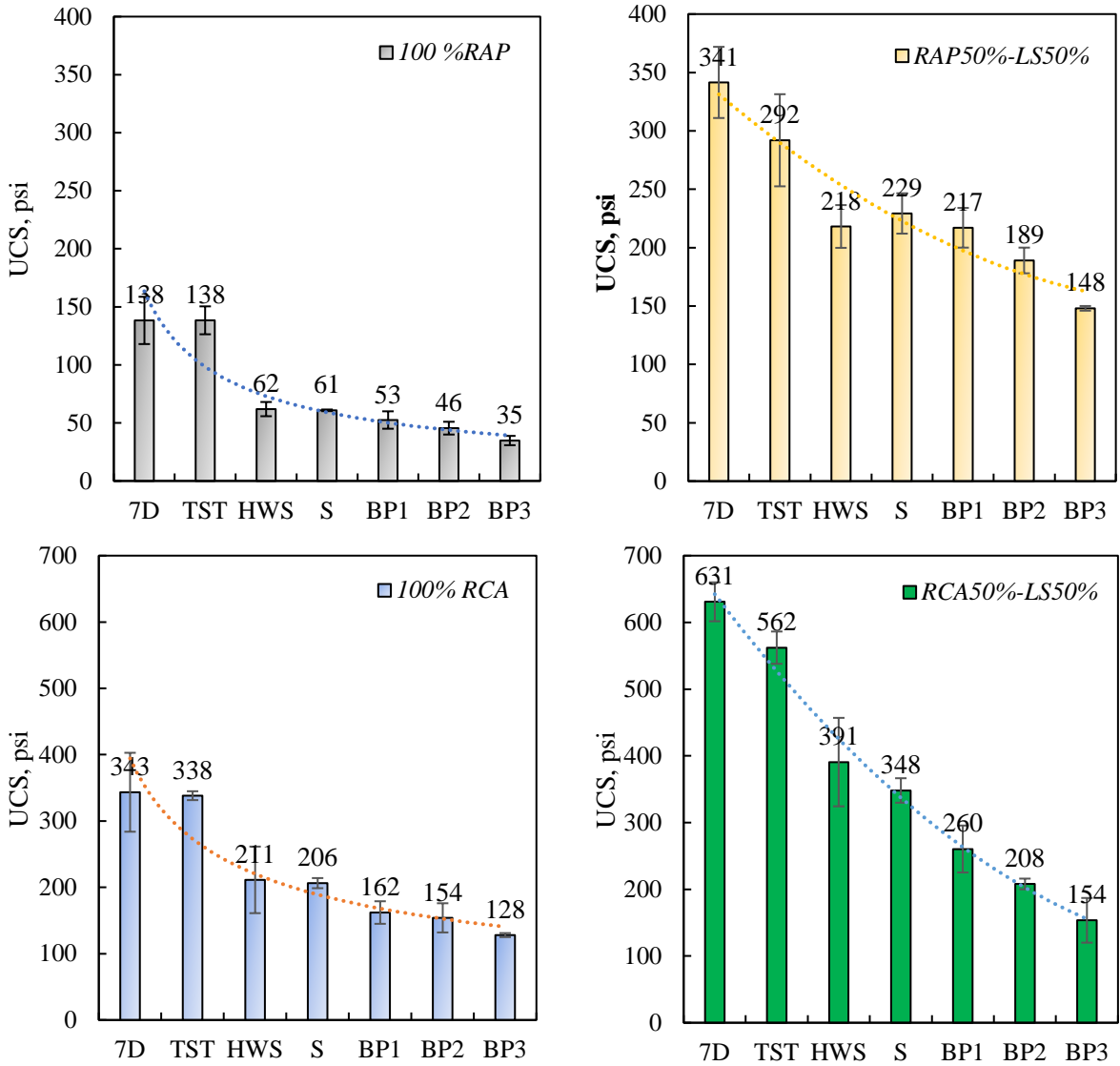


Figure 6-6: Unconfined Compressive Strength Results for Stabilized Recycled Materials with Different Curing Conditioning Procedures.

Figure 6-7 present unconfined compressive strengths test results for 5% cement stabilized sandy and clay subgrade soils subjected to various moisture curing/conditioning procedures. As indicated in the plot, both sand and clay soils yielded comparable results for the selected sources of subgrade materials in this study. The submergence protocol resulted in the lowest compressive strength for both sandy and clayey subgrade soils. This behavior can be attributed to the role of the confining pressure in the backpressure saturation tests. The 10 psi confinement can potentially help mitigate the disintegration of the particles and maintain the integrity of the stabilized specimen during the backpressure saturation procedure.

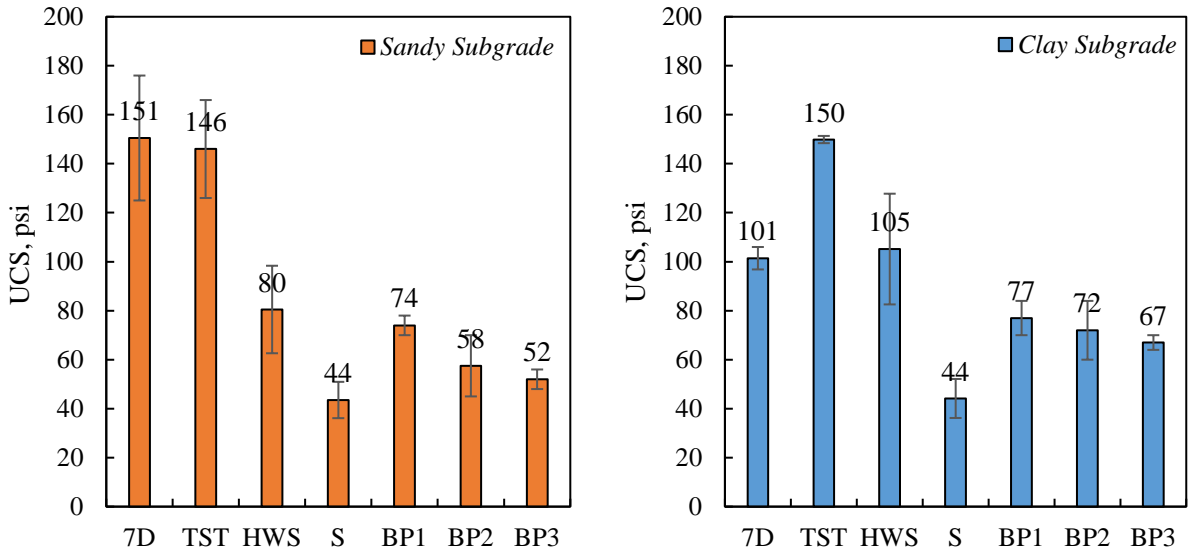


Figure 6-7: Unconfined Compressive Strength Results for 5% Cement Stabilized Subgrade Soils with Different Curing/Conditioning Procedures.

One of the major practical concerns in the submergence test for the subgrade soils are associated with the dissolution of outer specimen layer in water. The stabilized subgrade specimen disintegrates during the submergence process by absorbing water from all its sides. This issue was fully solved in this study by capping the subgrade specimens with porous stones and placing them in a rubber membrane sleeve to keep the uniformity of specimen during the submergence test. Figure 6-8 shows stabilized clayey and sandy subgrade specimens with and without membrane after submergence tests.

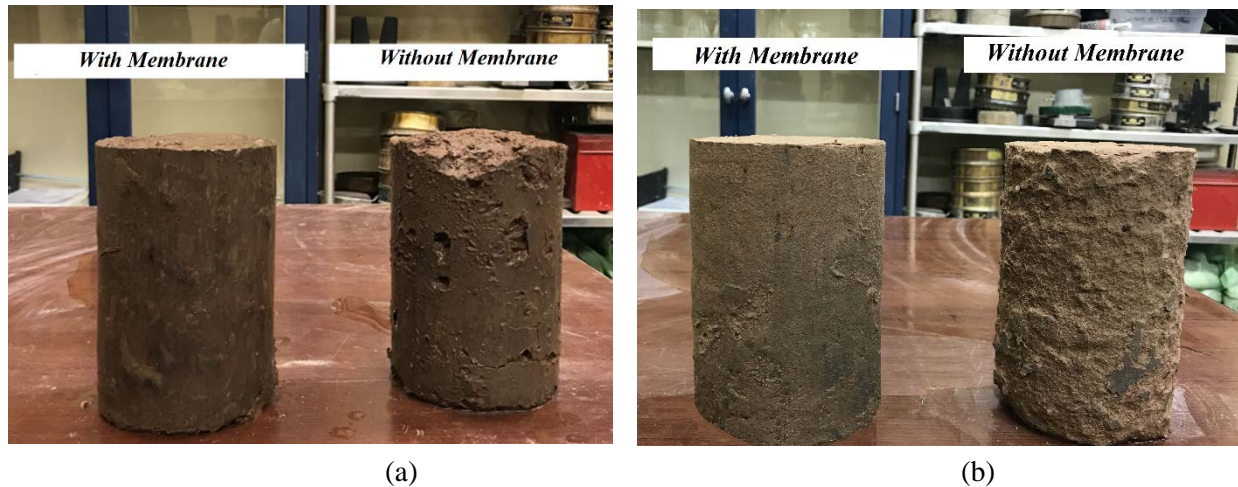


Figure 6-8: Stabilized (A) Clayey and (B) Sandy Subgrade Specimens with and without Membrane after Submergence Test.

Figures 6-9 to 6-11 shows the compression between different moisture susceptibility protocols for siliceous gravel materials sourced from Pharr, RCA sourced from Houston, and FDR materials sourced from Atlanta, respectively. All aforementioned materials showed lower unconfined

compressive strength when subjected to the fully saturated moisture susceptibility protocols such as backpressure and submergence procedures. The test results indicate the significant underperformance of FDR materials when subjected to the backpressure test for 2 and 3 days compared to other materials in the experiment design. For instance, the 2% cement stabilized FDR have approximately 73% and 62% lower compressive strength, respectively, when subjected to the 2-day and 3-day backpressure protocols. This indicate that the incorporation of the moisture susceptibility protocols provides a mechanistic approach for the quantification of the softening behaviour of the stabilized layers upon moisture intrusion. Another interesting observation that can be clearly visualized from the plots is the increase of strength properties with the addition of more stabilizer to the mix when subjected to different moisture susceptibility protocols for all reclaimed and marginal aggregates. As depicted in Figure 6-12, the compressive strength of FDR materials subjected to the 2-day backpressure test improved drastically from 56 psi to 223 psi, by slightly increasing cement content from 2% to 4%. This provides a valuable means for the selection of the type and source of the aggregates for the construction of cement stabilized base layers.

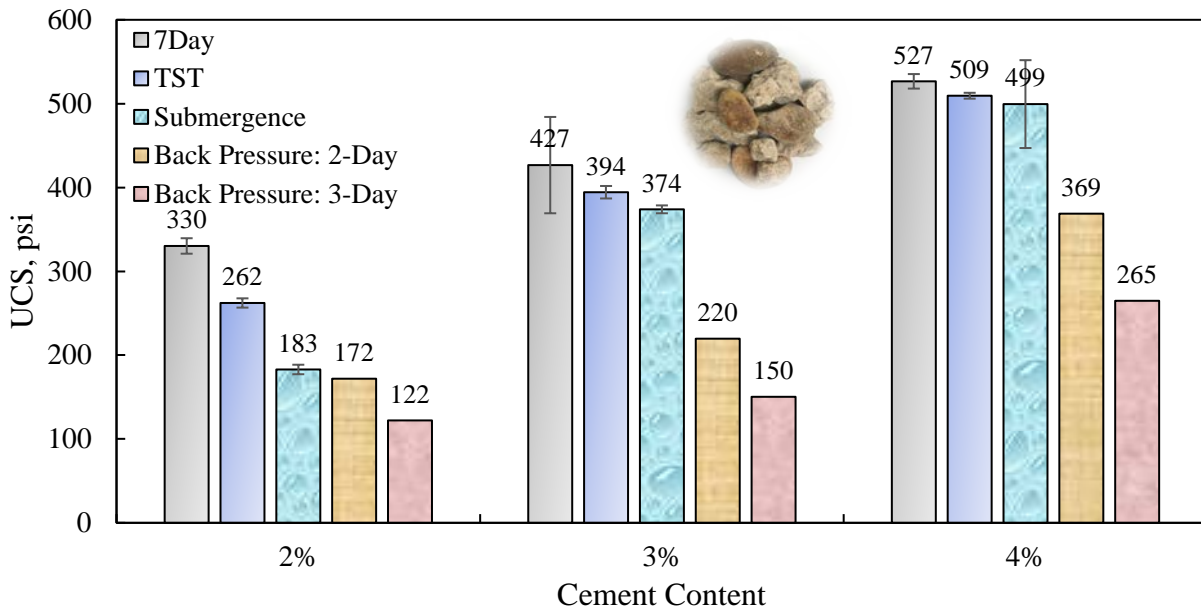


Figure 6-9: Unconfined Compressive Strength Results for Cement Stabilized Siliceous Gravel Sourced from Pharr with Different Curing/Conditioning Procedures.

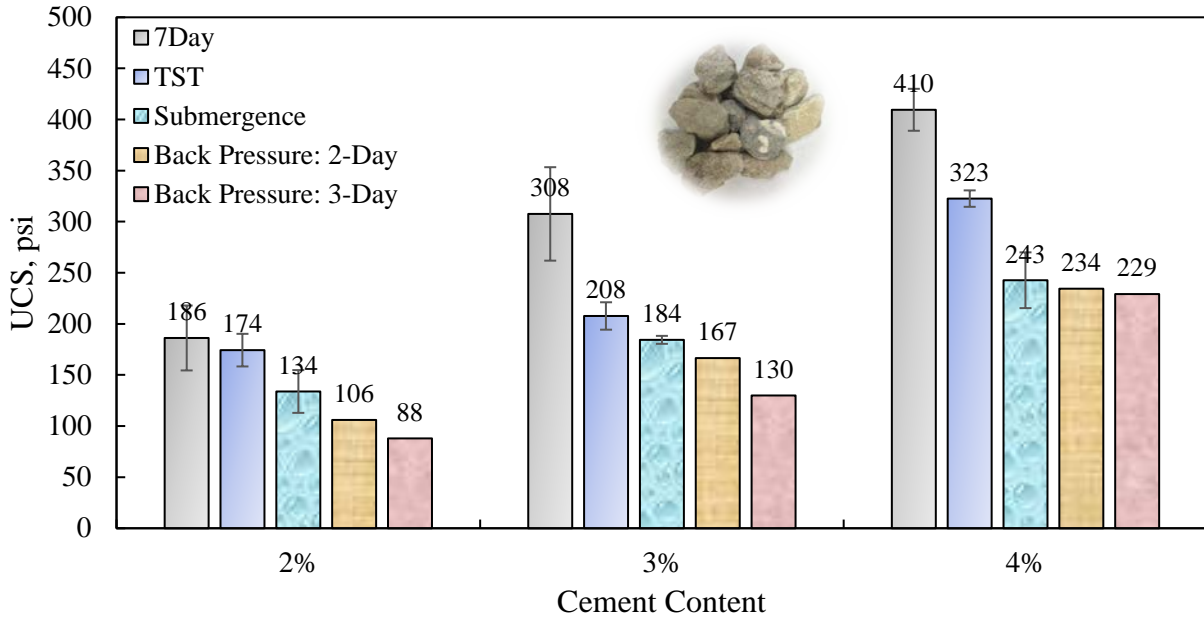


Figure 6-10: Unconfined Compressive Strength Results for Cement Stabilized RCA Materials Sourced from Houston with Different Curing/Conditioning Procedures.

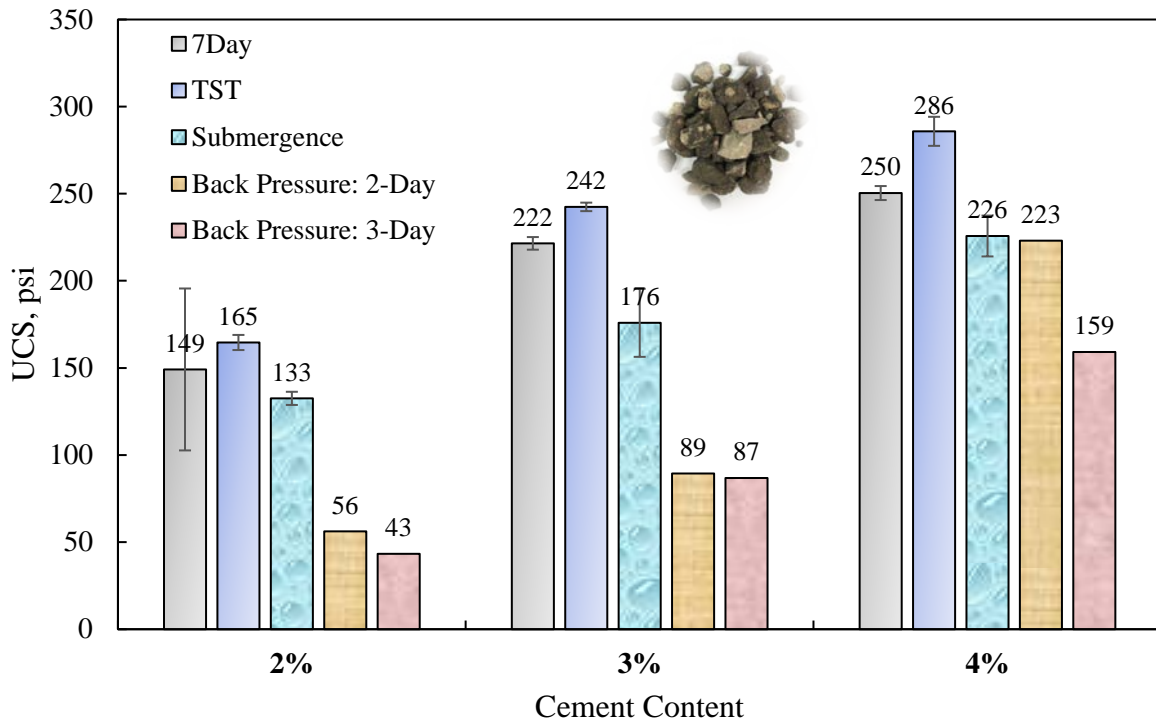


Figure 6-11: Unconfined Compressive Strength Results for Cement Stabilized FDR Materials Sourced from Atlanta with Different Curing/Conditioning Procedures.

6.3.3 Feasibility and Relevance of the Tube Suction Test

Figure 6-12 presents the average dielectric values after 10 days of capillary soak for crushed limestone base, four blends of reclaimed materials, and two different subgrade soils. Variations of the dielectric values (DV) with time provide valuable insight for comparative analysis of the moisture transport capacity of granular materials in this study. As observed in Figure 6-12, the average dielectric values measured at five points upon the completion of the 10-day tube suction procedure is highly dependent on the type of materials used in the mixture. Based on the laboratory measurements, 3% cement treated specimen consisted of 100% RAP materials outperformed other variants in terms of lower dielectric value. Specimens fabricated with 100% RCA resulted in the highest dielectric value of 18.8. The results suggest that the majority of stabilized base and subgrade sources were less moisture susceptible than the stabilized limestone base, which contradicts the UCS test results presented earlier in this chapter. This is primarily due to differences in moisture treatment mechanism in TST procedure and other presented protocols in this research effort. In the tube suction test, the moisture is provided in an upward manner against the gravitational forces by means of capillary action in the specimen, while in the backpressure saturation procedure, the water is forced through the pore structure by all-around confinement to maintain the fully saturated state throughout the test. Evidently, the slow and steady moisture provided by capillary in presence of un-hydrated alkaline earth partakes in strength-gain reactions and results in improvements in strength properties of the specimen. Despite the fact that the TST procedure can be a valuable means to characterize the moisture susceptibility of unbound aggregate systems, this procedure has significant limitations when used for stabilized granular soils. Submergence and backpressure saturation procedures are better suited to simulate loss of stiffness properties of pavement foundations at elevated saturated states during inundation periods.

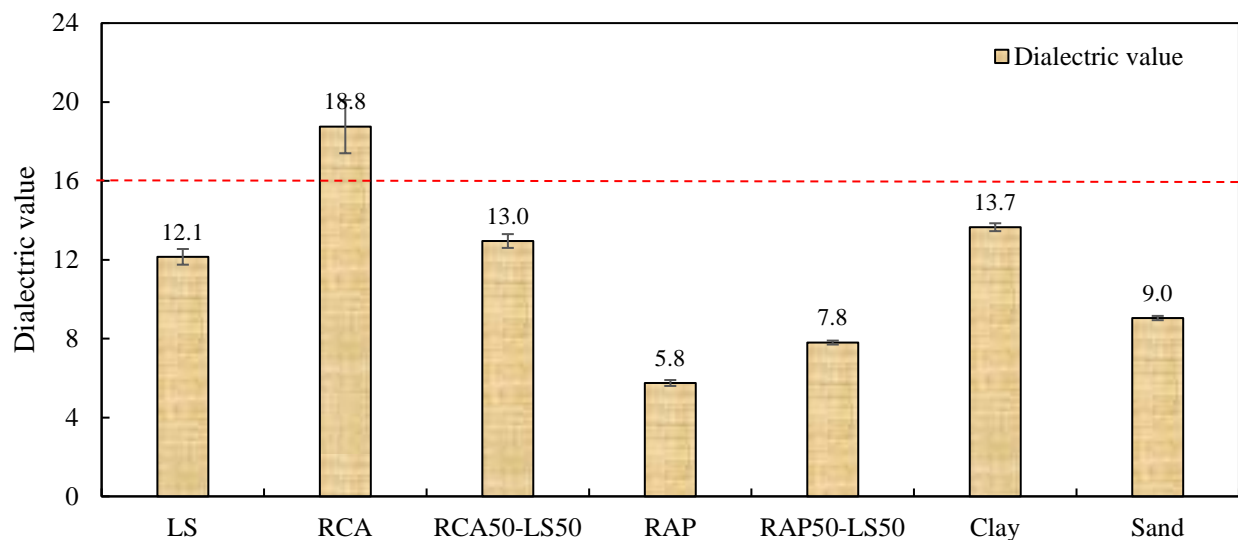


Figure 6-12: Average Dielectric Values after 10 Days of Capillary Soak for Limestone (LS), Aggregates, Reclaimed Concrete Aggregate (RCA), Reclaimed Asphalt Pavement (RAP), Sandy and Clayey Subgrade Materials.

Figure 6-13 demonstrates the variation of moisture content and degree of saturation with time for the RCA materials in the capillary soak procedure. The degree of saturation is calculated according to Equation 6-1 as:

$$S = \frac{G_s \times \gamma_w \times (1+W)}{e \times \gamma_t} - \frac{1}{e} \quad \text{Equation 6-1}$$

Where S is the degree of saturation, G_s is the specific gravity of aggregate, γ_w is the unit weight of water, e is the void ratio, and γ_t is the total (or wet) unit weight of specimen.

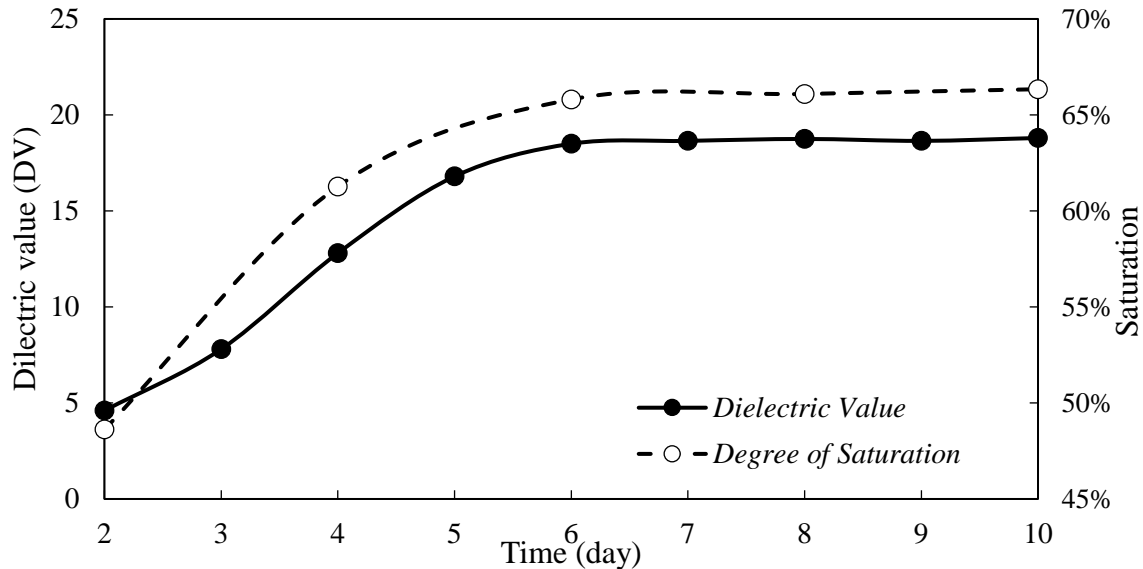


Figure 6-13: Variation of Degree of Saturation and Dielectric Values with Time for RCA Materials.

As observed in Figure 6-13, there is a rapid increase in the degree of saturation and consequently the dielectric value of the 3% cement stabilized system with 100% RCA in the early stages of the capillary soak test. The curves reach an asymptotic behavior after the fifth day of the test, as the degree of saturation remains approximately 65% and well below the fully saturated state. The calculations of the degree of saturation based on traditional phase-relationship equations confirmed the shortcoming of the TST test to replicate fully saturated states.

The visual inspection of the stabilized specimen subjected to capillary soak provided additional information regarding the uniformity of the distribution of water in the specimen. Based on the bundle of capillary analogy in the unsaturated soil mechanics, the inter-connected void system resembles nano-tubes that are responsible for the moisture transport in the soil structure. The soils internal void structure and therefore the diameters of capillary tubes are greatly influenced by the aggregate type, gradation, magnitude, and method of application of compaction energy, type and amount of the stabilizer, and other factors. Considering the fact that the height of the capillary rise is inversely related to the diameter of the capillary tube on one hand, and the random nature of the distribution of such capillary tubes on the other, the distribution of moisture in the specimen in the TST procedure is highly non-uniform as shown in Figure 6-14. Additionally, the presence of

multiple lifts during the compaction of the specimen results in the discontinuity of such capillary tubes at the lift interface which in turn results in an added component to the non-uniformity of moisture distribution in the specimen. Figure 6-15 provides comparative values of degree of saturation resulted from different moisture treatment protocols in this study. Evidently, the push created by the confining pressure in the backpressure saturation test was an efficient means to purge the air and replace it with water in the pore microstructure. The small deviation from the fully saturated states in the reported values in Figure 6-15 could be associated with small isolated air bubbles trapped in the specimen structure.

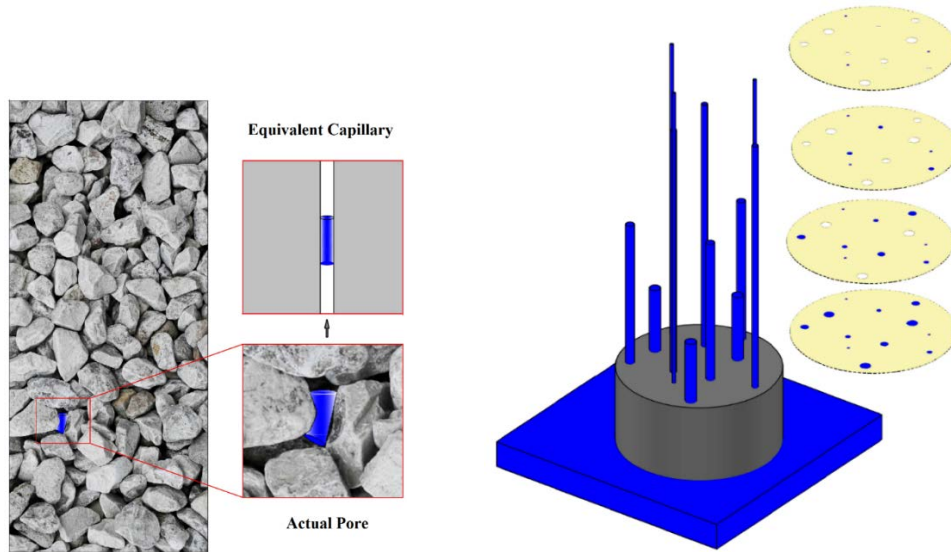


Figure 6-14: Capillary Rise in The Tube Suction Test.

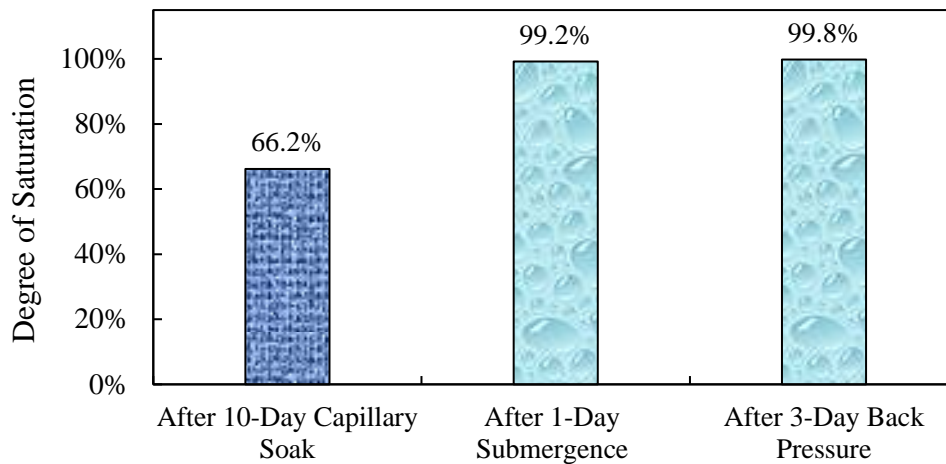


Figure 6-15: Degree of Saturation after Completion of Different Curing Conditioning Procedures.

6.4 Retained Unconfined Compressive Strength and Retained Inverse Diametrical Tensile Strength

Virgin, marginal, and recycled aggregate base materials were subjected to the 2-days backpressure saturation test and to the 1-day submergence test to determine the retained unconfined compressive strength (UCS) and the retained indirect diametrical tensile (IDT) strength defined in Equation 6-2 and Equation 6-3, respectively. The retained strength represents the percentage of the strength of a specimen cured for 7 days that remains after subjecting the specimen to moisture susceptibility tests.

$$R_{UCS} = (UCS_{mst}/UCS_{7dc}) \quad \text{Equation 6-2}$$

Where:

R_{UCS} : retained UCS

UCS_{mst} : UCS after subjecting the specimen to moisture susceptibility tests

UCS_{7dc} : UCS after curing the specimen for 7 days at 95% relative humidity and 23°C

$$R_{IDT} = (IDT_{mst}/IDT_{7dc}) \quad \text{Equation 6-3}$$

Where:

R_{IDT} : retained IDT strength

IDT_{mst} : IDT strength after subjecting the specimen to moisture susceptibility tests

IDT_{7dc} : IDT strength after curing the specimen for 7 days at 95% relative humidity and 23°C

The virgin material evaluated was limestone from El Paso, while the marginal material evaluated was gravel from Pharr. The recycled materials were RCA from Houston, FDR from Atlanta, and RAP as well as RCA from El Paso. The characteristics of these materials were described in Chapter 5. These aggregate base materials were treated with 3% cement and compacted using the impact hammer to fabricate two different sizes of cylindrical specimens: 4 in. x 6 in. and 4 in. x 4 in. for UCS and IDT testing, respectively.

Figure 6-16 shows the retained UCS values obtained. Materials subjected to the 1-day submergence test have higher retained UCS compared to materials subjected to the 2-days backpressure saturation test, in which the loss of compressive strength is higher. Gravel from Pharr is the material with the highest retained UCS (0.88) after being subjected to the submergence test for one day, while limestone from El Paso is the material with the highest retained UCS (0.80) after being subjected to the backpressure saturation test for two days. The lowest retained UCS value corresponds to RAP El Paso for both moisture susceptibility conditions: 0.44 after subjecting the specimen to 1-day submergence test and 0.33 after subjecting the specimen to 2-days backpressure saturation test.

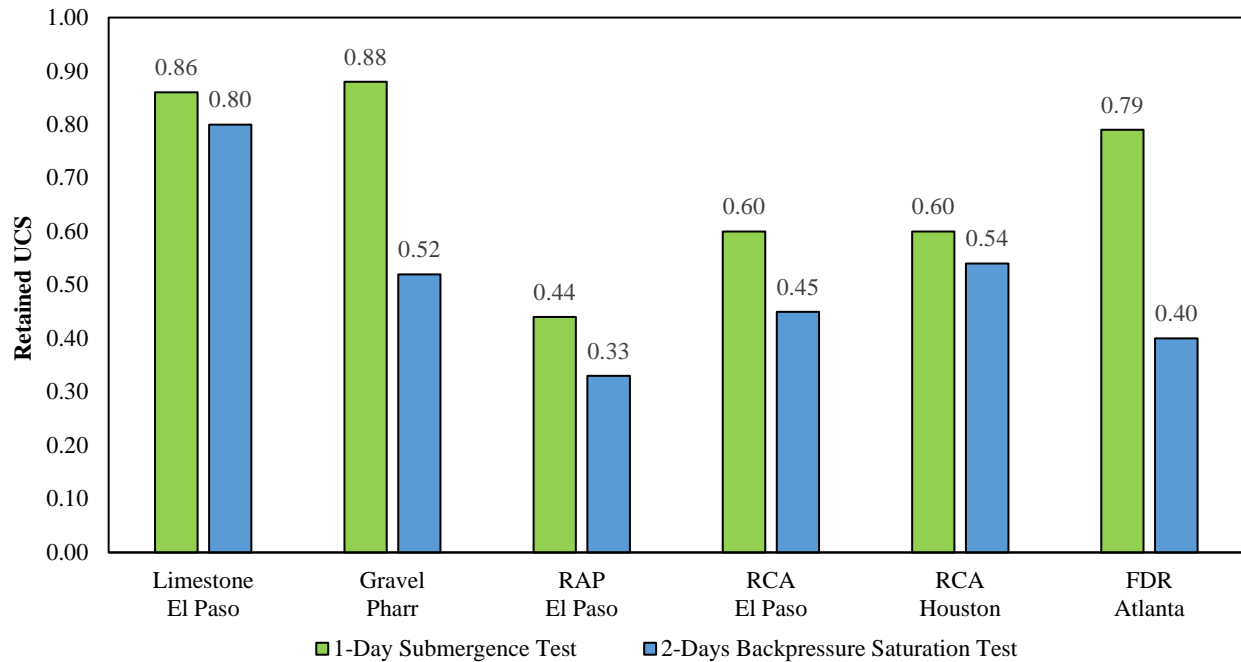


Figure 6-16: Retained UCS Values of Base Materials.

Figure 6-17 shows the retained IDT values obtained. Materials subjected to the 2-days backpressure saturation test have higher retained IDT strengths compared to materials subjected to the 1-day submergence test, in which the loss of tensile strength is higher. RAP from El Paso is the material with the highest retained IDT (0.73) after being subjected to the submergence test for one day, while both RAP El Paso and FDR Atlanta are materials with the highest retained IDT (0.88) after being subjected to the backpressure saturation test for two days. The lowest retained IDT values correspond to limestone El Paso for both moisture susceptibility conditions: 0.55 after subjecting the specimen to 1-day submergence test and 0.70 after subjecting the specimen to 2-days backpressure saturation test.

Figure 6-18 and Figure 6-19 display the comparison between retained UCS and retained IDT strength after subjecting the materials to 2-days backpressure saturation test and 1-day submergence test, respectively.

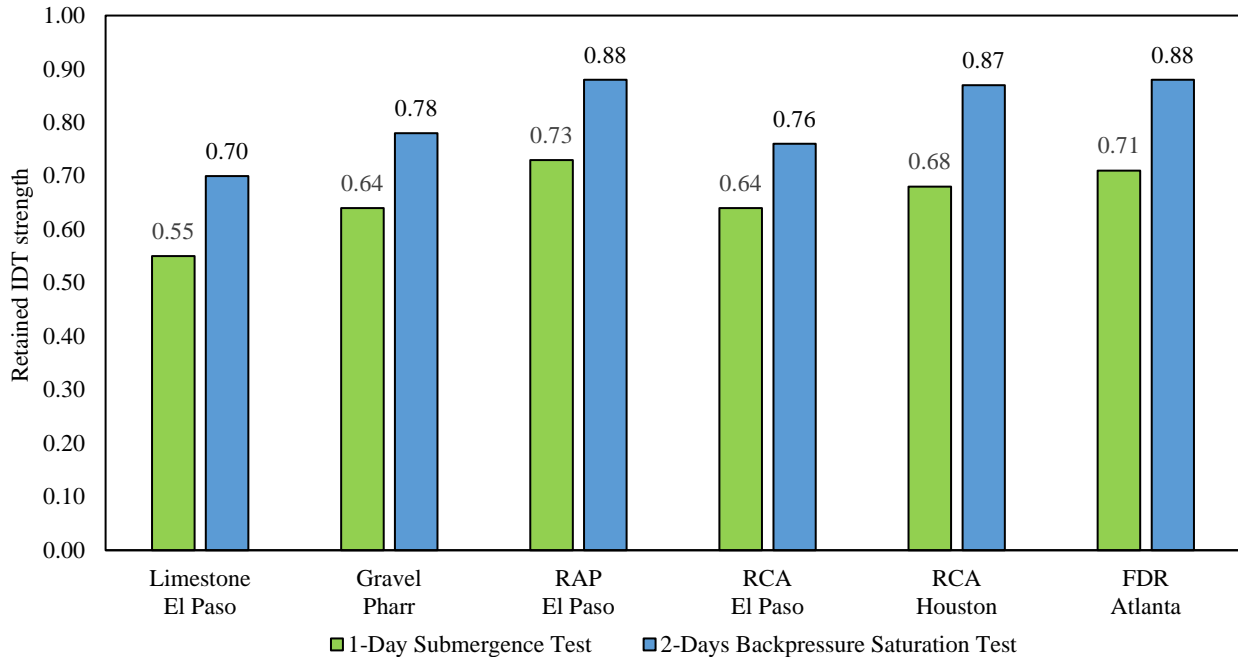


Figure 6-17: Retained IDT Strength Values of Base Materials.

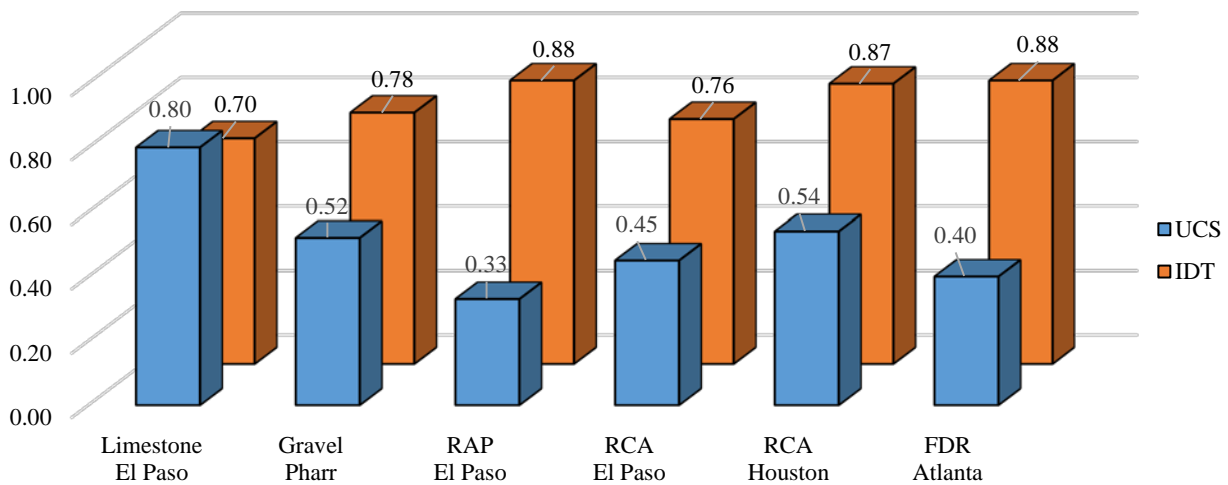


Figure 6-18: Comparison of Retained UCS and IDT Strength Values of Base Materials Subjected to 2-Day Backpressure Saturation Test.

It can be stated from Figure 6-18 that limestone from El Paso is the only material that exhibits close retained UCS and IDT strength values after being subjected to 2-days backpressure saturation test. For the other materials, the retained UCS is lower than the retained IDT strength after subjecting the specimens to the backpressure saturation test for two days.

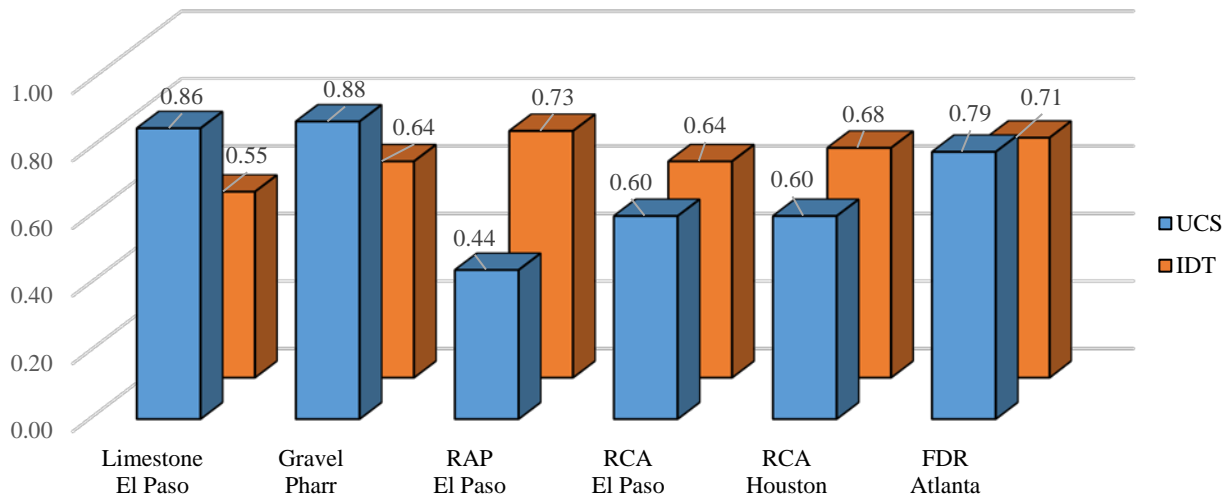


Figure 6-19: Comparison of Retained UCS and IDT Strength Values of Base Materials Subjected to 1-Day Submergence Test.

Similarly, based on Figure 6-19, RCA from El Paso, RCA from Houston, and FDR from Atlanta exhibit close retained UCS and IDT strength values after being subjected to 1-day submergence test. For RAP from El Paso, the retained UCS is lower than the retained IDT strength after subjecting the specimens to submergence test for one day. For limestone from El Paso and gravel from Pharr, the retained UCS is higher than the retained IDT strength after subjecting the specimens to submergence test for one day.

In conclusion, the determination of the minimum cement content for virgin, marginal, and reclaimed aggregate base materials treated with cement must include the compressive strength as well as the tensile strength of specimens subjected to moisture susceptibility conditions. The retained strength can be used as a criterion to accept or reject cement treated materials that will undergo prolonged saturated conditions during its service life.

6.5 Summary of the Major Points

The primary objective of this chapter was to explore alternative moisture susceptibility procedures in lieu of traditional TST protocol for realistic simulation of field conditions in the event of flooding and prolong saturation states of pavement facilities. To achieve this objective, several alternative moisture susceptibility procedures including tube suction protocol, multiple backpressure saturation procedures with different durations, and multiple submergence protocols were incorporated in this study to evaluate the influence of moisture ingress on the compressive strength properties of stabilized materials. The analysis of the compressive strength results showed that the TST protocol resulted in relatively similar to the 7-day moist-cured UCS values. This

contradicts the notion of using tube suction procedure to simulate stiffness loss associated with moisture intrusion in pavement foundations. Therefore, the research team devised a series of alternative moisture susceptibility procedures such as multiple submergence procedures with variable heat treatment protocols, and backpressure saturation at three different durations to better replicate the inundation scenarios during the service life of pavement structures. Contrary to the compressive strength results for specimen subjected to TST procedure, submergence and backpressure saturation procedures were able to detect early onset of damage in both cement treated base and subgrade specimen in the laboratory. Another noteworthy finding of this research pertains to the differences in behavior of cement treated reclaimed and virgin materials when subjected to various durability protocols. The analysis of the blend ratios provided in this study can serve as a starting point for efficient mixture design of cement treated base layers in areas with flooding potential. Evidently, inclusion of the representative moisture susceptibility procedure is an integral component of the mixture design of stabilized pavement layers in areas prone to prolong inundation periods and natural disasters. Ultimately, since the strength of a material in compression, after being subjected to moisture susceptibility procedures is not the same as the strength of a material in tension, the determination of the minimum cement content for virgin, marginal, and reclaimed aggregate base materials treated with cement must necessarily include both strengths. The retained strength can be used as a criterion to accept or reject cement treated materials that will undergo prolonged saturated conditions during its service life.

Chapter 7. Analysis of the Variability of the Laboratory Data

One of the goals of this research is to improve the procedures for the characterization of the cement treated materials and mixture design based on laboratory tests. These tests should produce reliable and repeatable results and be practical in nature for statewide application. For this reason, it is imperative to analyze the robustness of the laboratory procedures. The main objective of this chapter is to develop numerical and statistical analysis of the multi-dimensional features database to identify the reliability and repeatability of the laboratory tests. This chapter also outline the procedures to obtain and compare estimates of precision and bias among the data, and mathematical techniques used to select (or reject) laboratory specimens. These robust statistical techniques were then employed to analyze the variability of the data obtained from the UCS, IDT, and submaximal modulus tests. Additionally, analysis of the variability of proposed specimen preparation procedures using gyratory compactor, vibratory, and impact hammers was provided in order to investigate the repeatability and potential benefits of different compaction methods on the engineering properties of the cement treated materials.

7.1 Layout of the Experimental Procedure

The layout of the procedure requires *n- test* observations to be obtained for each test by three different operators and two types of materials namely level 1 and level 2 for properly covering full range of interest. Compressive strength, indirect tensile strength, and resilient modulus for the stabilized crushed limestone aggregates as test observations were extracted from the UCS, IDT, and submaximal tests, respectively. In this study, level 1 represented lightly stabilized materials or low level of strength (specimens stabilized with 2% cement content) and level 2 pertains to permutations of heavily stabilized systems or high strength variants (specimens stabilized with 4% cement content). The example database for this chapter was summarized in Table 7-1 for the analysis of the variability and repeatability of the laboratory tests.

Table 7-1: UCS, IDT, and Submaximal Tests Results.

Levels		Operators	Tests					
			UCS (psi)		IDT (psi)		Submaximal (psi)	
			Specimen #1	Specimen #2	Specimen #1	Specimen #2	Specimen #1	Specimen #2
Level 1	Lightly Stabilized Materials	Hector	235.2	261	45.6	44.5	800	1000
		Margarita	259.2	268.5	42.5	40	900	1050
		German	258	268.2	37	45.5	1100	1200
Level 2	Heavily Stabilized Materials	Hector	864.4	872.5	97	109.1	2200	1600
		Margarita	852.1	833.2	115	87	1550	1800
		German	833.9	873.8	93.5	98.2	2000	2200

7.1.1 Precision Assessment between Experimental Procedures

Standard deviation (SD) were used for comparing the precision of the laboratory test results. The standard deviation is a measure that is used to quantify the variation or dispersion of a set of data values. A low standard deviation indicates that the data points tend to be close to the mean (also called the expected value) of the set, while a high standard deviation indicates that the data points are spread out over a wider range of values as shown in Figure 7-1. Equation 7-1 presents the standard deviation formula:

$$SD_{ij} = \sqrt{\frac{\sum(X_{ij} - \bar{X}_{ij})^2}{N_{ij} - 1}} \quad \text{Equation 7-1}$$

Where:

X_{in} = Properties of materials obtained at the i^{th} level by the j^{th} method.

N_{ij} = Number of test results for each level and method cell.

SD_{ij} = Standard deviation results obtained at the i^{th} level by the j^{th} method.

In addition, the average, \bar{X}_{ij} for the i^{th} level using j^{th} method was calculated according to Equation 7-2:

$$\bar{X}_{ij} = \frac{\sum X_{ij}}{N} \quad \text{Equation 7-2}$$

Where:

\bar{X}_{ij} = Average results obtained at the i^{th} level by the j^{th} method.

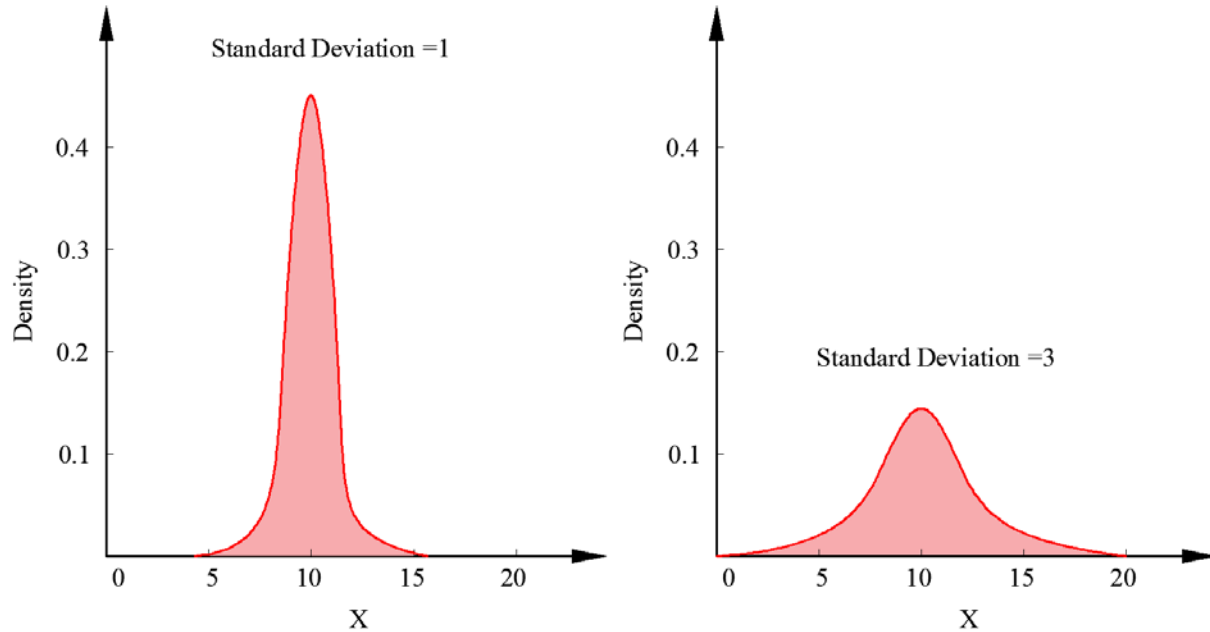


Figure 7-1: Variation within Samples with Low and High Variability.

The standard deviation is independent of the test and unit in which the measurement has been taken. For the comparison between datasets with different units or widely different means, coefficient of variation were used instead of the standard deviation as a dimensionless measure to identify the precision and repeatability of laboratory tests. The coefficient of variation (CV) is defined as the ratio of the standard deviation to the average as indicated in Equation 7-3:

$$CV_{ij} = 100 \times \frac{SD_{ij}}{\bar{X}_{ij}} \quad \text{Equation 7-3}$$

Where:

CV_{ij} = Coefficient of variation, expressed as a percentage, for the i^{th} level of the j^{th} method,

SD_{ij} = Standard deviation results obtained for the i^{th} level of the j^{th} method, and

\bar{X}_{ij} = Average of the test results for the i^{th} level of the j^{th} method.

Table 7-2 shows the standard deviation, average, and coefficient of variation for the UCS, IDT, and submaximal test results at two strength levels. The statistical analysis shows that aforementioned tests incorporated in this study have coefficient of variation lower than 20% (acceptable level considered for this study). This coefficient of variation range shows that most of the data are close to the average value and are highly forecastable. Therefore, performing UCS, IDT, and submaximal tests with three different operators and two replicates shows that these laboratory tests produce reliable and repeatable results.

Table 7-2: Average, Standard Deviation and Coefficient of Variation For Different Test Methods at Two Levels of Lightly and Heavily Stabilized Materials.

Levels		Tests								
		UCS			IDT			Submaximal		
		X	SD	CV	X	SD	CV	X	SD	CV
Level 1	Lightly Stabilized Materials	258	12	5	43	3.4	8.1	1008	143	14
Level 2	Heavily Stabilized Materials	855	18	2	100	10	10	1892	287	15

Another noteworthy observation in Table 7-2 is the difference of coefficient of variations between UCS and submaximal test. The results revealed that UCS test results with smaller coefficient of variations (2%~5%) are less dispersed than the submaximal modulus test results with larger coefficient of variations (14%~15%).

In the next step, F-distribution was drawn using the ratio of the between-group variability to the within-group variability when the null hypothesis is true. The null hypothesis is a general statement or default position, in which there is no relationship between two measured phenomena, or no association among groups. Then, a threshold (critical) value of F will be established. This F value can be obtained from statistical tables and is referred to as $F_{critical}$ or F_{α} , which is the minimum value for the test statistic to be able to reject the null hypothesis. The F-distribution, $F_{critical}$, and the location of acceptance and rejection regions are shown in Figure 7-2. Therefore, the F statistic, as the ratio of the variances for each level and for each test method, was calculated using Equation 7-4 and then the results were summarized in Table 7-3.

$$F_{ij} = \frac{(S_{Aij})^2}{(S_{Bij})^2} \quad \text{Equation 7-4}$$

Where:

$(S_{Aij})^2$ = the larger of the two variances for the i^{th} level of the j^{th} method.

$(S_{Bij})^2$ = the smaller of the two variances for the i^{th} level of the j^{th} method.

F_{ij} = the calculated F statistic for the i^{th} level of the j^{th} method.

Table 7-3: F-Static for Different Test Methods at Two Levels Of Lightly and Heavily Stabilized Materials.

Levels		Tests								
		UCS			IDT			Submaximal		
		Larger variance	Smaller variance	F-statistic	Larger variance	Smaller variance	F-statistic	Larger variance	Smaller variance	F-statistic
Level 1	Lightly Stabilized Materials	268.5	235.2	1.2	45.6	38.5	1.4	1200	800	2.25
Level 2	Heavily Stabilized Materials	873.8	833.2	1.1	115	87	1.75	2200	1550	2.01

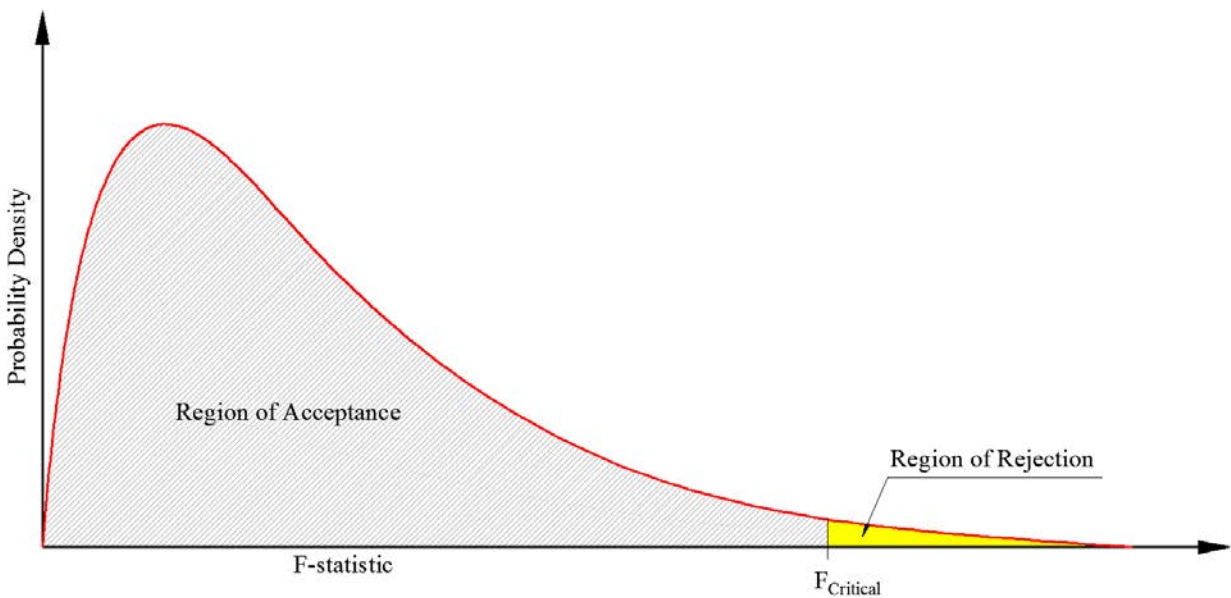


Figure 7-2: Distribution of the F-values.

Variances in the F-statistic are a measure of dispersion, or how far the data are scattered from the mean. Table 7-3 indicates that the submaximal test results have the larger values of F-statistic which represent greater dispersion in comparison with UCS and IDT tests. Subsequently, a threshold (critical) value of F was obtained according to the cut-off value of F in the F-distribution shown in Table 7-4 for a confidence level of 95% ($\alpha=0.05$). This critical value ($F_{\alpha} = 5.05$) is the minimum value for the test statistic to be able to reject the null hypothesis. Statistical analysis shows that all F-statistics for the IDT, UCS and submaximal modulus tests ranging from 1.1 to 2.25 were less than the critical value ($F_{\alpha} = 5.05$). This shows that all laboratory test results with a confidence level of 95% are in the acceptance region. Therefore, the IDT and submaximal modulus tests are robust laboratory procedures for inclusion in the draft specification for the characterization of cement stabilized base materials in this example database.

Table 7-4: Cut-Off Value of F in the F-Distribution Table for the Confidence Level of 95% (A=0.05)

Degree of Freedom	1	2	3	4	5	6	7	8	9	10
1	161.4	199.5	215.7	224.5	230.1	233.9	236.7	238.8	240.5	241.8
2	18.51	19.00	19.16	19.25	19.30	19.33	19.35	19.37	19.38	19.40
3	10.13	9.55	9.28	9.12	9.01	8.94	8.89	8.85	8.81	8.79
4	7.71	6.94	6.59	6.39	6.26	6.16	6.09	6.04	6.00	5.96
5	6.61	5.79	5.41	5.19	5.05	4.95	4.88	4.82	4.77	4.74
6	5.99	5.14	4.76	4.53	4.39	4.28	4.21	4.15	4.10	4.06
7	5.59	4.74	4.35	4.12	3.97	3.87	3.79	3.73	3.68	3.64
8	5.32	4.46	4.07	3.84	3.69	3.58	3.50	3.44	3.39	3.35
9	5.12	4.26	3.86	3.63	3.48	3.37	3.29	3.23	3.18	3.14
10	4.96	4.10	3.71	3.48	3.33	3.22	3.14	3.07	3.02	2.98

7.2 Assessing Variability of Gyratory Compactor and Impact Hammer

Uniform specimen preparation is of paramount importance for accurate and reliable characterization of the mechanical behavior of cement treated materials in the laboratory. Traditionally, impact hammer method is used to compact specimens in the laboratory to establish the moisture-density curves, perform strength tests, and to characterize the deformation potential of cement treated systems. Based on the laboratory test results, the specimen prepared using the impact method due to the nature of the application of compaction energy exhibit high levels of non-uniformity, which in turn jeopardizes the accuracy of the laboratory performance test results. Additionally, the methods of compaction energy in the field, such as static pressure, vibration, and kneading actions are vastly different from the impact hammer in the laboratory. This would ultimately result in significant differences in the void structure and preferred orientation of the aggregate particles. Therefore, the research team prepared the cement treated specimens using four compaction methods, namely Texas Gyratory Compactor (TGC), impact hammer, vibratory hammer, and gyratory compactor, in order to investigate the repeatability and potential benefits of using gyratory and vibratory compactors on the engineering properties of the cement treated materials.

Figure 7-3 represents the coefficient variations of unconfined compressive strength tests for various stabilized materials compacted with different compaction procedures. This plot is primarily based on the averages of CV for stabilized aggregates with 2%, 3%, and 4% cement content. As illustrated in Figure 7-3, stabilized reclaimed materials such as RCA and FDR fabricated with impact hammer exhibited considerably higher coefficient variations in comparison with other permutations. This can be an indication of higher scatter and lower precision of impact hammer for reclaimed materials compared to the other compaction procedures due to higher particle breakage and crushing potential of reclaimed materials.

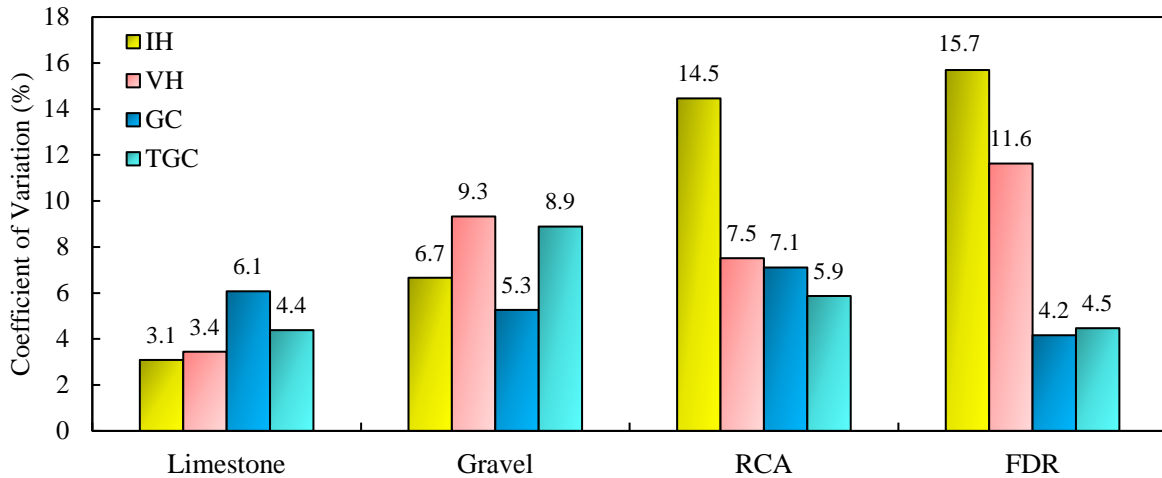


Figure 7-3: Coefficient Variations of Unconfined Compressive Strength Tests for Stabilized Specimens Compacted with Different Compactions Procedures.

7.3 Assessing Variability of Moisture Susceptibility Protocols

Figure 7-4 presents the average coefficient variations of UCS tests for stabilized specimens subjected to different moisture susceptibility protocols. The results indicated that alternative moisture susceptibility protocols such as backpressure and submergence tests incorporated in this study have coefficient of variation lower than 20% (acceptable level considered for this study). This coefficient of variation range shows that most of the data are close to the average value and is highly forecastable. Therefore, performing UCS test with two replicates shows that these moisture susceptibility tests produce reliable and repeatable results. Another noteworthy observation in Figure 7-4 is the difference of coefficient of variations between submergence and backpressure tests. The results revealed that the submergence test results with smaller coefficient of variations (6%~13%) is less dispersed than the backpressure test results with larger coefficient of variations (4%~24%).

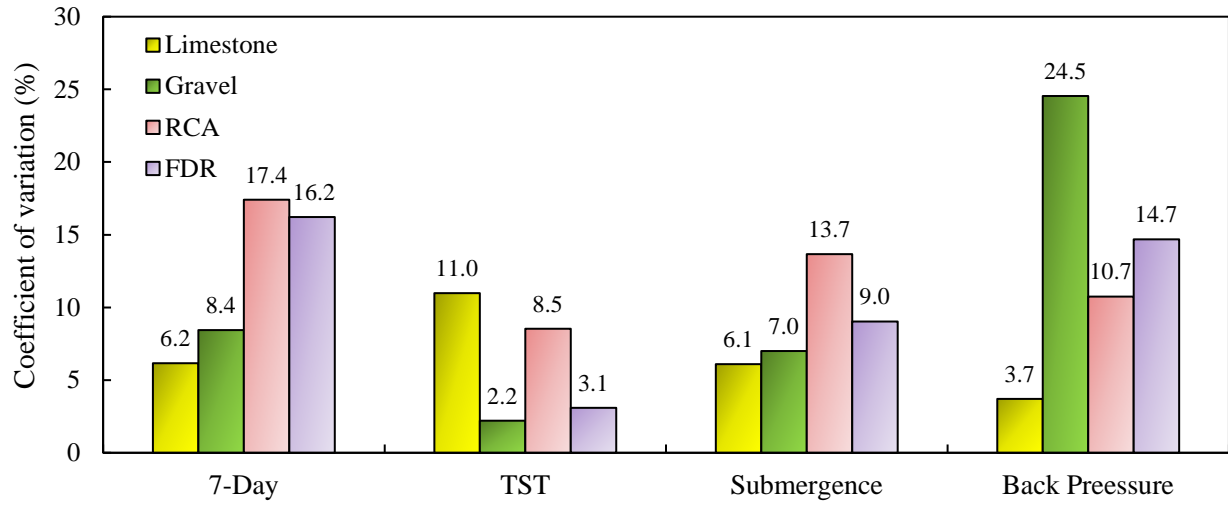


Figure 7-4: Coefficient Variations of Various Moisture Susceptibility Protocols for Stabilized Base Materials.

Chapter 8. Compaction Characterization

Uniform specimen preparation is of paramount importance for accurate and reliable characterization of the mechanical behavior of cement treated materials in the laboratory. Traditionally, impact hammer method is used to compact the specimen in the laboratory to establish the moisture-density curve, perform strength tests, and to characterize the deformation potential of cement treated systems. Based on the previous studies, due to the nature of the application of compaction energy, the specimen prepared using the impact method exhibit high levels of non-uniformity, which in turn jeopardizes the accuracy of the laboratory performance test results (Ping et al, 2003; Kaya et al., 2012; Du et a., 2018). Additionally, the methods of compaction energy in the field, such as static pressure, vibration, and kneading are vastly different from the impact hammer in the laboratory. This would ultimately result in significant differences in the void structure and preferred orientation of the aggregate particles. High variability of strength test results and presence of layer interface barrier between lifts can be other limiting factors in this compaction technique. Therefore, this chapter describes new compaction procedures for stabilized base and subgrade materials as an alternative to the traditional impact hammer compaction. In this study, the cement treated specimens – using four compaction methods, namely Texas Gyrotory Compactor (TGC), impact hammer, vibratory hammer, and gyrotory compactor – were prepared in order to investigate the potential benefits and effects of using gyrotory and vibratory compactors on the engineering properties of the stabilized materials (Figure 8-1).



Figure 8-1: Impact Hammer, Texas Gyrotory Compactor (TGC), Gyrotory Compactor, and Vibratory Hammer.

8.1 Impact Hammer

Impact hammer have been used for decades and is the most popular compaction procedure in the laboratory testing due to the fact that impact hammer was the first compaction technique to be standardized. In this method, the specimens were molded vertically in cylindrical molds by compacting the stabilized base and subgrade mixtures using impact hammer with a 10 lb. hammer

and 18 inches drop. Each layer with the thickness of 2 inches were compacted by applying 50 hammer blows on each flat end. This study followed the Tex-113-E and Tex-114-E standards for compacting the stabilized base and subgrade materials, respectively.

8.2 Vibratory Hammer

The vibratory hammer compaction uses a specific mechanism by rotating eccentric weight to induce a downward force in addition to the dead weight of the compaction machine. This compaction method delivers a quick sequence of blows to the stabilized base and subgrade mixtures. Layers of materials in the mold are affected by moving vibration. This sets the aggregates in motion and moves them closer together to achieve the target level of compaction. Previous studies showed that the vibratory compactor is especially effective in compacting cohesionless soil such as gravel and sand (Kelfkens 2008; Ping et al. 2003). In this compaction method, the specimens were molded vertically in cylindrical molds by compacting the stabilized base and subgrade mixtures in six lifts of 2 inches thickness using the vibratory hammer according to ASTM standard C1435 (ASTM, 2020). The hammer has a power consumption of 11 Watt (Joule/second) and operates at a frequency of 25 Hz. In this method, as the stabilized base mixture consolidate, mortar should fill in the annular space between the outer edge of tamping plate and the inside mold wall. During vibration, mortar forms a ring around the total perimeter of the tamping plate. The operator stops the vibratory hammer when the mortar ring forms completely around the tamping plate. According to the ASTM standard C1435 (ASTM, 2020), if a major portion of mortar ring does not form after 20 seconds, the vibratory hammer must be stopped and next layer of stabilized mixture should be added. Two types of circular steel tamping plate with the diameters of 5(3/4) and 3(3/4) inches were used for the compaction of molds with diameters of 6 and 4 inches, respectively. These plates are attached to a steel shaft, which is inserted into the vibratory hammer chuck as depicted in Figure 8-2.

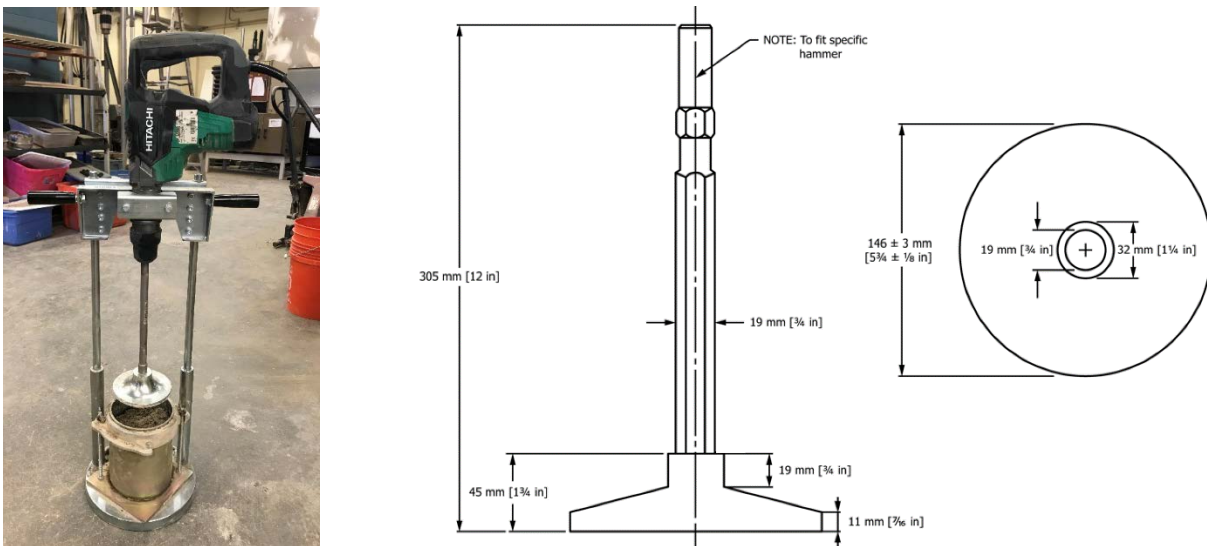


Figure 8-2: Impact Hammer Setup and Circular Steel Tamping Plate and Metal Shaft.

8.3 Gyrotory Compactor

Gyrotory compactors have been widely used in recent years for the compaction of asphalt mixtures. In this compaction method, material is compacted through simultaneous action of compressive pressure and shearing forces generated as a result of mold gyrations about its vertical axis. Literature is sparse regarding the compaction of soil and granular materials with the gyrotory compactor. In some of these few research studies, satisfactory results such as leading to a better simulation of field compaction were observed using the gyrotory compactor (Lee et al., 2019). Previous studies showed that the internal structure of samples prepared by a gyrotory compactor may show a closer resemblance to that resulting from actual field compaction. This compaction procedure has also the ability to simultaneously apply a vertical load in addition to self-adjusting kneading action which simulates the moving traffic load experienced by a flexible pavement system as shown in Figure 8-3 (McRae & McDaniel, 1965). Beside the physical similarities to field compaction, gyrotory compactors are generally more precise, effective, and repeatable than impact hammer. Therefore, the gyrotory compactor variables were studied to establish a standard procedure for the compaction of stabilized base aggregates and subgrade soils.

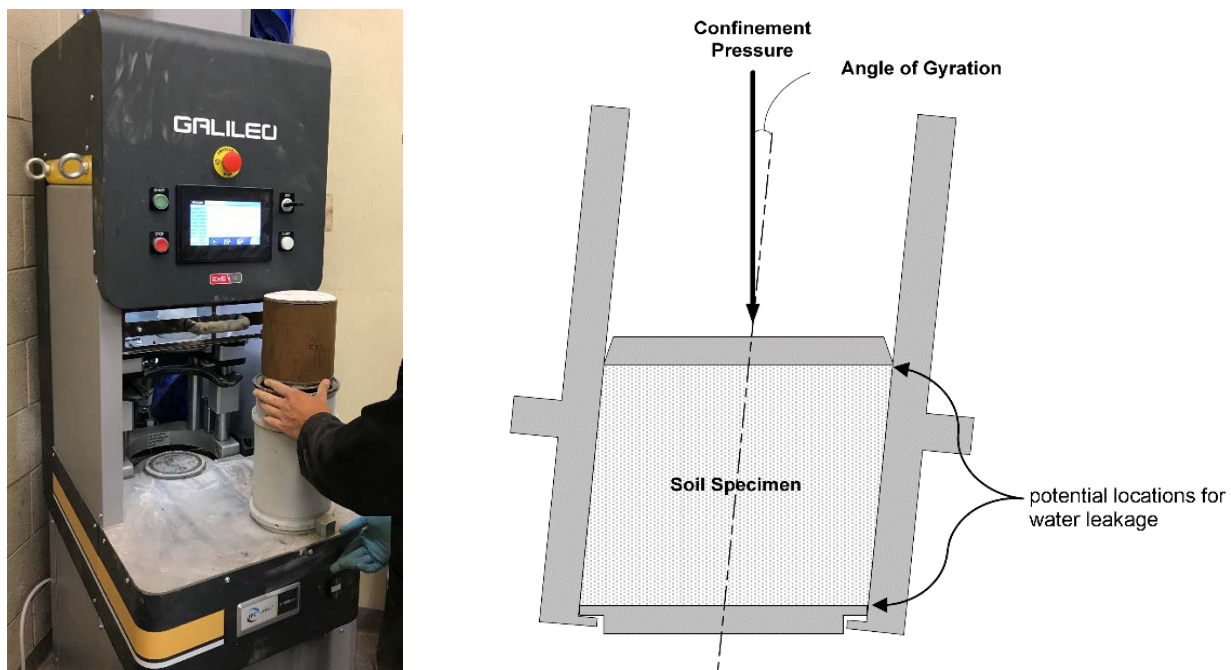


Figure 8-3: Schematic Cross-section and View of Gyrotory Compactor.

To begin the work, current state of practice and emerging research using gyrotory compactor were investigated, and then their compaction parameters were summarized in Table 8-1. Based on the previous studies, the main parameters of gyrotory compactor such as gyration rate, number of gyration, angle of gyration, compaction pressure, and specimen diameter may influence the gyrotory and field compaction simulation. Thus, a comprehensive factorial analysis is required to explore, in detail, the effect of these parameters on strength properties and density of cement stabilized materials after compaction.

Table 8-1: Main Variables of Gyrotory Compactor in Previous Studies.

References	Specimen diameter (in)	Gyration rate (gyration/min)	No. of Gyration	Angle of gyration	Compaction pressure	
					(kPa)	(psi)
MnDOT	6	30	50	1.25	600	87
U.S. Army Corps of Engineers	6	-	30 and 120	1 & 2	25 - 200	4-29
Montana State University	-	30	Up to maximum of SGC machine	1.25	200 - 600	29-87
Florida DOT		20	90	1.25	100 - 500	15-73
TxDOT for Base	6	30	Up to maximum of SGC machine	1.16	600 - 800	87-116
TxDOT for Subgrade	4	30		1.25	600	87

8.3.1 Factorial Analysis for Gyrotory Compactor Parameters

This section describes the comprehensive factorial analysis in order to fully investigate the effect of gyrotory compactor parameters on strength properties and density of the mixture. Based on the results from the literature review, gyration rate of 30 gyration/minute as well as the diameter of 6 inches and 4 inches were considered for all stabilized base and subgrade materials, respectively. Three main parameters of gyrotory compactor including angle of gyration, compaction pressure and number of gyration were examined for crushed limestone aggregate sourced from El Paso in the laboratory. Figures 8-4 and 8-5 present the variation density and height of specimen versus number of gyrations during gyrotory compaction. The ascending nature of the plots is an indication of the favorable influence of the number of gyrations to the improvement of density in stabilized materials. The results clearly show the densification of specimens around 120 number of gyrations for all compaction pressures. Another interesting observation was the slightly increase of density by increasing compaction pressure. For instance, ultimate density after 120 gyrations and with 1.25° angle of gyration were 151; 155; and 156 pcf for compaction pressure of 58, 87, and 116 psi, respectively.

However, higher compaction pressure, such as 116 psi, may subject the laboratory soil specimens to pressures and compaction energies that are greater than typical field construction condition. Additionally, high compaction pressure would likely result in more particle breakage than low compaction pressure. Therefore, the compaction pressure of 87 psi was used for all laboratory testing in this project.

The angle of gyration should be manually adjusted by changing the roller positions on the carriage body. This is a time and labor intensive process; consequently, for this factorial analysis two angle of rotation, namely 1.16° and 1.25°, were examined for all testing. Figure 8-6 illustrates variation of height of specimen versus number of gyration for different angles of rotation. The trend of the data shows the higher densification of stabilized materials by increase of angle of rotation in the compaction procedure. This is more pronounced for materials under the compaction pressure of

87 psi. For instance, the height of a specimen under 87 psi compaction pressure with 1.25° angle of gyration significantly decreased from 6.89 in to 5.31 in after 120 number of gyration, while the ultimate height of specimen with 1.16° angle of gyration was 5.55 in.

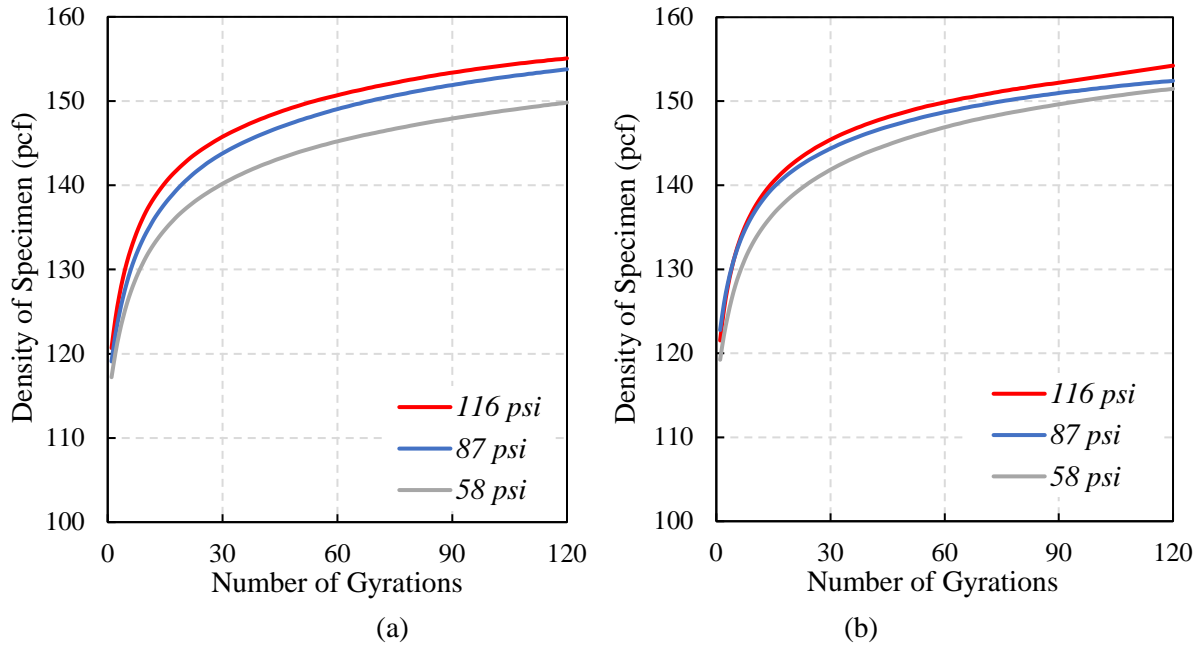


Figure 8-4: Variation of Density Versus Number of Gyration for Different Compaction Pressures (a) Angle of Rotation = 1.25° (b) Angle of Rotation = 1.16°

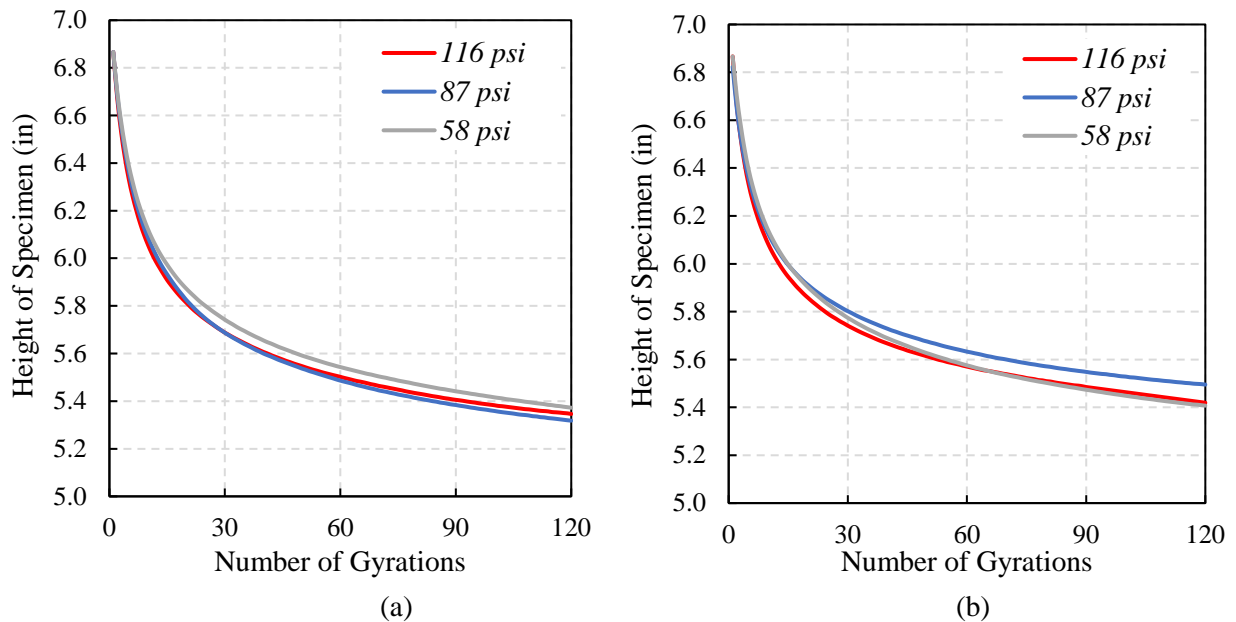


Figure 8-5: Variation of Height of Specimen Versus Number of Gyration for Different Compaction Pressures – (a) Angle of Rotation = 1.25° (b) Angle of Rotation = 1.16°.

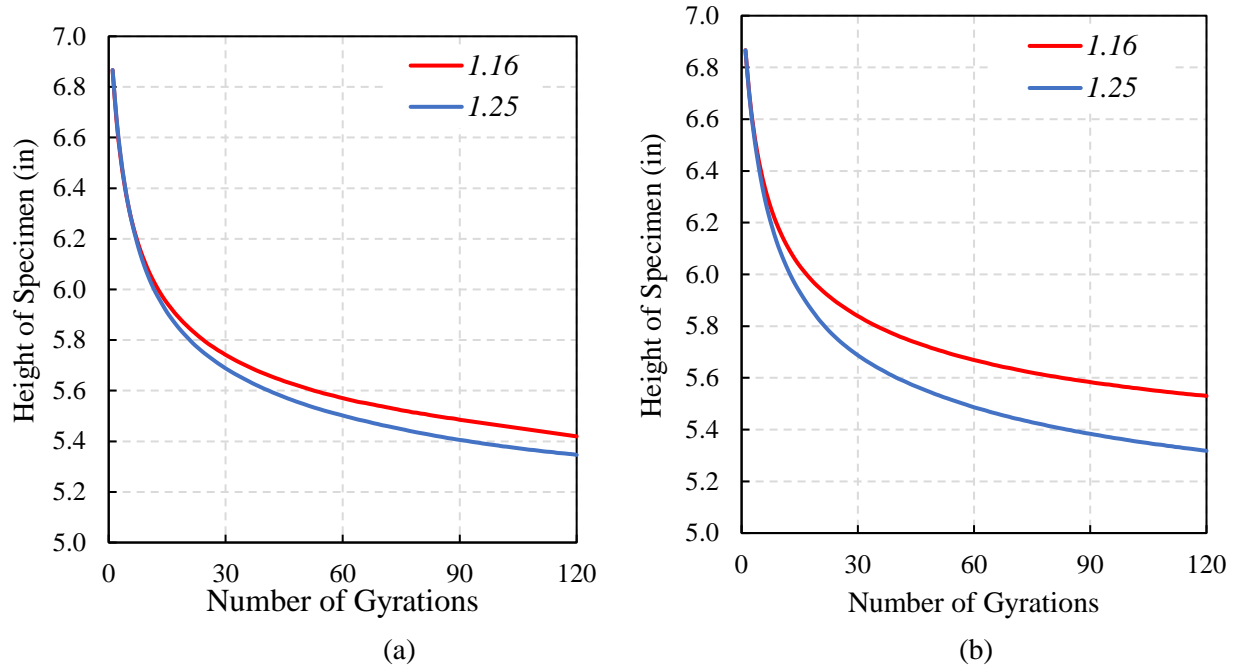


Figure 8-6: Variation of Height of Specimen Versus Number of Gyration for Different Angle of Rotations – (a) Compaction Pressure = 116 psi (b) Compaction Pressure = 87 psi.

Figure 8-7 and 8-8 represent unconfined compressive strength and density results for stabilized materials with different angle of rotations and compaction pressure, respectively. The plots show the beneficial role of the increase of angle of gyration on the compressive strength and density of stabilize base aggregates. As observed in the plots, compressive strengths for stabilized specimen with 1.25° angle of gyration were approximately 25% higher than the same specimen with 1.16° angle of gyration. This could be attributed to the higher packing of aggregate systems and particle orientation of specimens fabricated with gyratory compactor in higher angle of rotation. Aggregate particles subjected to compaction tend to rearrange themselves in a way as to increase particle contacts and reduce air voids to achieve maximum strength and density (Ashtiani, 2009). This information was utilized for the selection of the compaction parameters of cement stabilized materials for the gyratory compactor.

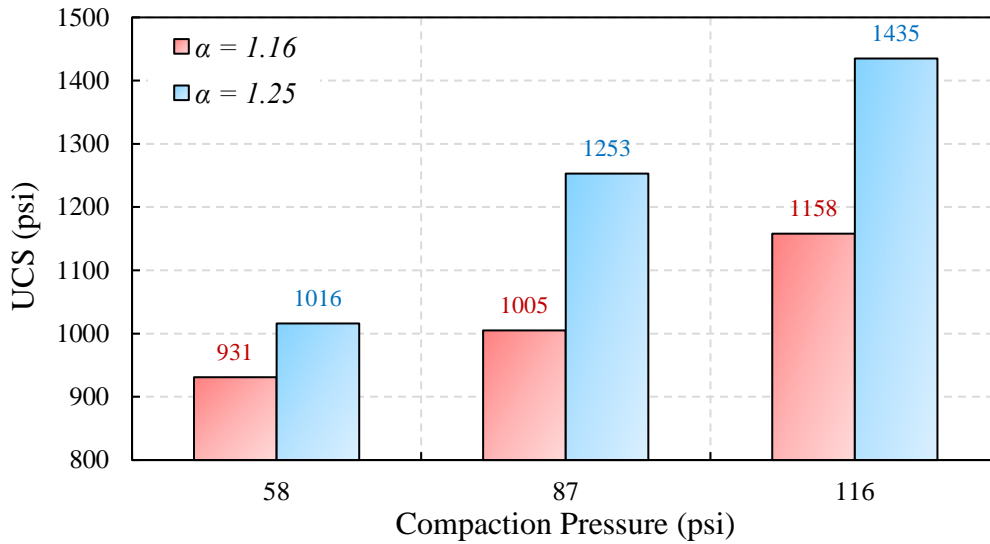


Figure 8-7: Unconfined Compressive Strength Test Results for Stabilized Materials with Different Angle of Rotations and Compaction Pressure.

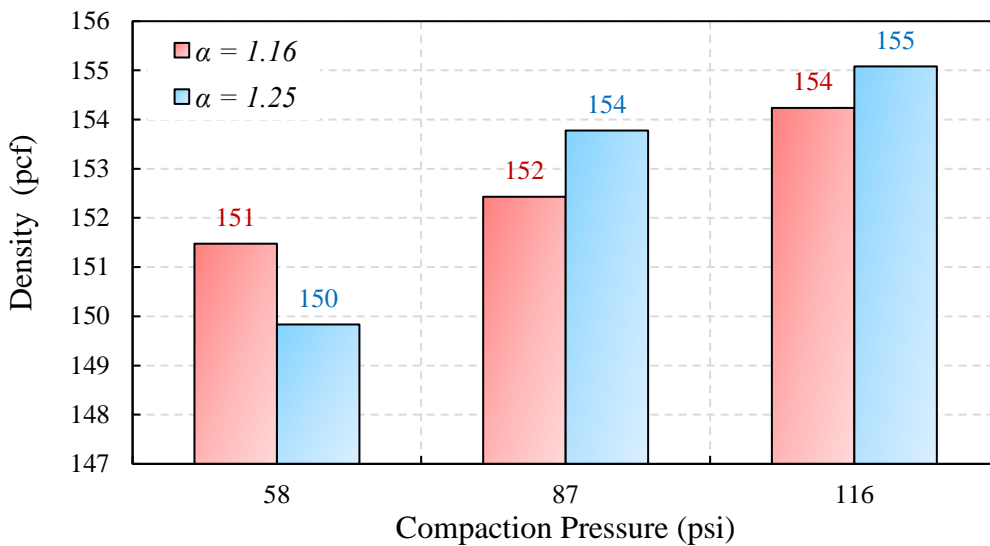


Figure 8-8: Density of Stabilized Materials Compacted by Gyratory Compactor with Different Angle of Rotations and Compaction Pressure.

Since there is no standard test procedure to compact stabilized base aggregates and subgrade soils with gyratory compactor, a new procedure was developed by applying the suitable compaction parameters obtained from both factorial analyses in this study and previous works. Table 8-2 lists the finalize compaction parameters used to compact the stabilized base aggregates and subgrade soils with the gyratory compactor.

Table 8-2: Main Variables of Gyrotory Compactor in Previous Studies.

Parameters	Values
Specimen diameter (in)	Base: 6 in. / Subgrade: 4 in.
Gyration rate	30 gyration/min
Number of Gyration	120
Angle of gyration	1.25°
Compaction pressure	87 psi

8.4 Compaction Energy

The work done by compacting the aggregates with a compactor is known as the compaction effort or compaction energy. Different compaction procedures apply different levels of compaction energy and mechanism on the stabilized mixture. For the impact hammer technique, the energy is transferred through the hammer to the soil. As illustrated in Table 8-3, the impact hammer compaction energy is determined by the height of drop, the hammer weight, the number of blows per layer, number of layers, and the volume of the mold. Vibratory hammer has a different mechanism of compaction. An estimate of the compaction effort for this procedure can be calculated by converting the electrical input to the compaction devices into energy. The energy applied per volume of aggregate compacted was computed with following equation developed by Arcement and Wright (2001):

$$CE = \frac{W \times e \times t \times f_s \times N_{layers}}{Volume} \quad \text{Equation 8-1}$$

Where W is the Electrical Input, e is the Efficiency of the Equipment, t is the time of vibration, f_s is the electrical input imparted into the aggregates, and N_{layers} is the number of layers. Based on the previous experience, values of 50% were assumed for the equipment efficiency and fraction of energy transmitted to the soil (TxDOT, 1874).

For the gyrotory compactor, the compaction energy is transferred to the soil through the vertical pressure and shear stress. The method of estimating the compaction energy in the gyrotory compactor is presented in Table 8-3. The results indicate that the compaction energy of the impact hammer is over 10% and 75% greater than energy created by the gyrotory compactor and vibratory hammer in the same mold size, respectively. This could be attributed to the fact that too much energy is lost during compaction in the impact hammer.

Table 8-3: Calculation of Compaction Energy for Different Compaction Procedures.

Compaction Type	Energy (N-m)	Equation for Calculation Compaction Energy	Parameters	Reference
Impact Hammer	32,849	$CE = \frac{\text{Height} \times \text{Weight} \times N_{\text{blows}} \times N_{\text{layers}}}{\text{Volume}}$	N_{blows} : Number of blows N_{layers} : Number of layers	Tex-113-E
Vibratory Hammer	18,102	$CE = \frac{W \times e \times t \times f_s \times N_{\text{layers}}}{\text{Volume}}$	W : Electrical Input e : Efficiency of the Equipment t : time of the vibration	TxDOT-1874 report (Arcement & Wright, 2001)
Gyratory Compactor	29,752	$CE = P_{\text{vertical}} \times A_{\text{sample}} \times \left(\frac{H_{\text{before}} - H_{\text{after}}}{A_{\text{force}}} \right)$	H_{after} : Height of specimen after compaction H_{before} : Height of specimen after compaction P_{vertical} : Vertical Force	Florida DOT report (Ping et al., 2003)

8.4.1 Moisture-Density Evaluation

Moisture density relationships were developed for various material types and different compaction methods in order to determine the applicability of the gyratory compactor and vibratory hammer to prepare a uniform cement stabilized specimen in the laboratory, as shown in Figures 8-9 and 8-10. The results indicated that the maximum dry density of specimens fabricated with gyratory compactor were significantly higher than specimens compacted with impact and vibratory hammers. For instance, the stabilized RCA materials compacted with gyratory compactor had approximately 10% and 15% higher density when compared to the results obtained from impact and vibratory hammer compaction procedures, respectively. This could be attributed to either providing more uniform specimens or minimizing the interface barrier between layers when using the gyratory compactor.

The stabilized base materials are compacted in six lifts by impact and vibratory hammers. This produces interfaces between lifts which ultimately result in higher air void contents. However, in the gyratory compaction, all layers were compacted and gyrated together at one time. This indicates that impact and vibratory hammer compaction methods are not sufficient to compact soils.

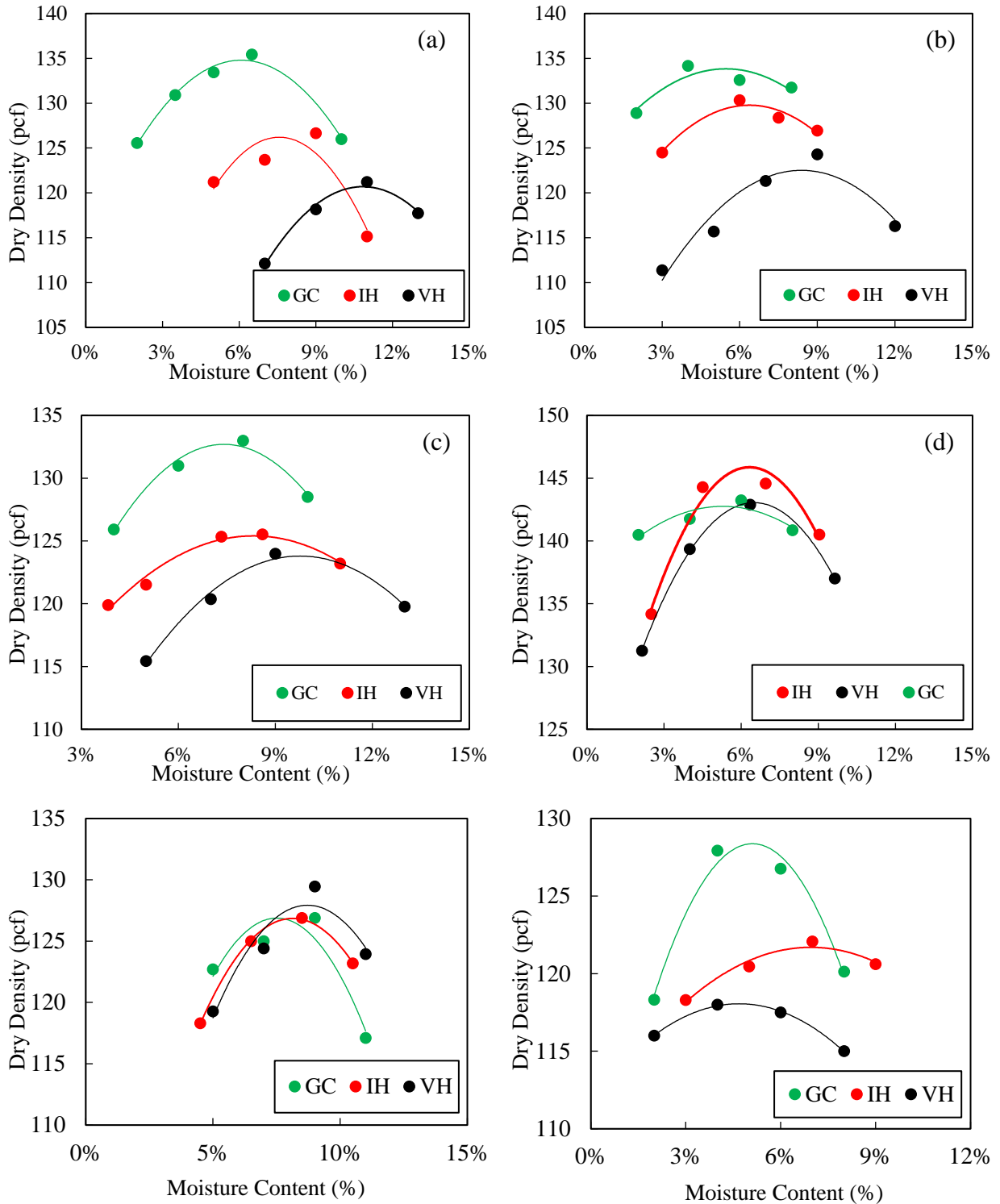


Figure 8-9: Moisture-Density Curves for (a) RCA Materials Sourced from Houston, (b) FDR Materials Sourced from Atlanta, (c) Siliceous Gravel Materials Sourced from Pharr, (d) Limestone Aggregates Sourced from El Paso, (e) Limestone Aggregates Sourced from Houston, and (f) RAP materials Sourced from Atlanta.

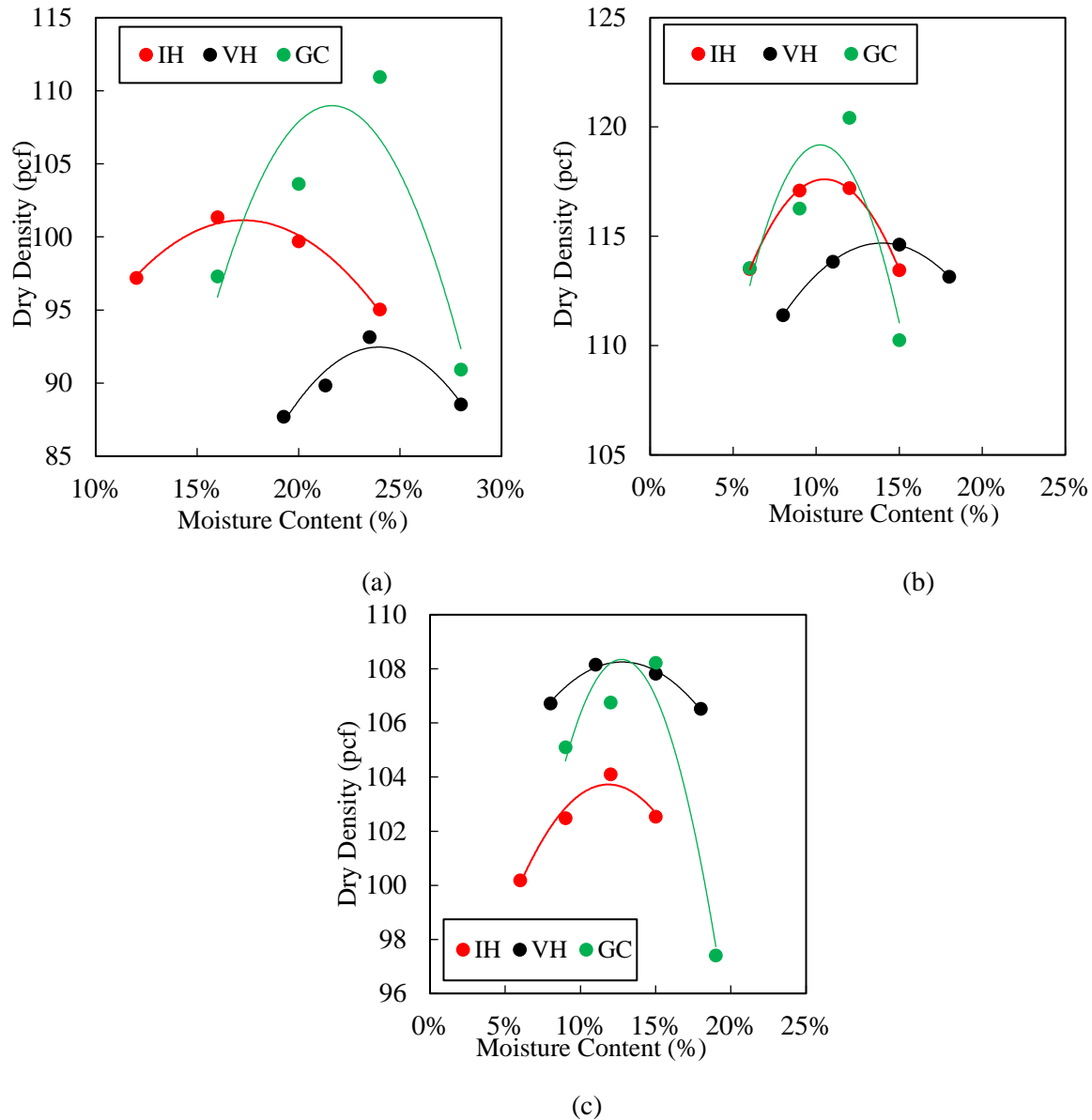


Figure 8-10: Moisture-Density Curves for (a) Clayey Materials Sourced from Sierra Blanca, (b) Sandy Soils Sourced from El Paso, and (c) Sandy Soils Sourced from Corpus Christi.

Figures 8-11 and 8-12 show the variation of optimum moisture content for stabilized base aggregates and subgrade soils with different compaction procedures, respectively. All base aggregates and subgrade soils except of RAP materials compacted with vibratory hammer yielded considerably higher OMC values compared to gyrotory compactor and impact hammer. This could be due to the low compaction energy in the vibratory hammer in comparison with other compaction procedures which results in the need of high moisture content to achieve the target density. Additionally, stabilized base aggregates compacted with the impact hammer exhibit greater optimum moisture contents than the gyrotory compactor. This could be due to the high particle breakage and fine generation in the impact hammer, which likely caused an increase in the surface

area of the crushed particles. The growth of surface area of aggregate particles during the compaction increases the optimum moisture content values in the stabilized mixture.

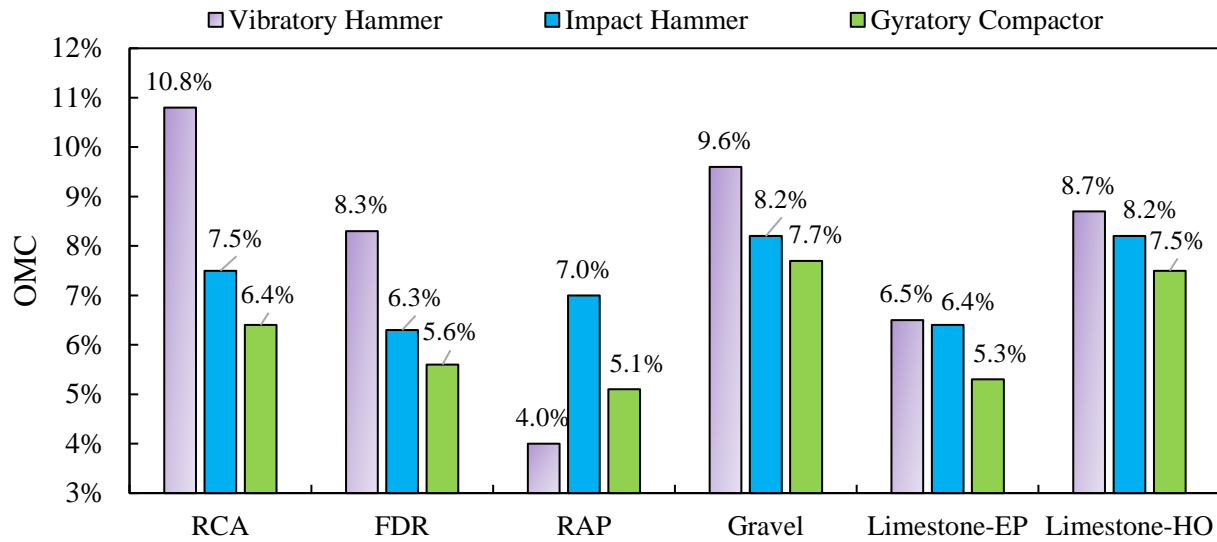


Figure 8-11: Optimum Moisture Content for Different Types of Stabilized Base Aggregates with Different Compaction Procedures.

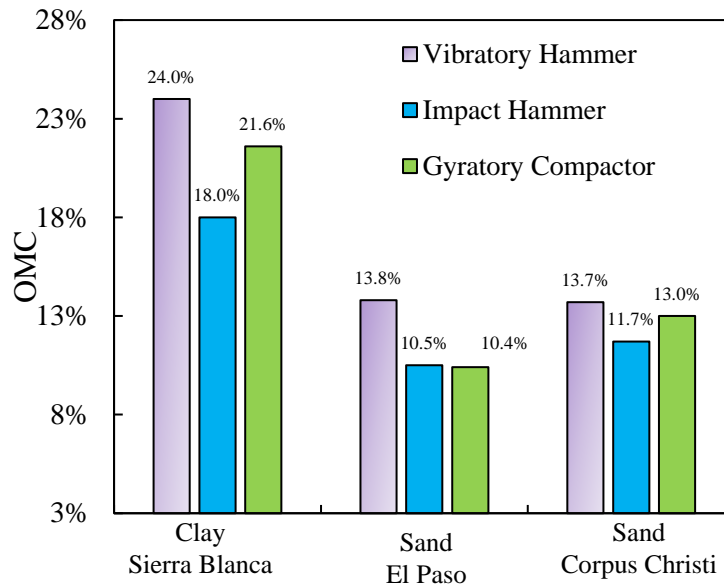


Figure 8-12: Optimum Moisture Content for Different Types of Stabilized Subgrade Soils with Different Compaction Procedures.

Figures 8-13 and 8-14 represent the maximum dry density for different types of stabilized base aggregates and subgrade soils with different compaction methods. The plots show that the reclaimed materials and marginal aggregates prepared with the gyrotory compactor provided considerably higher maximum dry density values compared to other compaction methods. For instance, the maximum dry density obtained from RCA materials sourced from Houston was 7%

and 12% higher than the density obtained from impact and vibratory hammers, respectively. One reason for higher maximum dry density in the specimens prepared with gyratory compactor can be the fact that the gyratory compaction can provide more uniform specimens and the interface barrier between layers is minimized. In the impact and vibratory hammers, the stabilized base and subgrade materials are poured and compacted in few lifts. Therefore, there are interfaces between lifts that have higher void contents and ultimately lower density (Sebesta et al., 2009).

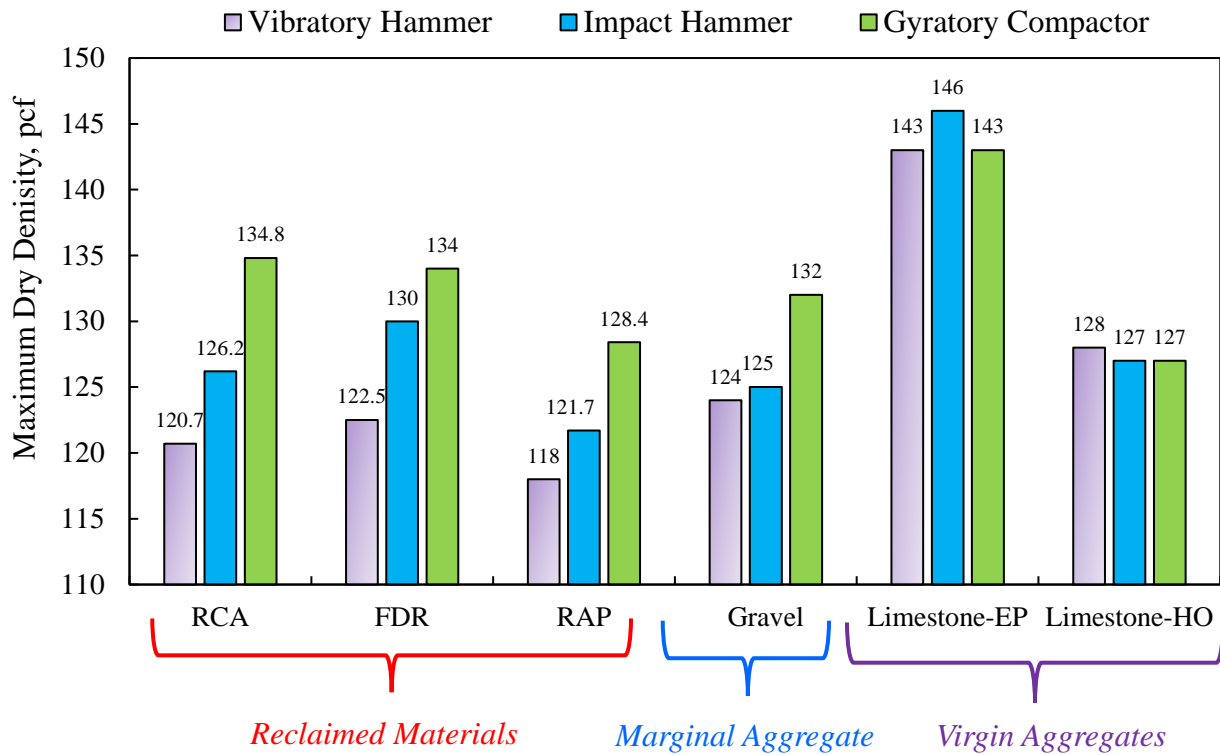


Figure 8-13: Maximum Dry Density for different Types of Stabilized Base Aggregates with Different Compaction Procedures.

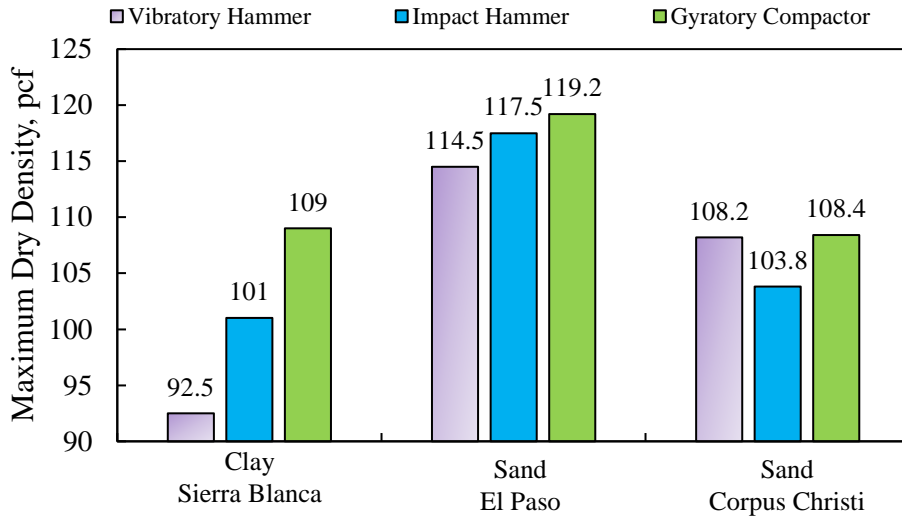


Figure 8-14: Maximum Dry Density for Different Types of Stabilized Subgrade Soils with Different Compaction Procedures.

Figure 8-15 represent the comparison between the impact hammer and gyrotory compactor for different stabilized materials. The radar chart revealed that density of stabilized materials obtained from gyrotory compactor is significantly higher than impact hammer for the majority of materials. This information can provide valuable insight on the selection of compaction procedures in the laboratory to simulate the field compacted conditions.

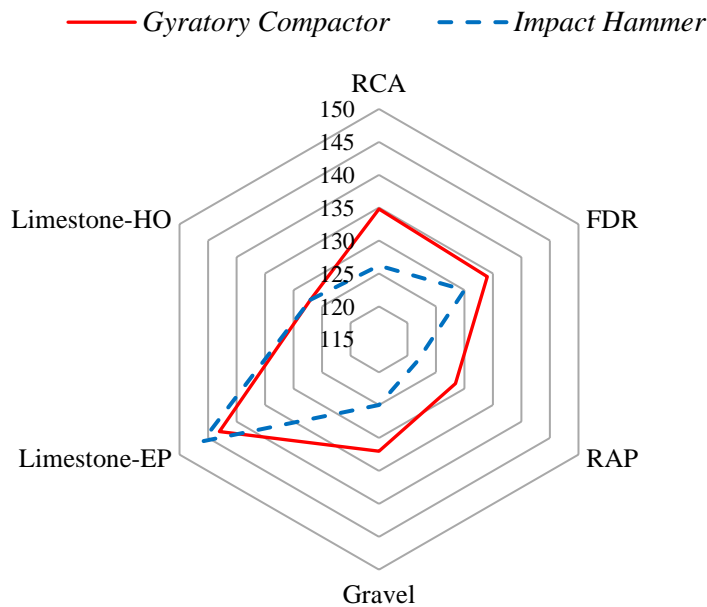
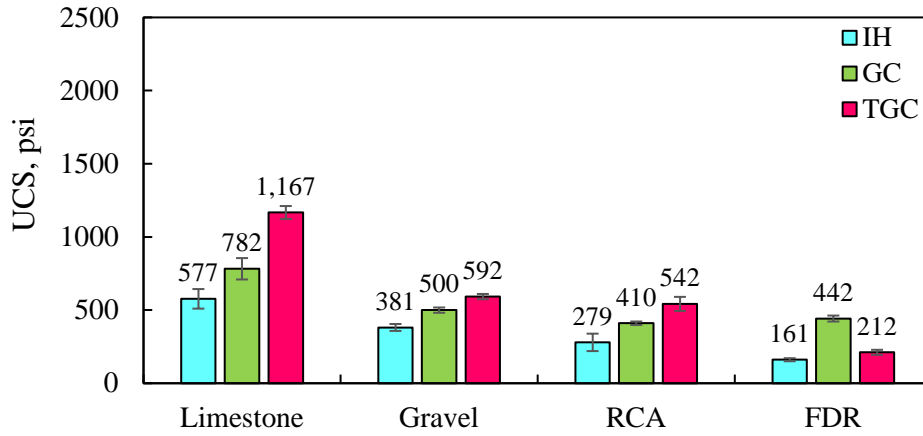


Figure 8-15: Maximum Dry Density for Different Types of Stabilized Base Aggregates Compacted with Impact Hammer and Gyrotory Compactor.

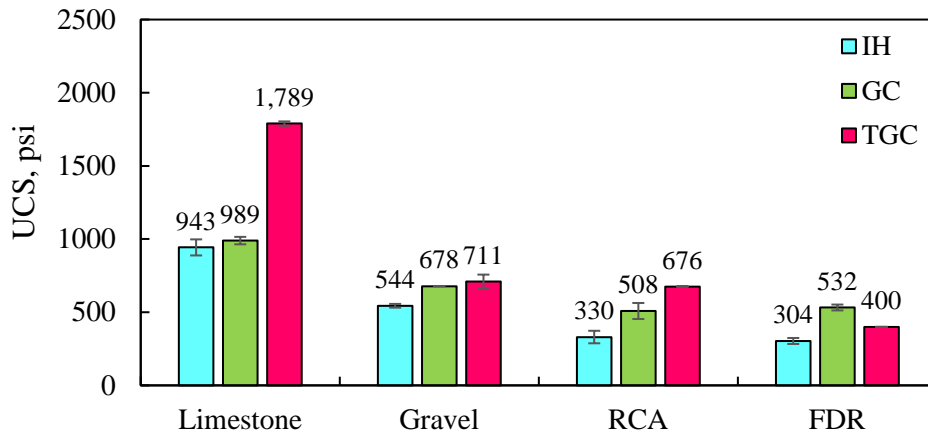
To compare the effect of the different laboratory compaction methods on strength properties of cement stabilized materials, UCS and IDT tests were conducted on the specimens compacted with

the four different compaction methods. Figure 8-16 shows the unconfined compressive strength results for samples stabilized with different cement contents ranging from 2% to 4% and compacted with impact hammer, gyratory compactor, and TGC. A notable observation in these plots is the significant underperformance of stabilized materials fabricated with impact hammer compared to other compaction methods. The underperformance of compacted specimens with impact hammer is more pronounced at low stabilized content. For example, the compressive strength of RCA specimens stabilized with 2% cement content drastically improved by 47% and 95%, respectively, by using gyratory compactor and TGC instead of impact hammer compaction method.

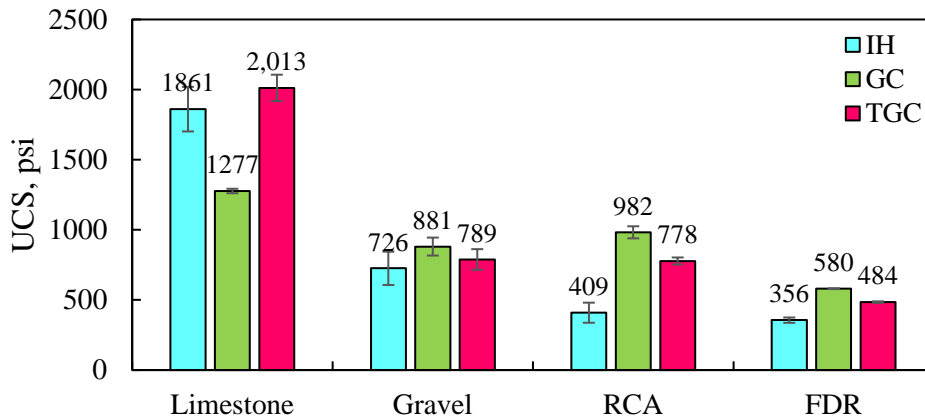
Unconfined compressive strength results for stabilized specimens compacted with impact hammer were compared against the results from vibratory hammer as observed in Figure 8-17. Stabilized specimens compacted with the impacted hammer exhibited relatively similar compressive strength to the specimens fabricated with the vibratory hammer. For instance, the compressive strength for gravel materials stabilized with 4% cement content was 418 and 410 psi, respectively, when the specimens were compacted with the impact hammer and vibratory hammer.



(a)

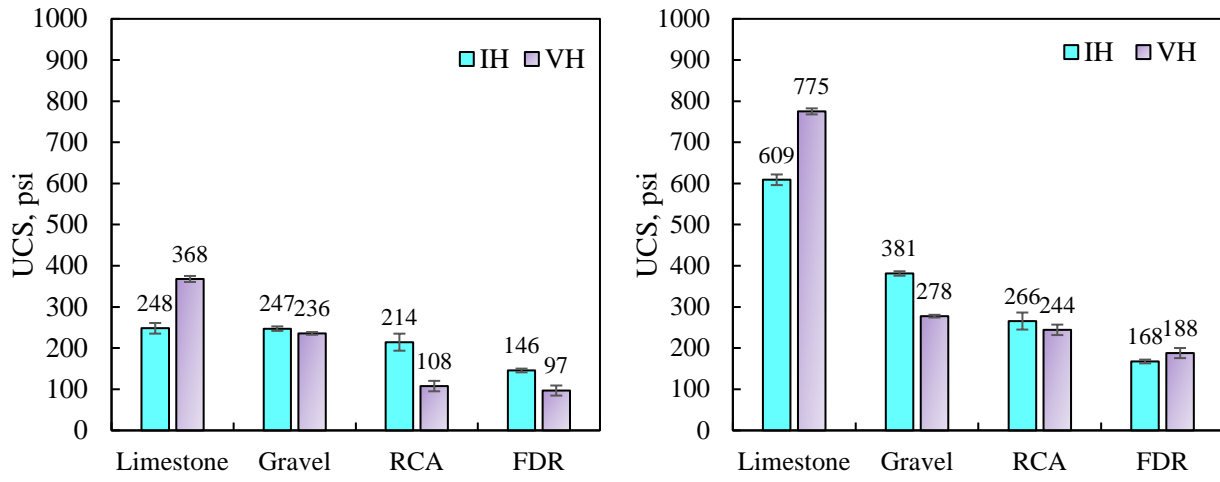


(b)



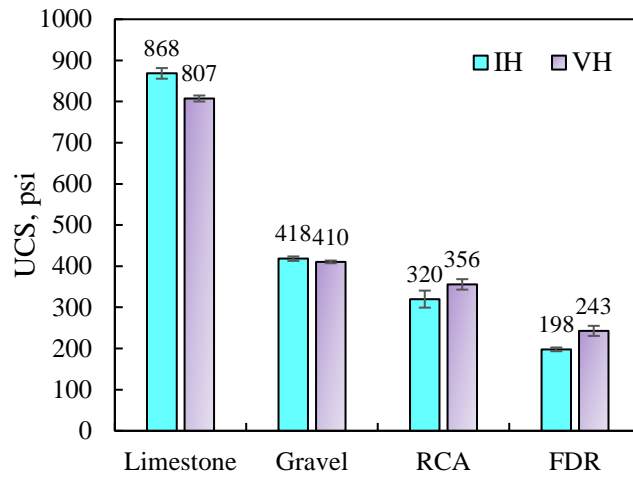
(c)

Figure 8-16: Unconfined Compressive Strengths Results for Samples Stabilized with (a) 2%, (b) 3%, and (c) 4% Cement Contents and Compacted with Different Compaction Procedures.



(a)

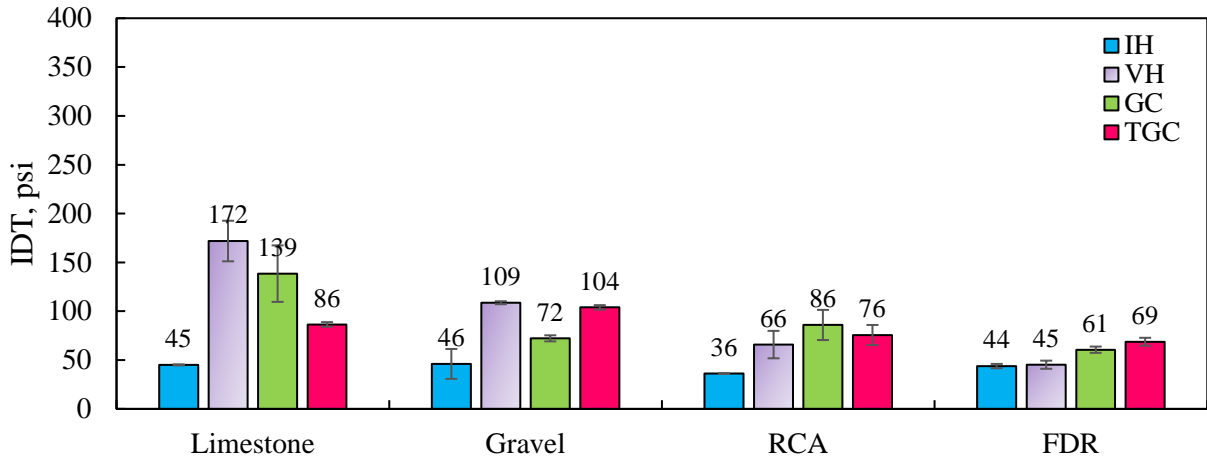
(b)



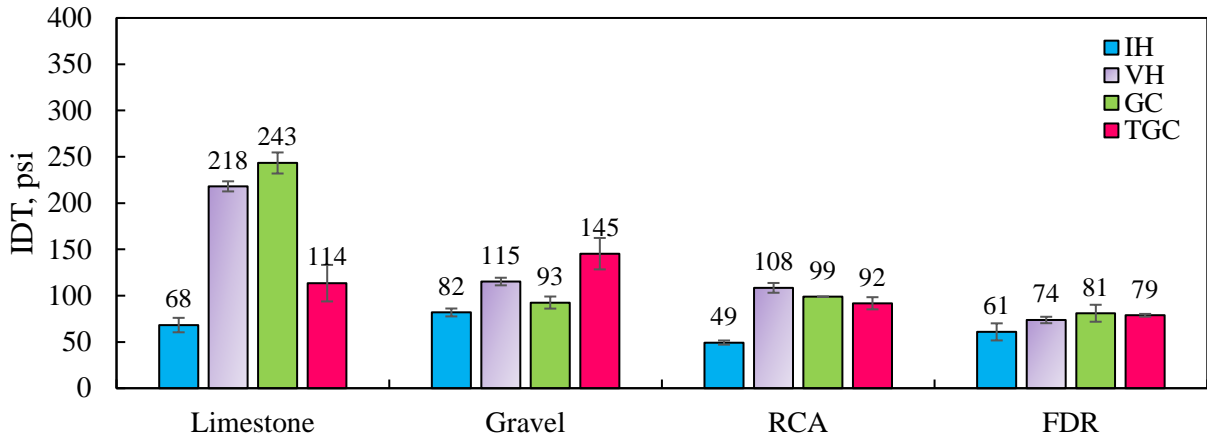
(c)

Figure 8-17: Unconfined Compressive Strengths Results for Samples Stabilized with (a) 2%, (b) 3%, and (c) 4% Cement Contents and Compacted with Different Compaction Procedures – (L/D ratio = 2).

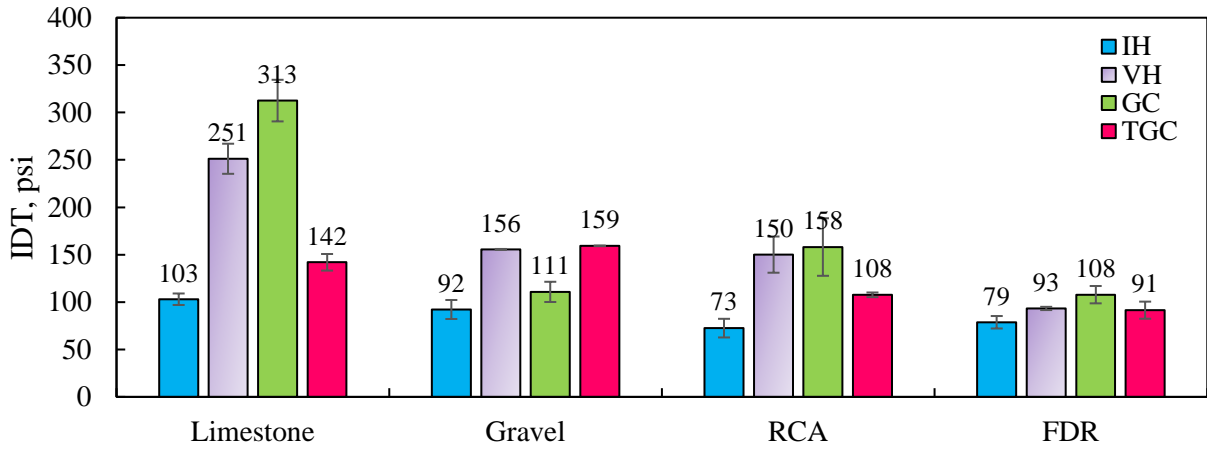
Strain controlled indirect tensile strength tests were performed on 4×4 inches stabilized specimens compacted with four different compaction methods. Similar to the UCS and moisture density tests results, the lightly stabilized specimen compacted with the impact hammer did not provide sufficient tensile strength, as observed in Figure 8-18. For instance, the tensile strength of RCA specimens stabilized with 2% cement content and compacted with impact hammer was 36 psi, while the same percentage of cement content for the specimens fabricated with gyratory compactor, vibratory hammer, and TGC resulted in approximately 85%, 140%, 115% improvement in the IDT strength, respectively. This underscores the influence of the compaction procedure for the analysis of strength properties of geomaterials in the laboratory.



(a)



(b)



(c)

Figure 8-18: Indirect Tensile Strength Results for Samples Stabilized with (a) 2%, (b) 3%, and (c) 4% Cement Content and Compacted with different Compaction Procedures.

8.5 Aggregate Breakdown in Impact Hammer

Due to particle breakage while using the impact hammer, sieve analysis was also performed after each compaction methods to identify particle loss and fines generation in different compaction process. This analysis deems necessary due to the disintegration and crumbling potential of some aggregate materials as observed in Figure 8-19.



Figure 8-19: Aggregate Breakage during the Impact Hammer Compaction.

Figure 8-20 present the schematic diagrams of aggregate breakage after impact hammer compaction for different base materials. The plot indicates that aggregate particle with a sieve number size over #4 degraded most seriously for the majority of base materials. For instance, the percentage of RAP particles with the size of 3/8 inches significantly reduced around 35% after the impact hammer compaction. Figure 8-21 represents the average percentage of the particle breakage for all base materials after subjecting them to the impact hammer. The results clearly indicate that the coarse particle size base aggregates ranging from 3/8 to 1 3/4 tend to be finer particles. The percentage of materials passing sieve #200 increased notably by 41% after compaction with the impact hammer for different geomaterials. This indicates the remarkable influence of the impact hammer on the performance of cement stabilized materials. Figure 8-21 also shows that 40% of the gravel size aggregates was reduced after impact hammer compaction and the breakdown aggregates became sand and fine materials in the mixture. This is due to the fact the large-sized particles, which generally undertook skeleton effects, were crushed more easily when subjected to impact hammer compaction.

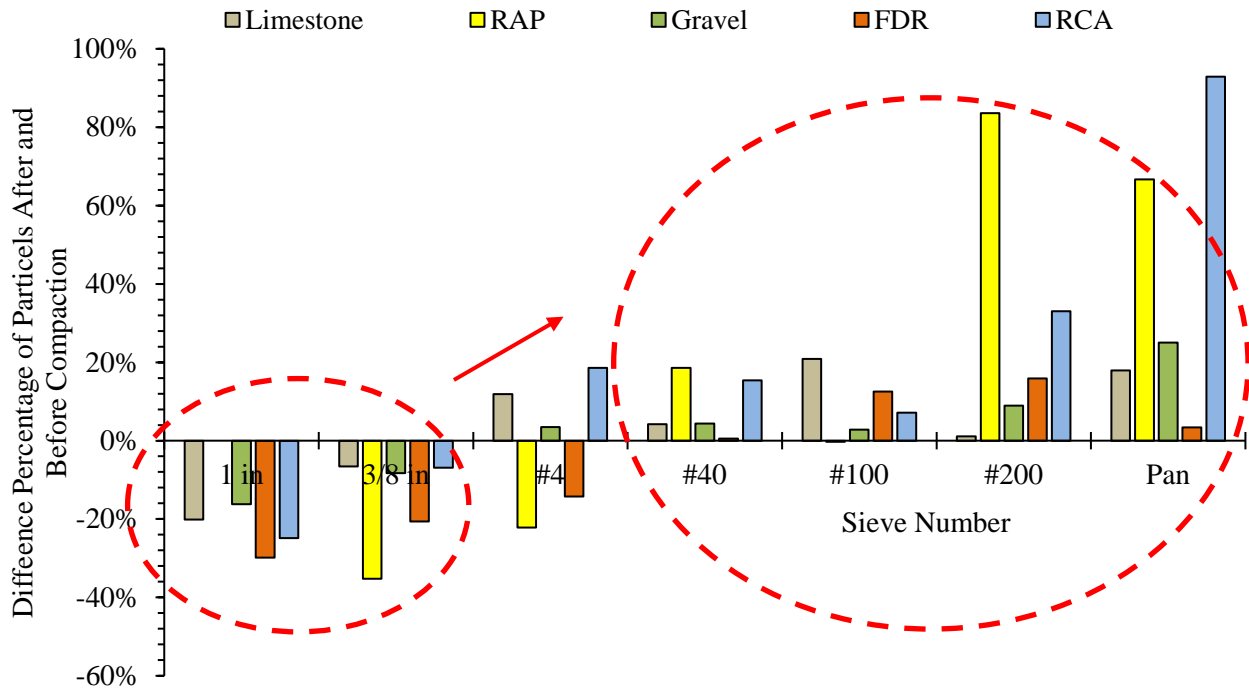


Figure 8-20: Schematic Diagrams of Aggregate Breakage after Impact Hammer Compaction for Different Base Materials.

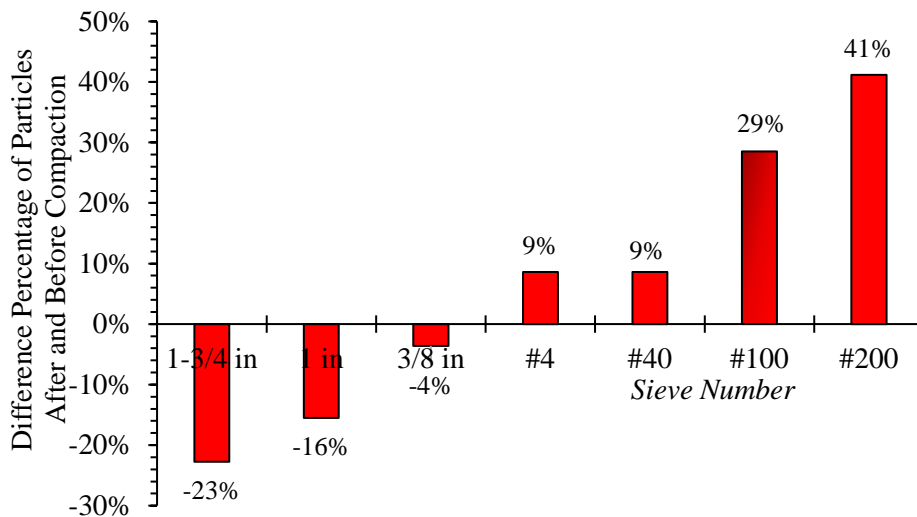


Figure 8-21: Schematic Diagrams of Aggregate Breakage after Impact Hammer Compaction for all Base Materials.

Schematic diagrams of aggregate breakage after different compaction methods for limestone aggregates sourced from El Paso is shown in Figure 8-22. The results revealed that the particle loss and fines generation after vibratory hammer and gyratory compactor was considerably lower than the impact hammer for limestone aggregates. For instance, the percentage of particle breakage

with 1-inch size was 20%, 10%, and 3%, respectively, for impact hammer, vibratory hammer, and gyratory compactor. In other words, the aggregates after gyratory compactor degraded the least. This indicates that gyratory compaction could better maintain the skeleton of cement stabilized base materials.

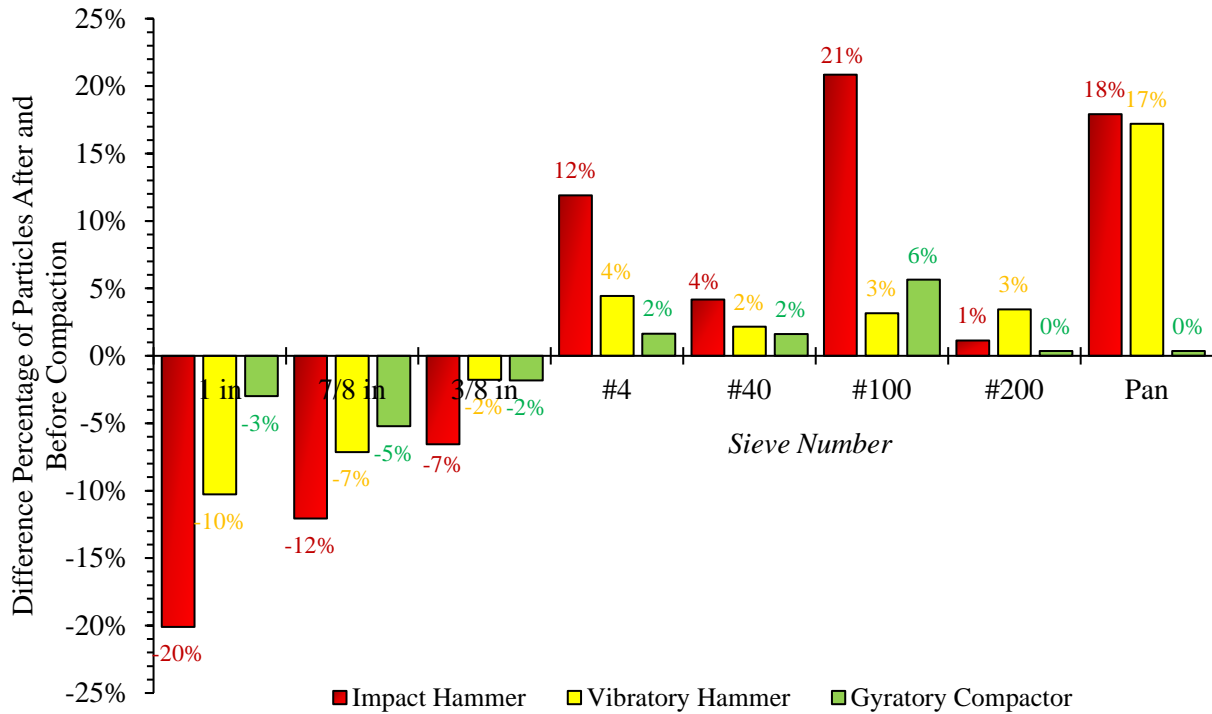


Figure 8-22: Schematic Diagrams of Aggregate Breakage after Different Compaction Methods for Limestone Aggregates Sourced from El Paso.

Chapter 9. Strategies to Improve Orthogonal Strength Capacity and Volumetric Stability of Expansive Soils

9.1 Introduction

In many parts of the United States, expansive soils pose serious challenges such as excessive rutting, swelling, and cracking of pavement structures. These highly plastic soils are prone to adsorb a significant amount of moisture and expand upon moisture intrusion due to seasonal moisture variation. Stabilization technique with calcium-based stabilizers has been proven to be a cost-saving option to mitigate the swelling potential and improve the volumetric stability of expansive soils in lieu of soil replacement or thickening of the base course layer. Although the solution appears simple and straight forward, engineering properties of fine-grained soils may vary widely due to heterogeneity in soil composition and differences in physical and chemical interactions with calcium-based stabilizers. Such chemical additives usually do not provide effective treatment for clay soils containing large amounts of soluble sulfates. New methods such as the use of polypropylene fibers are still needed for the reinforcement and stabilizations of expansive soils to reduce swelling and enhance mechanical properties of subgrade soils. Therefore, this chapter was designed to investigate the effectiveness of polypropylene fiber along with chemical additives on the strength properties and volumetric stability of expansive soils. To accomplish this objective, different quantities of chemical additives such as cement, lime, and fly ash as well as different proportionate of polypropylene fibers were mixed with two types of high plasticity soils of variable sulfate content. More than 500 stabilized samples were prepared and subjected to the unconfined compressive strength test, one dimensional swell test, swell pressure test, methylene blue value test, and Atterberg limits test.

9.2 Methodology

For the experimental program of this study, three fine-grained subgrade soils collected from Houston and Bryan (East of Texas) and Sierra Blanca (West of Texas) were incorporated in this research (Figure 9-1). All these soils are classified as a clay with high plasticity (CH) in accordance with the Unified Soil Classification System (USCS). Different chemical stabilizer additives such as Cement Type I/II, Lime, Fly Ash class C ranging from 3% to 7% were added to each permutation of the experiment design to achieve permanently modified properties, and improve strength and compactability of subgrade soils. Additionally, polypropylene fibers with a length of 0.75 inches were used as the reinforcements at proportionate quantities of 0.2% and 0.4% of the dry weight of the soil. The combination of fibers with different dosages of cement binders to enhance the improving effect of fibers for increasing the mechanical properties of soft clays were also investigated in this research study. Subsequently, the variants of the experiment matrix were subjected to several laboratory tests to characterize the compressive behavior, moisture adsorption potential, plasticity, and swelling potential of stabilized subgrade soils as depicted in Figure 9-2.

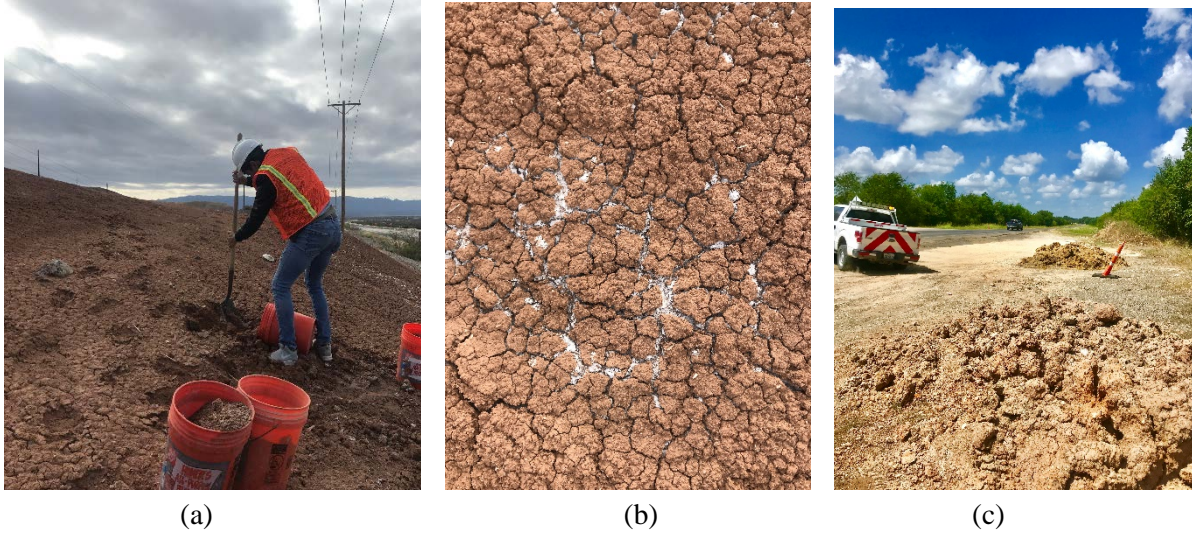


Figure 9-1: Expansive Subgrade Soils sourced from (a and b) Sierra Blanca, and (c) Bryan.

The moisture-density tests were performed on untreated materials to identify the Optimum Moisture Content (OMC) and Maximum Dry Density (MDD) following the standard test method specified by Texas Department of Transportation (Tex-114-E specification). The Atterberg limits tests were also performed to determine the Plastic Limit (PL), Liquid Limit (LL), and the Plasticity Index (PI) of the subgrade materials following Tex-104-E, Tex-105-E, and Tex-106-E specifications, respectively. Additionally, soluble sulfate content of soils was calculated by using the colorimetric method according to Tex-145-E specification. Table 9-1 presents parameters pertaining to the Atterberg limits, moisture-density, and sulfate content tests for subgrade soils evaluated in this study. The table indicates that clayey materials sourced from Sierra Blanca with sulfate concentration of 24,320 ppm was referred as the high sulfate (HS) soil. This value for clay sourced from Houston was 480 ppm, which is referred to as the low sulfate (LS) soil. The results also show that the clayey materials sourced from Bryan had highest plasticity index (PI=45), therefore, it is referred to as the high plasticity (HP) soil.



Figure 9-2: Testing Program for Expansive Subgrade Soils.

Table 9-1: Atterberg Limits and Moisture-Density Test Results

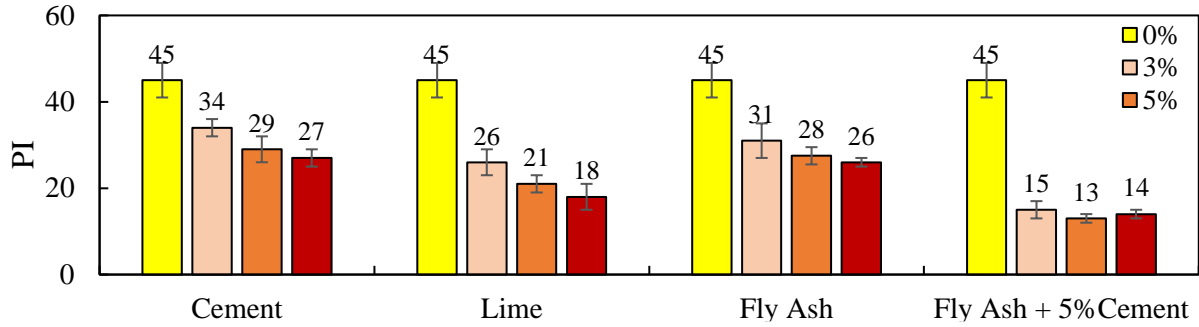
Soil Properties	Clay (HS)	Clay (HP)	Clay (LS)
	Sierra Blanca	Bryan	Houston
Liquid Limit (LL)	48	63	53
Plasticity Index (PI)	37	45	36
Maximum Dry Density (pcf)	101	102	103
Optimum Moisture Content	17.2%	20.1%	18.5%
Sulfate Content (ppm)	24,320	13,093	480

For the determination of the rate of volumetric strain in clayey subgrade materials stabilized with chemical additives, one dimensional swell and swell pressure tests were performed in this study. These swell tests characterized the swelling potential of expansive soils upon addition of cement, lime, fly ash, and polypropylene fibers in the mix in presence of moisture.

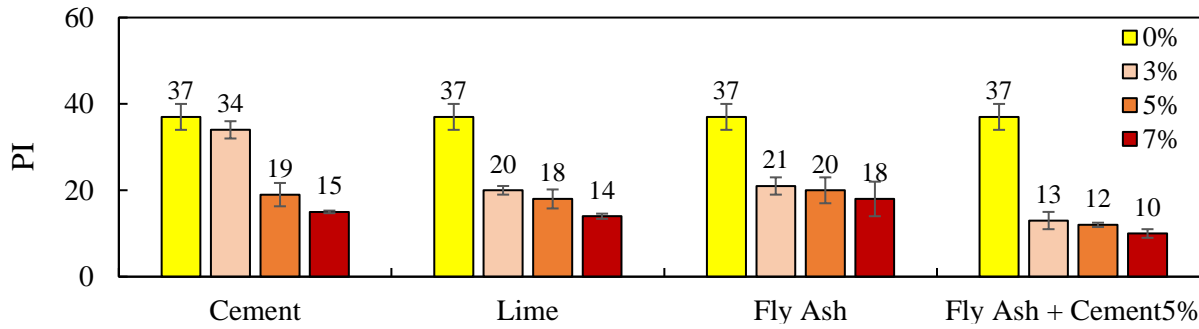
9.3 Atterberg Limits and Methylene Blue Value Test Results

Figure 9-3 show the plasticity index for all expansive subgrade soils with different stabilizers type and content. The Atterberg limits test results clearly indicate that a small amount of lime significantly changes the plasticity index of the LS soil. For instance, a small addition of 3% lime

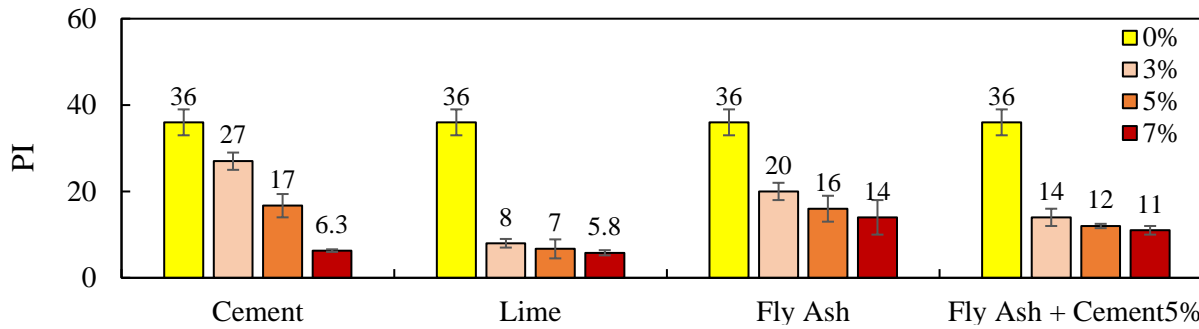
dramatically reduces the plasticity index of the LS soil from 36 to 8. Comparatively, calcium-based additives, whether lime or cement, do not work well on PI reduction for high sulfate (HS) bearing soils compared to the LS soil. This could be attributed to the sulfate attack on stabilized soils, which results in the deterioration of the cement-soil matrix. Another interesting observation depicted in this graph is that all expansive soils did not benefit more from the cement binders in terms of PI reduction unless a large amount of cement (such as 7%) was added to the mixture. These trends indicate that the strength of stabilized soils should be higher for cement stabilization at higher cement content. This expected behavior has been justified in the following section (UCS test results). Higher strengths for higher cement content can be attributed to the calcium hydroxide crystals as a rigid network produced during cement hydration. This rigid network is formed by the cement reaction products. At small dosages, the network may be small and isolated; at larger dosages, the reaction products may form large interconnected networks. These well connected networks leads to improve the strength and reduce plasticity of cement stabilized soils.



(a)



(b)



(c)

Figure 9-3: Plasticity Index for (a) the HP Soil, (b) the HS Soil, and (c) the LS Soil at Different Stabilizer Types and Contents.

Figure 9-4 present the methylene blue value (MBV) for all expansive soils stabilized with different chemical types and additives. As discussed in previous section, the methylene blue value indicates the moisture adsorption potential of fine grained soils. The results show that the methylene blue value decreases considerably after treatment with all chemical additives. Similar to the Atterberg limits test results, the methylene blue value was further decreased by adding lime to the mixture compared to other stabilizers. The MBV for both high and low sulfate soils was greatly reduced from 50 and 43 to 15 and 11 by adding only 3% lime content to the mixture, respectively. This indicates that small amount of lime decreases considerably the moisture adsorption potential of expansive soils, which leads to the reduction of activity and swell potential of plastic clays. Higher effect of lime on bringing down the plasticity and moisture absorption of clay subgrade soils can

be attributed to the higher concentration of calcium hydroxide in lime compared to cement and fly ash. Stocker (1975) found that cement generates calcium hydroxide at a rate of approximately 31% of its weight, while this rate for lime is considerably higher and is around 90%.

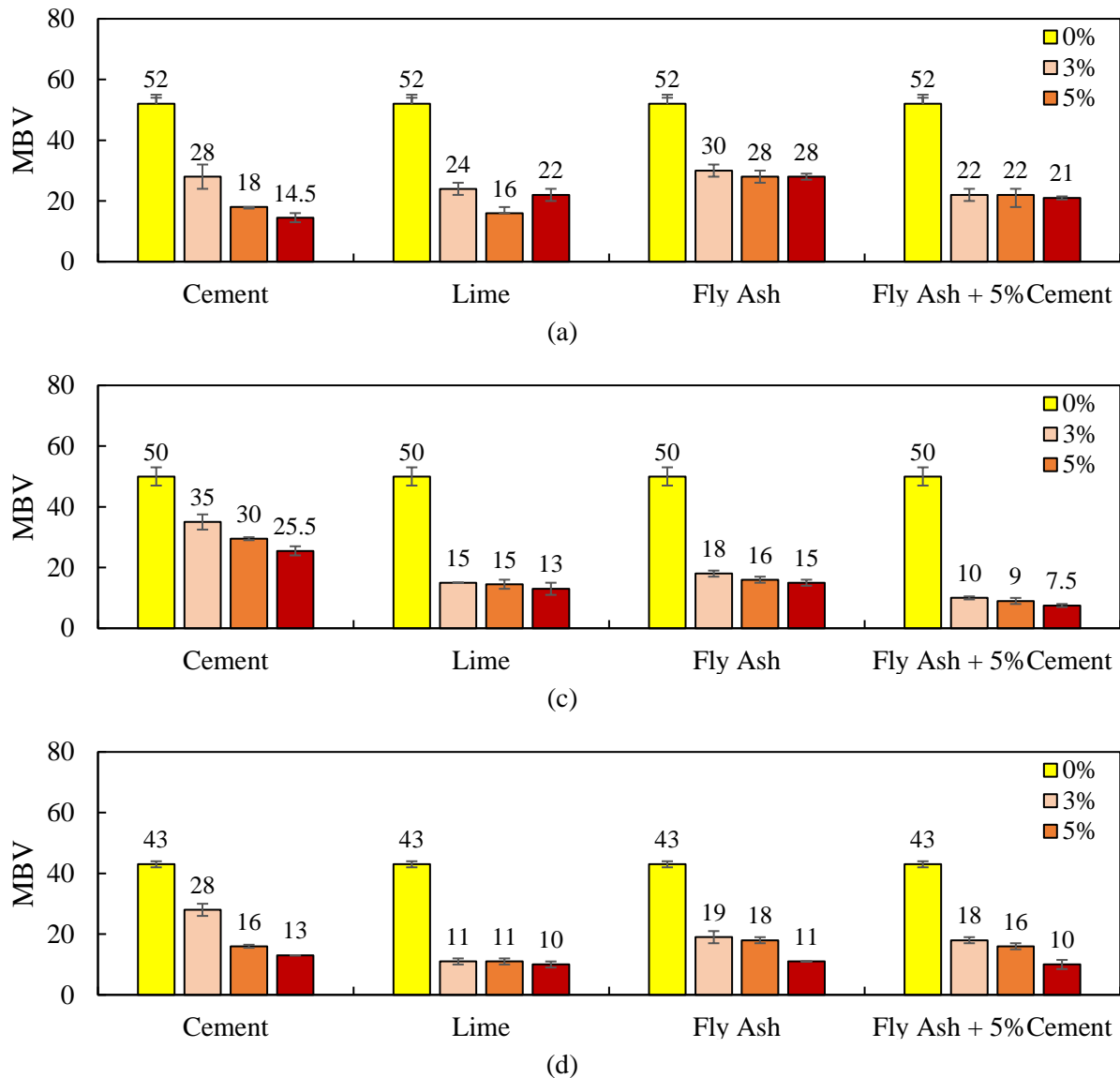


Figure 9-4: Methylene Blue Value for (a) the HP Soil, (b) the HS Soil, and (c) the LS Soil with Different Stabilizer Types and Contents.

The results of plasticity index were juxtaposed with the pH test as an excellent indicator of optimum lime content. The pH test is based on the philosophy of adding sufficient lime to a soil to satisfy cation exchange capacity of the soil and sustain the strength-producing lime-soil reactions. These reactions continue as long as the pH remains high and lime and pozzolans are available. Figure 9-5 demonstrate the results of the plasticity index and pH tests for high sulfate clay materials sourced from Sierra Blanca and Bryan. The results show that the plasticity index of lime treated clay soils had direct relationship with the pH value in the mixture. Little (1995)

reported that if the pH reading go to 12.40, the lowest percentage of lime that give a pH of 12.40 is the percentage required to stabilize the soil. These design lime percentage are 5% and 6% for expansive clayey soils sourced from Sierra Blanca and Bryan, respectively.

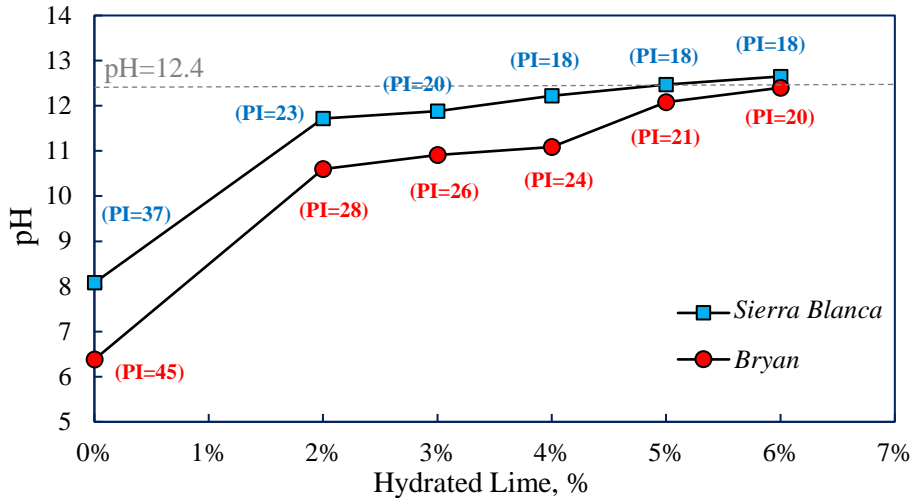


Figure 9-5: pH Test Results.

9.4 Swell Behavior of Expansive Soils

Expansive soils and high sulfate content soils in any layer of a pavement system are detrimental to its performance, creating problems such as swelling and cracking. Typically, highly plastic soils are prone to adsorb significant amount moisture and expand upon moisture intrusion. Cementitious stabilization often is used to mitigate the swell tendencies of expansive soil and sulfate-induced heave. In this study, one dimensional swell and swell pressure tests were performed to measure the rate of volumetric change in expansive soils.

Figure 9-6 demonstrates the swell pressure for all expansive soils with different binder types and contents. These plots clearly show how swell pressure of stabilized expansive subgrade soils is mitigated by the increase of chemical additives in the mixes. In general, when calcium-based additives are used to stabilize expansive soils, pH of the stabilized soil-mixture increases as shown in Figure 9-5. This leads to the formation of Calcium Silicate Hydrate (C-S-H) and Calcium Aluminum Hydrate (C-A-H) gels by dissolving the silica and alumina present in the clay, as indicated in Equations 9-1 and 9-2 (Eades & Grim, 1966). These gels are known to be the basic hydration product that contributes to the strength improvement and volumetric stability of the stabilized expansive soils.



Another noteworthy observation was the relatively higher swell pressure of high sulfate soil in comparison with low sulfate soil. This could be due to delayed formation of gypsum and ettringite in high sulfate materials.

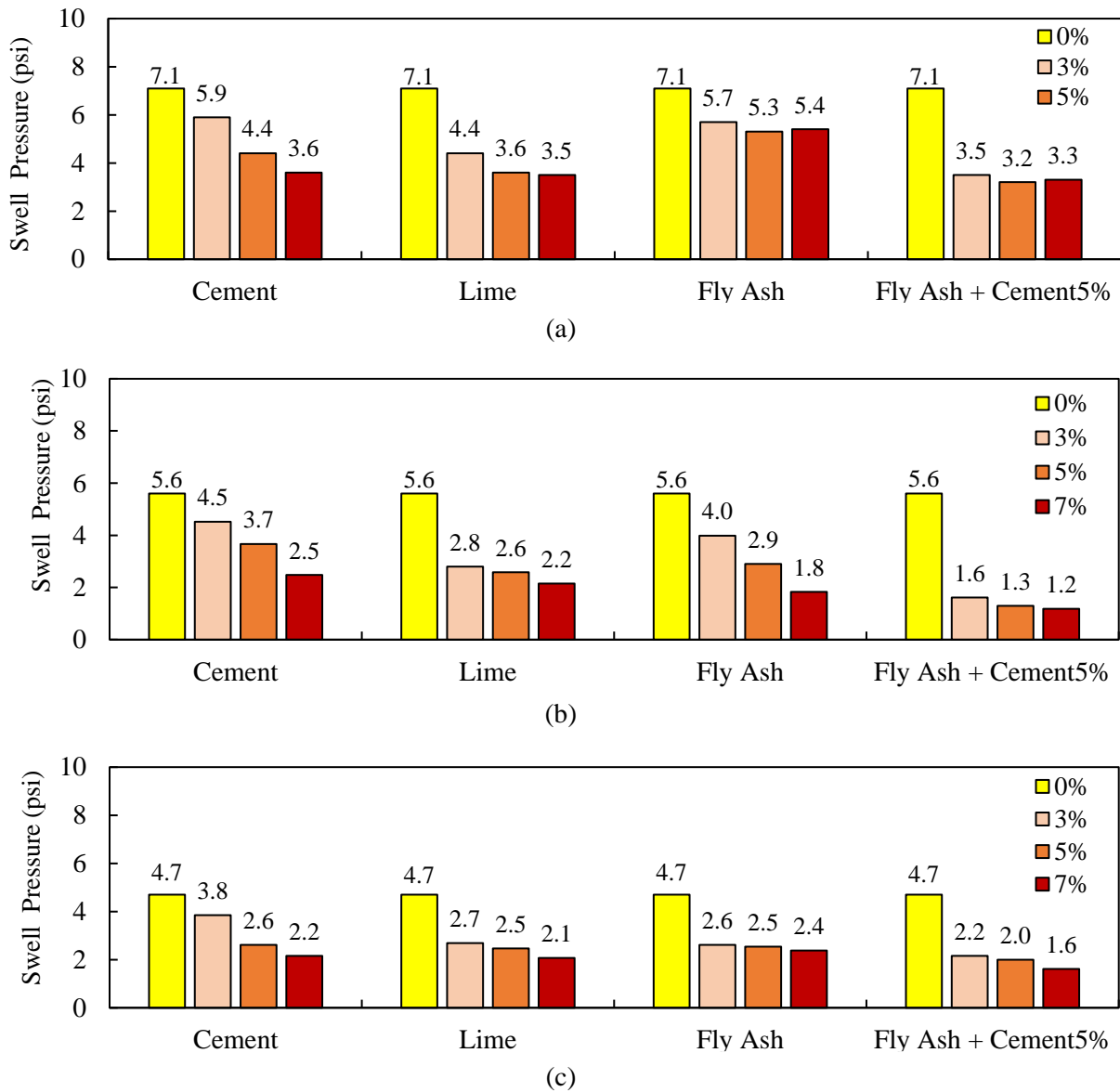


Figure 9-6: Swell Pressure for (a) the HP Soil, (b) the HS Soil, and (c) the LS Soil with Different Stabilizer Types and Contents.

Swell index obtained from one dimensional swell test for the expansive soils is presented in Figure 9-7. It is clearly seen that cement-fly ash combination had a substantial influence on the swell index of expansive soils compared to other chemical additives. For instance, the swell index of expansive soil sourced from Sierra Blanca was dramatically reduced from 12.7% (for unstabilized sample) to 1.3% by adding only 3% fly ash and 5% cement content to the mixture. Comparatively, the addition of 5% cement binder solely reduced the swell index of expansive soils to 6.3%. With

the increase of fly ash binders in the soil-cement mix, the pozzolanic activity of fly ash gradually appeared. As fly ash gradually reacts with $\text{Ca}(\text{OH})_2$, C-S-H gel will be formed, which constitutes a durable binder. This is an indication of the favorable contribution of fly ash and cement binders for improving the volumetric stability of expansive soils. This information can also provide valuable insight on the benefit-cost-ratio for the selection of stabilizer types and contents.

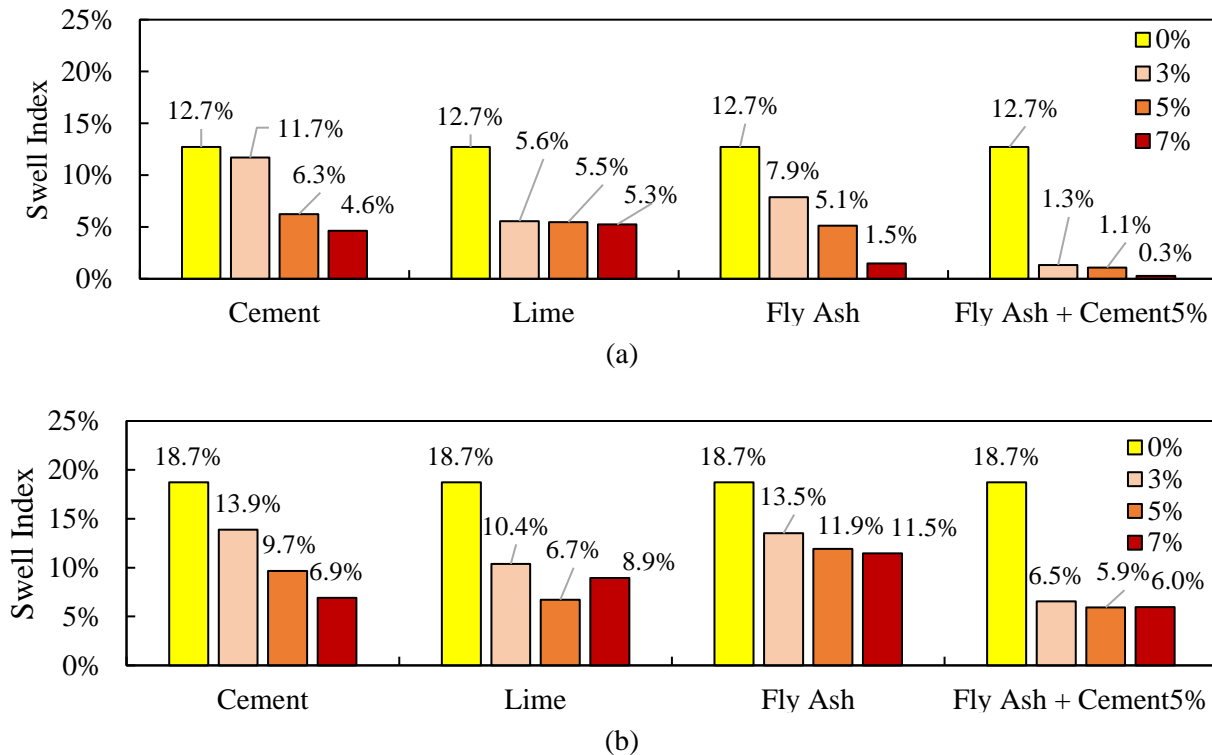


Figure 9-7: Swell Index and Swell Pressure for (a) the HS Soil and (b) the HP Soil with Different Stabilizer Types and Contents.

Figure 9-8 illustrates the combined role of chemical stabilization and fiber reinforcement on the swell behavior of expansive soils. Polypropylene fibers as a cross linking agent at proportionate quantities of 0.2% and 0.4% were added to the stabilized clay specimens with 0% to 7% cement content. As a result of fiber reinforcement, the swell index of cement stabilized clay samples exhibited a significant reduction. For instance, increasing polypropylene fibers from 0% to 0.2% for high sulfate clayey soil, resulted in more than 50% reduction in the swell index; while increasing cement binder from 0% to 3%, for the same subgrade soil, resulted in approximately 8% reduction in swell index. In optimal cases, the addition of 0.2% fibers along with 3% cement significantly decreased the swell index of the high sulfate clayey soil from 12.7% (for the unsterilized sample) to 4.1%. This underscores the influence of the fiber reinforcement, with environmentally friendly features, as a potential candidate for stabilized highly expansive subgrade soils.

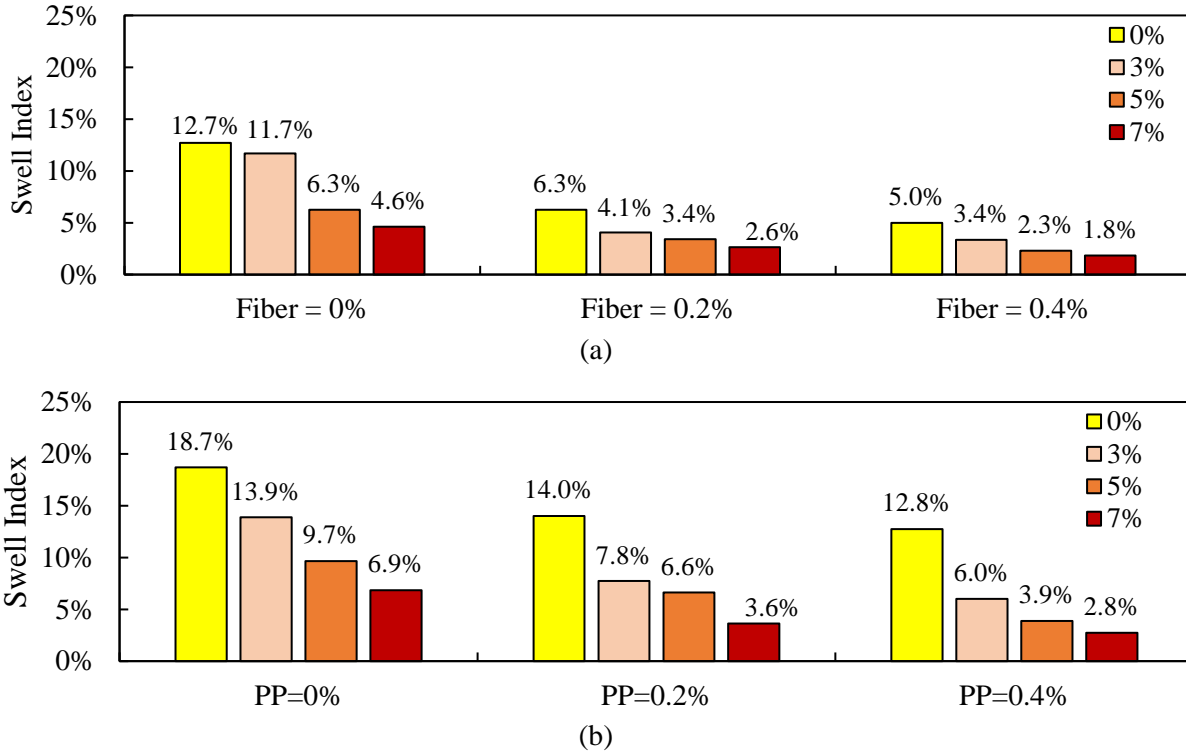


Figure 9-8: Swell Index for (a) the HS Soil and (b) the HP Soil with Different Stabilizer Types and Contents.

9.5 Statistical Modelling

Figures 9-9 to 9-11 provides the relationships between the methylene blue values with plasticity index, swell index, and swell pressure. The ascending nature of the trend lines suggest direct correlations of MBV, as an indication of the moisture adsorption potential, with PI, swell pressure, and index of expansive soils. In other words, permutations with higher MBVs exhibited higher plasticity index, swell pressure, and swell index compared to other counterparts in the experiment matrix. Equations 9-3, 9-4, and 9-5 presents the relationship between the MBV with PI, Swell Index (SI), and Swell Pressure (SP), respectively:

$$PI = 0.73 \times MBV + 4.3 \quad (R^2=0.64) \quad \text{Equation 9-3}$$

$$SI (\%) = 0.38 \times MBV - 0.39 \quad (R^2=0.72) \quad \text{Equation 9-4}$$

$$SP (\text{psi}) = 0.10 \times MBV + 0.17 \quad (R^2=0.61) \quad \text{Equation 9-5}$$

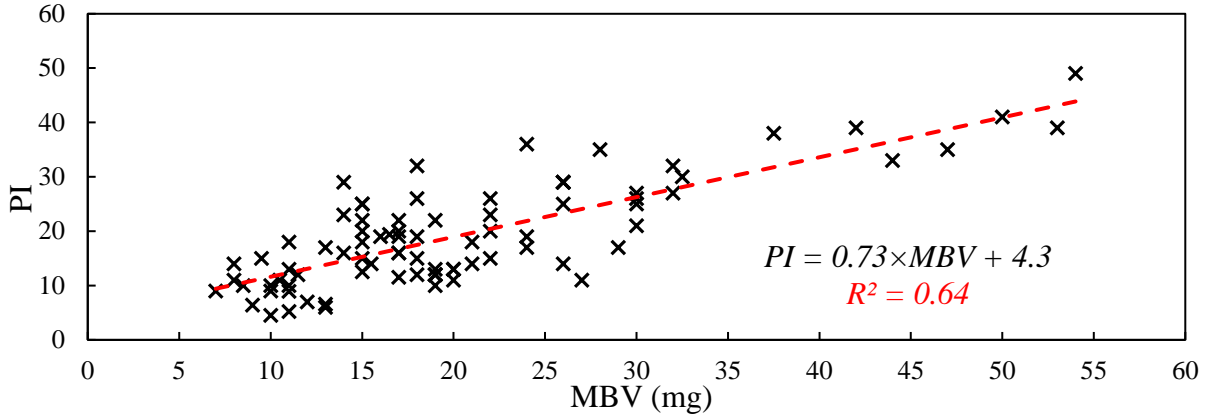


Figure 9-9: Relationship between Methylene Blue Value and Plasticity Index.

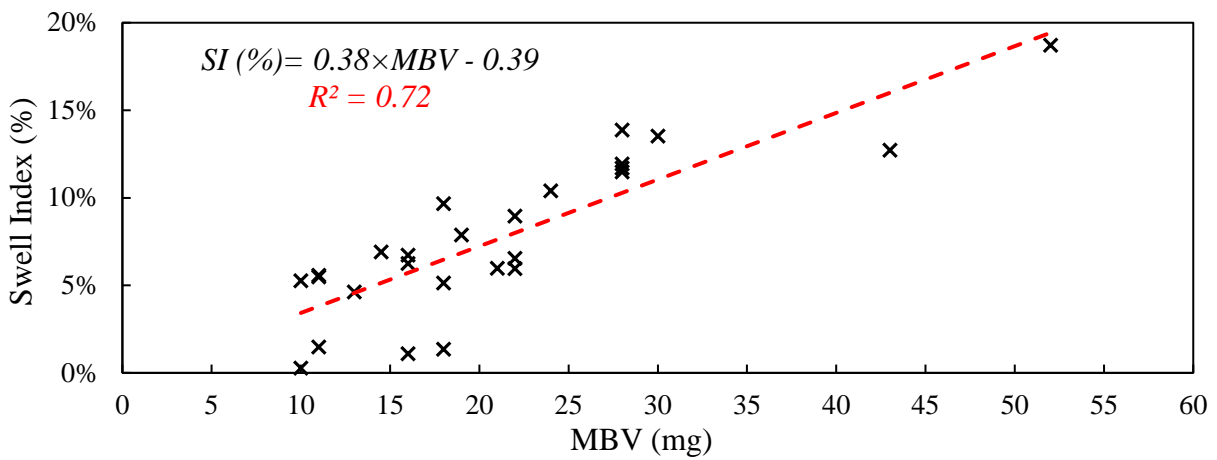


Figure 9-10: Relationship between Methylene Blue Value and Swell Index.

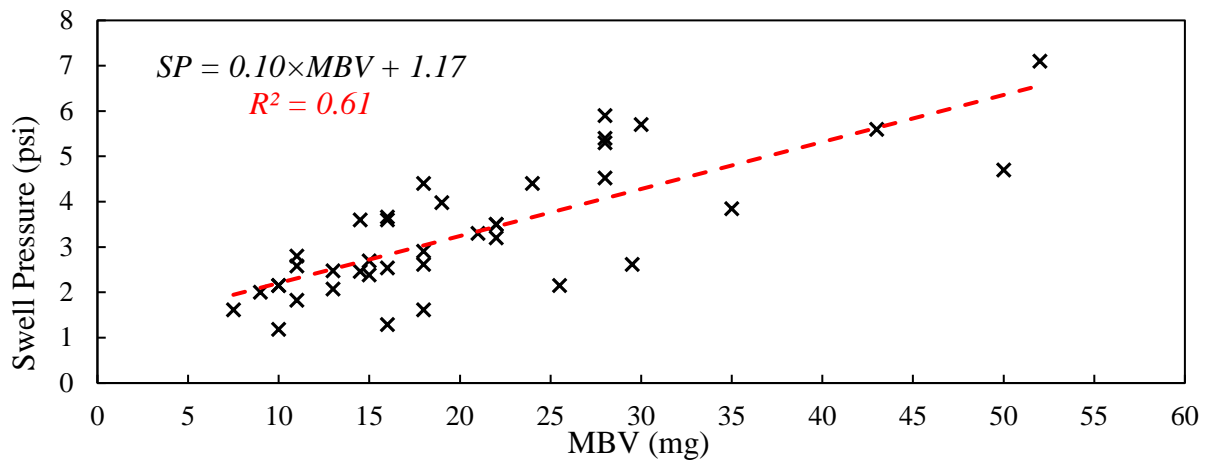


Figure 9-11: Relationship between Methylene Blue Value and Swell Pressure.

These relationships show that the plasticity and swell behavior of expansive clayey soils can be directly related to the potential of moisture adsorption of fine grained soils. In other words, MBV is capable of classifying the plasticity and volumetric change of expansive soils. This was the

reason to compare the repeatability of the measurement of MBV and PI. As evidenced in the statistical analysis, the measurement of MBV had significantly less variability than that of PI. This revealed that the methylene blue value is much more reliable and repeatable indicator than the PI.

Figures 9-12, 9-13, and 9-14 present the relationships between plasticity index, swell pressure, and swell index. Satisfactory correlations were observed between PI, swell pressure, and swell index, which are shown in Equations 9-6, 9-7, and 9-8. The results clearly underscore the role of plasticity of fine grained soils on the swell tendency in subgrade soils. This indicates that the PI is also capable of classifying the swell behavior of expansive soils.

$$SI (\%) = 0.38 \times PI - 0.09 \quad (R^2=0.76) \quad \text{Equation 9-6}$$

$$SP (\text{psi}) = 0.13 \times PI + 0.75 \quad (R^2=0.73) \quad \text{Equation 9-7}$$

$$SP (\text{psi}) = 33 \times SI (\%) + 1.1 \quad (R^2=0.96) \quad \text{Equation 9-8}$$

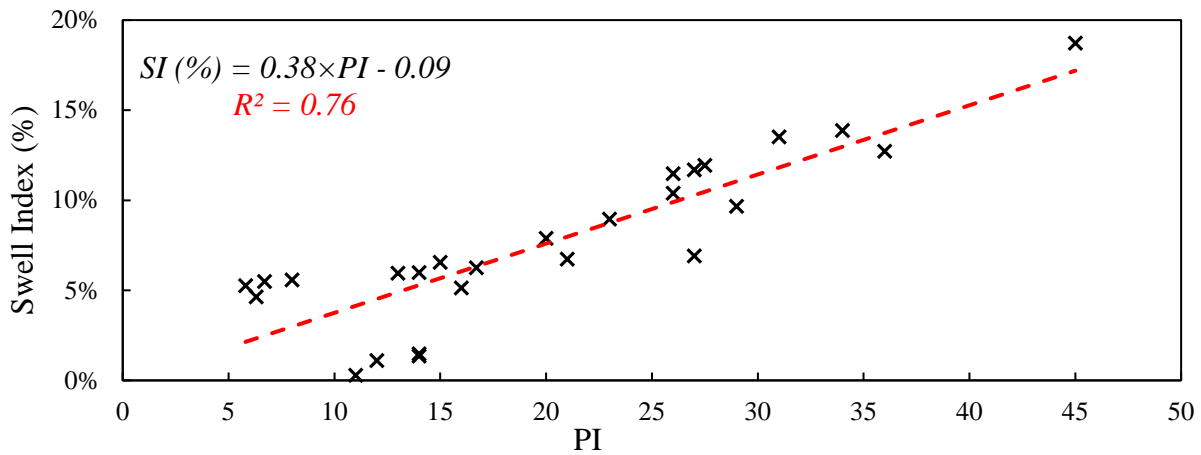


Figure 9-12: Relationship between Plasticity Index and Swell Index.

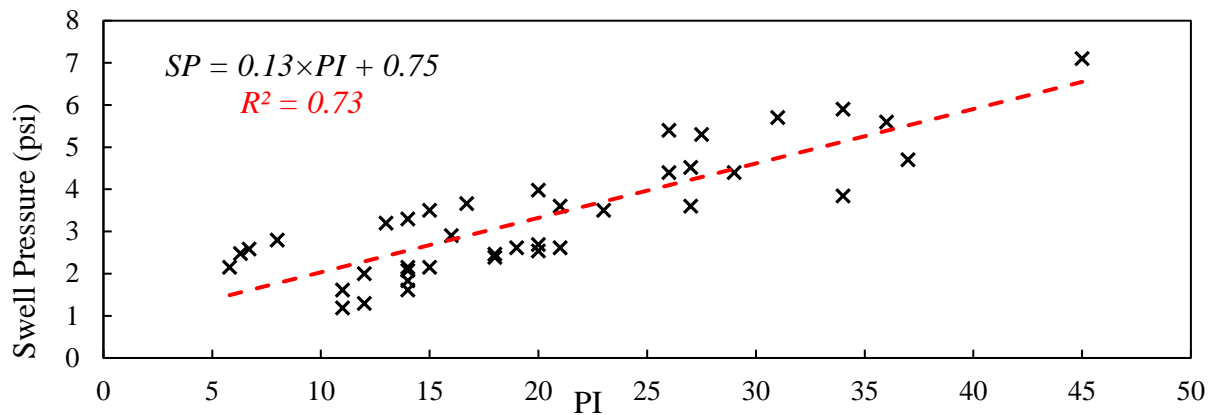


Figure 9-13: Relationship between Plasticity Index and Swell Pressure.

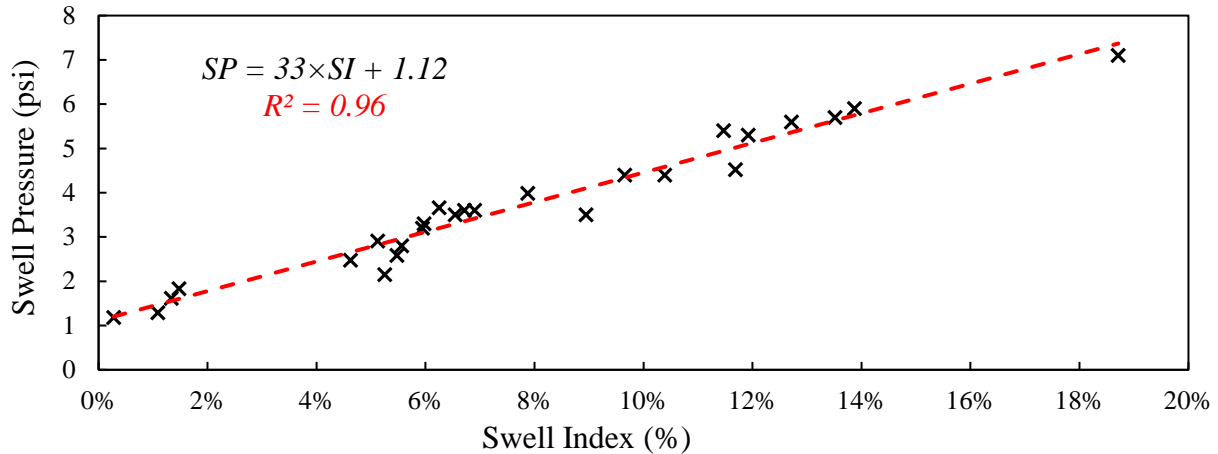


Figure 9-14: Relationship between Swell Index and Swell Pressure.

9.6 Unconfined Compressive Strength Test Results

As previously stated in this paper, different chemical stabilizer additives such as cement Type I/II, lime, class C fly ash as well as polypropylene fibers were added to each permutation of the experiment design to achieve permanently modified properties and improve strength of subgrade soils. Figure 9-15 demonstrates the unconfined compressive strength results for the HS soils with different stabilizer types and contents. The plots show the beneficial role of the increase of stabilizer content on the compressive strength of expansive soils. This favorable influence is more pronounced for cement stabilized specimens. For instance, compressive strength of specimens treated with 7% cement content were up to four times greater than those specimens treated with 3% cement content. This substantial improvement by the increase of cement binders can be attributed to the formation of the calcium hydroxide crystals as a rigid networks during the cement hydration process. These rigid networks are small and isolated in the “cement-modified soil” with a relatively small proportion of cement. However, high quantities of cement binder (such as 7%) in the “soil-cement” form large interconnected networks that lead to a significant improvement of the strength properties of subgrade soils.

Figure 9-15 also indicates that the combination of cement and fly ash appears to be the most suitable chemical additive for the stabilization of expansive soils. The high sulfate soil specimens stabilized with cement-fly ash blend showed highest strength compared to the other type of stabilizers. For instance, the HS soil specimens stabilized with 7% lime and 7% cement had a relatively lower compressive strength of 65 and 89 psi, respectively. Conversely, the UCS was drastically improved to 116 psi for the same specimen stabilized with 5% cement and 3% fly ash contents. Therefore, replacing a portion of cement binders with fly ash in cement stabilized soils is more beneficial to improve compressive strength of subgrade soils in pavement foundations.

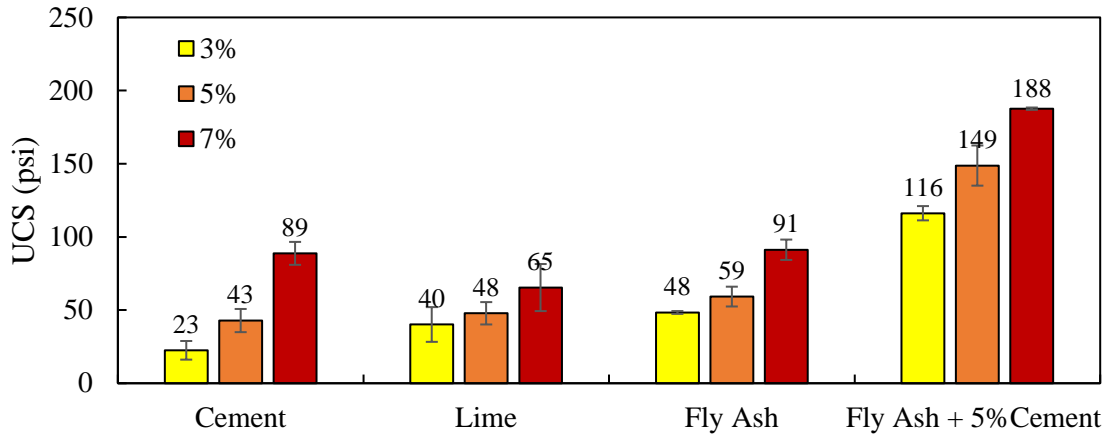
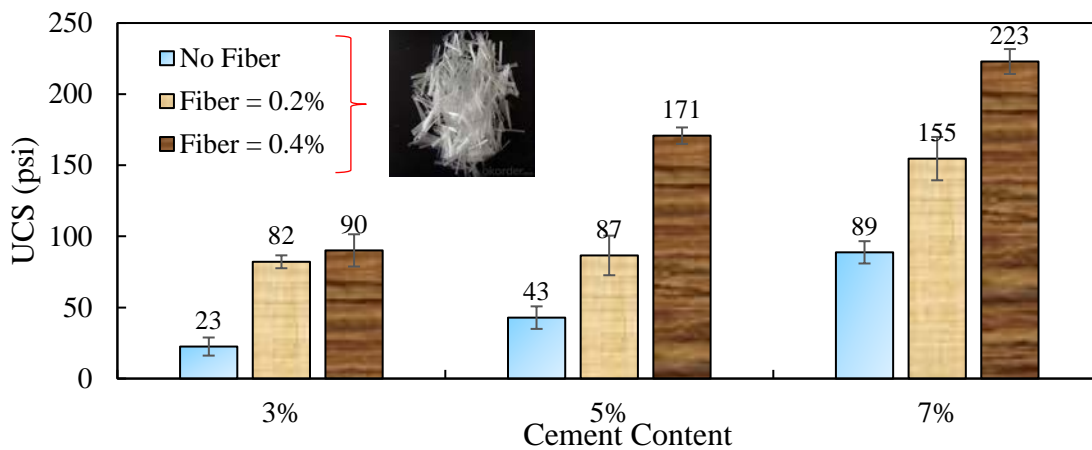


Figure 9-15: Unconfined Compressive Strength of HS Soils with Different Stabilizer Types and Contents.

Figure 9-16 demonstrates the contribution of fibers and cement binders for improving the compressive strength of the HS and HP soils. As evidenced in the plot, the reinforced soil-cement specimens with polypropylene fiber exhibited a significant UCS improvement compared to the unreinforced soil. The compressive strength for stabilized HS soil specimens with 3% and 5% cement content increase significantly from 23 to 90 psi and from 43 to 171 psi after 0.4% fiber is added to the mixture, respectively. The plot also shows that the increase in strength of combined cement and polypropylene fiber inclusions is significantly higher than the sum of the increase caused individually by them.



(a)

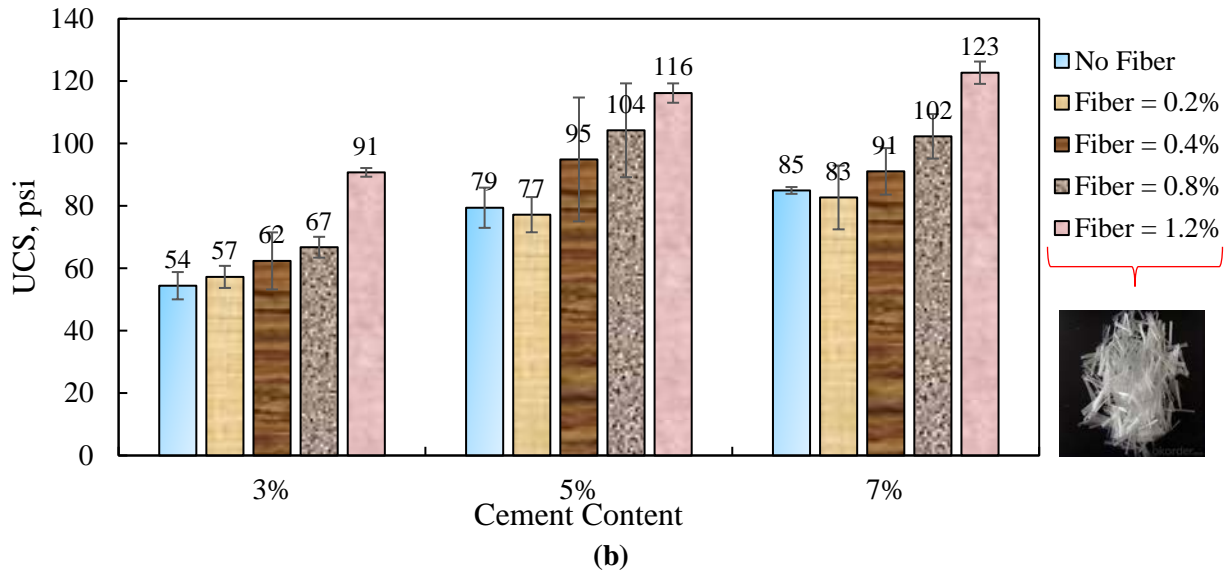


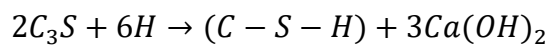
Figure 9-16: Unconfined Compressive Strength of (a) HS Soils and (b) HP soils with Different Stabilizer Types and Contents.

Another interesting observation that can be clearly visualized from Figures 9-15 and 9-16 is the superior performance of the combination of cement-fiber in terms of higher compressive strength compared to the combination of cement-fly ash in stabilized expansive soils. For instance, the soil specimen stabilized with 5% cement and 5% fly ash contents had approximately 15% lower unconfined compressive strength compared to the stabilized specimen with 5% cement content and 0.4% fibers. Figure 9-17 also shows the initiation of the crack in highly plastic and sulfate clay materials sourced from Bryan for different types of stabilizers after 7-day moist curing. The results demonstrate the superior performance of stabilized specimens with the combination of fiber-cement in terms of lower crack area compared to other permutation of experiment design. Therefore, the addition of fiber-cement to expansive soils can be considered as an efficient strategy for improving compressive strength of subgrade soils with high plasticity and high sulfate contents.

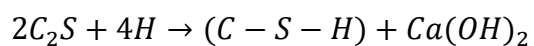


Figure 9-17: Stabilized Clay Soils Sourced from Bryan District after 7 Days of Curing.

The cementitious reaction between cement and clay takes place as primary and secondary processes. In the primary process, cement hydration forms a network of calcium hydroxide to bind soil particles together, as indicated in Equations 9-9 and 9-10. These products provide available calcium for cation exchange, flocculation and agglomeration, and Calcium Silicate Hydrate (C-S-H), which provide strength and structure in the soil matrix.



Equation 9-9



Equation 9-10

Where $H=H_2O$, $C-S-H = C_3S_2H_3$, C_3S = tricalcium silicate, and C_2S =dicalcium silicate.

In the secondary process, the fresh calcium hydroxide formed in the primary phase reacts slowly with the silica and alumina in the clay to form additional cementitious material as previously shown in Equations 9-1 and 9-2. Thus, the clayey material itself contributes somewhat to the strength development of treated clay mixtures with calcium-based stabilizers during the curing time.

Figures 9-18 and 9-19 presents the variation of unconfined compressive strength with curing time over 28 days for stabilized HS and HP soils, respectively, with different chemical additives. The compressive strength of each specimen treated with cement, lime, and fly ash increased with the curing period. The increased strength can be attributed to the decreased moisture content in the cured samples due to hydration and pozzolanic reactions. For the specimens stabilized with cement, the rate of increase in strength was not significant beyond 14 days of curing. This means that curing after this time does not have any considerable influence on strength gain of cement stabilized expansive soils. On the contrary, unconfined compressive strength of HS soils stabilized with lime and fly ash kept increasing with the increase of curing time. This could be attributed to the fact that lime provides more free calcium and fly ash provide more silica and aluminum for the pozzolanic reaction as a secondary process of soil stabilization. The pozzolanic reactions take place slowly, over months, and can further strengthen a stabilized expansive soil.

As shown in the plot, different trend of UCS versus time was observed for the HS soil stabilized with the combination of cement and fly ash (5% cement + 5% fly ash). The compressive strength of cement-fly ash specimens initially enhanced with increase of time, while the strength drastically decreased beyond the curing of 7 days. This indicates that excessive amount of chemical additives (such as 10%) resulted in overly rigid systems that are prone to shrinkage cracking. The growth of these cracks in expansive subgrade soils can significantly compromise the structural integrity, serviceability, and life of pavement structures. Therefore, it is imperative to establish an upper bound limit for the strength properties of the calcium-based stabilized soils to protect the subgrade against shrinkage cracking. Hence, the proper selection of the type and the amount of the calcium-based stabilizers in the mix design is of paramount importance to ensure the longevity of pavement foundations.

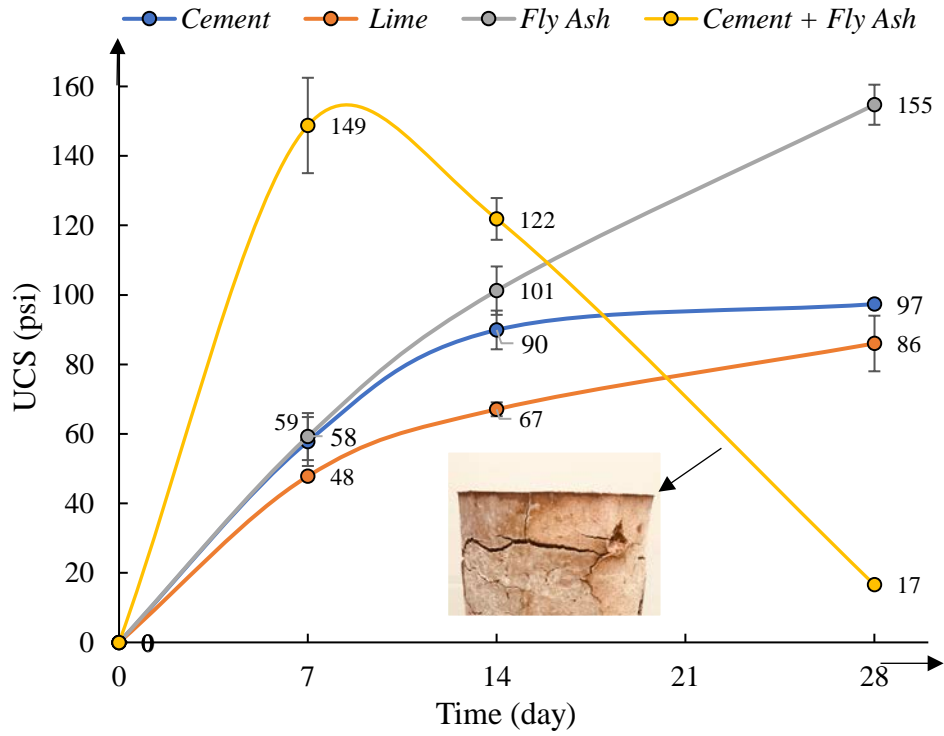


Figure 9-18: Unconfined Compressive Strength of HS Soils Stabilized with 5% Cement, 5% Lime, 5% Fly Ash, and the Combinations of the Cement and Fly Ash (5% Cement+5%Fly Ash) versus Curing Time.

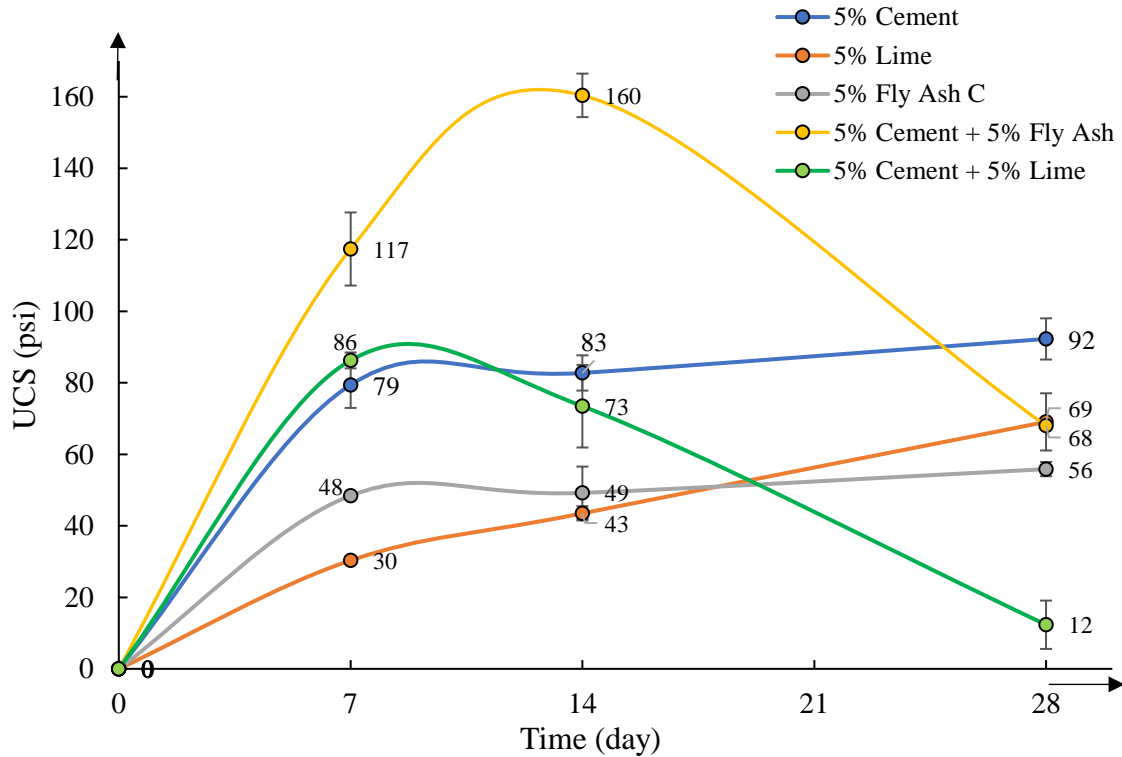


Figure 9-19: Unconfined Compressive Strength of HP Soils Stabilized with 5% Cement, 5% Lime, 5% Fly Ash, the Combinations of the Cement and Fly Ash (5% Cement+5%Fly Ash) and the Combinations of the Cement and Lime (5% Cement+5%Lime) versus Curing Time.

Figure 9-20 presents the unconfined compressive strength of stabilized expansive soils sourced from Bryan with different stabilizer types and contents after 7-day and 28-day curing. As observed in the plot, the compressive strength of cement-fly ash and cement-lime specimens after 7-day curing initially increased, while the compressive strength drastically decreased after the curing of 28 days. This shows again that excessive amount of chemical additives (ranging from 8% to 12%) resulted in overly rigid systems that are prone to shrinkage cracking. The growth of these cracks in expansive subgrade soils is shown in Figure 9-21. These cracks can significantly compromise the structural integrity, serviceability, and life of pavement structures.

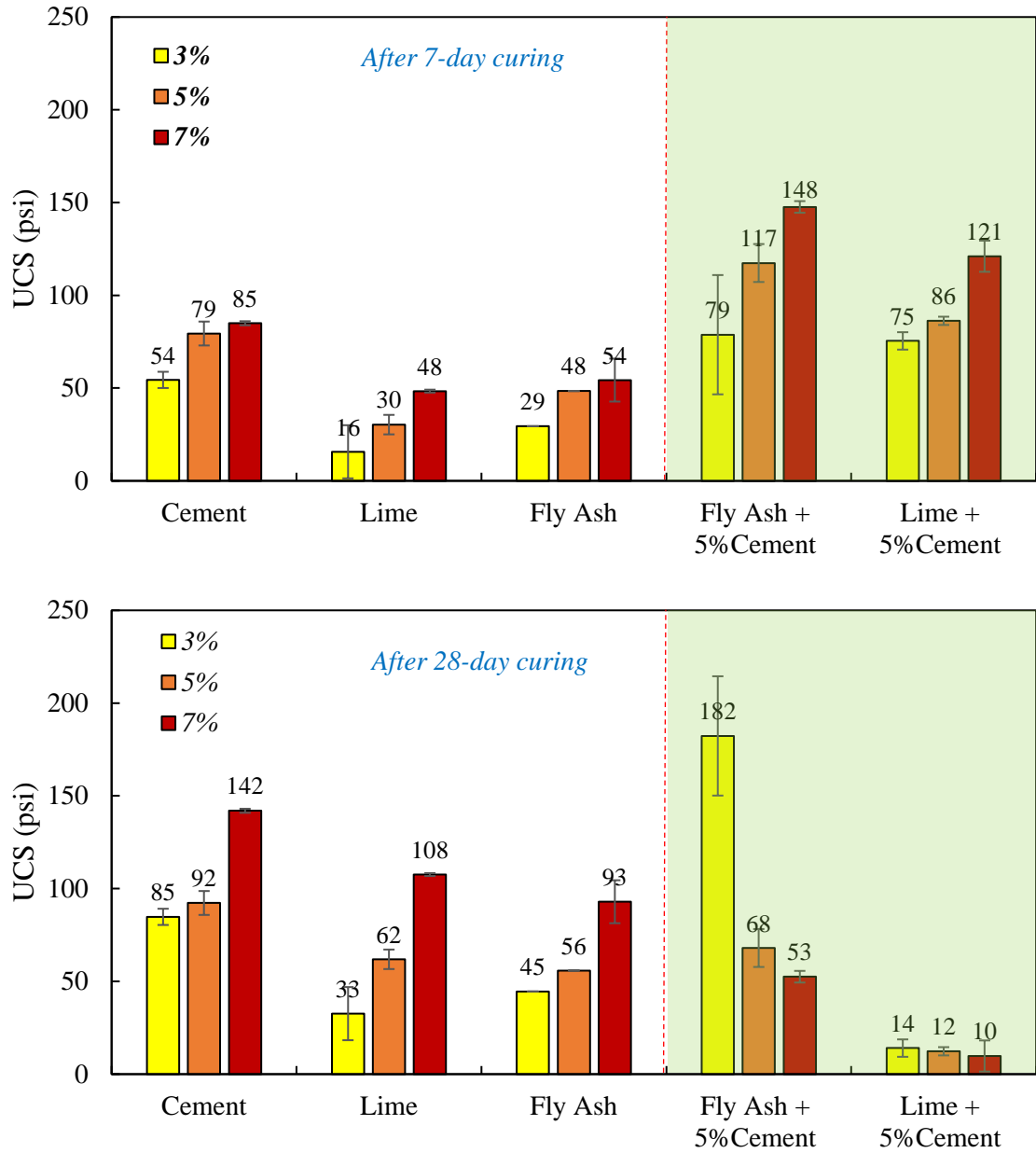


Figure 9-20: Unconfined Compressive Strength of Stabilized Expansive Soils Sourced from Bryan with Different Stabilizers Type and Content After 7-Day and 28-Day Curing.



Figure 9-21: Stabilized Clay Soils with 5% Fly Ash and 5% Cement after 7-day, 14-day, and 28-day Curing.

9.7 Summary of the Major Points

The focus of this chapter was to investigate the performance of polypropylene fiber and chemical additives on the strength properties and volumetric stability of expansive soils. This objective was achieved by the execution of a comprehensive experiment design consisted of three types of expansive soils, different quantities of calcium-based stabilizers such as cement, lime, fly ash, and cement-fly ash blend, and different proportionate of polypropylene fibers. The major observations and conclusions of this chapter are itemized in the following:

- Atterberg limits and Methylene Blue tests results showed that a small amount of lime considerably decreases the plasticity and moisture adsorption potential of expansive soils with low sulfate content. Comparatively, all calcium-based additives including lime, cement, and fly ash, did not work well on PI reduction for high sulfate bearing soil due to the sulfate attack on stabilized soils, which results in the deterioration of cement-soil matrix.
- The relationships between the methylene blue values, plasticity index, swell index and swell pressure were developed in this study. This relationship indicates that MBV is capable of classifying the plasticity and volumetric change of expansive soils. Accordingly, the repeatability of the measurement of MBV and PI were evaluated by statistical analysis. The results showed that the MBV is much more reliable and repeatable indicator than the PI.
- Combination of cement and fly ash appeared to be suitable chemical additive in terms of compressive strength and volumetric stability for the stabilization of expansive soils. The laboratory test results revealed that replacing a portion of cement binders with fly ash in cement stabilized soils is more beneficial to improve compressive strength of subgrade soils in pavement foundations. However, excessive amount of cement-fly ash blend

resulted in overly rigid systems that are prone to shrinkage cracking in expansive subgrade soils. The growth of these cracks can significantly compromise the structural integrity, serviceability, and life of the pavement structure.

- The combined role of chemical stabilization and polypropylene fiber reinforcement as a cross linking agent was investigated on the strength and swell behavior of expansive soils. The post processing results showed the superior performance of the combination of cement-fiber compared to the combination of cement-fly ash and other chemical additives in stabilized expansive soils. Hence, the addition of fiber-cement to expansive soils can be considered as an efficient strategy for improving strength and volumetric stability of subgrade soils with high plasticity and high sulfate contents.

Chapter 10. Development of Material Models

Traditionally, the compressive strength of the cement stabilized materials is obtained by the unconfined compressive strength test, while the tensile strength is estimated based on the third point bending beam flexural or split tension tests. The resilient properties of the cement stabilized materials can be obtained based on the stress path tests or the submaximal modulus test. Detailed discussions regarding the advantages and the shortcomings of the laboratory procedures and the parameters of the stress path protocols for the estimation of the resilient properties of the stabilized materials were provided in Chapter 2. Execution of all the laboratory tests is a costly and time consuming undertaking for many state agencies. Customarily, due to the lack of equipment availability, time constraints, operator concerns, and budgetary issues, among others, many design engineers rely on the past experience for the selection of the type and stabilizer content in pavement projects. Therefore, this section was designed to provide a series of practical and robust relationships among routine laboratory tests using regression analysis for the estimation of pavement design input parameters. The developed relationships are valuable means in the hierarchical pavement design approach for incorporation in the design and analysis.

10.1 Relationship between the UCS and IDT

The primary focus of this section was to investigate the inter-relations between the strength characteristics of cement stabilized materials in tension and compression using the traditional multivariate regression models.

To better understand the inter-relations between the mixture parameters and laboratory derived strength properties of the stabilized materials, the research team initially developed a series of regression models as the basis to study the underlying relationships between the mixture parameters and tensile and compressive strength properties of the tested variants of the experiment design. This step was the prelude to the regression analysis provided in the next section of this chapter.

Figure 10-1 provides the relationship between the unconfined compressive strength and the indirect diametrical tensile tests results. The ascending nature of the trend line suggests a direct correlation between the compressive and tensile behavior of the cement stabilized materials. In other words, permutations with higher compressive strength exhibited higher tensile strength compared to other counterparts in the experiment matrix.

Equation 10-1 presents the relationship between the compressive and tensile strength of cement stabilized systems. The model is based on the UCS and IDT testing of 288 permutations in the laboratory. The relationship developed between the IDT strength (S_{IDT}) and the UCS is presented in Equation 10-1.

$$S_{IDT} = 5.53 \times UCS^{0.41} \quad (R^2=0.50) \quad \text{Equation 10-1}$$

The proposed model is in good agreement with models developed by other researchers as provided in Table 10-1.

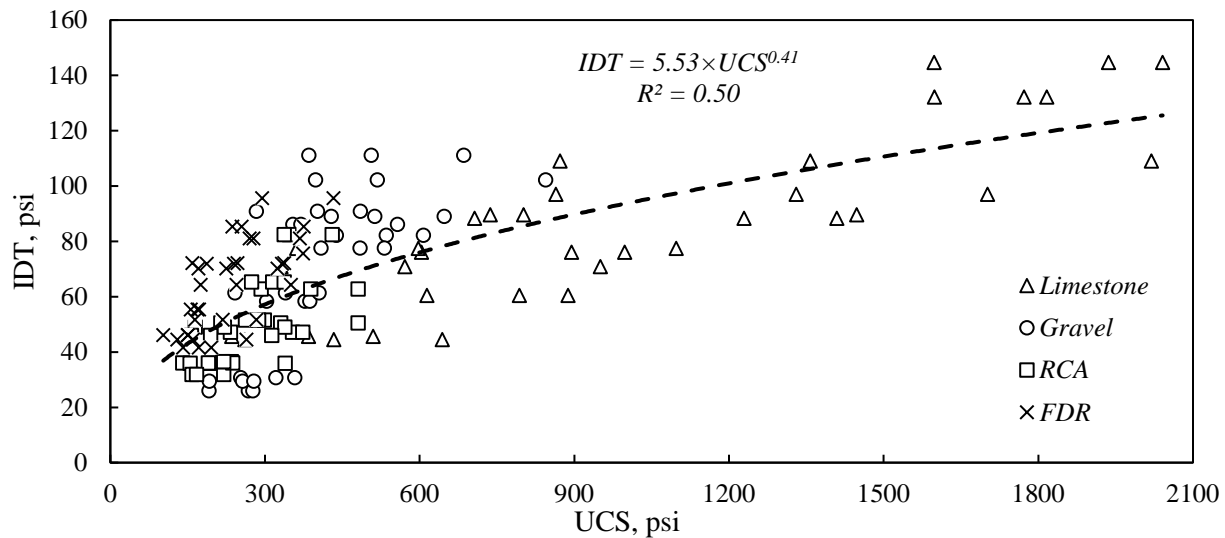


Figure 10-1: Relationship between UCS and IDT Strength for Cement Stabilized Base Materials in the Laboratory.

Table 10-1: Available Relationships for IDT Strength and UCS.

Relationship (psi)	Researcher	Year
$S_{IDT} = 0.166 \times UCS - 11.38$	Kennedy	1973
$S_{IDT} = 0.114 \times UCS$	Piratheepan et al.	2010
$S_{IDT} = 0.177 \times UCS - 9.31$	Scullion	2012
$S_{IDT} = 0.12 \times UCS$	Wen and Edil	2014

The developed model in this study has several advantages compared to the previous studies outlined in Table 10-1. The first advantage is associated with the range of the cement contents added to the mixes. As previously stated in this chapter, all three aggregate sources were stabilized with 2% up to 4% cement. Therefore, the models incorporate both lightly stabilized systems as well as rigid aggregate matrices. The overly rigid aggregate systems are not desirable in pavements as they may be prone to shrinkage cracking. For this reason, several state agencies defined thresholds for the UCS to protect the pavements against distresses related to reflective cracking. Another major advantage of the newly developed model is attributed to the incorporation of durability tests. The simultaneous monitoring of the unbound moisture and the rate of strength gain (or loss) in the TST test provided valuable information on the moisture susceptibility of the stabilized mixes. A detailed discussion regarding the pair-wise plots of dielectric value and seismic modulus, and the procedure for the characterization of the moisture susceptibility of stabilized materials were provided in previous chapters. In addition, four aggregate sources with different

mineralogy including stabilized reclaimed materials such as FDR and RCA as well as virgin aggregates such as crushed limestone and siliceous gravel materials were incorporated in this model. In summary, incorporation of four aggregate sources, three increment of cement content, and integration of the durability tests potentially enhanced the generalization of the relationships developed in this study.

Figure 10-2 underscores the influence of the stabilizer content on the compressive and tensile behavior of the cement stabilized materials. As expected, increase in cement content resulted in improvements on both compressive and tensile properties of the stabilized systems. Additionally, this plot clearly shows the synergistic influence of the aggregate mineralogy and the cement content on the mechanical behavior of cement treated materials. The spread of the data points corresponding to the tensile and compressive behavior of stabilized specimens can be explained by the schematic data cloud analogy. As evidenced in Figure 10-2, the cloud of the data is relatively rounded for lightly stabilized materials. However, the increase in the cement contents resulted in larger spread of the cloud of the data. This variation is more pronounced for 4% cement stabilized systems as depicted with the elongated ellipse. In other words, the results indicate that the distance from the mean increases with the increase in the cement contents. This can potentially be attributed to the role of the mineralogy and surface properties of the aggregates, and their influence on the tensile and compressive behavior of cement treated systems. Another plausible explanation can be attributed to the initiation of the micro-cracks in overly rigid stabilized mixes.

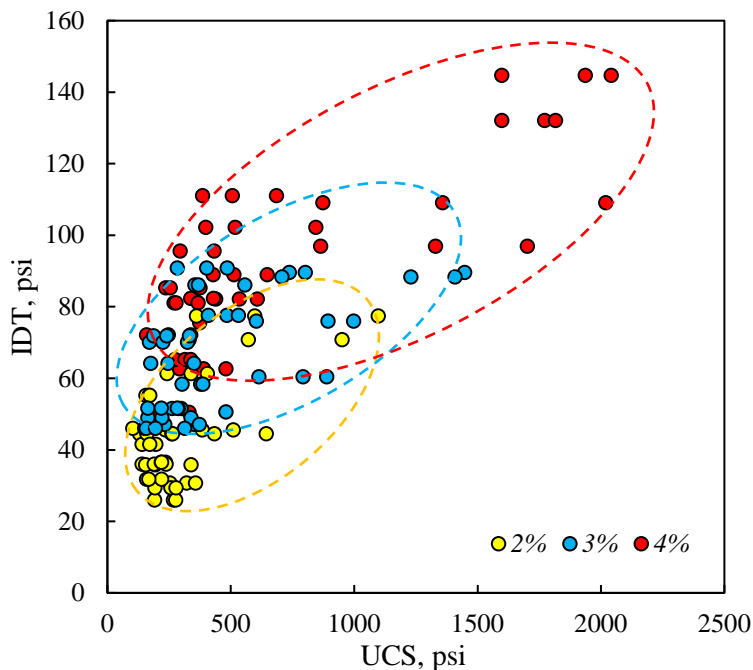


Figure 10-2: Relationship between UCS and IDT Strength for Cement Stabilized Base Materials Categorized Based on the Cement Content.

Another noteworthy observation is the distinct transition of lightly stabilized materials that resembles soil cement, to the heavily stabilized materials that behave more like concrete. This was the motivation to establish a new relationship exclusively for the 4% cement stabilized materials and compare it with conventional concrete models. The general power form function used by American Concrete Institute ACI (1981) and Oluokon (1966) was adopted for direct comparison of the models. Equation 10-2 presents the model based on the 4% cement stabilized materials for four different aggregate sources.

$$S_{IDT} = 7.77 \times UCS^{0.38} \quad (R^2=0.56) \quad \text{Equation 10-2}$$

Figure 10-3 illustrates the comparison between the widely used concrete relationships and the model developed for the highly cement stabilized materials in this study. As expected, the envelope for the cement treated materials were contained below the traditional concrete models. Additionally, the rate of tensile strength gain with the increase in UCS is shown to be significantly higher for concrete. In other words, the slope of the concrete models is much higher compared to the cement stabilized materials.

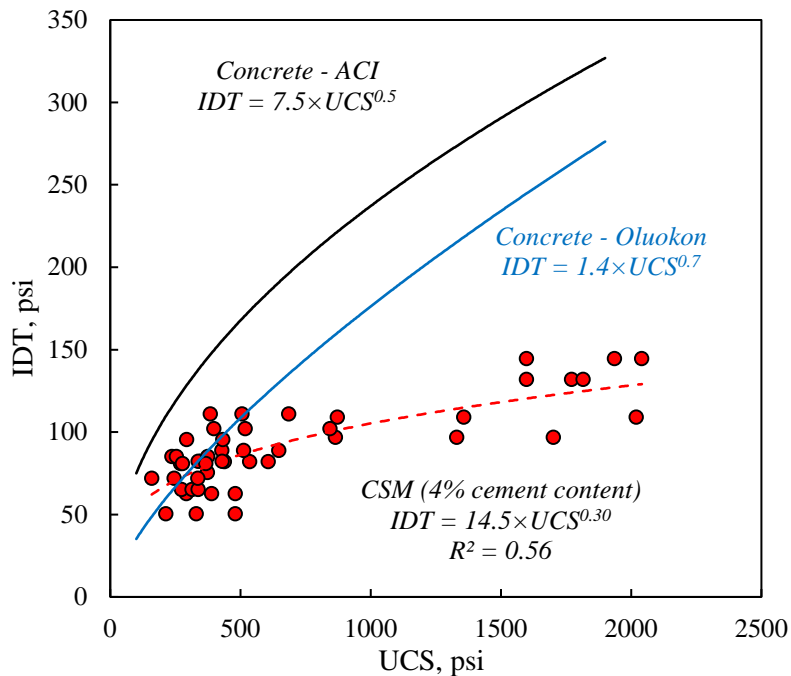


Figure 10-3: Comparisons of Tensile and Compressive Strengths for Heavily Cement Stabilized Materials and Conventional Concrete Models.

Figure 10-4 provides the IDT and UCS results categorized based on the aggregate type. As previously stated, four aggregate sources, namely crushed limestone aggregates, FDR, RCA, and siliceous gravel material stabilized with 2% to 4% cement content were evaluated in this study. The results clearly underscore the role of the aggregate mineralogy on the mechanical performance of the cement stabilized materials. As shown in Figure 10-4, the slope of the best fit lines in the

UCS-IDT plots are appreciably different for the four types of materials tested in this study. This underscores the influence of the type of virgin and reclaimed materials to partake in hydration and strength reactions, and therefore result in mixtures with different compressive and tensile strength properties. The results also showed that both FDR and RCA materials benefitted less from the increase in the cement contents, and therefore underperformed other variants in the experiment design. The lackluster results for these reclaimed materials are in agreement with other laboratory performance tests such as repeated load permanent deformation tests, and resilient modulus tests executed in this study.

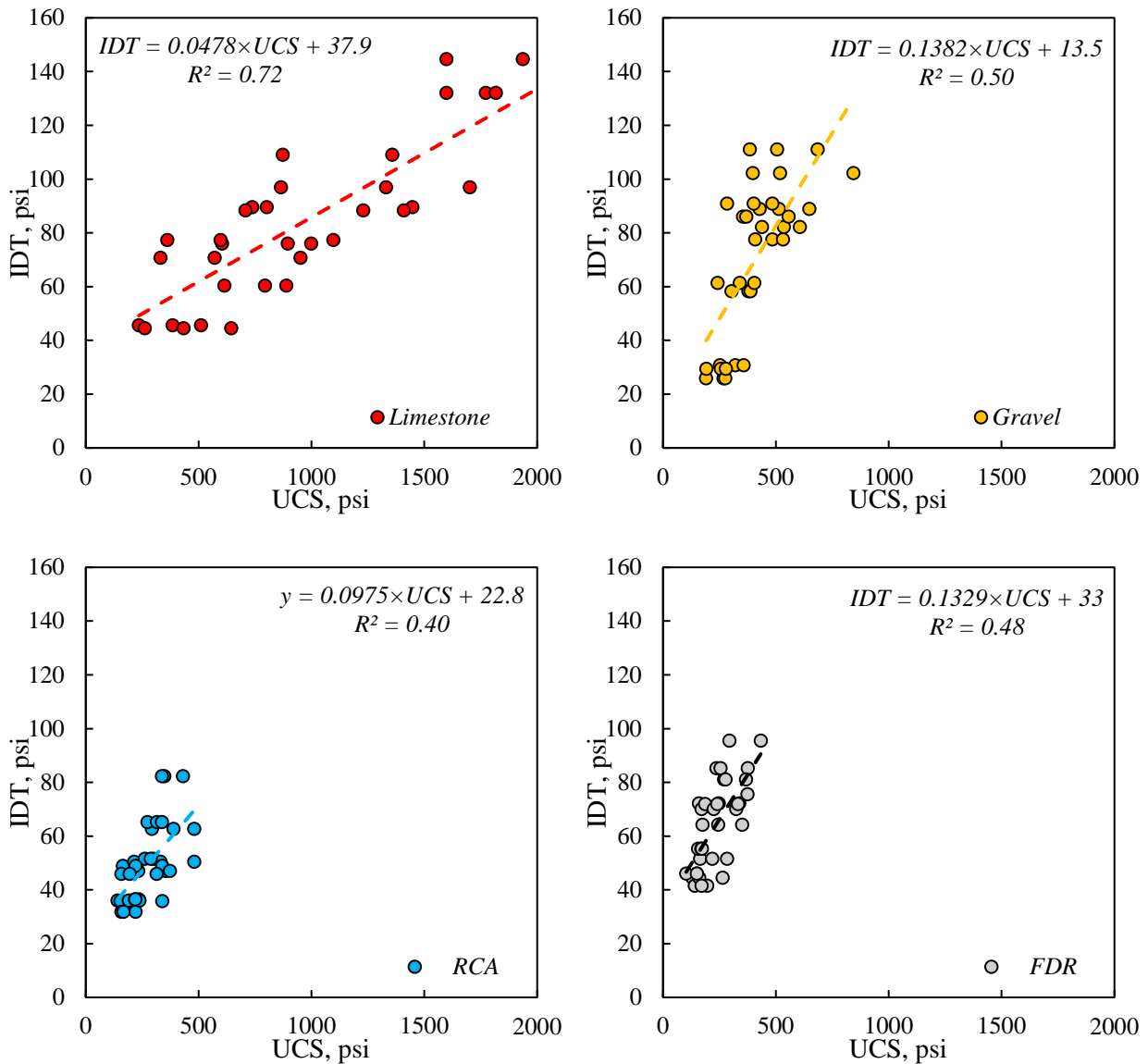


Figure 10-4: Relationships between the UCS and IDT Categorized by Aggregate Type.

Figure 10-5 provides the relationship between IDT and UCS test results categorized based on the different compaction procedures conducted in this study. As previously stated, stabilized

specimens were fabricated with four compaction procedures, namely impact hammer, vibratory hammer, gyratory compactor, and Texas gyratory compactor. The plot shows that the IDT strength for stabilized materials compacted with impact hammer is approximately 8.4% of the unconfined compressive strength, while this fraction for the stabilized specimens fabricated with vibratory hammer is 34.3%. This underscores the influence of the compaction procedure for the analysis of strength properties of geomaterials in the laboratory.

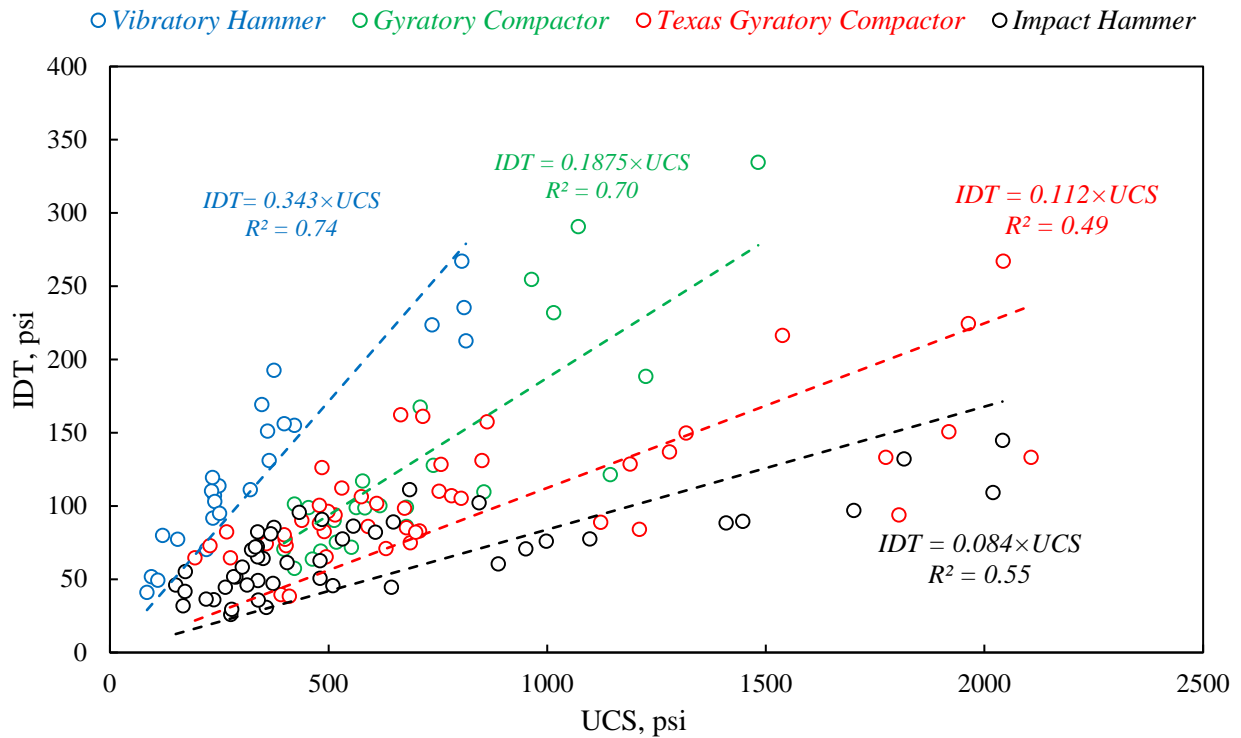


Figure 10-5: Relationships between the UCS and IDT Categorized by Compaction Methods.

Figure 10-6 presents the relationship between the compressive and tensile strength of the cement stabilized systems categorized based on the different specimen dimension, characterized by length to diameter ratio. Length to diameter ratio (L/D) of test specimens is one of the influencing factors that greatly impacts the UCS test results. The plot indicates that the slope of the best fit lines in the UCS-IDT plots obtained from testing specimens having L/D ratio of 1 exhibited flatter slope in comparison to specimens with L/D of 1.5 and 2. This underscores the influence of the specimen dimension on the compressive and tensile behavior of the cement treated reclaimed and virgin mixes.

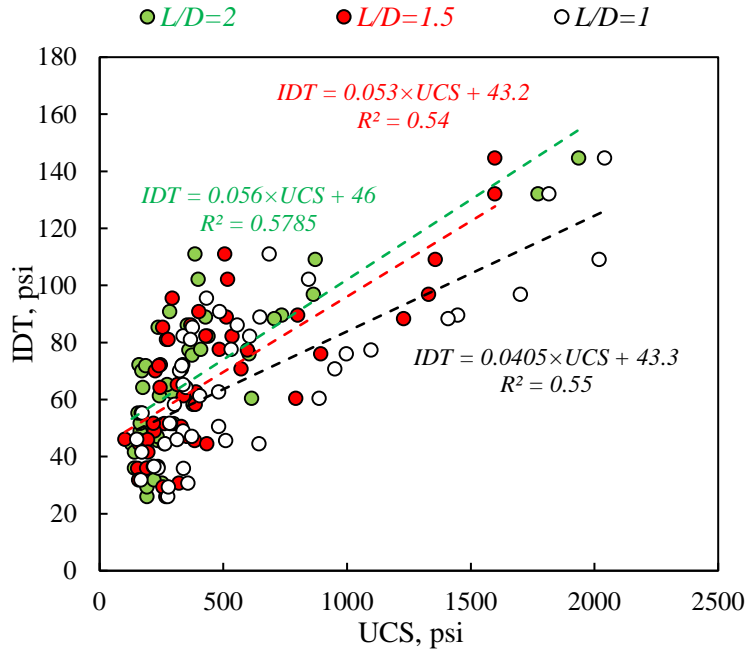


Figure 10-6: Relationships between the UCS and IDT Categorized by Specimen Dimension.

10.1.1 Genetic Expression Programming

As previously discussed in the regression analysis section, the compressive and tensile strength properties of stabilized reclaimed systems are greatly influenced by the material type, the cement content, and specimen size in the mix. Additionally, the compaction procedure also shown to play a pivotal role in the laboratory achieved tensile and compressive strength properties of the mixes. Therefore, the authors explored alternative mathematical approaches, using genetic expression programming, to develop robust relationships between mixture parameters, such as cement content (C%), specimen dimension (L/D), on one hand, and strength properties of the laboratory specimen on the other hand, such as tensile strength in the modified split tension test (S_T) and unconfined compressive strength (S_C). The primary motivation to develop such models was to assist the laboratory mixture design practitioners with a starting point to estimate the tensile strength of materials without the need to incorporate the IDT test in the experiment matrix.

Due to the significant influence of the compaction procedure on the strength properties of the mixes presented earlier under Figure 10-5, the datasets for different compaction methods were separated and four sets of models were prepared for the prediction of the compressive and tensile strength properties of the stabilized reclaimed systems. This step was imperative to show significant differences in the mechanical performance of stabilized specimens fabricated with different compaction procedures in the laboratory. Equations 10-3 and 10-4 provide the tensile strength prediction models for the specimens compacted with impact hammer in the laboratory.

$$S_T = 1838 \times C\% + 0.054 \times S_C \times \frac{L}{D} + 497.9 \times S_C \times C\%^3 - 8.07 - 1.25 \times S_C \times \frac{L}{D} \times C\%$$

Equation 10-3

$$S_T = 377.54 \times C\% \times S_C^{0.284}$$

Equation 10-4

Where S_T is the tensile strength (psi), $C\%$ is the cement content percentage, L/D is the length over diameter ratio, S_C is the unconfined compressive strength (psi).

Equations 10-5, 10-6, and 10-7 provide the tensile strength prediction models for the three categories of gyratory compactor, vibratory hammer, and TGC, respectively.

$$S_T = S_C \times \sqrt{C\%}$$

Equation 10-5

$$S_T = \left(\frac{S_C \times e^{S_C \times C\%^2}}{C} \right)^{0.5}$$

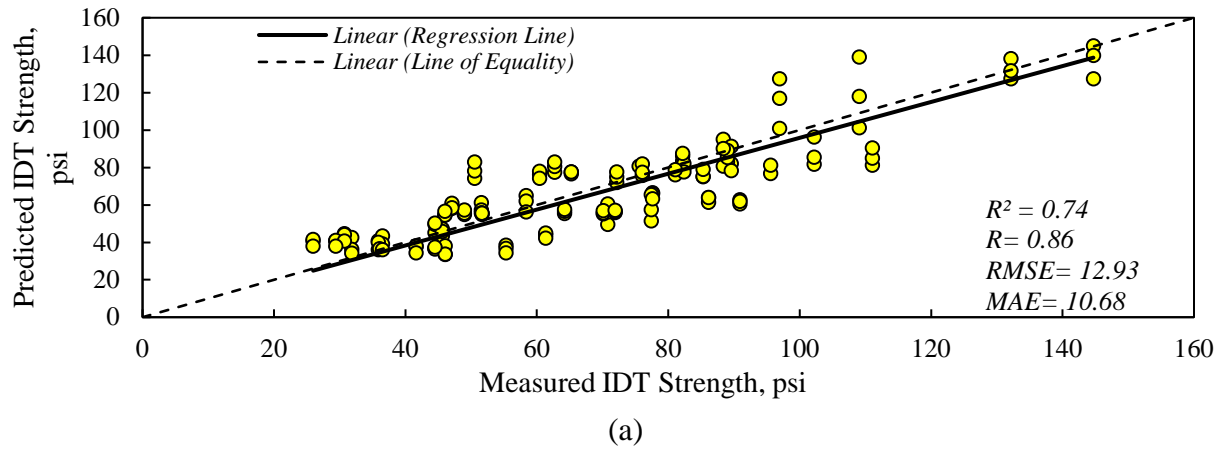
Equation 10-6

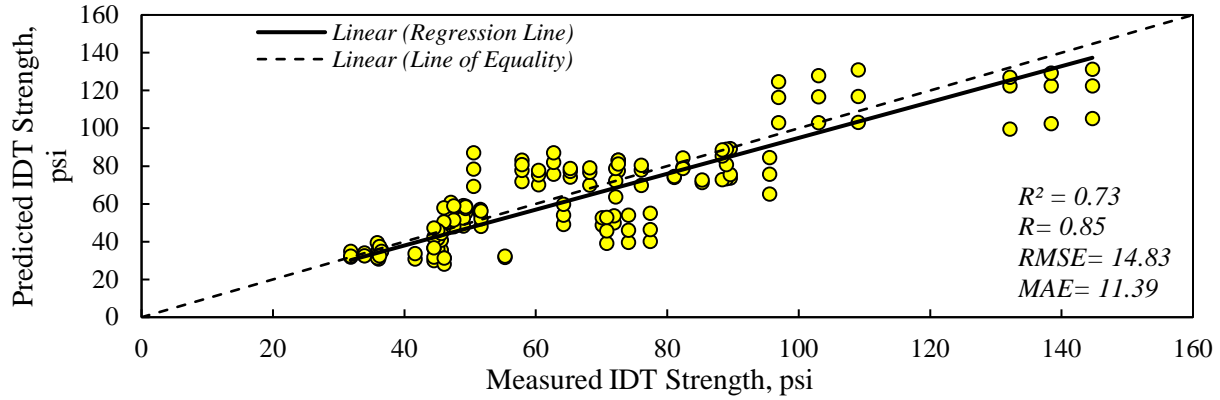
$$S_T = (239.87 \times C\% \times S_C)^{0.5}$$

Equation 10-7

Figures 10-7 and 10-8 provide the measured versus predicted tensile strength values based on the models developed in this study. The statistical parameters and performance measures for each subset of models are also provided in these plots.

Smith (1986) recommended that for a coefficient of determination of $|R| > 0.8$, a strong correlation exists between the input and output layers of the models. The proposed models showed acceptable prediction capability as the correlation coefficient for all models was more than 0.80 as indicated in Table 10-2. The error values are also within the acceptable range for all models.





(b)

Figure 10-7: Measured Versus Predicted IDT Strength for Specimens Compacted with Impact Hammer Using Genetic Programming Models for (a) Equation 10-3 and (b) Equation 10-4.

Table 10-2: Statistical Measures for the Performance of the Models.

Equation	R	R ²	RMSE	MAE
10-3	0.86	0.74	12.93	10.68
10-4	0.85	0.73	14.83	11.39
10-5	0.87	0.75	37.25	24.69
10-6	0.94	0.89	20.14	14.78
10-7	0.87	0.75	15.65	12.53

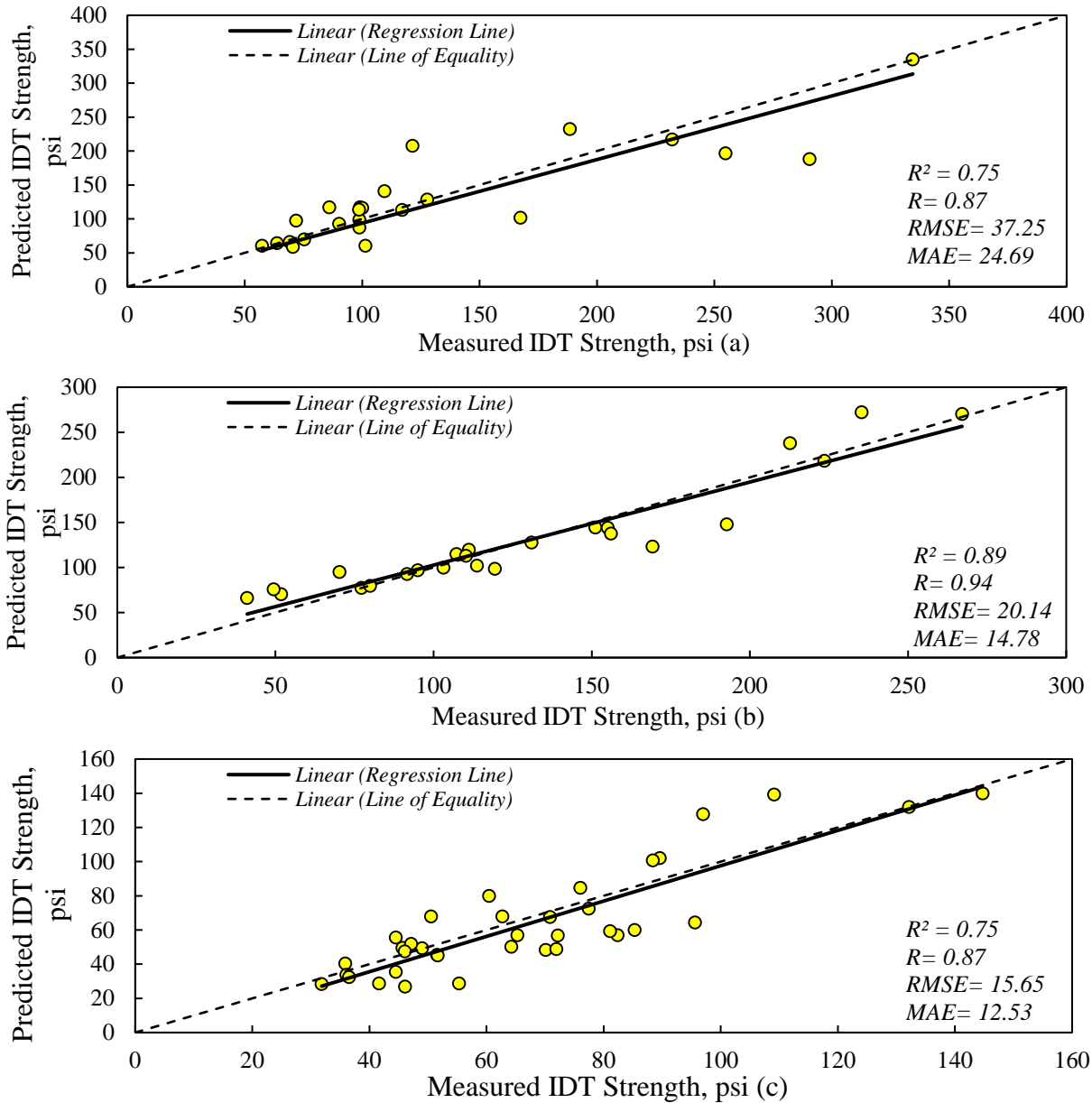


Figure 10-8: Measured Versus Predicted IDT Strength for Specimens Compacted with (a) Gyratory Compactor, (b) Vibratory Hammer, and (c) TGC Using Genetic Programming Models.

10.2 Resilient Modulus of Cement Stabilized Materials

The new Mechanistic-Empirical Pavement Design Guide (MEPDG) requires a measure of the resilient modulus for the analysis and design of pavements. This information is required for the calculation of the responses of pavements subjected to traffic loads. Therefore, the submaximal modulus tests at two Strength Ratios (SR) were performed on 7-day moist-cured and 10-day capillary soak specimen in the laboratory. As earlier discussed, pre-determined fractions of the UCS-value, namely 25% and 50% were cycled for 5,000 repetitions to calculate the resilient modulus of the stabilized mixes. Execution of the full spectrum of the submaximal modulus test

is a costly and time-consuming undertaking for small projects. Therefore, a series of relationships between the UCS and the resilient modulus tests at different strength ratios were developed in this study using the traditional multivariate regression models and genetic expression programming. Such models can serve as a starting point to provide an estimate of the resilient modulus of cement treated layers for the practitioners and the pavement design engineers.

10.2.1 Regression Analysis

A series of regression models were initially developed as the basis to study the underlying relationships between the mixture parameters and resilient properties of stabilized base materials. The results from developed models in this section were the prelude to the genetic expression programming provided in the next section.

Figure 10-9 provides the resilient modulus and unconfined compressive strength results categorized based on the aggregate type. The results clearly underscore the role of the aggregate mineralogy on the resilient and strength properties of the cement stabilized materials. As illustrated in the plot, the slope of the best fit lines in the UCS- M_r plots are considerably different for the four types of materials tested in this study. Stabilized reclaimed materials such as FDR and RCA had lower range of resilient modulus and compressive strength compared to siliceous gravel and crushed limestone aggregates. This underscores the influence of the type of materials to partake in hydration and strength reactions, and therefore result in mixtures with different stiffness and strength performance. These results provide a valuable means for the selection of the type and source of the aggregates for the construction of cement stabilized base layers.

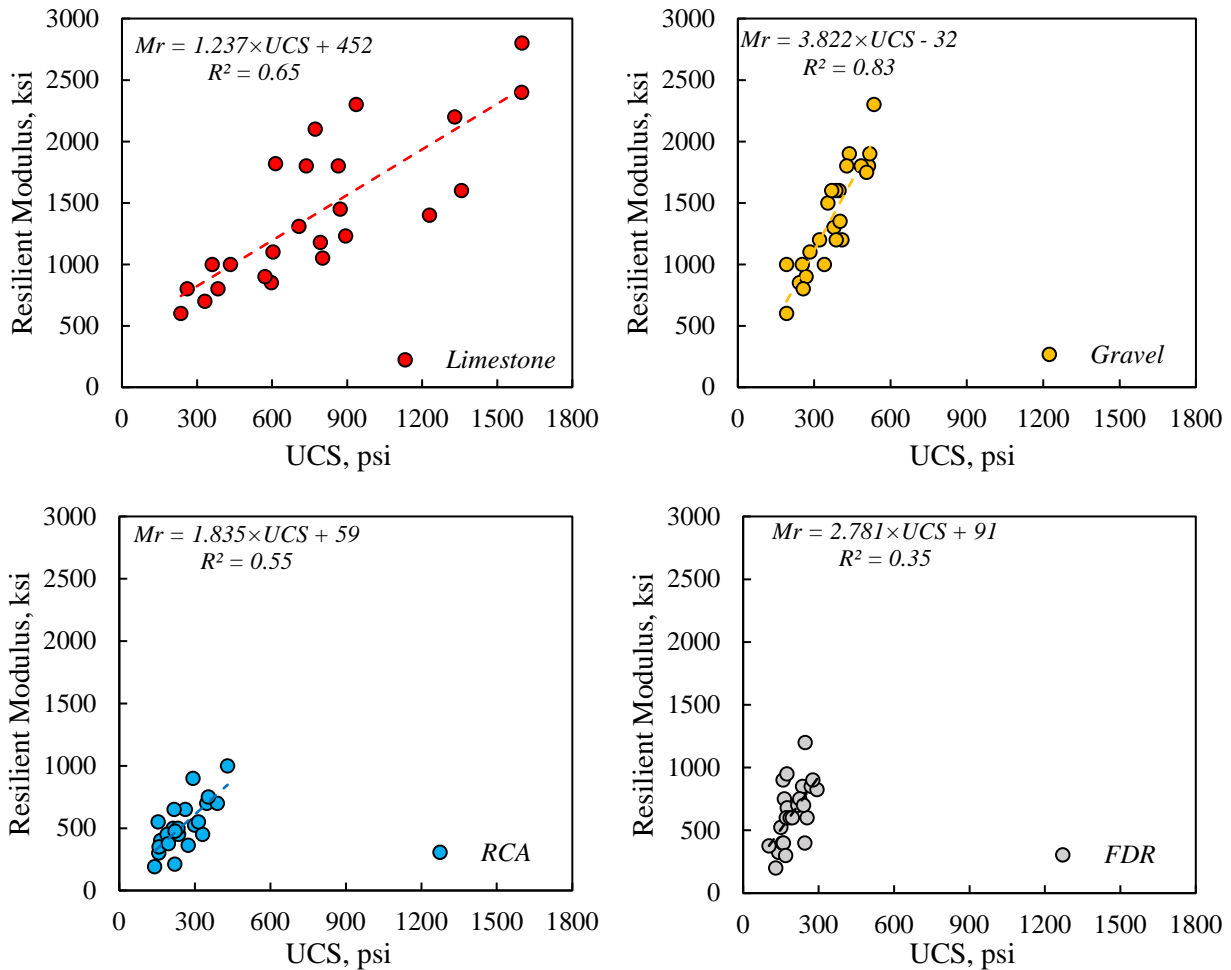


Figure 10-9: Relationship between Resilient Modulus and Unconfined Compressive Strength Categorized by Aggregate Type.

The stress path protocol had a considerable effect on the resilient modulus of the cement stabilized materials. The results showed that the variants subjected to less taxing stress paths had higher resilient modulus values. This is due to the low-stress excitation levels and therefore low induced strains in the SR=25% loading protocol. Conversely, SR=50% stress path protocols induce higher strains and the net effect will be lower modulus values. Therefore, it deems necessary to consider the strain levels imposed by traffic loads on pavement layers for the realistic selection of the resilient modulus for the design and analysis of pavements.

Figure 10-10 presents the relationship between resilient modulus and unconfined compressive strength at 25% and 50% strength ratio. Two relationships based on the strength ratio levels were developed in this study to cover small-strain and intermediate-strain level behavior of stabilized layers. Small strain behavior could be associated with pavements with thick/stiff surface layers. In such pavements, most of the traffic-induced stresses dissipate within the stiff/thick surface layer, and therefore the magnitude of the stresses transmitted to the stabilized layer will be relatively small. Subsequently, the small stress excitations will result in low strain levels induced by traffic

loads. A similar argument is valid for inverted pavements for which the stabilized layer is located below the asphalt and the unbound granular base layers. Such cases are plausible scenarios for the small strain behavior of stabilized base layers in the field.

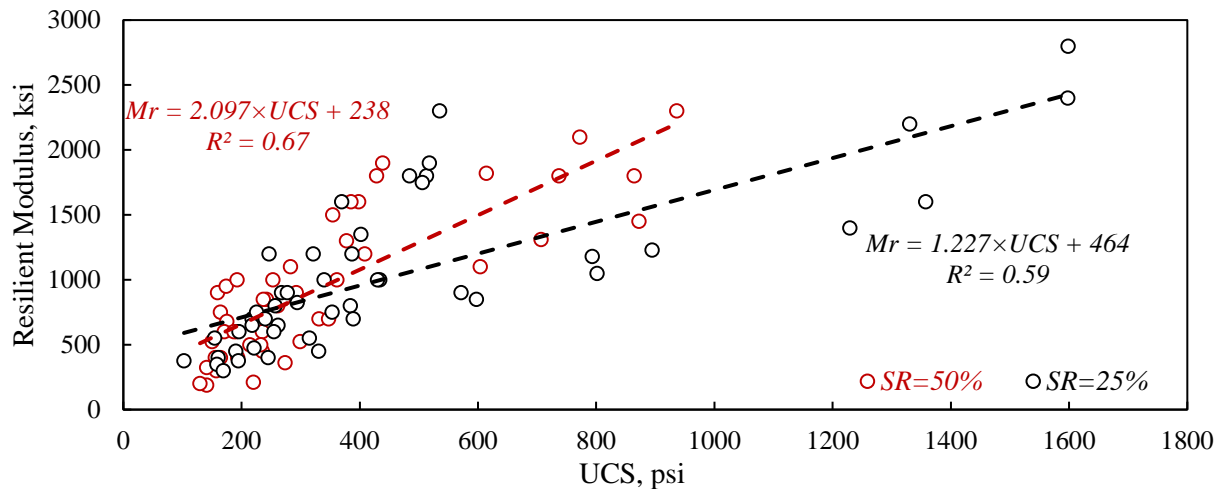


Figure 10-10: Relationship between Resilient Modulus and Unconfined Compressive Strength at 25% and 50% Strength Ratios.

Equations 10-8 and 10-9 provide relationships between the UCS and resilient modulus for small strain and intermediate strain levels. The small strain behavior model was primarily developed based on the SR=25%, and the intermediate strain model is based on the SR= 50%.

$$M_r = 1.227 \times UCS + 464 \quad (R^2 = 0.53) \quad \text{Equation 10-8}$$

$$M_r = 2.097 \times UCS + 238 \quad (R^2 = 0.81) \quad \text{Equation 10-9}$$

Figure 10-11 provides the relationship between the unconfined compressive strength and the resilient modulus for all material types and stress ratios based on the 192 permutations in the laboratory. The ascending nature of the trend line suggests that permutations with higher compressive strength exhibited higher resilient modulus compared to other counterparts in the experiment matrix. The developed general relationship between resilient modulus and compressive strength of cement stabilized materials is presented in Equation 10-10:

$$M_r = 9.16 \times UCS^{0.78} \quad (R^2=0.63) \quad \text{Equation 10-10}$$

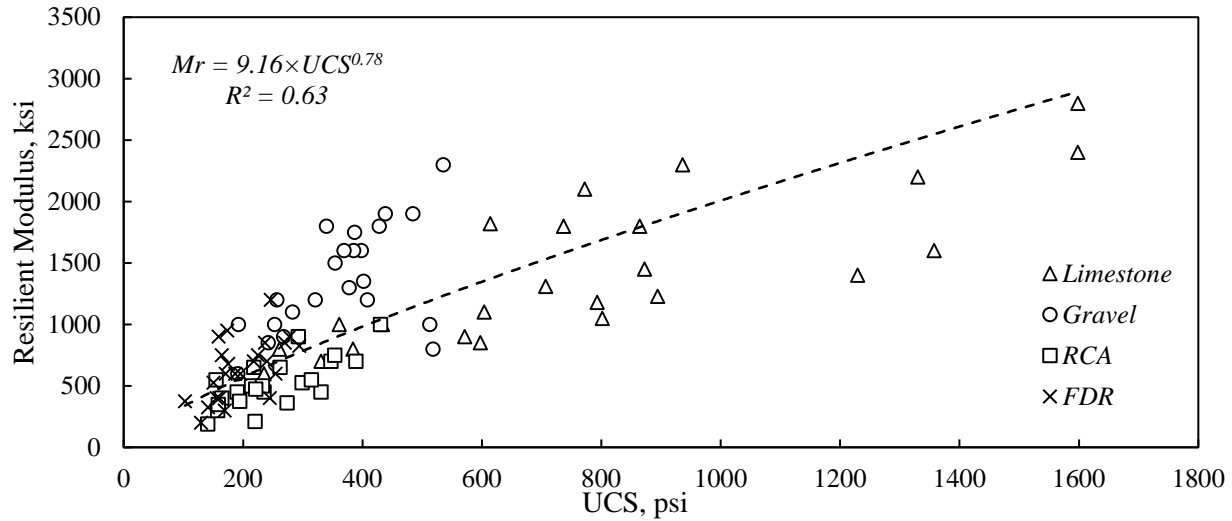


Figure 10-11: Relationship between Resilient Modulus and Unconfined Compressive Strength.

The resilient modulus relationships developed in this research was juxtaposed on prominent studies such as National Lime Association by Little (1995), Barenberg (1977), American Coal Ash Manual (1990), and Australian Road Research Laboratory (1998) as illustrated in Table 10-3. This table provides a comparison of the models developed under various sample preparation procedures, base/subgrade materials, and different calcium-based stabilizers.

Table 10-3: Available Relationships for IDT Strength and UCS.

Relationship	Material Type	Researcher(s)	Year
$M_r \text{ (MPa)} = 2240 \times \text{UCS (MPa)}^{0.88} + 1,100$	Cement Stabilized Subgrade Soils	Australian Road Research Laboratory	1998
$M_r \text{ (ksi)} = \text{UCS (psi)} + 0.498$	Lime Stabilized Soils	National Lime Association	1995
$M_r \text{ (ksi)} = \text{UCS (psi)} + 500$	Fly Ash Stabilized Materials	American Coal Ash pavement Manual	1990
$M_r \text{ (ksi)} = 1.2 \times \text{UCS (psi)}$	Untreated Coarse Sand	Barenberg	1977
$M_r \text{ (ksi)} = 9.16 \times \text{UCS (psi)}^{0.78}$	Cement Stabilized Materials	Rashidi & Ashtiani	2019

As previously discussed in the regression analysis section, the resilient properties of stabilized systems are greatly influenced by the cement content in the mix. It was also shown that the resilient modulus of the stabilized bases is a stress-path dependent property. Therefore, both stabilizer content and stress dependency of the resilient properties of the cement stabilized materials should be considered for the selection of the design modulus values. In this section, alternative mathematical approaches, using genetic expression programming approach, was explored to develop robust relationships between mixture parameters such as cement content, the stress path protocol, on one hand, and compressive strength properties and resilient performance of the cement stabilized base materials in the laboratory. Equation 10-11 provide the resilient modulus prediction

model as a function of unconfined compressive strength of the laboratory specimens (S_C), cement content (C%), and strength ratio (SR):

$$M_r = \sqrt{123461 \times S_C \times C\% \times SR^{0.396}} \quad \text{Equation 10-11}$$

Figure 10-12 presents a comparison of the measured and predicted resilient modulus of stabilized base materials. This developed relationship revealed that the incorporation of stress ratio and cement content in predicting the resilient modulus of stabilized mixes significantly improved goodness of the fit of the model compared to traditional regression-based prediction models (Equation 10-10).

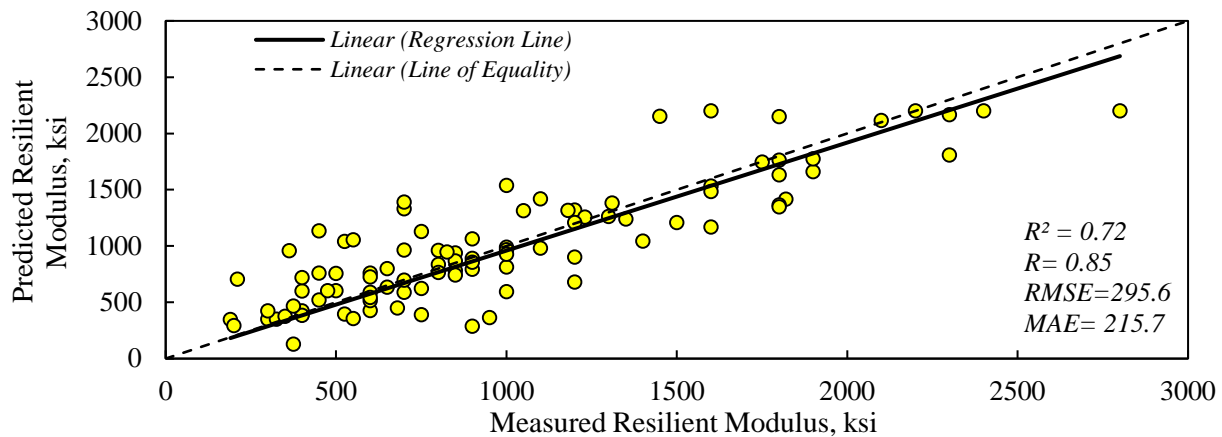


Figure 10-12: Measured Versus Predicted Resilient Modulus for Cement Stabilized Materials.

10.3 Practical Estimation for Shrinkage Strain of Stabilized Materials

As previously stated in this chapter, the proper selection of the amount of calcium-based stabilizers in the mix design is of paramount importance to ensure the longevity of the pavement foundations. Excessive amounts of stabilizers will result in overly rigid systems that are prone to shrinkage cracking. The propagation of the cracks to the surface of the asphalt layers can significantly compromise the structural integrity, serviceability, and life of pavements. Therefore, it is imperative to establish the new prediction model to estimate autogenous shrinkage of the calcium-based stabilized materials to protect pavements against reflective cracking.

Figure 10-13 present the relationship between shrinkage strain and unconfined compressive strength for different cement stabilized materials. The ascending nature of the trend line suggests that permutations with higher compressive strength exhibited higher shrinkage strain compared to other counterparts in the experiment matrix. This is more pronounced for the FDR materials that showed nearly quadruple the rate of increase of shrinkage strain as compared to other stabilized materials. This underscores the influence of the lithology and surface properties of the geomaterials as potential candidates for stabilized layers. Additionally, this indicates that cement treatment greatly alter the shrinkage rate of stabilized layers in the pavement structure.

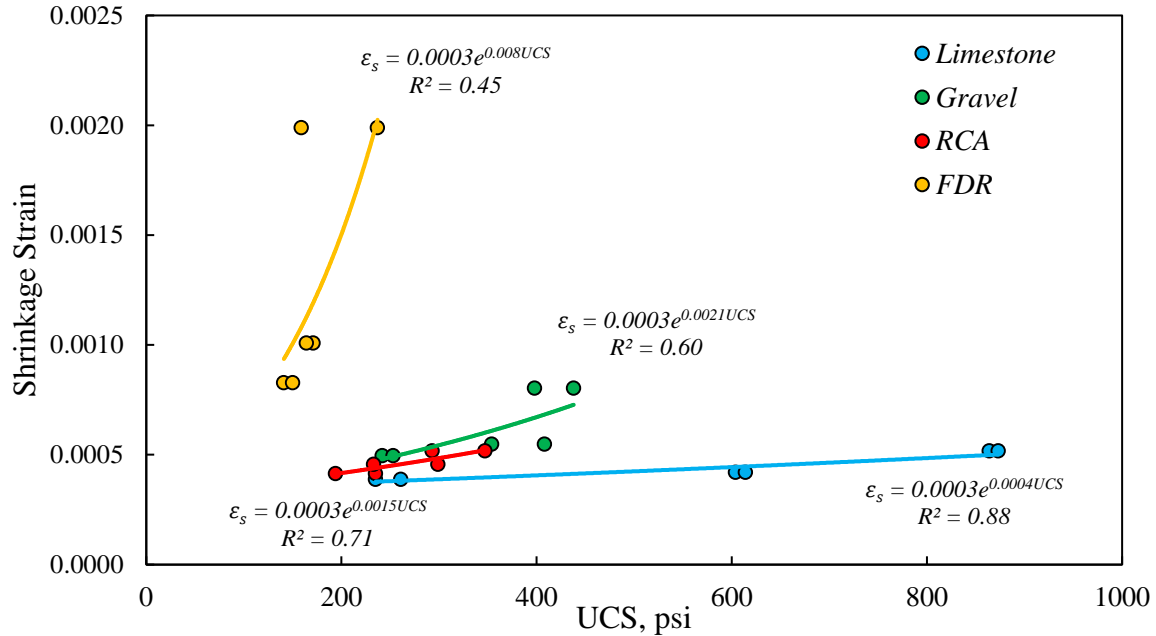


Figure 10-13: Relationship between Shrinkage Strain and Unconfined Compressive Strength for Different Cement Stabilized Materials.

The experimental results of Figure 10-13 were analyzed by using Equation 10-12, and the regression parameter (K) for different stabilized materials are tabulated in Table 10-4.

$$\epsilon_s = 0.0003 \times e^{K \times S_c} \quad \text{Equation 10-12}$$

Table 10-4: Regression Parameter (K) in Shrinkage Prediction Model for Different Materials.

Material	K
FDR	0.0080
Gravel	0.0021
RCA	0.0015
Limestone	0.0004

Figure 10-14 demonstrates the relationship between shrinkage strain and unconfined compressive strength for cement stabilized materials with different cement percentages. The plot underscores the influence of the stabilizer content on the shrinkage behavior of the cement stabilized materials. As expected, the increase in cement content resulted in the increase in shrinkage strain of the stabilized systems. Additionally, this plot clearly shows the synergistic influence of the strength properties and the cement content on the shrinkage behavior of cementitious materials. For instance, the stabilized mixture with higher cement content and lower compressive strength resulted in higher shrinkage strain. Such significant volumetric change can manifest itself in the form of shrinkage cracks in the cement treated base layers. These cracks can propagate to the

asphalt surface layers and jeopardize the longevity of pavement structures. Therefore, it is imperative to properly develop models for the volumetric characteristics of cement treated materials.

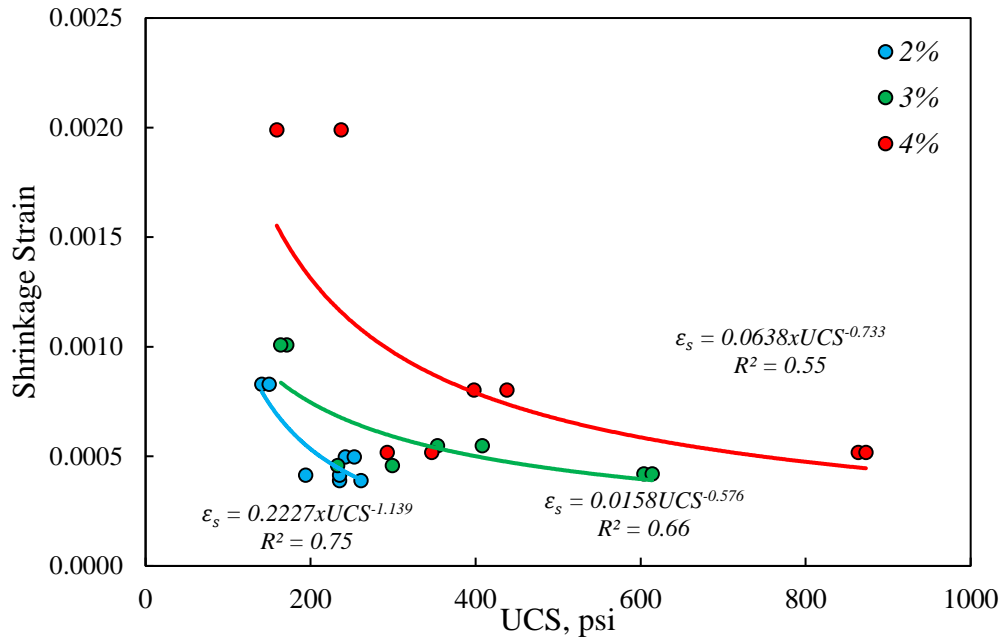


Figure 10-14: Relationship between Shrinkage Strain and Unconfined Compressive Strength for Cement Stabilized Materials with Different Cement Percentages.

Figures 10-13 and 10-14 shows that the shrinkage behavior of stabilized reclaimed systems are greatly influenced by the compressive strength and the cement content in the mix. Therefore, alternative mathematical approaches were explored, using the genetic expression programming, to develop robust relationships between shrinkage strain, cement content, and compressive strength. The primary motivation to develop such models was to assist the laboratory mixture design practitioners with a starting point for the reasonable estimate of the shrinkage strain of the materials without the need to incorporate the shrinkage test in the experiment matrix.

Equation 10-13 provide the model for the prediction of the shrinkage strain of the stabilized systems.

$$\epsilon_s = 0.000187 + 156.16 \times \frac{C\%^2}{S_C} \quad \text{Equation 10-13}$$

Where ϵ_s is the shrinkage strain, $C\%$ is the cement content percentage, and S_C is the unconfined compressive strength (psi).

As shown in Figure 10-15, the prediction model gives a reasonably good estimate of the autogenous shrinkage of stabilized base materials. Moreover, the results show that the difference

between the predicted and measured values is not large and that the prediction model properly estimates the relative autogenous shrinkage with acceptable correlation coefficient ($R=0.85$).

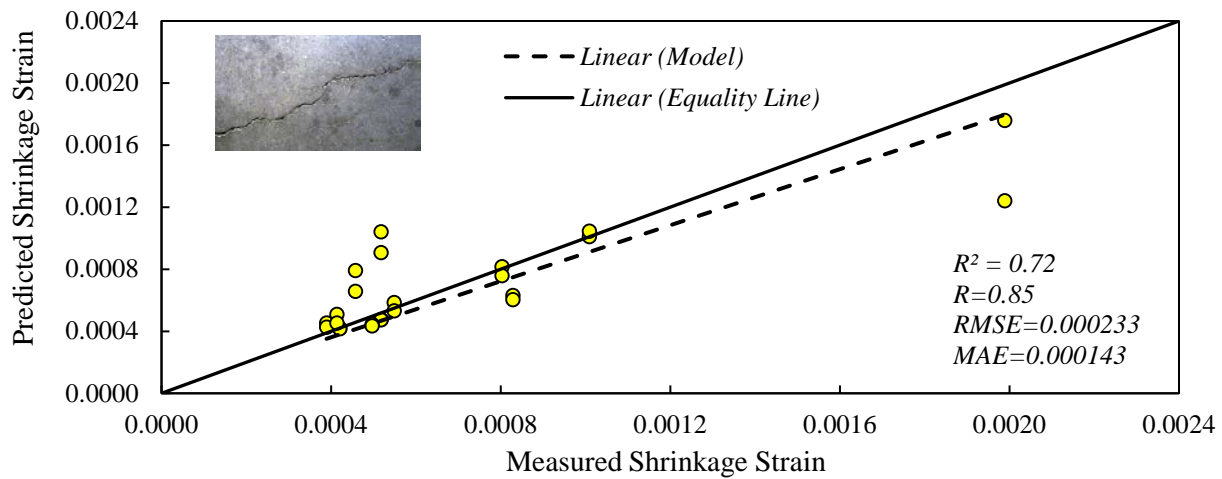


Figure 10-15: Measured Versus Predicted Shrinkage Strain for Cement Stabilized Materials.

10.4 Summary of the Major Points

The primary objective of this research was to explore the feasibility of using genetic expression programming as a computational intelligence technique to develop closed-form solutions to better understand the influence of the mixture design parameters on the strength and stiffness properties of stabilized reclaimed materials in the laboratory.

The relation between the resilient modulus and compressive strength properties of the stabilized mixes were also investigated in this study. The submaximal modulus tests at two strength ratios were performed to study the behavior of the systems at small-strain and intermediate-strain levels. Consequently, the relationships between the resilient modulus, UCS, strength ratio, and the cement content were developed in this study.

The incorporation of moisture susceptibility tests, diversity of aggregate sources, and wide range of the cement treatments were the main prerogative of this study. This can potentially enhance the generalization of the models for improved prediction of the resilient and strength properties of the stabilized systems. The proposed models can serve the pavement design industry to provide an estimate of the tensile strength and the resilient modulus of cement stabilized materials for the analysis and design of pavement structures.

Chapter 11. Field Testing Database

The main objective of this chapter is to develop the database of pavement type, layer configurations, and layer thicknesses using the nondestructive testing (NDT) equipment such as Falling Weight Deflectometer (FWD) and Ground Penetrating Radar (GPR). To accomplish this objective, a pavements feature database was developed using the combination of the NDT results of representative pavement sections and the datasets from previous studies across the state. The nondestructive testing equipment such as FWD and GPR on representative pavement sections were utilized for the assessment of current pavement conditions. The results of field testing using continues GPR survey of the network and FWD deflection basins on selected pavement sections was outlined for further post processing and calibration of models. Then, the development of the database of 64 pavement sections located in Texas was provided in this chapter to serve as a representative sample for the local and global calibration of the fatigue performance models. This field performance data contains information on the location, pavement type, layer stiffness properties, layer configurations, and layer thicknesses.

11.1 Ground Penetrating Radar

GPR is a geophysical survey method used to remotely and non-destructively obtain an image of subsurface materials. The technique is based on sending an electromagnetic pulse through the antenna to the pavement surface and then recording the reflected pulses from the internal interfaces. At each interfaces, a contrast in the dielectric properties is exhibited, as depicted in Figure 11-1. The measured time difference between the reflected pulses (i.e., t_1) can be used in conjunction with the dielectric properties of the surveyed layer to determine its thickness. For example, the thickness of the HMA layer in this study was computed according to equation 11-1:

$$h_{HMA} = \frac{c \times t_1}{2 \times \sqrt{\epsilon_{HMA}}} \quad \text{Equation 11-1}$$

Where h_{HMA} is the HMA layer thickness, t_1 is the electromagnetic wave two-way travel time through the HMA layer as shown in Figure 11-1, c is the speed of light in free space ($c = 3 \times 10^8$ m/s), and ϵ_{HMA} is the dielectric constant of the HMA layer, which was computed according to Equation 11-2:

$$\epsilon_{HMA} = \left[\frac{1 + \frac{A_1}{A_m}}{1 - \frac{A_1}{A_m}} \right]^2 \quad \text{Equation 11-2}$$

Where A_1 is the amplitude of surface reflection; and A_m is the amplitude of reflection from a large metal plate in volts (this represents the 100 percent reflection case).

Similar expressions could be developed for the Cement Treated Base (CTB) layer as indicated in Equation 11-3:

$$h_{CTB} = \frac{c \times t_2}{2 \times \sqrt{\epsilon_{CTB}}} \quad \text{Equation 11-3}$$

Where h_{CTB} is the CTB layer thickness, t_2 is the electromagnetic wave two-way travel time through the CTB layer as shown in Figure 11-1, and ϵ_{CTB} is the dielectric constant of the CTB layer, which was computed in this study according to Equation 11-4:

$$\epsilon_{CTB} = \epsilon_{HMA} \times \left[\frac{1 - \left(\frac{A_1}{A_m}\right)^2 + \left(\frac{A_2}{A_m}\right)^2}{1 - \left(\frac{A_1}{A_2}\right)^2 - \left(\frac{A_1}{A_m}\right)^2} \right]^2 \quad \text{Equation 11-4}$$

Where A_2 is the amplitude of reflection from the top of the CTB layer.

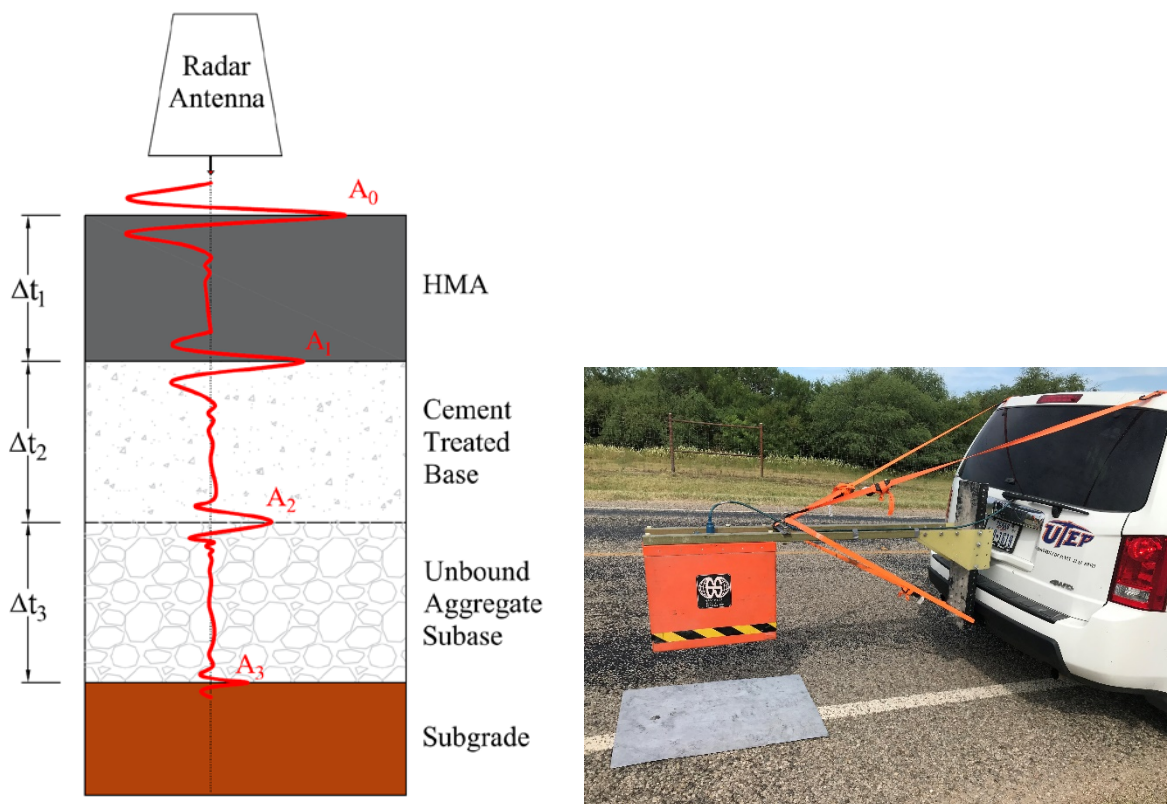


Figure 11-1: Typical GPR Reflections from a Pavement System.

11.2 Falling Weight Deflectometer

The Falling Weight Deflectometer (FWD) is a non-destructive testing method that provides modulus values for pavement layers and the subgrade as shown in Figure 11-2. The test is conducted by applying an impulse load by dropping it from a particular height to a 12-inch diameter circular loading plate that remains in contact with the surface of the pavement layers being tested. By changing the mass as well as the drop height of the weight, different loadings can be simulated and the applied load can be measured using load cells. The resulting surface deflections are measured using seven geophone sensors positioned at various distances such as 0,

12, 18, 24, 30, 36, and 48 inches from the center of the loading plate as shown in Figure 11-2. The resilience modulus of pavement layers in a test section as well as the depth of the underlying layers are measured with the response of the pavement layers via geophones. The resilience moduli are then determined by a back-calculation process using MODULUS software program.

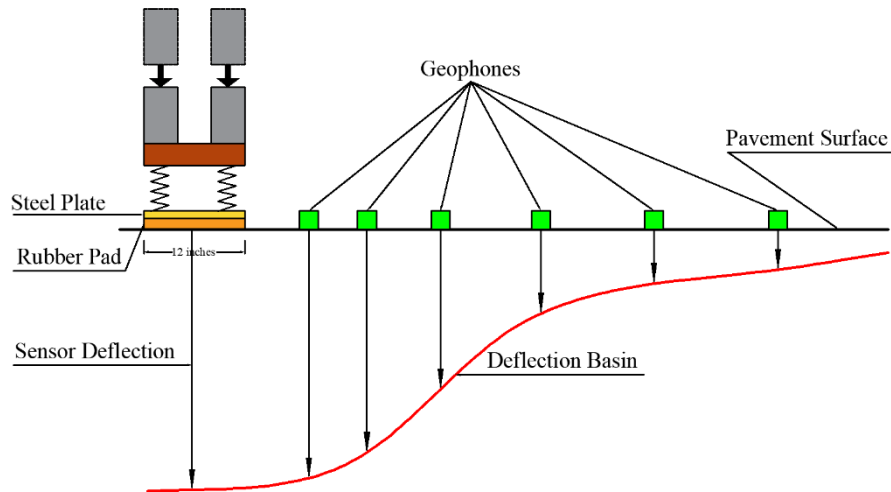


Figure 11-2: Pavement Deflection Basin resulted from FWD Device.

11.3 Field Testing Results

SH-123 and SH-72 are heavily trafficked transportation facilities that serve the energy developing areas of east Texas in the vicinity of four major cities in San Antonio, Houston, Austin, and Corpus Christi, as shown in Figure 11-3. Both roadways were selected as the representative sites for this study for the assessment of current pavement conditions. The original construction plan stated that the SH-123 was 52 ft. wide and had inverted pavement sections with 5 inches of asphaltic material as a surface layer, 8 inches of unbound aggregate material as a flexible base layer, and 8 inches of cement treated base layer as shown in Figure 11-4. As the first step in the field testing, GPR survey on SH-123 was conducted to examine the test section variability and to check layer thicknesses.



Figure 11-3: Location of SH-123 and SH-72 in Texas.

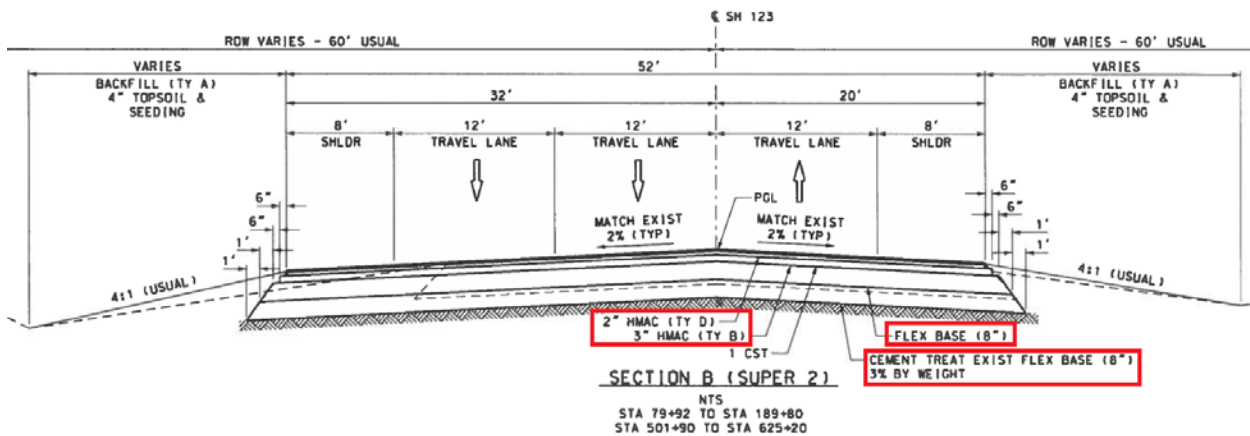


Figure 11-4: Pavement Construction Section and View of SH-123 in Corpus Christi.

Figure 11-5 shows a representative GPR image from the inverted pavement section in State Highway 123 in Corpus Christi. In general, the identification of the layer interfaces was clear except for the interface between CTB and subgrade soils as GPR cannot effectively penetrate to a depth of 20 inches. The plot also indicated that thickness of HMA layer varied between 4 to 6 inches, and the base layer thickness was about 8 inches. The GPR results are in agreement with the design blueprints provided in Figure 11-4.

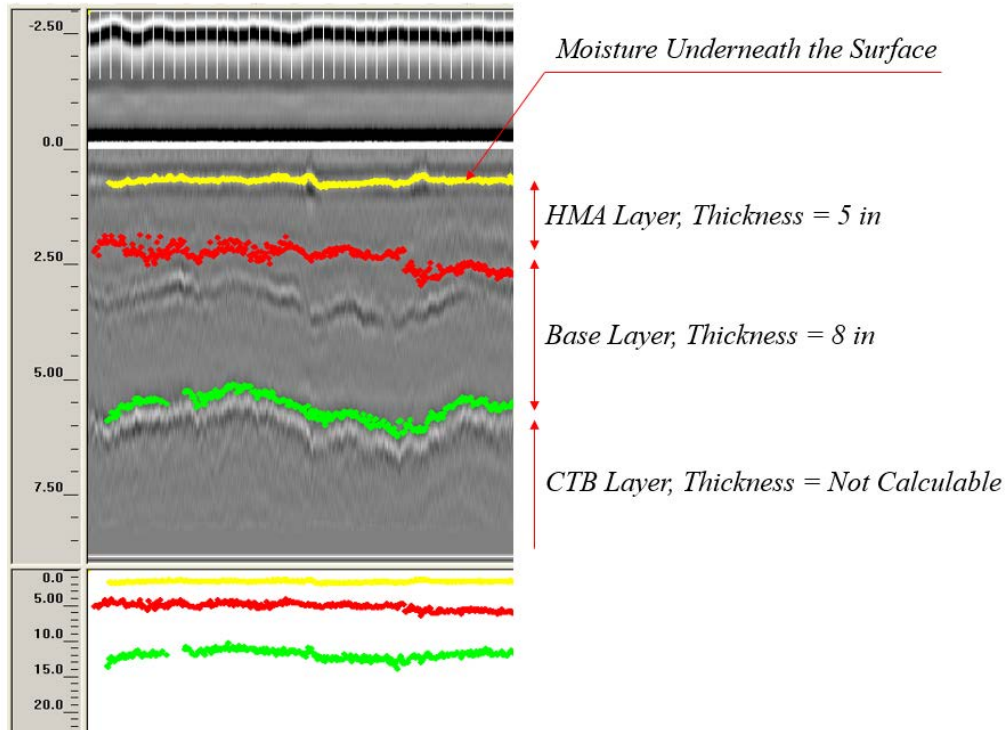


Figure 11-5: GPR Data of SH-123 in Corpus Christi.

In the next step, FWD data was collected on a section of SH-123 in the Karnes County after two years of completion of pavement construction. Table 11-1 shows the FWD data from inverted pavement section of SH-123 in Corpus Christi. The R1 to R7 columns showed the measured deflection at 12 inches intervals away from the load plate. The average maximum deflection (R1) with 10,000 lb. loading was 8.41 mils. Post processing analysis results showed a modulus of 615 ksi as the back-calculated value for 8 inches of cement treated material. This value is in the acceptable range for cement treated base materials with 3% cement content. This information will be instrumental for the performance analysis of pavement sections with cement treated layers.

Table 11-1: FWD Data of SH-123 in Corpus Christi.

TTI MODULUS ANALYSIS SYSTEM (SUMMARY REPORT)																
District	CRP								Modulus Range (psi)							
County	Karnes								Thickness (in)		Minimum		Maximum		Poisson's Ratio	
Highway/Road	SH-123								Pavement:		100		2000		0.35	
									Base:		10		150		0.20	
									Subbase:		10		2000		0.25	
									Subgrade:		150.64(by DB)		15		0.40	
	Load	Measured Deflection (mils):												Absolute	Depth to	
Station	(lb.)	R1	R2	R3	R4	R5	R6	R7	SURF(E1)	BASE(E2)	SUBB(E3)	SUBG(E4)	Err/Sens	Rock	Limit	
0	11118	7.95	5.8	3.95	2.91	2.16	1.71	1.44	1839.2	53.2	524.6	16.4	0.9	186.5		
0.1	10811	13.37	9.94	6.65	4.74	3.47	2.71	2.23	1272.2	22.1	414.4	10	1.08	195.2		
0.2	10701	10.05	7.52	5.35	4.03	3.03	2.39	1.95	1422.4	57.5	226.7	11.5	0.59	183.4		
0.301	10701	5.99	4.36	3.21	2.57	2.02	1.64	1.34	1851.6	97.9	1161.2	15.1	0.46	142.3		
0.4	10548	5.21	3.91	3.02	2.54	2.1	1.79	1.61	2000	150	355.2	17	8.31	300	*	
0.499	10318	9.91	7.19	4.76	3.41	2.47	1.93	1.46	1449.8	31	489.5	13.5	0.97	155.8		
0.6	10252	8.22	6.13	4.26	3.15	2.35	1.87	1.56	2000	34.3	1073	13.2	0.78	216.5	*	
0.7	10154	9.4	6.91	4.85	3.63	2.73	2.18	1.73	1635.5	30.9	1086.8	11.1	0.88	140.1		
0.8	9946	13.61	10.3	7.17	5.31	3.98	3.14	2.55	1055.6	36	139	8.2	1.05	199.2		
0.9	9989	10.35	8.1	5.91	4.53	3.47	2.76	2.33	1888.5	32.9	571.4	8.4	0.41	242.7		
1	9902	10.41	7.9	5.27	3.57	2.45	1.8	1.44	1656.1	44.1	46	14.8	0.93	113.2		
1.1	9858	7.21	5.35	3.95	3.16	2.51	2.07	1.76	1427.1	88.5	622.8	11.4	0.85	300		
1.2	9803	9.72	7.46	5.26	3.84	2.79	2.15	1.7	1711.1	51.1	112	12.1	0.7	144.7		
1.302	9737	8.33	6.32	4.55	3.47	2.6	2.04	1.64	1588.2	76.9	177.5	12.4	0.65	151.6		
1.4	9770	8.07	5.87	4.1	3.09	2.35	1.87	1.55	1671.7	36.9	1251.7	12.4	0.66	211.7		
1.468	9825	5.7	4.2	3.17	2.54	2.02	1.66	1.37	1907.8	94.7	1264.2	13.3	0.56	163.7		
1.509	9814	4.47	3.12	2.31	1.83	1.42	1.15	0.97	1753.4	138.4	1230.1	20.5	0.7	300		
1.573	9672	8.08	5.72	3.85	2.83	2.13	1.65	1.3	1310.3	49.9	442.9	14.8	0.62	127.8		
1.654	9727	4.85	3.38	2.5	2.04	1.65	1.37	1.12	1620.6	150	881.3	18	1.85	132	*	
1.779	9683	7.35	5.47	3.88	2.92	2.17	1.68	1.33	1643.4	85.8	185.5	15.1	0.55	130.4		
Mean:		8.41	6.25	4.4	3.31	2.49	1.98	1.62	1635.22	68.1	612.79	13.46	1.18	171.6		
Std. Dev.		2.53	1.97	1.29	0.88	0.62	0.48	0.4	252.71	40.75	429.19	3.1	1.7	46.9		
Var Coeff(%):		30.09	31.57	29.35	26.62	25.06	24.28	24.49	15.45	59.84	70.04	23.06	145.2	27.3		

Figure 11-6 shows the initial construction plan and view of State Highway 72 in Corpus Christi. As observed in the map, SH-72 consisted of a thick cement treated base layer (16 inches) supporting a 6.5 inches thick asphalt surface layer. As evidenced in Figure 11-7, the GPR results of the asphalt layer thickness is in conformity with the design profile displayed in Figure 11-6. A network level FWD testing plan was devised to determine the layer stiffness properties inside and outside of the wheel path. Figure 11-8 provides an example of the MODULUS 7.0 output file that the research team used for the back-calculation of the layer moduli of pavement sections. The post processed field data resulted in 232 ksi as the modulus of 1% cement treated base layer for this pavement section. The research team will contrast this information with the laboratory data to cross validate the results.

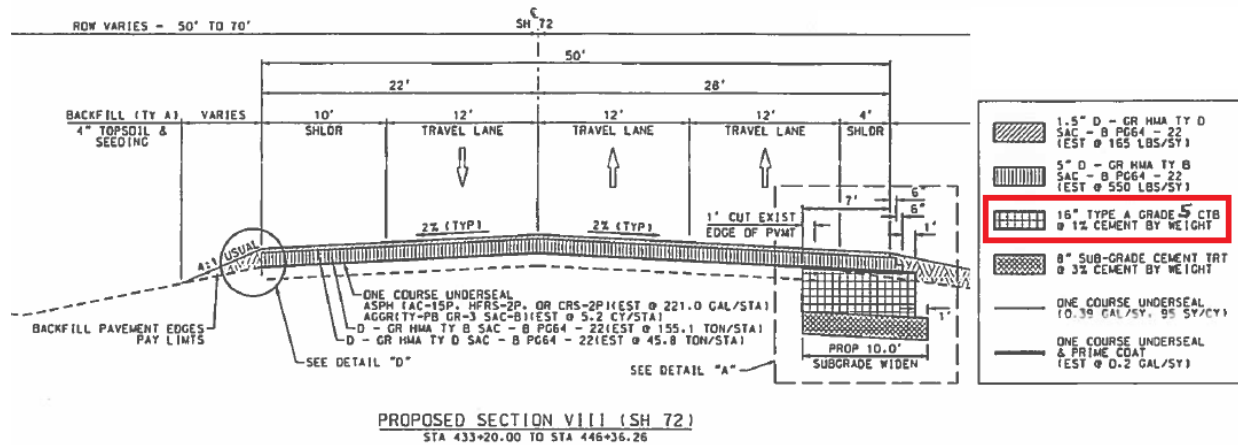


Figure 11-6: Pavement Construction Section and View of SH-72 in Corpus Christi.

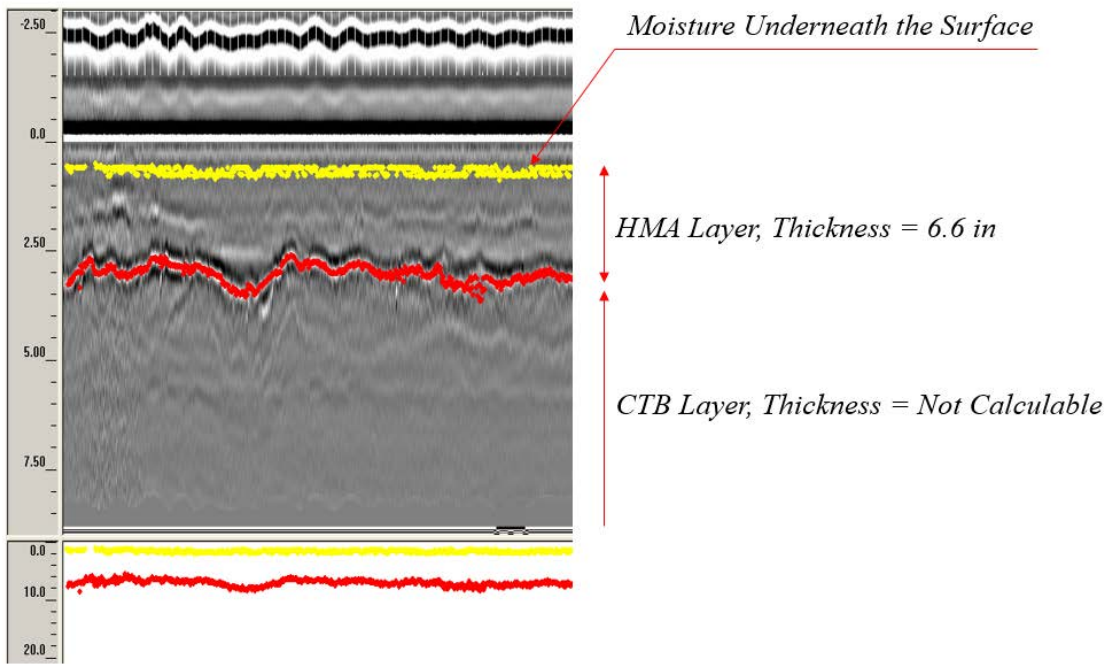


Figure 11-7: GPR Data of SH-72 in Corpus Christi.

TTI MODULUS ANALYSIS SYSTEM (SUMMARY REPORT)													(Version 7.0)			
District:									MODULI RANGE (psi)							
County :			Thickness (in)						Minimum		Maximum		Poisson Ratio Values			
Highway/Road:			Pavement:			Base:			Subbase:			Subgrade:			H1: v = 0.35	
			6.60			16.00			8.00			114.80 (by DB)			H2: v = 0.25	
			400,000			200,000			20,000			10,000			H3: v = 0.35	
			1,040,000			1,000,000			50,000						H4: v = 0.40	
Station	Load (lbs)	Measured Deflection (mils):							Calculated Moduli values (ksi):				Absolute Dpth to			
		W1	W2	W3	W4	W5	W6	W7	SURF(E1)	BASE(E2)	SUBB(E3)	SUBG(E4)	ERR/Sens	Bedrock		
0.000	11,016	10.41	6.57	4.59	3.48	2.72	2.11	1.69	400.0	200.0	20.0	11.0	9.23	144.1 *		
0.270	10,801	14.46	7.54	4.92	3.78	2.98	2.39	1.94	400.0	200.0	20.0	8.6	17.47	165.4 *		
0.513	10,968	14.20	8.51	5.58	4.17	3.28	2.47	1.98	400.0	200.0	20.0	7.8	17.55	129.1 *		
0.764	10,110	23.54	14.77	9.02	6.07	4.66	3.40	2.59	400.0	200.0	20.0	3.5	32.16	300.0 *		
1.015	10,627	13.07	10.84	7.34	4.82	3.37	2.51	1.91	400.0	200.0	20.0	6.3	23.59	136.6 *		
1.264	10,265	22.58	13.13	7.54	5.02	3.76	2.75	2.17	400.0	200.0	20.0	4.7	33.36	300.0 *		
1.511	10,531	14.65	10.84	7.87	5.70	4.15	3.07	2.38	400.0	200.0	20.0	5.0	19.59	133.6 *		
1.781	10,750	6.65	4.53	3.89	3.30	2.84	2.38	2.00	400.0	522.9	50.0	9.2	1.80	300.0 *		
2.022	9,939	31.93	20.62	11.48	7.20	5.41	4.12	3.24	400.0	200.0	20.0	2.4	40.05	137.2 *		
2.251	10,690	11.06	8.26	6.01	4.44	3.37	2.60	2.05	400.0	200.0	20.0	7.5	11.30	144.6 *		
2.506	10,694	10.48	7.56	5.67	4.13	2.86	1.96	1.35	400.0	200.0	20.0	9.1	14.60	91.1 *		
2.760	10,484	10.62	7.46	5.33	4.08	3.26	2.59	2.02	400.0	200.0	20.0	8.1	8.48	129.8 *		
3.010	10,774	6.08	4.25	3.53	3.01	2.51	2.09	1.76	400.5	587.5	34.1	10.8	1.10	300.0 *		
3.271	10,678	5.99	4.59	3.72	3.19	2.76	2.28	1.91	696.4	404.7	50.0	9.2	1.60	300.0 *		
3.525	10,233	14.71	8.55	6.21	4.60	3.44	2.51	1.87	400.0	200.0	20.0	6.3	19.40	111.9 *		
3.783	10,348	14.89	9.48	5.42	3.53	2.59	1.96	1.54	400.0	200.0	20.0	8.3	27.89	191.1 *		
3.981	10,484	11.71	7.26	5.30	4.47	3.61	2.82	2.31	400.0	200.0	20.0	7.4	7.79	149.9 *		
4.335	10,459	9.69	6.17	4.17	3.23	2.53	1.94	1.55	400.0	200.0	20.0	11.5	9.29	131.8 *		
4.546	10,384	13.80	9.63	6.12	4.42	3.45	2.53	1.97	400.0	200.0	20.0	6.5	19.43	114.4 *		
4.754	10,317	17.57	10.72	7.48	5.66	4.41	3.40	2.63	400.0	200.0	20.0	4.5	19.35	135.5 *		
5.006	10,301	11.62	8.95	7.30	5.75	4.67	3.56	2.76	400.0	200.0	20.0	5.0	6.34	135.5 *		
5.258	10,535	4.61	3.52	3.06	2.65	2.30	1.52	1.65	735.4	817.8	50.0	10.0	0.46	300.0 *		
5.515	10,416	9.60	5.79	4.34	3.25	2.60	2.07	1.67	400.0	200.0	20.0	11.2	6.34	161.1 *		
5.758	10,400	5.99	4.81	3.91	3.09	2.57	2.03	1.65	1040.0	226.1	48.6	10.2	1.59	153.2 *		
5.977	10,547	8.12	6.00	4.34	3.02	2.19	1.62	1.30	400.0	200.0	20.0	13.2	9.30	118.3 *		
6.260	10,074	19.43	9.66	4.55	2.92	2.29	1.60	1.35	400.0	200.0	20.0	9.3	36.63	118.8 *		
6.510	9,963	33.22	12.22	5.05	3.37	2.54	1.97	1.70	400.0	200.0	20.0	7.1	43.78	62.6 *		
6.773	10,070	16.95	8.57	3.96	2.38	1.71	1.33	1.09	400.0	200.0	20.0	12.1	37.66	93.7 *		
7.018	9,967	22.90	11.67	6.15	4.39	3.33	2.56	2.06	400.0	200.0	20.0	5.4	32.90	300.0 *		
7.261	9,816	19.33	13.47	9.31	7.02	5.39	4.20	3.39	400.0	200.0	20.0	3.0	21.99	198.1 *		
7.520	10,285	26.26	10.14	3.98	2.31	1.51	1.28	0.98	400.0	200.0	20.0	12.2	47.66	54.3 *		
7.754	10,154	16.74	8.27	5.59	4.07	3.15	2.41	1.96	400.0	200.0	20.0	6.9	21.79	162.4 *		
7.959	9,931	19.14	9.72	6.88	4.88	3.67	2.63	1.95	400.0	200.0	20.0	5.2	25.45	120.0 *		
8.265	10,205	15.64	7.17	4.46	2.87	2.37	1.69	1.23	400.0	200.0	20.0	10.2	25.86	176.3 *		
8.510	9,864	17.54	10.27	6.43	4.55	3.33	2.37	1.78	400.0	200.0	20.0	5.7	27.52	106.2 *		
8.753	10,225	9.70	5.56	3.55	2.73	2.33	1.75	1.48	400.0	200.0	20.0	13.0	10.88	300.0 *		
9.029	10,146	18.34	9.65	5.68	4.11	3.02	2.31	1.85	400.0	200.0	20.0	6.7	27.60	150.2 *		
9.268	10,245	13.78	8.74	5.88	4.22	3.29	2.47	1.92	400.0	200.0	20.0	6.8	18.46	135.0 *		
9.523	10,376	9.63	6.33	4.61	3.30	2.32	1.63	1.19	400.0	200.0	20.0	11.5	13.74	96.6 *		
9.804	9,971	19.15	8.74	5.39	3.76	2.85	2.15	1.66	400.0	200.0	20.0	7.1	28.03	134.6 *		
10.042	9,900	14.33	9.08	6.40	4.16	2.74	1.74	1.26	400.0	200.0	20.0	7.4	30.53	86.4 *		
10.351	9,276	35.31	14.52	7.40	5.09	3.67	2.51	1.82	400.0	200.0	20.0	3.9	41.93	300.0 *		
10.672	9,665	25.80	11.60	4.96	2.47	1.69	1.24	0.95	400.0	200.0	20.0	10.1	52.63	59.3 *		
10.933	10,213	15.06	9.69	5.16	3.30	2.31	1.63	1.19	400.0	200.0	20.0	9.1	32.58	97.2 *		
11.165	10,420	7.26	5.73	4.33	3.24	2.45	1.90	1.45	547.9	200.0	20.0	12.0	4.36	110.9 *		
11.335	10,372	12.40	9.07	6.90	5.28	4.09	3.08	2.43	400.0	200.0	20.0	5.6	11.62	140.7 *		
11.502	10,400	10.01	7.30	5.54	4.12	3.23	2.53	1.93	400.0	200.0	20.0	8.2	7.57	119.9 *		
11.672	10,392	11.04	6.97	4.56	3.47	2.72	2.17	1.76	400.0	200.0	20.0	9.7	13.06	159.0 *		
Mean:	15.15	8.85	5.64	4.04	3.09	2.34	1.84	1.29	429.6	232.5	22.8	8.0	20.28	145.4		
Std. Dev:	7.09	3.16	1.67	1.14	0.86	0.66	0.52	0.35	112.0	115.6	8.4	2.8	13.41	64.0		
Var Coeff(%):	46.84	35.66	29.58	28.12	27.97	28.02	28.25	26.1	26.1	49.7	37.1	34.3	66.16	44.0		

Figure 11-8: FWD Data of SH-72 in Corpus Christi.

11.4 Data Collection

A comprehensive database of section parameters and material properties from NDT, such as FWD and GPR was compiled for further incorporation in the calibration algorithm of the fatigue performance model. Table 11-2 summarize the dataset from 64 pavement sections across Texas. This database contains the location of these pavement sections, thickness, back-calculated FWD modulus, and materials type for the cement stabilized layers. In addition to these particulars, the field collected data consists of (1) the materials properties for stabilized materials such as unconfined compressive strength, maximum dry density, optimum moisture content, and (2) layer configurations, layer thickness, and back-calculated FWD modulus for each layer of representative

pavement sections. This database will be instrumental for the calibration of the fatigue performance models.

Table 11-2: General Overview of the Database Compiled from NDT in Texas.

No.	Location	CTB Layer				References
		Thickness (in.)	FWD Modulus (psi)	Materials	Stabilizer	
1	SH-123 - San Antonio	8	612,790	Virgin Aggregate	3% Cement	TxDOT-0-6949
2	SH72 - Corpus Christi	16	232,500	Virgin Aggregate	1% Cement	
3	US-290 - Bryan	14	919,200	Virgin Aggregate	3.5% Cement	Scullion et al. (2008)
4	US-290 - Bryan	14	500,000	Virgin Aggregate	3.5% Cement	
5	FM-378 - Lubbock	7	320,000	25% RAP-75% Virgin	2% Cement	TxDOT-6084
6	FM-448 - Yoakum	8	128,000	50% RAP-50% Virgin	3% Cement	
7	FM-448 - Yoakum	8	343,000	50% RAP-50% Virgin	3% Cement	
8	FM-2415 - Fort Worth	10	629,000	60% RAP-40% Virgin	4% Cement	
9	FM-2415 - Fort Worth	10	684,000	60% RAP-40% Virgin	4% Cement	
10	SH-121 - Paris	9.5	2,900,000	Virgin Aggregate	9% Cement	TxDOT-6658
11	US-271 - Paris	9	2,089,600	Virgin Aggregate	9% Cement	
12	US-59 - Atlanta	10	316,600	Virgin Aggregate	Lime-Fly Ash	
13	US-59 - Atlanta	10	228,400	Virgin Aggregate	Lime-Fly Ash	
14	US-59 - Atlanta	10	468,200	Virgin Aggregate	Lime-Fly Ash	
15	US-59 - Atlanta	10	212,800	Virgin Aggregate	Lime-Fly Ash	TxDOT (No.474PV1A007)
16	SH-72 - Karnes	10.5	360,000	Sandy material	4% Cement	
17	SH-72 - Karnes	8	125,000	Sandy material	2% Cement	
18	SH-72 - Karnes	11	125,000	Sandy material	2% Cement	
19	SH-72 - Karnes	8	50,000	Sandy material	3% Lime	TxDOT (No.474PV1A008)
20	FM-99 - Corpus Christi	11	410,000	Virgin Aggregate	3% Cement	
21	FM-99 - Corpus Christi	8	323,300	Virgin Aggregate	3% Cement	
22	FM-99 - Corpus Christi	11	448,300	Virgin Aggregate	3% Cement	
23	FM-99 - Corpus Christi	8	198,700	Virgin Aggregate	3% Cement	Si et al. (2007)
24	Amarillo District	12	53,000	Limestone Base	2% Cement	
25	Amarillo District	12	21,000	Limestone Base	8% Fly Ash	
26	Amarillo District	12	57,000	Limestone Base	3% Lime	Chenet al. (2007, 2011)
27	SH-24 - Paris	11	2,000,000	Virgin Aggregate	3% Cement	
28	US-290	12	1,000,000	Crushed Stone	3.5% Cement	TxDOT-4052
29	Riverside Campus	6	362,000	Marginal Gravel	4% Cement	
30	Riverside Campus	6	947,000	Marginal Gravel	4% Cement	
31	Riverside Campus	6	417,100	Marginal Gravel	8% Cement	
32	Riverside Campus	6	1,690,600	Marginal Gravel	8% Cement	
33	SH-16 - San Antonio	12	93,700	Virgin Aggregate	2% Cement	
34	SH-16 - San Antonio	11.5	340,100	Virgin Aggregate	2% Cement	
35	SH-16 - San Antonio	7	138,400	FDR	3% Cement	
36	SH-16 - San Antonio	7	160,700	FDR	3% Cement	
37	SH-16 - San Antonio	11.6	609,800	Virgin Aggregate	2% Cement	
38	SH-16 - San Antonio	7	169,200	FDR	3% Cement	
39	SH-16 - San Antonio	7	153,900	FDR	3% Cement	
40	SH-16 - San Antonio	11.4	429,600	Virgin Aggregate	2% Cement	
41	SH-16 - San Antonio	7	137,700	FDR	3% Cement	
42	SH-16 - San Antonio	12	257,200	Virgin Aggregate	2% Cement	
43	Riverside Campus	6	1,012,900	Marginal Gravel	4% Cement	

No.	Location	CTB Layer				References
		Thickness (in.)	FWD Modulus (psi)	Materials	Stabilizer	
44	Riverside Campus	6	771,400	Marginal Gravel	4% Cement	
45	Riverside Campus	6	1,712,000	Marginal Gravel	8% Cement	
46	Riverside Campus	6	850,000	Marginal Gravel	8% Cement	
47	Riverside Campus	6	1,164,400	Marginal Gravel	4% Cement	
48	Riverside Campus	6	1,086,700	Marginal Gravel	4% Cement	
49	Riverside Campus	6	2,038,300	Marginal Gravel	8% Cement	
50	Riverside Campus	6	1,278,400	Marginal Gravel	8% Cement	
51	Riverside Campus	6	1,392,100	Marginal Gravel	4% Cement	
52	Riverside Campus	6	1,305,200	Marginal Gravel	4% Cement	
53	Riverside Campus	6	2,075,800	Marginal Gravel	8% Cement	
54	Riverside Campus	6	1,258,600	Marginal Gravel	4% Cement	
55	Riverside Campus	6	1,190,500	Marginal Gravel	4% Cement	
56	Riverside Campus	6	2,899,400	Marginal Gravel	8% Cement	
57	Riverside Campus	6	1,647,100	Marginal Gravel	8% Cement	
58	Riverside Campus	6	1,758,800	Marginal Gravel	4% Cement	
59	Riverside Campus	6	2,357,000	Marginal Gravel	8% Cement	
60	SH-47 - Bryan	14	347,000	FDR	3% Cement	
61	SH-47 - Bryan	14	347,000	FDR	3% Cement	
62	SH-16 - San Antonio	5	359,000	FDR	2% Cement	
63	Riverside Campus	6	850,000	Marginal Gravel	4% Cement	
64	Riverside Campus	6	2,100,000	Marginal Gravel	8% Cement	

Chapter 12. Field Calibration of the Fatigue Performance Model

12.1 Introduction

Fatigue cracking in the cement stabilized layers considerably reduces the support provided to the surface pavement layers. This will accelerate the manifestation of distresses in the asphalt surface layers, such as bottom-up fatigue fracture that ultimately lead to a premature failure of the pavement structure. The fatigue performance models in the TxME have never been calibrated due to the lack of field data and reliable laboratory tests in the past. Thus, it is necessary to calibrate this model for implementation in local setting by taking into account local materials, traffic information, and environmental conditions. The main focus of this chapter is to develop and calibrate the fatigue performance model for cement stabilized layers in flexible pavement based on the laboratory test results and field database.

12.2 Fatigue Performance Model in the TxME

The TxME requires a measure of the 28-day flexural modulus of the cement treated layers to estimate the fatigue life of pavements. Equation 12-1 provides a general form of the fatigue performance model in the TxME.

Equation 12-1

$$\log N_f = \frac{0.972 \times \beta_{c1} - \left(\frac{\sigma_t}{M_{rup}} \right)}{0.0825 \times \beta_{c2}}$$

Where N_f is number of load repetitions to fatigue cracking of the stabilized layer,

σ_t is maximum traffic induced tensile stress at the bottom of the stabilized layer (psi),

M_{rup} is the 28-days modulus of rupture or flexural strength (psi),

β_{c1}, β_{c2} are field calibration factors.

Traditionally the ASTM C78 (ASTM, 2018) third point flexural loading test is used for the estimation of the 28-day modulus of rupture. Major practical challenges associated with this test for cement treated materials in the laboratory were outlined by Ashtiani et al. (2016) at the Tx-06812 project, as:

- Practicality issues associated with incurring damage to the large beams (6x6x20 in) during de-molding and handling of the prismatic specimen in the laboratory. The authors reported that a significant number of lightly stabilized beams were disintegrated during de-molding, handling, and transportation to the test setup.
- Issues associated with the uniformity of compaction of the stabilized materials in the large beam specimen. Uniformity of the compaction cannot be assured due to the long and relatively shallow nature of the molds in the conventional third point test. The wall

effect was exhibited in most of the stabilized samples, which is an indication of non-uniform compaction effort. The inconsistency in compacted materials can potentially manifest itself in reduced reliability of the test results.

- Issues associated with labor intensive process of the bending beam test. The authors reported that at least two operators are required to safely transport the 60 lb. prismatic beams to the tests setup without damaging the specimen.
- Due to the large size of the prismatic beams, the third point beam test requires significantly larger amount of material for testing in the laboratory.

Several researchers reported inconsistencies with the bending beam test and explored alternative testing methods to estimate the tensile behavior of stabilized materials (Majumder et al., 1999; Sobhan & Das, 2007; Midgley & Yeo, 2008; Flintsch et al., 2008; Gnanendran & Piratheepan, 2009; Yan et al., 2011; Arnold, 2012). Ashtiani et al. (2016) performed several FE analysis considering different material properties and stress paths to investigate the systematic error associated with the bending beam test for stabilized materials in the laboratory. As evidenced in Figure 12-1a, due to the pure bending mechanism in the bending beam test, the top portion of the beam is in compression, while the bottom fibers experience tension. They concluded that approximately 60% of the beam is still in compression due to the pure bending loading in the third point test based on the parameters selected for the finite element analysis. Additionally, the distributions of the stress follow a highly nonlinear pattern in the mid-span cross section of the prismatic beam. They also showed the capability of the Indirect Diametrical Tensile (IDT) test as an alternative to the bending beam test to induce a relatively uniform tension along the axis of loading in the specimen as observed in Figure 12-1b. The exaggerated deformed meshes showed small compression zones immediately beneath the loading platform and adjacent to the support at the bottom of the specimen, however the majority of the specimen stays in tension upon the application of the axial load.

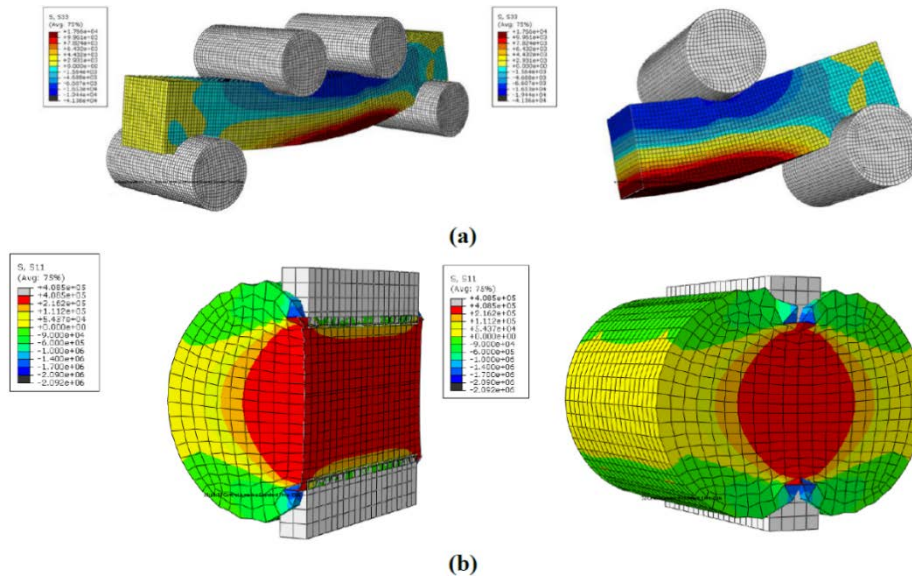


Figure 12-1: Nature of Stress Distributions in Traditional Tension Tests: (a) Third Point Bending Beam Test, and (b) Indirect Diametrical Tensile (IDT) Test (Ashtiani et al., 2016).

Therefore, the theoretical issues and practical aspects of the third point beam test underscore using IDT as an alternative test method to effectively and efficiently develop the fatigue performance model for cementitious materials in the laboratory.

The current TxME fatigue model uses the accumulated damage concept to estimate the fatigue damage (D) based the Miner's Law, as indicated in Equation 12-2:

Equation 12-2

$$D = \sum_{i=1}^T \frac{n_i}{N_{fi}}$$

Where:

T is total number of load applications,

n_i is actual traffic for load i , and

N_{fi} is calculated repetitions to failure for load i .

The TxME proposed an empirical relationship between damage in the cement treated layer to surface cracking damage, as shown in Equation 12-3:

Equation 12-3

$$C = \frac{1000}{1 + e^{(1-D)}}$$

C is cement stabilized base layer cracking in units of ft of cracking per 500-ft-long sections,

D is the cement stabilized base damage level.

Calculation of surface cracking damage based on the empirical Equation 12-3 does not appear to be logical. For instance, if the base damage from Equation 12-2 is 0 (the case of no damage in pavement foundation), entering a zero in Equation 12-3 will compute a C value of 269 ft. of cracking per 500-ft-long section.

Another shortcoming arises when the computed stresses are not increased to account for shrinkage cracking in the TxME fatigue model. As discussed before, time and temperature dependent cement hydration process influences the shrinking behavior of the cement treated layers. Such volumetric change can manifest itself in the form of shrinkage cracks in the cement treated base layers. These cracks can propagate to the asphalt surface layers and jeopardize the longevity of pavement structures. Therefore, it is imperative to properly consider the impact of shrinkage cracking in the fatigue performance model of the cement stabilized base layer.

12.3 Development and Calibration of the Fatigue Performance Model

This section presents the development and calibration of the TxME predictive models for fatigue performance of the stabilized base layer in flexible pavements design. To accomplish this objective, relevant databases were collected from the laboratory test results, FE simulation, and field testing. Results from the submaximal modulus test, shrinkage test, static and dynamic IDT test were initially used in this study to develop the fatigue performance model in the laboratory. The development of the database of 102 pavement sections (64 pavement sections located in Texas) were used as a representative sample for the local and global calibration of the fatigue performance models. Figure 12-2 presents the process for the development and calibration of the fatigue performance model for cement stabilized layers. The process of model development, calibration and validation will be performed using the following five-step procedure:

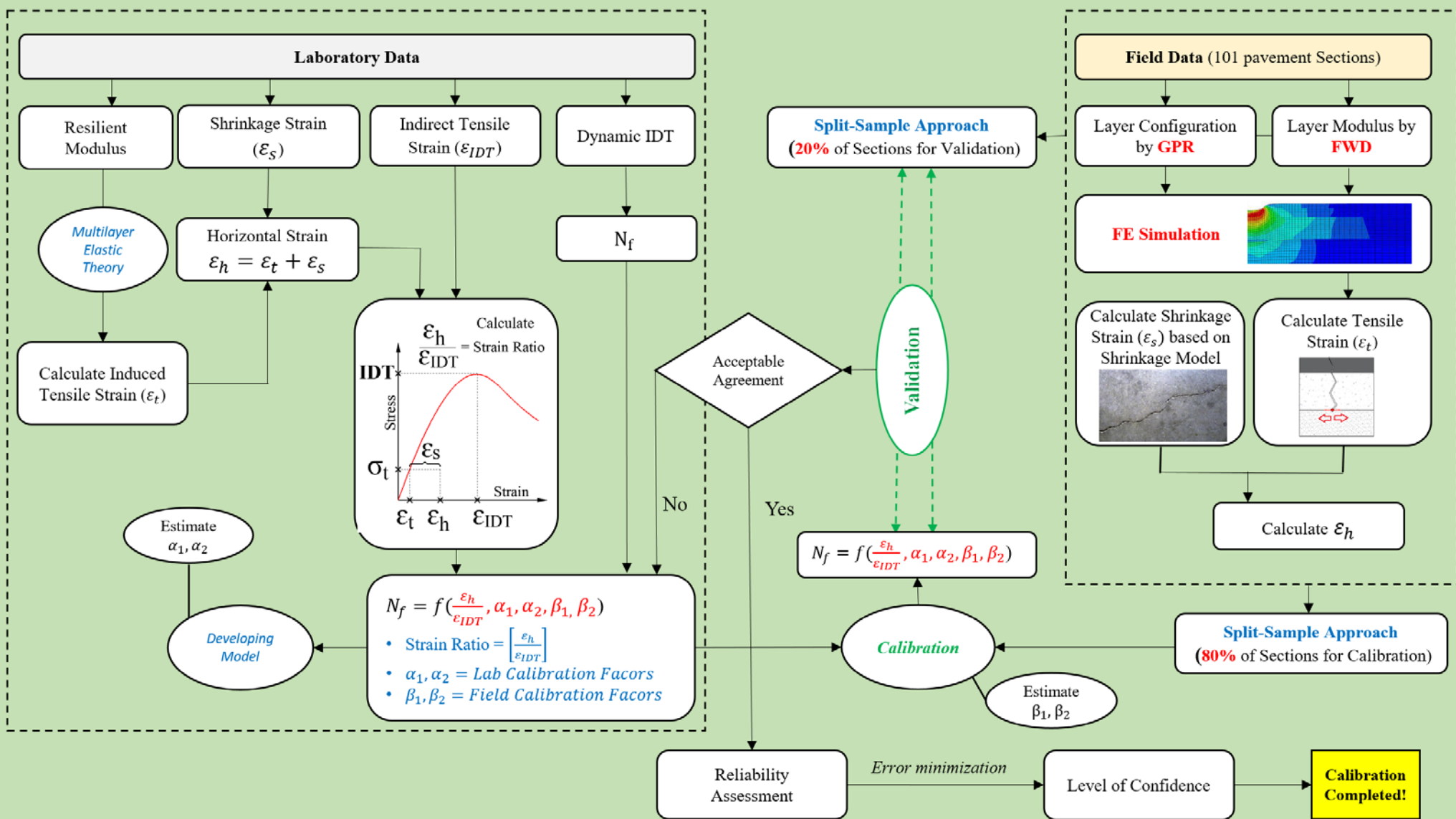


Figure 12-2: Calibration of the Fatigue Performance Model

12.3.1 Step 1: Determination of Strain Ratio

The current TxME model used to predict the fatigue life of cement stabilized base layer is thoroughly depended on the stress ratio as demonstrated in Equation 12-1. With decreasing stress ratio of the cement stabilized layer, fatigue life of pavement structure considerably increases. Thus, maximum tensile stresses derived from available traffic loads at the bottom of the stabilized layer and flexural strength of stabilized materials are the main parameters in the TxME model. In this traditional procedure, the impact of shrinkage cracking was not considered in the fatigue performance model. Therefore, new developed model uses strain ratio in lieu of stress ratio in order to properly incorporate the component of shrinkage strain to predict the fatigue life of cement stabilized base layers. Figure 12-3 shows that strain ratio of the fatigue performance model developed in this study was determined based on the strain value, which corresponds to tensile strength of materials (ϵ_{IDT}) and horizontal strain (ϵ_h). As observed in the plot, the shrinkage strain (ϵ_s) is added to induced tensile strain (ϵ_t) for the calculation of the total horizontal strain (ϵ_h) to consider the impact of shrinkage cracking in cement treated base layers.

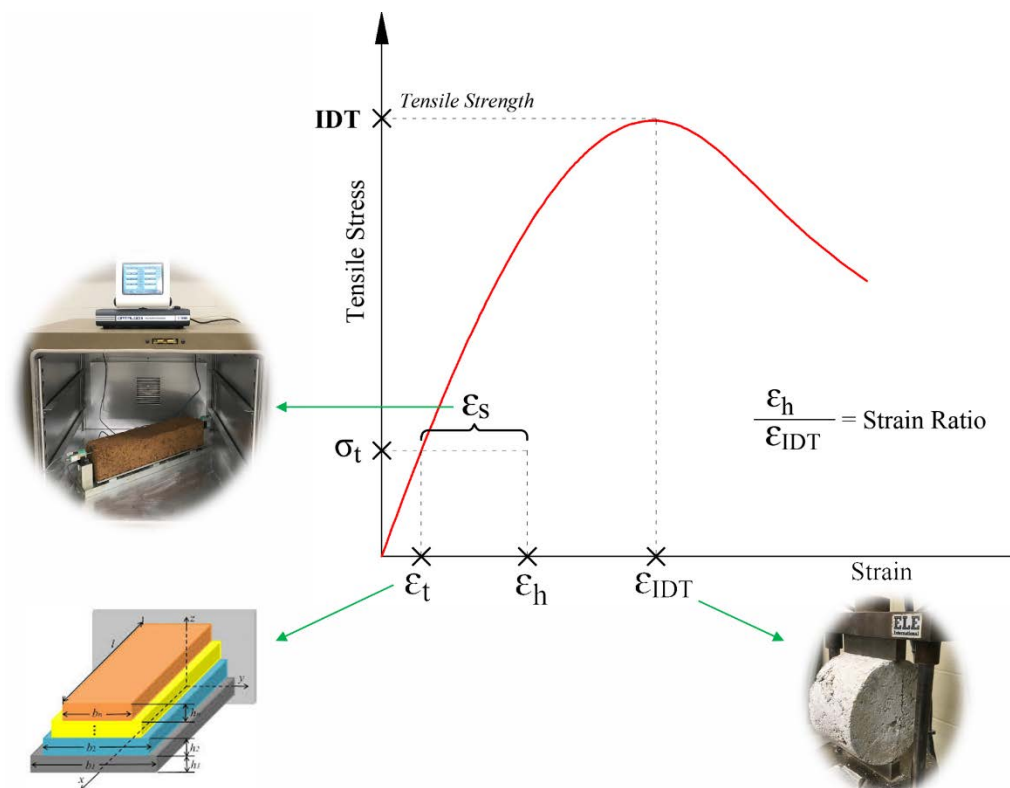


Figure 12-3: Calculation of Strain Ratio.

Strain value that corresponds to the maximum tensile strength of materials (ϵ_{IDT}) and shrinkage strain (ϵ_s), were obtained from static IDT test and shrinkage test in the laboratory, respectively. The multilayer linear elastic analysis was conducted to compute induced horizontal strain (ϵ_t) in the pavement sections under the cement treated layer for the following assumed conditions:

- HMA layer with a thickness of 3 in. and a resilient modulus of 360 ksi.
- Cement treated layer with a thickness of 8 in.
- Infinite subgrade thickness with a resilient modulus of 12 ksi.
- A dual wheel with tire pressure of 115 psi, contact area of 42.5 in², and wheel spacing of 12 in, which is most frequent truck class and tire pressure in Texas according to the TxDOT-0-6949 Project (Ashtiani et al., 2019).

In the multilayer linear elastic analysis, the modulus values for cement treated layer were obtained from the performance of submaximal modulus test in the laboratory for the relevant materials.

12.3.2 Step 2: Development of the Fatigue Performance Model

After determining the strain ratio, the fatigue performance model was developed to determine the bottom-up tensile-fatigue life of the cement stabilized layers. The number of load applications to failure (N_f) in the dynamic IDT tests, the strain ratio ($\frac{\epsilon_h}{\epsilon_{IDT}}$), α_1 and α_2 as regression parameters, and β_1 , as the field calibration factor, are the main parameters of the developed model, as shown in the following Equation:

$$N_f = f\left(\frac{\epsilon_h}{\epsilon_{IDT}}, \alpha_1, \alpha_2, \beta_1\right) \quad \text{Equation 12-4}$$

Figure 12-4 presents the number of load application to failure (N_f) for different types of stabilized base materials. As evidenced from the plot, stabilized limestone aggregates and FDR materials had the highest and lowest number of load application in the dynamic IDT tests, respectively. The plot also illustrates the typical damage evolution obtained for the limestone specimen stabilized with 4% cement content. The high plastic strain rate was observed during the first load cycles, then it decreases to a nearly constant level. This constant level followed by a sharp increase in the permanent deformation after around 5,000,000 load applications is depicted in the graph. Such dramatic change in permanent deformation is considered due to the propagation of cracks in the stabilized mixture and represents true failure. These results were used in this project to develop the fatigue performance model for cement stabilized materials.

Materials	Cement	Nf
Limestone	2%	1,352,321
	3%	5,010,021
	4%	4,947,979
Gravel	2%	2,017,945
	3%	3,380,187
	4%	473,329
RCA	2%	3,351,617
	3%	4,512,653
	4%	1,534,013
FDR	2%	62,335
	3%	512,865
	4%	1,135,491

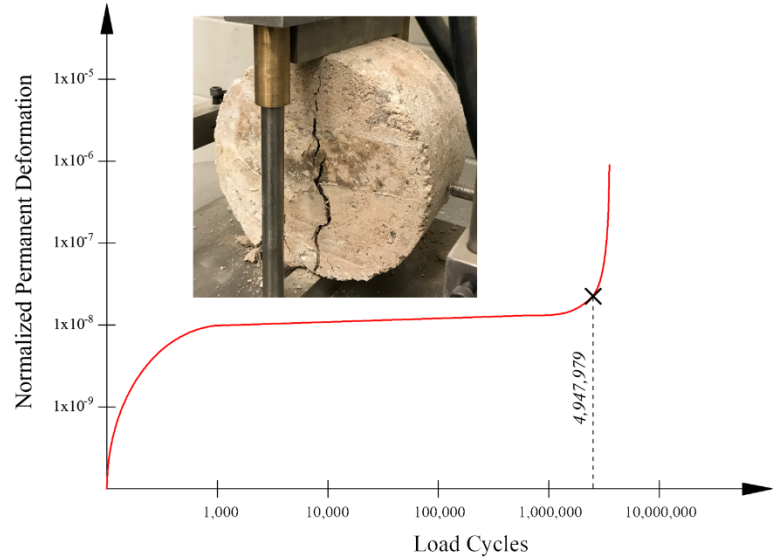


Figure 12-4: Number of Load Application to Failure (N_f) for Different Types of Stabilized Base Materials and Typical Damage Evolution.

Figure 12-5 provides the relationship between number of load application to failure (N_f) in the dynamic IDT tests and the strain ratio for cement stabilized base materials in the laboratory. The descending nature of the trend line suggests a direct correlation between the number of load application to failure and strain ratio of cement stabilized materials. In other words, permutations with higher shrinkage strain and induced tensile stress exhibited lower fatigue life compared to other counterparts in the experiment matrix.

Equation 12-5 presents the relationship between the strain ratio and the bottom-up tensile-fatigue life of cement stabilized layers. The model is based on the submaximal modulus, static IDT, shrinkage, and dynamic IDT results of four different types of materials tested in the laboratory.

$$\ln(N_f) = \left[\frac{\alpha_1 - \frac{\epsilon_h}{\epsilon_{IDT}}}{\alpha_2} \right] \quad \text{Equation 12-5}$$

Where N_f is the number of load application to failure, $\frac{\epsilon_h}{\epsilon_{IDT}}$ is strain ratio, and the laboratory regression factors are $\alpha_1 = 0.6643$ and $\alpha_2 = 0.04$.

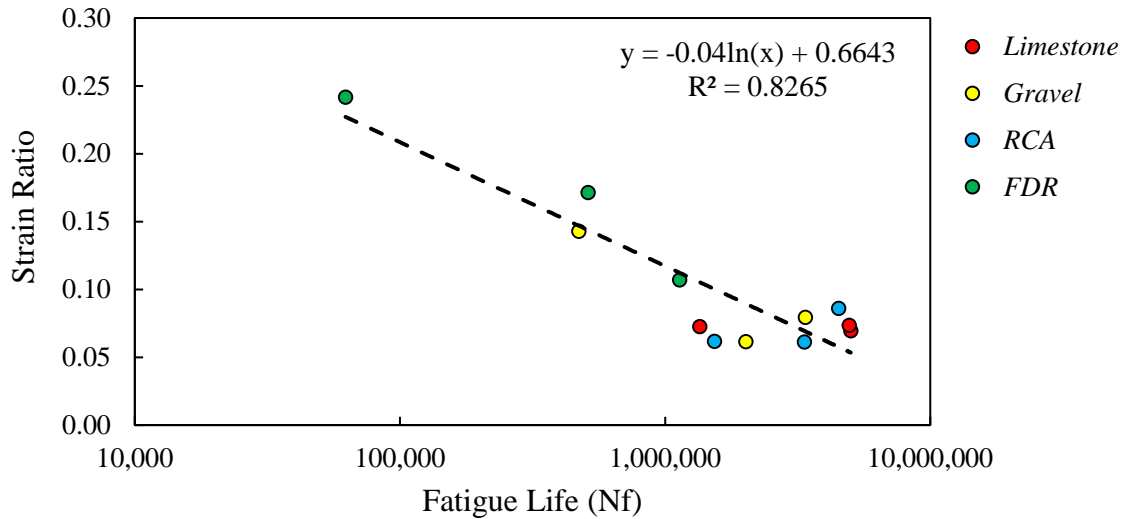


Figure 12-5: Relationship between Number of Load Applications to Failure and Strain Ratio for Cement Stabilized Base Materials in the Laboratory.

Due to the significant influence of the types of materials on the strength properties of the mixes, datasets for different material types were separated and two sets of fatigue performance models were developed for stabilized virgin aggregate materials and stabilized reclaimed systems. As previously stated, two groups of materials, namely crushed limestone aggregates and siliceous gravel as virgin materials and FDR and RCA as reclaimed materials were incorporated in this study. Figure 12-6 shows the fatigue performance model categorized based on the aggregate type. As shown in Figure 12-6, the slope of the best fit lines in the fatigue failure and strain ratio plots are appreciably different for the two groups of materials tested in this study. This underscores the influence of the type of virgin and reclaimed materials to partake in hydration and strength reactions, thus resulting in mixtures with different fatigue performance models.

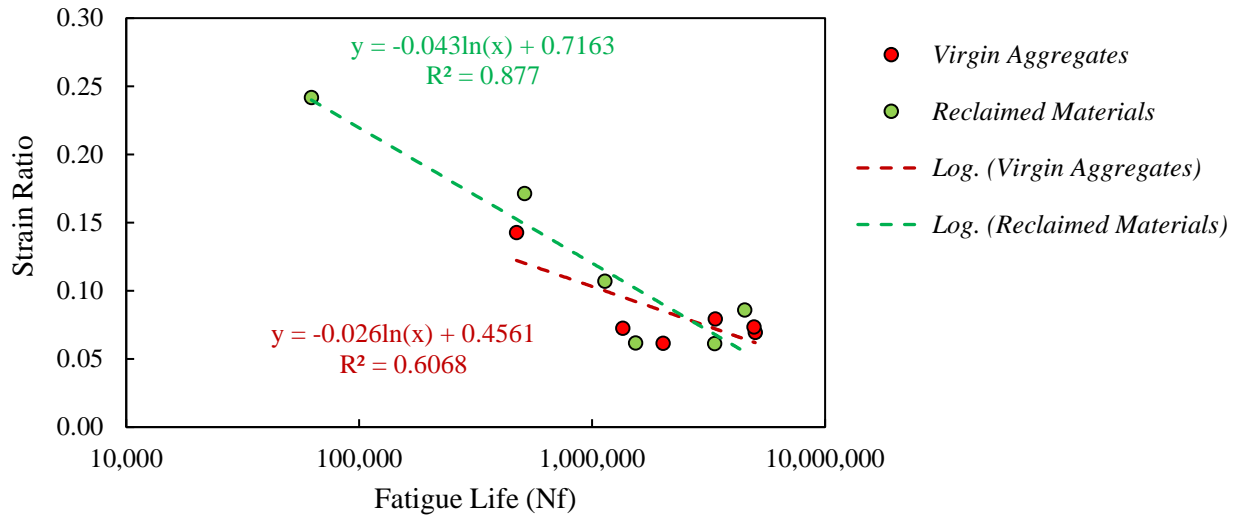


Figure 12-6: Relationship between Number of Load Applications to Failure and Strain Ratio for Stabilized Virgin Aggregates and Reclaimed Materials.

Table 12-1 shows the laboratory regression factors (α_1 and α_2) of the fatigue performance model for virgin aggregates and reclaimed materials.

Table 12-1: Laboratory Regression Factors of Fatigue Performance Models.

Equations	α_1	α_2	R^2
Equation for Virgin Aggregates	0.4561	0.026	0.61
Equation for Reclaimed Materials	0.7163	0.043	0.88

The proposed models have several advantages compared to the previous developed models. The first advantage is associated with incorporation of four aggregate sources in this model. As previously outlined in the Chapter 4, RCA and FDR, crushed limestone aggregates, and siliceous gravel materials were incorporated in this study. Another major advantage of the newly developed model is attributed to the range of the cement contents added to the mixes. As previously stated in the Chapter 4, all four aggregate sources were stabilized with 2% up to 4% cement in this study. Therefore, the models incorporate both lightly stabilized systems as well as rigid aggregate matrices. In addition, lower strain ratios and impact of shrinkage cracking on the cement stabilized layers were considered in the new fatigue performance model to realistically simulate field conditions. In summary, the incorporation of four reclaimed and virgin aggregate sources, the three increment of cement content, and the integration of the shrinkage tests potentially enhanced the generalization of the relationships developed in this study.

12.3.3 Step 3: Field Data Collection

The research team compiled a comprehensive database of section parameters and material properties using NDT equipment, such as FWD and GPR, from this project and previous TxDOT projects. This field database was incorporated in the calibration algorithm of the fatigue performance model. This database contains the location of these pavement sections, thickness, back-calculated FWD modulus, and type of materials for the cement stabilized layers (Figure 12-7). In addition, the field collected data consists of (1) materials properties for stabilized materials such as unconfined compressive strength, maximum dry density, optimum moisture content, (2) layer configurations, layer thickness, and back-calculated FWD modulus for each layer of representative pavement sections.

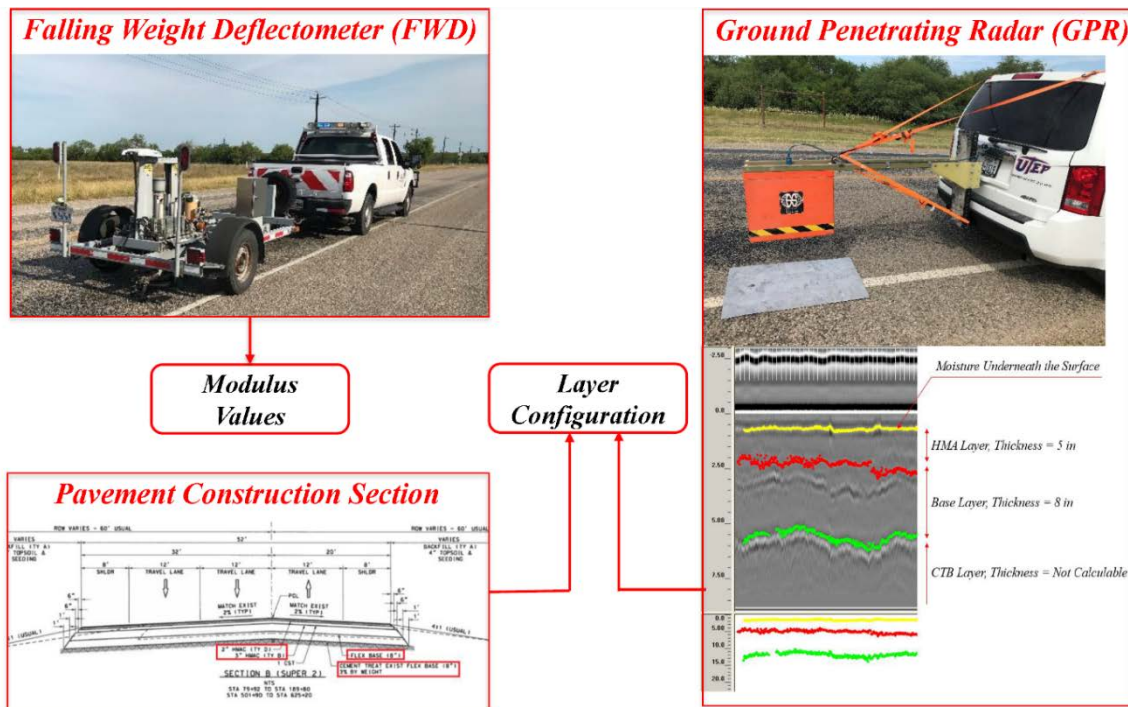


Figure 12-7: Compiling Pavement Section Parameters and Material Properties from NDT (SH-123 – San Antonio).

12.3.4 Step 4: Filed Simulation by Finite Element Method

To simulate the field condition and calculate critical pavement responses, the commercial finite element software ABAQUS was used to model 64 field pavement structures in Texas. Different layers of pavement structure consisting of Asphalt Concrete (AC), Cement Treated Base (CTB), and subgrade (SG) soils were simulated in the finite element program as exhibited in Figure 12-8. Site-specific structural properties of the pavement layers such as the layer thickness, layer configurations and modulus values obtained from GPR and FWD testing were assigned for each representative field roadway section in the FE model. Since entire three dimensional model is symmetric, the research team only simulate a quarter size of the model in the FE program which

leads to optimize the computational efficiency of the finite element analysis. The research team also defined a finer mesh under the wheel path as the most critical response points in the procedure of pavement performance analysis are located in this region. A coarser mesh in region far from loading areas were used to reduce the output file size and expedite the computation time as shown in Figure 12-8.

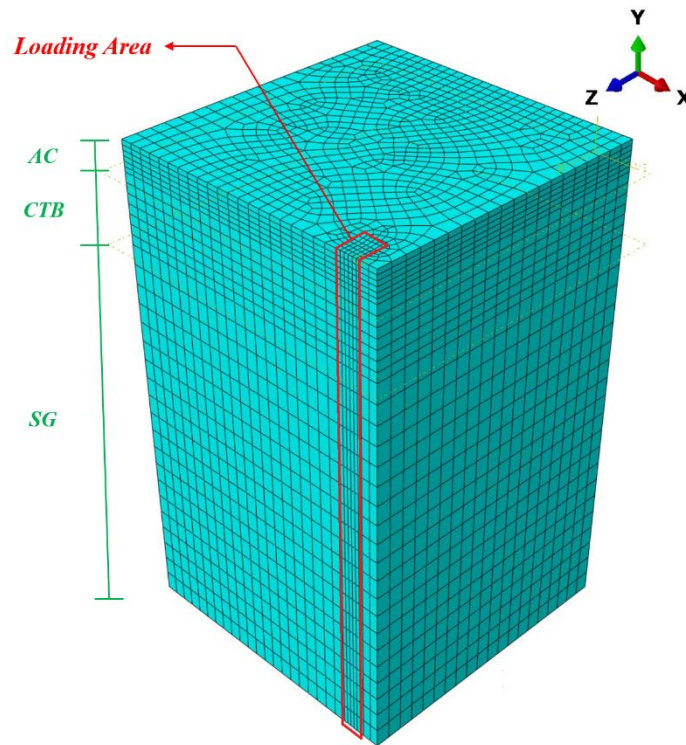


Figure 12-8: Meshing and Pavement Layers Simulations in ABAQUS.

Bottom and lateral boundaries of the FE model were set far enough to minimize the boundary effect. The boundary conditions were appropriately defined in the FE model by constraining the displacement and/or rotation of boundaries to assure a realistic field model. Thus, the research team restrained the displacement and rotation in all direction at the bottom of subgrade layer to simulate bedrock. Moreover, two other boundary conditions were defined in the FE models to restrict the horizontal displacement at the lateral boundaries.

Traffic loads were considered for the simulation of field pavement sections based on most frequent truck classes and tire pressure in Texas as reported in TxDOT project No. 6965 (Table 12-2). According to the average measured values, FE models were developed in this study based on tandem wheel loads with 9.6 kips, a contact area of 42.5 in², a tire pressure of 113 psi, and a wheel spacing of 12 inches. Then, the research team analyzed the pavement structures associated with distinct materials properties and layer configuration for specific sites to obtain the maximum induced tensile strain (ϵ_t) at the cement treated base layer for all pavement sections as depicted in Figure 12-9.

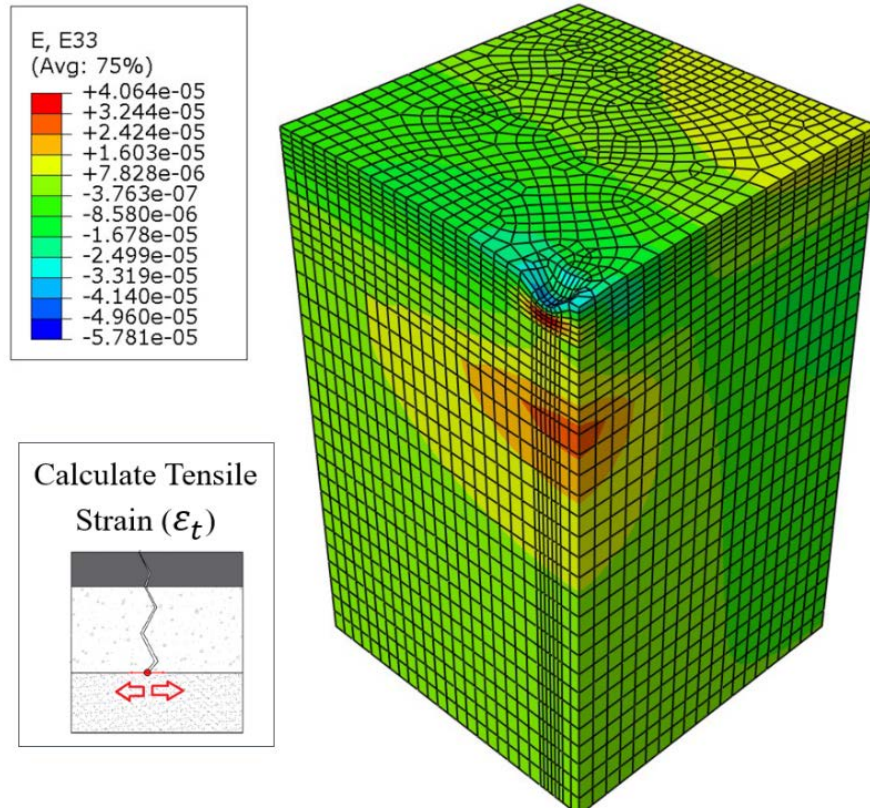


Figure 12-9: Pavement Responses Contours for Horizontal Tensile Strain (ϵ_t).

Table 12-2: Most Frequent Truck Classes and Tire Pressures in Texas (TxDOT 6965)

Most Frequent Traffic Loads	Vehicle Classification	Axle Type	Contact Area (in ²)	Weight per Axle Side (lb.)	Tire Pressure (psi)
	Class 6	Tandem Axle	42.2	9780	116
	Class 9	Tandem Axle	42.8	9440	110
Average			42.5	9610	113

12.3.5 Step 5: Determination of Strain Values in the Field

Because no values for the shrinkage strain of cement stabilized layers were measured in the field, shrinkage values were assumed based on the model developed in this study. As previously outlined in Chapter 5, the shrinkage behavior of stabilized base systems is greatly influenced by the compressive strength and the cement content in the mix. Therefore, mathematical approaches were explored, using regression analysis, to develop robust relationships between shrinkage strain, cement content, and compressive strength. The primary motivation to develop such models was to assist the laboratory mixture design practitioners with a starting point for the reasonable estimate of the shrinkage strain of the materials without the need to incorporate the shrinkage test in the experiment matrix.

Equation 12-6 provide the regression model for the prediction of the shrinkage strain of the stabilized systems.

$$\epsilon_s = 0.000187 + 156.16 \times \frac{C\%^2}{S_C} \quad \text{Equation 12-6}$$

Where: ϵ_s is the shrinkage strain, $C\%$ is the percentage of cement content, and S_C is the unconfined compressive strength (psi).

As shown in Figure 12-10, the prediction model gives a reasonably good estimate of the autogenous shrinkage of stabilized base materials. Moreover, the results show that the difference between the predicted and measured values is not large and that the prediction model properly estimates the relative autogenous shrinkage with an acceptable correlation coefficient ($R=0.85$).

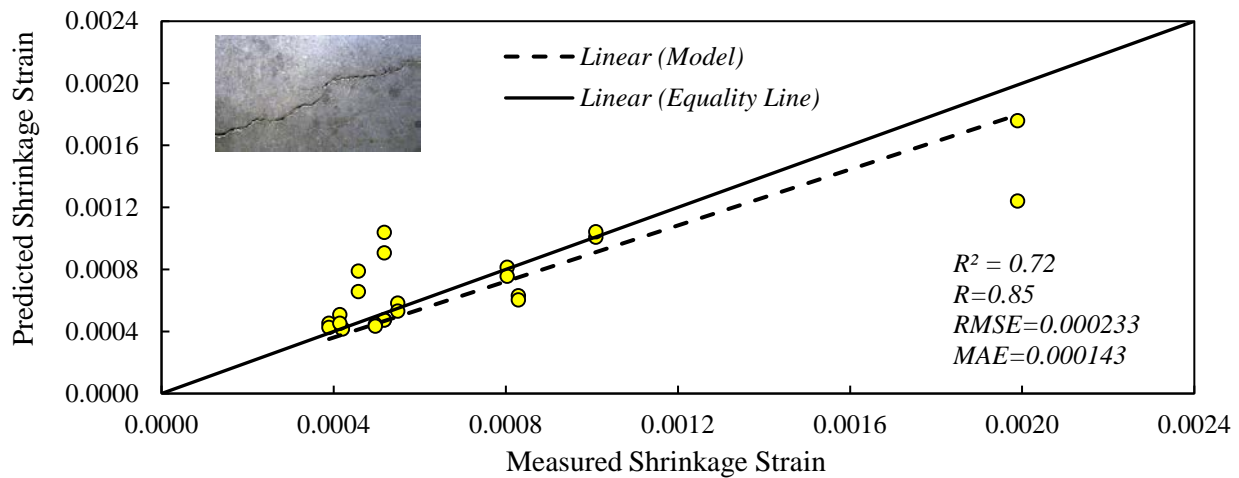


Figure 12-10: Measured Versus Predicted Shrinkage Strain for Cement Stabilized Materials.

Shrinkage strain (ϵ_s) for cement stabilized layers in the field pavement sections were calculated based on the model developed in the laboratory for different reclaimed and virgin aggregates. Then, the maximum horizontal strain (ϵ_h) as the critical pavement response for fatigue performance model was calculated based on the summation of induced tensile strain (ϵ_t) and shrinkage strain (ϵ_s) in order to consider the impact of shrinkage behavior on the cement treated base layers in the field.

Figure 12-11 shows the relationship between tensile strain at failure and tensile strength. As shown in the straight line fitted to the data points, relatively constant values of tensile strain at failure (0.007) are obtained for different types of materials with different stabilizer percentages. For each material, coefficient variation and range of tensile strain at failure was calculated as depicted in Figure 12-12. The plot shows that the average value for the tensile strain at failure for reclaimed materials and virgin aggregate was 0.007 and 0.0072, respectively. The statistical analysis also shows that the failure tensile strain in this study have coefficient of variation lower than 20%. This

coefficient of variation range shows that most of the data are close to the average value and is highly forecastable. Therefore, tensile strain at failure for all pavement section in the field was considered to be 0.007 to determine the strain ratio.

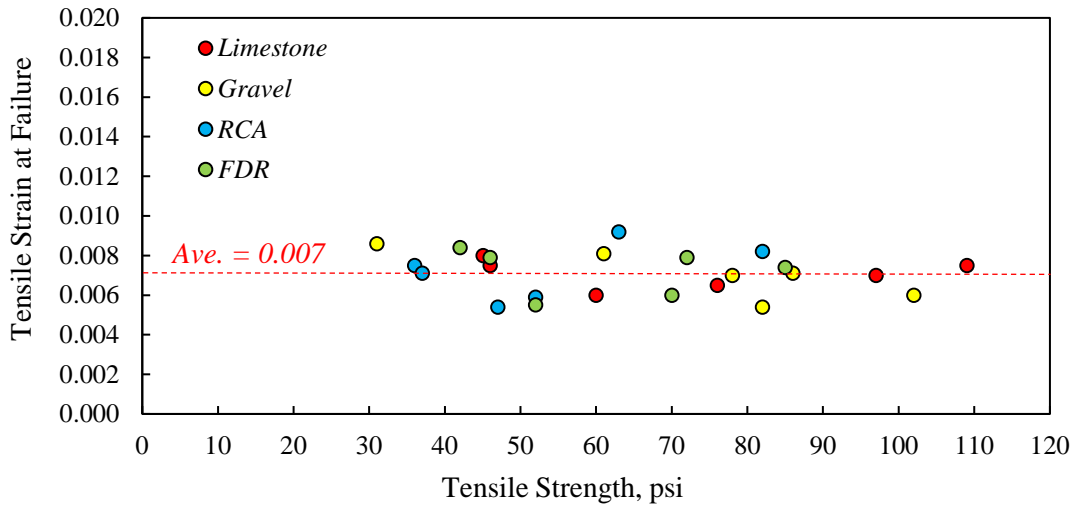


Figure 12-11: Relationship between Tensile Strain at Failure and Tensile Strength.

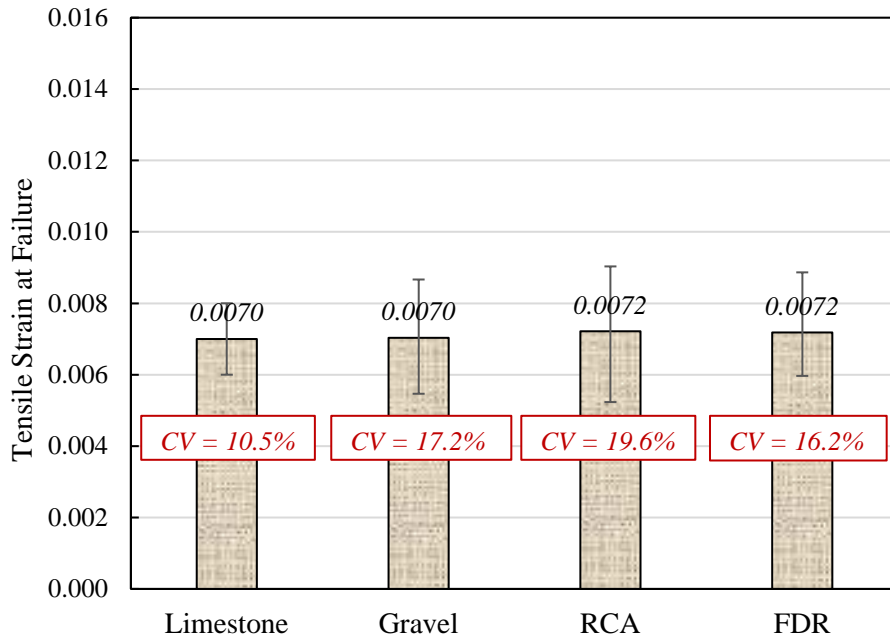


Figure 12-12: Tensile Strain at Failure for Different Cement Stabilized Materials.

Figure 12-13 presents the variation of shrinkage versus time for FDR materials with high subgrade fractions stabilized with 6% cement content. These shrinkage cracking was only observed in the laboratory for the cement stabilized base materials with high level of fine content and cement content. Excessive amounts of stabilizers and fines will result in overly rigid systems that are prone to shrinkage cracking. The plot shows the initiation of cracks in stabilized FDR materials at

shrinkage strain of 0.007. This indicates that cement stabilized materials at tensile strain of 0.007 can potentially failed whether by induced shrinkage or tensile loads.

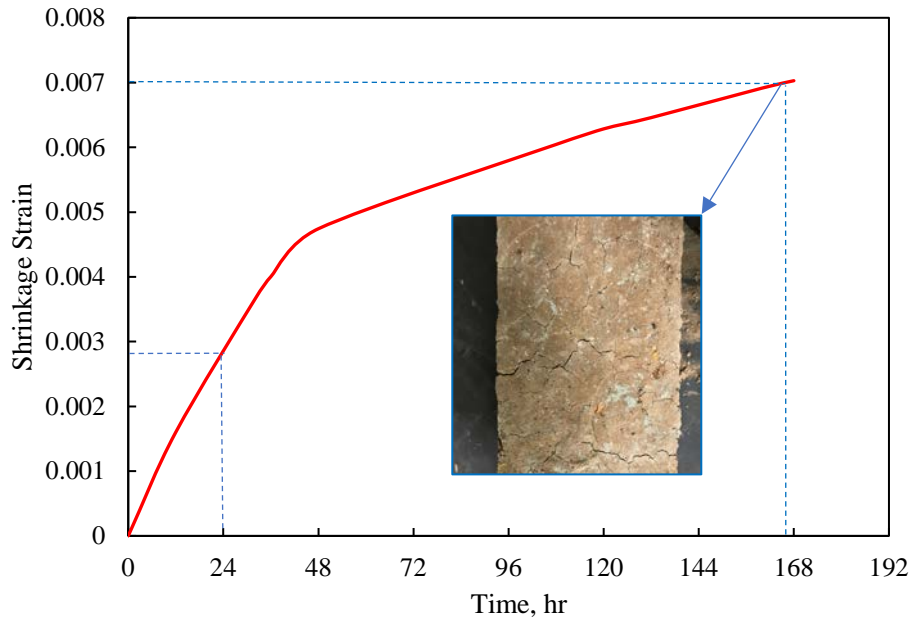


Figure 12-13: Relationship between Shrinkage Strain and Time.

12.3.6 Step 6: Model Calibration

Model calibration was incorporated in this study as a process of adjustment of the model parameters within the margins of the uncertainties to reduce or minimize the total error or difference between measured and predicted distresses. The predicted fatigue performance model for the cement stabilized layers must be compared with the performance of pavement sections in the field. Due to differences in the filed practices and conditions, the fatigue performance model predicted by the laboratory fatigue prediction model may have higher bias and lower precision when compared with the filed measured fatigue performance. As shown in Figure 12-14, through field calibration, the coefficients of these distress prediction models may be adjusted to improve precision of the fatigue performance model. Thus, the fatigue performance model developed in this study was locally calibrated using representative field database of pavement test sites (64 pavement sections) across the Texas.

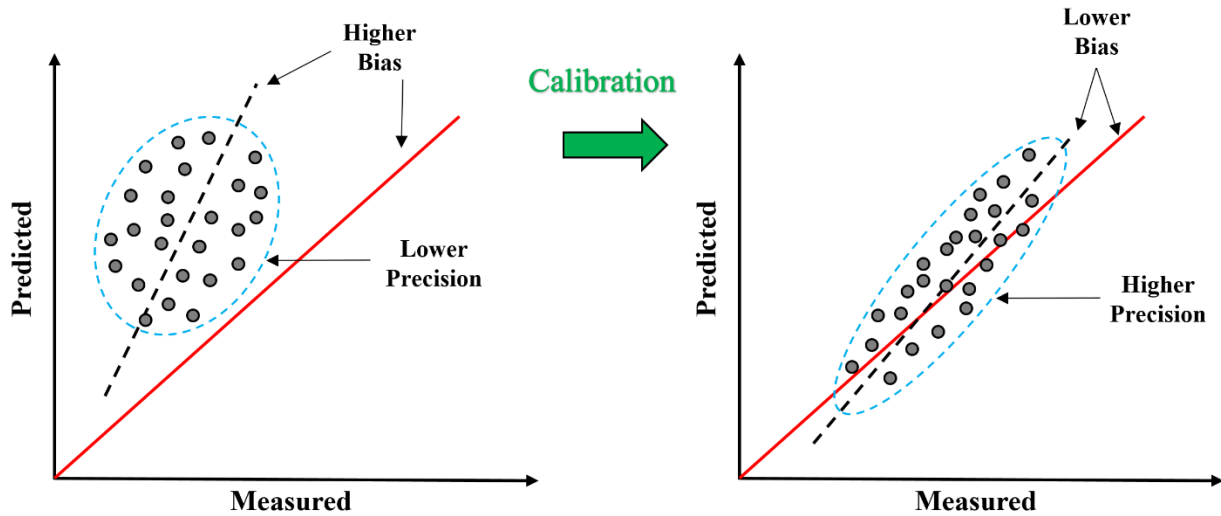
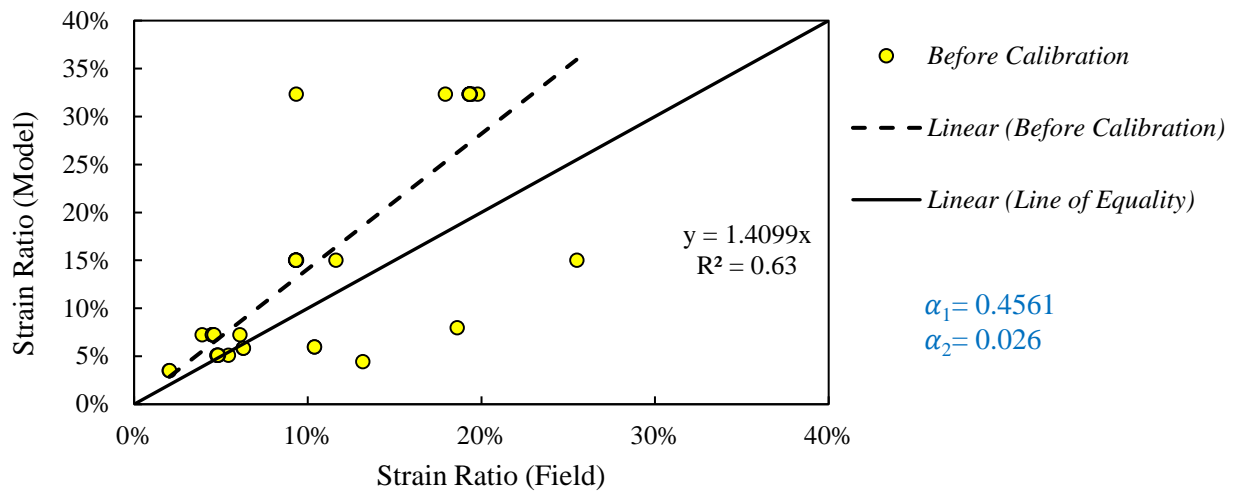
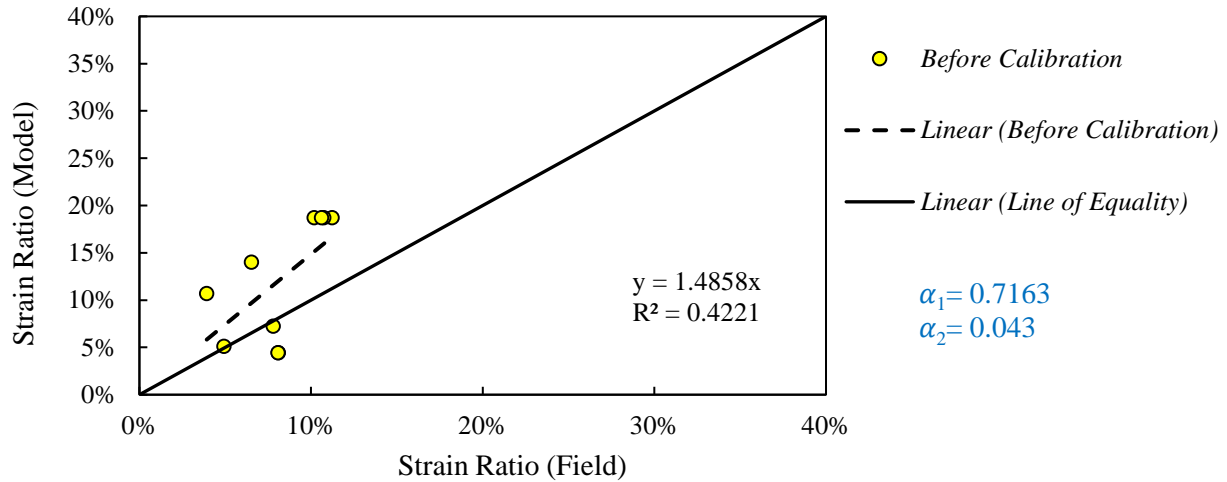


Figure 12-14: Improvement of Bias and Precision through Field Calibration.

After determining the strain ratio for all field pavement sections, field model coefficients (β_1 and β_2) were calibrated to eliminate the bias and reduce the standard error between the predicted and the measured strain ratio. The split-sample approach was used to confirm the accuracy of the prediction models during this calibration effort. Approximately 80% of the sections (51 field pavement sections) were randomly selected for calibration purposes and 20% of the sections (13 field pavement sections) were selected for the validation process. Figure 12-15 compares the predicted strain ratio after considering shrinkage effects in the laboratory with the strain ratio obtained from the 41 and 10 field pavement sections based on the collected field database for the stabilized virgin aggregates and reclaimed materials, respectively.



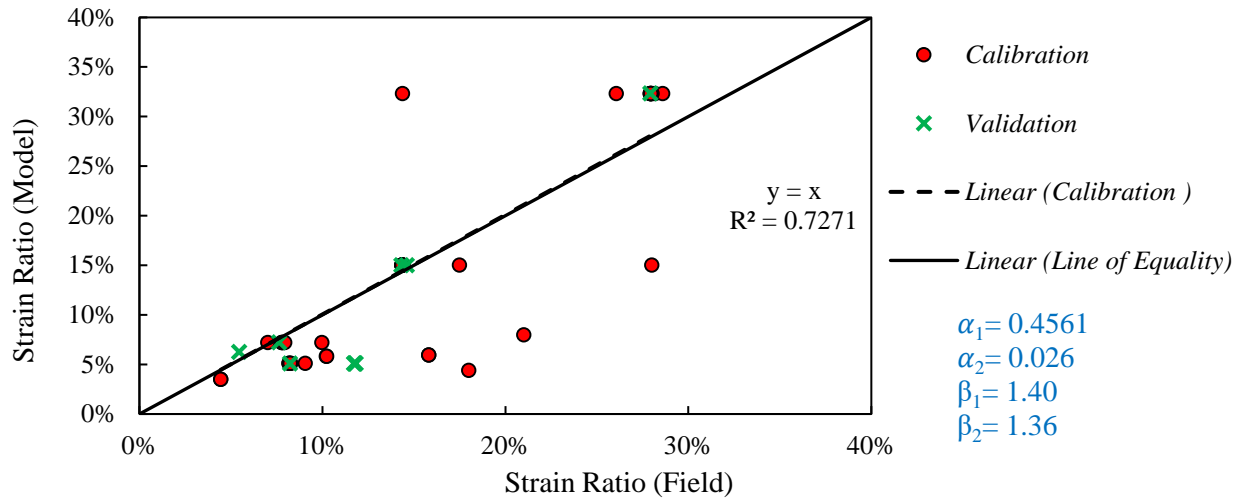
(a)



(b)

Figure 12-15: Predicted (Model) Versus Measured (Field) Strain Ratio before Local Calibration for (a) Stabilized Virgin Base Layers and for (b) Stabilized Reclaimed Base Layers.

The field calibration factors (β_1 and β_2) in the fatigue model were determined by regression analysis. Figure 12-16 shows the predicted and measured strain ratios using the calibration factors for pavement section with stabilized virgin and reclaimed base layers. As observed in the plot, bias was eliminated and the precision was improved for the developed fatigue performance models.



(a)

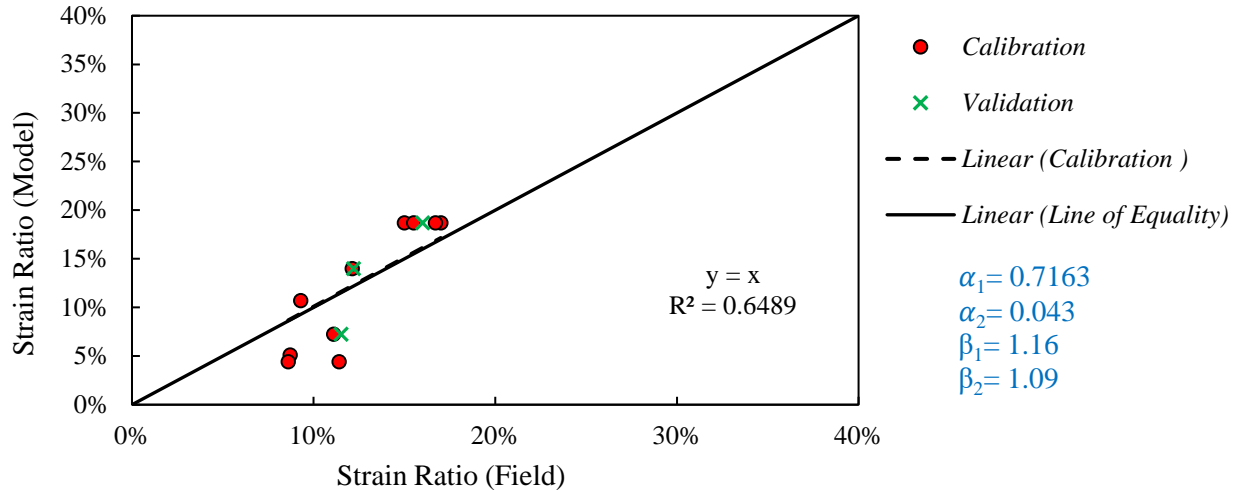


Figure 12-16: Predicted (Model) Versus Measured (Field) Strain Ratio After Local Calibration for (a) Stabilized Virgin Base Layers and for (b) Stabilized Reclaimed Base Layers.

Equation 12-17 provide the calibrated model for the prediction of the fatigue life of the stabilized base layers in pavement foundation. The regression parameters of this model for different stabilized materials are tabulated in Table 12-3. The results show that the difference between the predicted and measured values is not large after calibration and the prediction models properly estimate the fatigue life with acceptable correlation coefficients ($R > 0.80$).

$$\ln(N_f) = \frac{\beta_1 \times \alpha_1 - \frac{\epsilon_h}{\epsilon_{1DT}}}{\beta_2 \times \alpha_2} \quad \text{Equation 12-7}$$

Table 12-3: Local Field Calibration Factors and Laboratory Regression Factors of Fatigue Performance Models

Fatigue Performance Models	α_1	α_2	β_1	β_2	R	R ²
Model for Virgin Aggregates	0.4561	0.026	1.40	1.36	0.85	0.73
Model for Reclaimed Materials	0.7163	0.043	1.16	1.09	0.81	0.65

The field calibrated model was then validated using an independent set of data (20% of the field dataset) to check for the reasonableness of the performance predictions as previously shown in Figure 12-16. The fatigue performance model was successfully validated to the field conditions for pavement design engineers. The bias and precision statistics of the model were similar to those obtained from the calibration when applied to the validation dataset. In other words, the calibrated model produces relatively robust and accurate predictions for field pavement sections.

12.4 Summary of the Major Points

The newly developed model for the fatigue performance of cement stabilized layers has the following advantages compared to the current TxME model:

- Incorporation of different types of cement stabilized materials: (1) Virgin Aggregates, (2) Full Depth Reclamation (FDR), (3) Marginal Aggregates, (4) Reclaimed Materials (RCA).
- Considering the impact of shrinkage cracking in the CTB layer.
- Inclusion of IDT test in the new developed model and removal of the Flexural Beam test due to practical and theoretical challenges.
- Full Calibration of developed model in local and global levels based on 101 pavement sections

Chapter 13. Analysis and Design of Inverted Pavements

The main objective of this chapter is to provide a concise description of the analysis and design of inverted pavement structures based on relevant literature and findings obtained from the assessment of real inverted pavement sections constructed in the United States. This section will focus on inverted pavements' structural characteristics, mechanical behavior, advantages, shortcomings, and field construction techniques required to ensure an adequate performance of inverted structures, also called sandwiched structures. The results of a numerical analysis of an inverted pavement segment constructed in State Highway SH-123 at Corpus Christi, Texas, will also be presented and compared to an existing conventional flexible pavement design at the same highway. An inverted pavement is a structure composed of an asphalt layer placed on top of a well-compacted unbound granular base layer, which lies over a stabilized granular subbase layer that is, typically, cement treated. Since the unbound granular base layer works as a crack-mitigation medium, it contributes to the reduction of reflective cracking that is originated in the stabilized subbase layer. Furthermore, the stiffnesses of both base and subbase layers, lead to a significant reduction in the compressive stresses at the top of the subgrade; thus, subgrade rutting is eliminated. During construction, since the stabilized subbase layer constitutes a robust platform, satisfactory density levels can be reached during the compaction of the unbound granular base layer. Inverted pavements design concept provide a promising alternative with better mechanical performance, longer service life, and reduced life cycle costs in lieu of conventional pavements.

13.1 Inverted Pavement Structure

The typical order of the layers (from the surface down) in a conventional pavement structure consists of an asphalt layer at the surface, followed by a stabilized granular layer, and finally ending with an unbound granular layer at the bottom. These three layers are supported by the subgrade. In an inverted pavement structure, the order of the two layers located below the asphalt layer is switched: the second layer is an unbound flex base while the third layer is stabilized. The unbound granular base layer is sandwiched between the asphalt layer and the cement stabilized granular subbase layer, as shown in Figure 13-1. The thickness of the asphalt concrete layer in an inverted pavement is less than that of a conventional pavement.

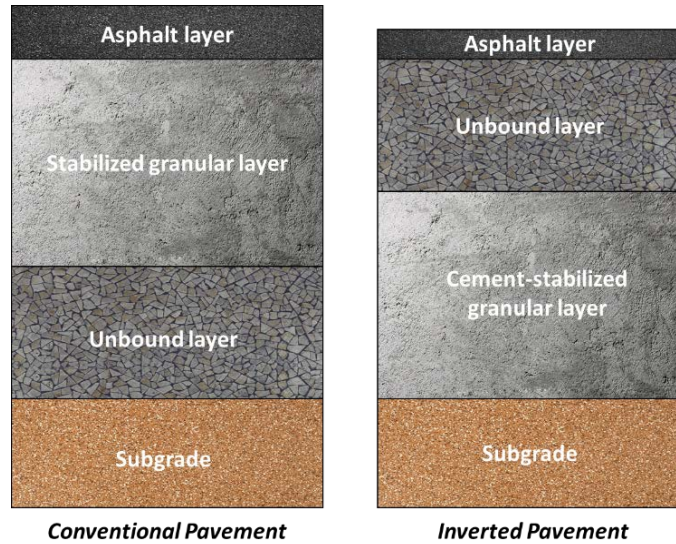


Figure 13-1: Side by Side Comparison of Conventional and Inverted Pavement Structure.

Conventional asphalt pavement designs place stiffer unbound granular layers on top of the subgrade to protect the layer below (Vaughan, 2014; Weingart, 2018). That is the reason why in a conventional pavement design, the stiffness properties of the layers successively increase from the bottom to the top; meaning that the stiffness of the upper layers are greater than that of the lower layers. On the other hand, as it is shown in Figure 13-2, in an inverted pavement, the stiffness of a lower layer, which corresponds to the cement-stabilized granular subbase layer, is greater than that of the upper layers.

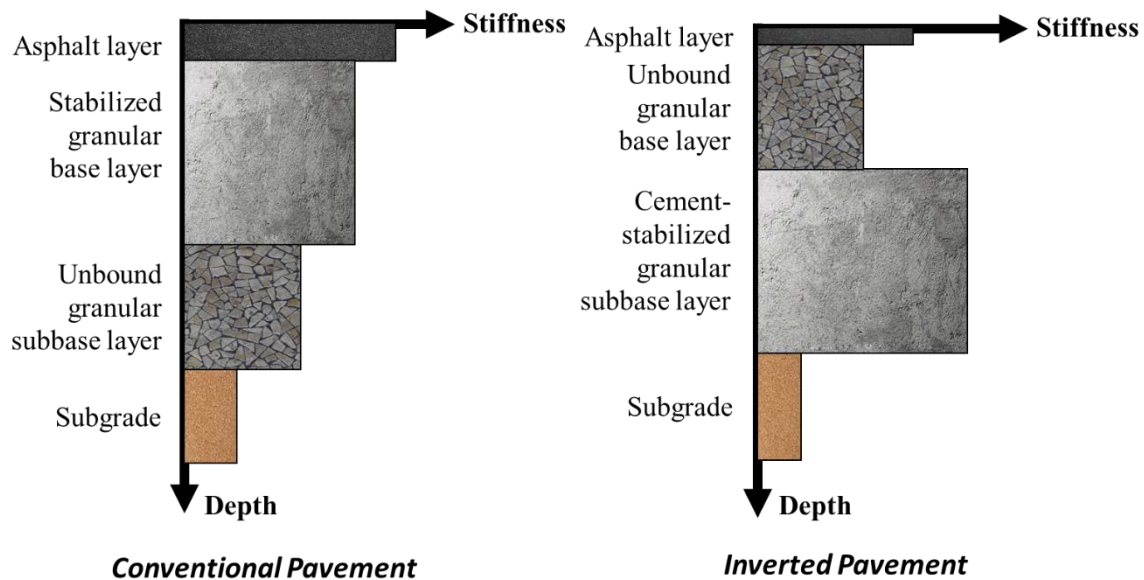


Figure 13-2: Schematic of the Different Stiffness Values per Layer in Conventional and Inverted Pavement Structures. Adapted from Papadopoulos (2014) and Boudreau et al. (2016).

13.2 Mechanical Behavior

The mechanical behavior of any pavement structure is related to the stress dissipation based on the thickness and stiffness of the layers. In conventional asphalt pavement structures, successive stiffer layers are placed from the subgrade up, meaning that the layer with the highest stiffness is placed closest to the surface. Then the stiffnesses of the following layers decrease in a descending order from the top to the bottom. Each of the layers absorbs the load as it is distributed to the subgrade. As shown in Figure 13-2, in inverted pavement designs, the unbound granular base layer, which has the lowest stiffness, is placed between two stiffer layers: the asphalt layer and the cement stabilized granular subbase layer. The distribution of stresses within inverted pavements is significantly different from that of conventional pavements due to the different stiffness values between successive layers (Papadopoulos & Santamarina, 2016).

13.2.1 Unbound Granular Base Layer

The unbound granular base layer is primarily a structural load-carrying component that causes the orthogonal dissipation of the traffic stresses through inter-particle contact (Cortes, 2010; Tutumluer, 2013). This layer leads to a substantial reduction in tensile stresses at the interface between the asphalt layer and the unbound layer, thus significantly reducing the occurrence of reflective cracking. Furthermore, the unbound granular base layer behaves as a crack-arrest medium; therefore, it also contributes to the mitigation of reflective cracking that is initiated in the cement stabilized granular subbase layer and propagated to the surface. The unbound granular base layer is subjected to higher stress states and its stress path presents a pronounced slope.

Also, the unbound granular base layer exhibits a more evident load-induced anisotropy due to the closeness of the unbound granular base layer to the surface where the loads are applied. The shape properties of the aggregates have an influence on the arrangement of the particles and its optimum packing when a granular layer is being compacted. After the compaction of the unbound granular base layer, the maximum dimension of the particles tends to align horizontally (Ashtiani, 2016). Thus, the stiffness of the unbound granular base layer is intrinsically anisotropic and stress dependent in nature (Yimsiri & Soga, 2002; Papadopoulos et al., 2015, Ashtiani, 2016).

13.2.2 Asphalt Concrete Layer

The thin asphalt concrete layer can exhibit thicknesses ranging between 0.5 in and 2 in (De Beer, 2012). With those thicknesses, the asphalt layer deforms as a membrane rather than a beam and its failure mechanism is evidenced through top-down cracking, which is a distresses easy to identify and treat (Lewis, 2012; Papadopoulos, 2017). Nevertheless, higher shear at the load edges is developed at the thin flexible asphalt layers (Papadopoulos & Santamarina, 2014). The asphalt layer provides a smooth ride quality and acts as a water sealer, preventing water from infiltrating into the structure (Jooste & Sampson, 2005). Therefore, the purpose of the thin asphalt concrete layer is mainly to protect the unbound granular base layer from water penetration. Preventive

maintenance activities on the surface layer, such as crack sealings, have to be considered during the life-cycle of the inverted pavement (SARB, 1998).

13.2.3 Cement Stabilized Granular Subbase Layer

The layer with the highest stiffness corresponds to the cement-stabilized granular subbase layer, which causes the upper layers (i.e. asphalt layer and the unbound granular base layer) to perform mostly in compression (Tutumluer, 2013; Boudreau et al., 2016). As a consequence, the development of tensile stresses is mitigated; therefore, reflective cracking is prevented.

Cement-stabilized granular layers that contain crushed stones as aggregates can reach higher levels of stiffness and strength, and lower levels of shrinkage cracking compared to cement-stabilized granular layers composed of natural soils, such as gravel (Barksdale & Todres, 1983). The cement-stabilized granular subbase provides a suitable foundation during compaction and during the service life of the unbound granular base layer (Jooste & Sampson, 2005).

Finally, the combined structural capacity of the unbound granular base layer and the cement stabilized granular subbase layer results in a substantial reduction of the vertical compressive stresses originated at the top of the subgrade, thus preventing pavement failure due to rutting.

13.3 Construction Considerations

During the construction process of an inverted pavement, the compaction of the unbound granular base layer is the most critical step. Proper equipment (e.g. grid rollers, vibratory rollers, pneumatic tire rollers, etc.) must be used to appropriately densify the material. No special equipment is needed for the construction of inverted pavement structures (Cortes & Santamarina, 2013). Only for the unbound granular base layer, additional efforts have to be taken into account to assure the high-density level that is required (Boudreau et al., 2016).

The required density for the unbound granular base layer corresponds to 86% of the apparent specific gravity of the material, which coincide with a density ranging from approximately 100% up to 105% of the maximum dry density obtained with the Modified Proctor test. Only in inverted pavement structures, in which the unbound granular base layer is compacted on top of a cement stabilized subbase, these density levels can be achieved. The unbound granular layer can achieve significantly higher densities compared to an unbound granular layer compacted on top of the subgrade, which is the case of a conventional pavements (Weingart, 2018).

The aggregates used for the construction of the granular layers consist of crushed rocks with non-plastic fine content. Crushed rock aggregates exhibit rough surfaces and angular shapes. The rough surface and the angular shape of crushed stones lead to a better interlocking of the aggregates during compaction; thus, increasing the stability of the unbound granular layer (Cho et al., 2006; Pan et al., 2006; Tutumluer, 2013). The absence of plastic fines is important to prevent degradation of the material due to moisture susceptibility (Ashtiani & Little, 2007).

There are not current gradation specifications, accepted in the United States for unbound base layers in inverted pavement structures. Since inverted designs have been used in South Africa since the 1970s as the main pavement structure for local and highway roads (Buchanan, 2011), South African specifications for the gradation and quality of crushed aggregate materials used in base layers of inverted pavements are going to be used as a reference and compared against TxDOT specifications. South African specifications for the base layer of inverted pavements, called G1 base, are presented in Table 13-1. Two types of G1 base materials are defined based on the nominal maximum size of the aggregate.

Figure 13-3 shows the gradation curves of the South African G1 base designs corresponding to two nominal maximum size values: 37.5 mm and 26.5 mm. These two gradations were compared to the particle size distributions for base layers (Grade 1-2, and 3) indicated in TxDOT Standard Specification, Item 247, for flexible base layers (TxDOT, 2014). As shown in Figure 13-3, South African gradation limits are narrower than TxDOT gradations. South African gradation G1 (NMS of 37.5 mm) falls perfectly within almost all the gradation limit points specified in TxDOT gradation Grade 1-2. Minor differences are found at the beginning of the upper limit points of G1 (NMS of 37.5 mm) and Grade 1-2 gradations. While comparing the gradation G1 (NMS of 37.5 mm) with gradation Grade 3, much more differences in both, lower and upper limit points, can be found. South African gradation G1 (NMS of 26.5 mm) does not fall within any TxDOT gradations.

Table 13-1: Material Requirements for South African G1 Base Layers. Adapted from TRH (1985), Buchanan (2010), Tutumluer (2013), and Boudreau et al. (2016).

Property	G1, 37.5 mm Nominal Maximum Size (NMS)	G1, 26.5 mm Nominal Maximum Size (NMS)
<i>Particle Size Distribution</i>		
<i>Percent Passing</i>		
~1.5 in (37.5 mm)	100	
~1.0 in (26.5 mm)	84-94	100
~¾ in (19.0 mm)	71-84	85-95
~½ in (13.2 mm)	59-75	74-84
#400 (4.75 mm)	36-53	42-60
#100 (2.00 mm)	23-40	27-45
#400 (0.425 mm)	11-24	13-27
#200 (0.075 mm)	4-12	5-12
Liquid Limit	< 25%	
Plasticity Index	< 4	
Linear shrinkage	< 2%	
Flakiness (sphericity)	< 35%	
Density	86% - 88% of apparent solid density	
Aggregate crushing value ^(a)	≤ 29%	
10% fine aggregate crushing value ^(b)	≥ 110 kN	

^(a)The aggregate crushing value can be defined as “the mass of material, expressed as a percentage of the test sample that is crushed finer than a 2.36-mm sieve when a sample of aggregate passing the 13.2-mm and retained on the 9.50-mm sieve is subjected to crushing under a gradually applied compressive load of 400 kN” (Tutumluer, 2013).

^(b)The 10% fine aggregate crushing value can be defined as “the force in kilonewtons required to crush a sample of aggregate passing the 13.2-mm and retained on the 9.5-mm sieve so that 10% of the total test sample will pass a 2.36-mm sieve” (Tutumluer, 2013).

A constant monitoring of the optimum moisture content of the layer during compaction also needs to be taken into consideration to ensure a dense packed arrangement of the material. During the placement and compaction of the base layer, the high stiffness of the cement-stabilized subbase layer, facilitates the achievement of the target density levels. The stabilized subbase layer constitutes a robust platform that allows a better compaction of the base layer that is placed above the subbase. After compaction, a prime coat followed by a hot mix asphalt layer can be placed.

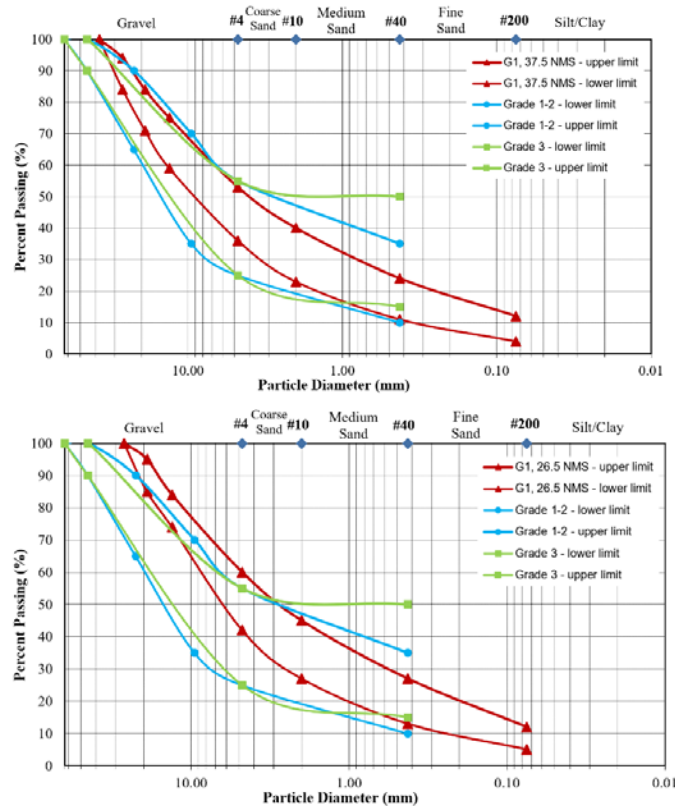


Figure 13-3: Gradation Limits for TxDOT Base Layers and South African G1 Base Layers with 37.5 mm NMS (top) and 26.5 mm NMS (bottom).

13.4 Advantages and Shortcomings

The advantages of using an inverted pavement design are presented as follows:

- In inverted pavement designs, tensile stresses at the interface between the asphalt layer and the unbound base layer are reduced. In addition, the crack-mitigation medium that is created by the unbound granular base, results in a significant reduction of reflective cracks (Titi et al., 2003).
- The varying stiffness of the different layers in an inverted pavement lead to a substantial reduction of compressive stresses originated at the bottom of the subbase layer; therefore, subgrade rutting is eliminated. Since reflective cracking and rutting are reduced significantly in inverted pavement structures, its service life is prolonged (Lewis et al.,

2012).

- During construction, due to the high compaction levels of the robust cement stabilized subbase, the compaction levels of the unbound granular base layer, placed on top of the subbase, are easier to reach (Barksdale & Todres, 1983; Terrel et al., 2003; Tutumluer, 2013). Typical construction processes and common equipment for compaction is needed to successfully achieve the density levels required for the layers (Lewis et al., 2012).
- The asphalt layer thickness in an inverted pavement design is lower compared to the thickness of an asphalt layer for a conventional pavement. Therefore, inverted pavements constitute a sustainable alternative to reduce the use of asphalt concrete during pavement construction (Tutumluer, 2013).

The shortcomings of using an inverted pavement design are presented as follows:

- Since the unbound granular base is the principal structural layer for stress dissipation, it is prone to exhibit permanent deformation, which will result in pavement failure due to rutting. Therefore, appropriate compaction during the construction of the unbound granular base layer is important (Metcalf et al., 1998; Tutumluer, 2013).
- The initial material cost for inverted pavements is not always lower as compared to conventional asphalt pavements (Titi et al., 2003). However, the significant increase in load-bearing capacity, which results in an extension of the inverted pavement's service life, can bring about considerable cost savings over the life-cycle of the pavement (Titi et al., 2003; Buchanan, 2010).
- The use of a cement stabilized subbase in northern climates of the United States represents a potential risk for pavement cracking due to shrinkage and cycles of freezing and thawing. The Portland Cement Association recommends cement contents of 2% to 3% in cement-stabilized granular layers to reduce cracking (Tutumluer, 2013).
- Since the structural behavior of inverted pavements is different compared to conventional pavements' behavior, the structural design of inverted pavement structures cannot be analyzed based on existing design procedures. A mechanistic approach should be used to simulate inverted pavements' performance (Papadopoulos & Santamarina, 2017).

13.5 Numerical Analysis

A numerical analysis was performed using WinJULEA, which is a multi-layer linear elastic software developed by the Engineering Research and Development Center of the United States Army Corps of Engineers. One inverted pavement and two conventional pavements were analyzed with the purpose of comparing the different critical stresses and strains developed in the structures due to variations in the stiffness properties of each particular layered system. One of the conventional pavement structures corresponds to the existing flexible pavement in State Highway SH-123 at Corpus Christi, Texas. The inverted pavement section is also located at State Highway

SH-123 close to Karnes City. The other structure is a simulated conventional pavement, as a hypothetical sections, for comparison purposes. The layers configuration, thicknesses, seasonal Modulus values, and Poisson’s ratios are shown in Table 13-2.

Table 13-2: Pavement Layers Configuration and Material Properties.

Pavement Type	Layer	Thickness (in)	Moduli (psi)		Poisson Ratio
			Summer	Winter	
SH-123 Inverted Pavement	Asphalt Concrete Layer	5	550,000	705,000	0.35
	Unbound Granular Layer	8	40,000	45,000	0.40
	Cement-Stabilized Layer	8	400,000	400,000	0.20
	Subgrade	-	7,000	8,200	0.45
Simulated Conventional Pavement	Asphalt Concrete Layer	5	550,000	705,000	0.35
	Cement-Stabilized Layer	8	400,000	400,000	0.20
	Unbound Granular Layer	8	40,000	45,000	0.40
	Subgrade	-	7,000	8,200	0.45
SH-123 Conventional Pavement	Asphalt Concrete Layer	5.5	550,000	705,000	0.35
	Unbound Granular Layer	15	40,000	45,000	0.40
	Subgrade	-	7,000	8,200	0.45

The layers configuration and thicknesses of the *SH-123 Inverted Pavement* were obtained from the cross-section plan of the structure provided by TxDOT. For the *SH-123 Conventional Pavement*, the configuration of the layers and its thicknesses were obtained from the Technical Report No. FHWA/TX-19/0-6965-1 of the project entitled “Characterization and Quantification of Traffic Load Spectra in Texas Overweight Corridors and Energy Sector Zones” (Ashtiani et al., 2019). As part of that project, Ground Penetrating Radar testing was performed on several pavement segments located at the Permian Basin and the Eagle Ford Shale region in Texas, including State Highway SH-123. The Modulus values for the asphalt concrete layer, unbound granular layer, and subgrade material, considered for the three pavements, were obtained from the same technical report. As part of the project, Modulus values of layers were estimated by conducting Falling Weight Deflectometer testing on certain pavement segments in Texas (including SH-123) during summer and winter. Poisson ratios and the Modulus for the cement-stabilized granular layer were assumed based on research teams’ knowledge.

With respect to the loading conditions, a tridem axle with dual tires was selected for the analysis. The axle characteristics include an axle load of 114,000 lb. and an axle spacing of 50 in. These values were obtained from the Technical Report No. FHWA/TX-19/0-6965-1 (Ashtiani et al, 2019). During that project, as it is shown in Figure 13-4, portable weight-in-motion (WIM) devices were used to collect the traffic data on several pavement segments located at the Permian Basin and the Eagle Ford Shale region in Texas, including State Highway SH-123. Additionally, a critical pressure of 120 psi was considered for each tire according to the same previously mentioned technical report, in which the tire pressure was calculated based on the tire footprint, measured by

using the print of painted tires on papers, and based on direct measurements of axle weights (See Figure 13-5). The value of 120 psi was selected as the most critical condition for the tire pressure and was also validated through a finite element analysis.



Figure 13-4: Portable WIM Equipment Setup for Traffic In-Situ Measurements.



Figure 13-5: Tire Pressure Estimation. A: Painting of Vehicle Tires. B: Print of Painted Tires on Papers. C: Axle Weight Measurements.

Figure 13-6 displays the tire contact areas of the tridem axle over the pavement surface. One set of dual tires at the middle axle (Axle 2) is going to be evaluated. A plan view and a cross-section view of the two contact areas of analysis are highlighted in Figure 13-6. Vertical stresses, tensile strains, and compressive strains are going to be calculated in four points of analysis located between the two tires (point A), on both sides of a tire (points B and D), and at the middle of a tire

(point C). Tensile strains are going to be evaluated at the bottom of the asphalt concrete layer and the vertical stresses as well as the compressive strains are going to be evaluated at the top of the subgrade.

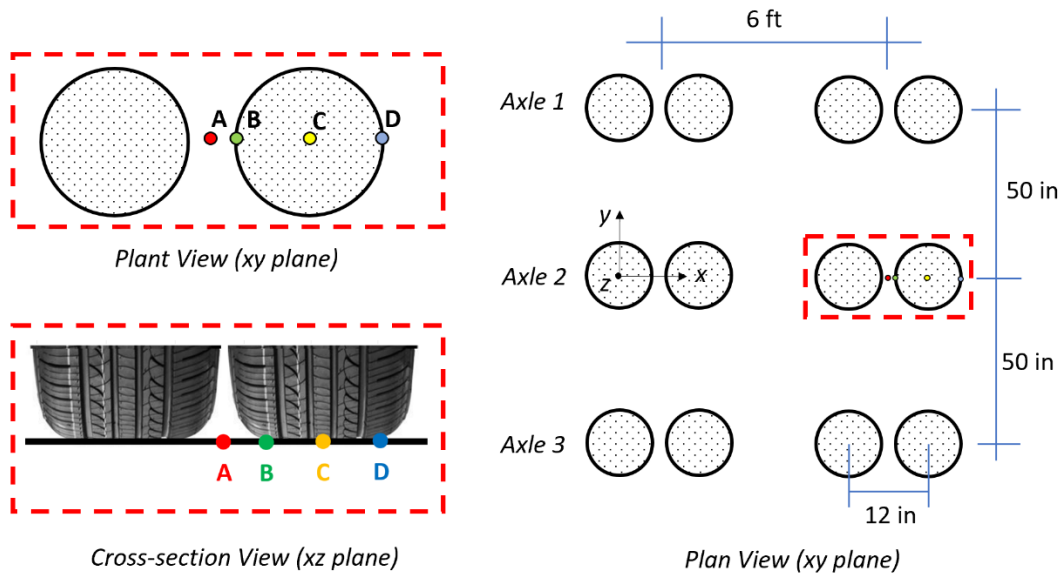


Figure 13-6: Tridem Axle Tire Contact Area of Analysis.

Figure 13-7A shows the tensile strains at the bottom of the asphalt concrete layer in each of the four points of analysis for the three pavement structures during summer and winter season. Strains at points A, B, and D at the *Simulated Conventional Pavement*, act in compression. Only below point C, the strain at the bottom of the asphalt concrete layer in the *Simulated Conventional Pavement*, is in tension. The highest tensile strain values were found below point C, which is located in the middle of the tire. At that critical point, the *Simulated Conventional Pavement* has a tensile strain 97% lower than that of the *SH-123 Inverted Pavement*, meaning that the conventional pavement has a better fatigue cracking performance and should last more longer than the inverted pavement. Comparing the two existing pavements, the *SH-123 Conventional Pavement* has a tensile strain 44% higher than that of the *SH-123 Inverted Pavement*, meaning that the inverted pavement has a better fatigue cracking performance and should last longer than the conventional pavement. As it is shown in Figure 13-7B, different strain values are obtained during the winter season, but similar tendencies as in summer are evidenced. The differences in strains are due to the changes in the Moduli of the layers from summer to winter.

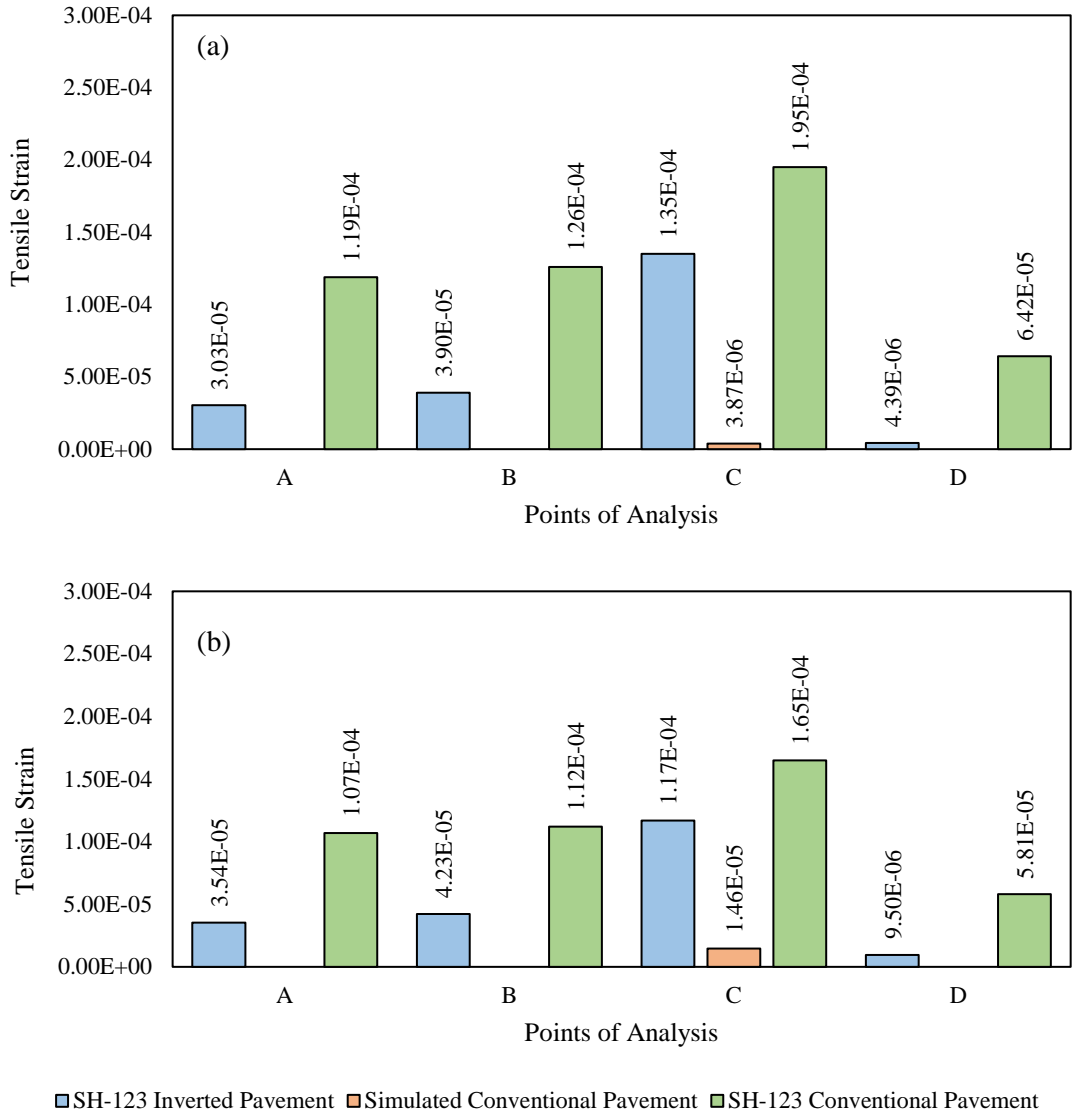


Figure 13-7: Tensile Strains at the Bottom of the Asphalt Concrete Layer for the Three Pavement Structures. (a) Summer Season. (b) Winter Season.

Figure 13-8 shows the compressive strains at the top of the subgrade in each of the four points of analysis for the three pavement structures during summer and winter season. The only point in which the highest strains are simultaneously obtained in all the pavements is point A, which is located between the tires. At that critical point, the *Simulated Conventional Pavement* has a compressive strain 21% higher than that of the *SH-123 Inverted pavement*, meaning that the inverted pavement has a better permanent deformation performance and should last longer than the conventional pavement. Comparing the two existing pavements, the *SH-123 Conventional Pavement* has a compressive strain 90% higher than that of the *SH-123 Inverted Pavement*, meaning that the inverted pavement has a better permanent deformation performance and should last longer than the conventional pavement. As it is shown in Figure 13-8, lower strain values are

obtained during the winter season, but similar tendencies as in summer are evidenced. The differences in strains are due to the increase in the Moduli of the layers in the winter season.

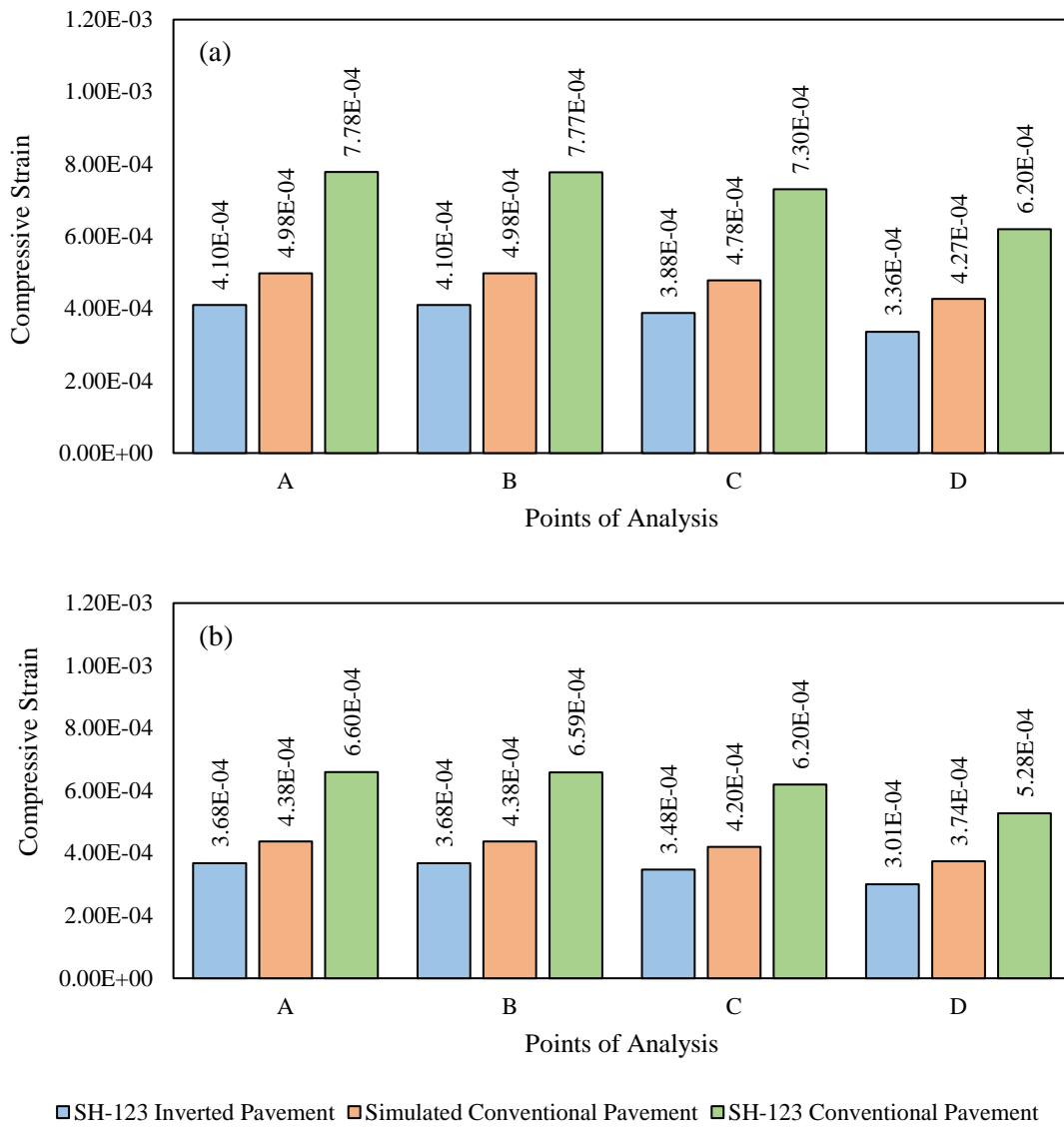


Figure 13-8: Compressive Strains at the Top of the Subgrade for the Three Pavement Structures. (a) Summer Season. (b) Winter Season.

Figure 13-9 shows the vertical stresses at the top of the subgrade in each of the four points of analysis for the three pavement structures during summer and winter season. The only point in which the highest stresses are simultaneously obtained in all the pavements is point A, which is located between the tires. At that critical point, the *Simulated Conventional Pavement* has a compressive stress 3% lower than that of the *SH-123 Inverted Pavement*, meaning that the dissipation of the stresses in the conventional pavement is slightly better. Comparing the existing pavements, the *SH-123 Conventional Pavement* has a vertical stress 41% higher than that of the *SH-123 Inverted Pavement*, meaning that the dissipation of stresses in the inverted pavement is

better. As it is shown in Figure 13-9, different stress values are obtained during the winter season, but similar tendencies as in summer are evidenced. The differences in stresses are due to the changes in the Moduli of the layers from summer to winter.

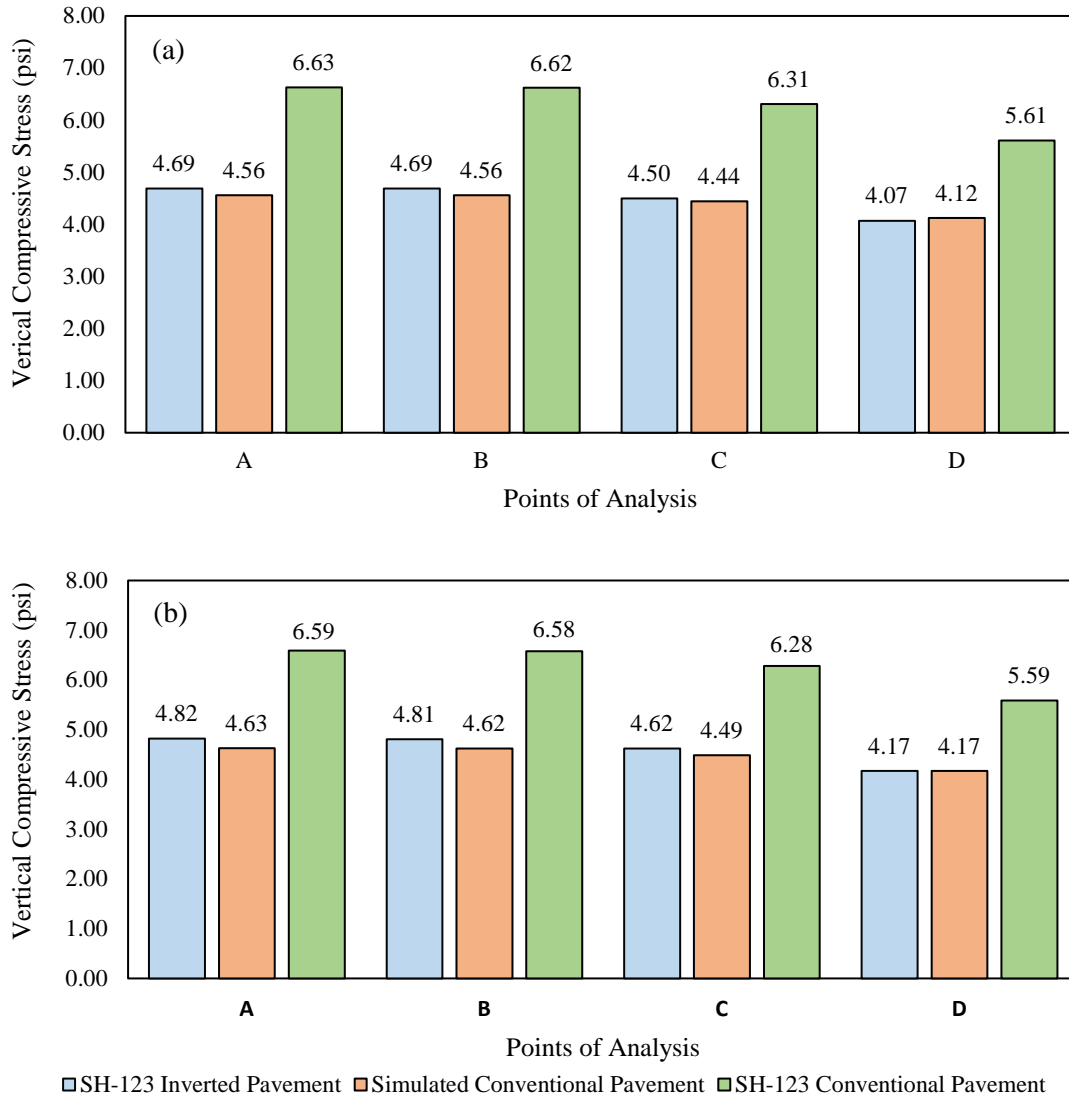


Figure 13-9: Vertical Stresses at the Top of the Subgrade for the Three Pavement Structures. (a) Summer Season. (b) Winter Season.

13.6 Summary of the Major Points

The main objective of this chapter was to provide a succinct description of the design and analysis of inverted pavement structures focusing on the structural characteristics, mechanical behavior, advantages, shortcomings, and field construction techniques required to ensure an adequate performance of the road. The results of a numerical analysis of an inverted pavement section constructed in State Highway SH-123 at Corpus Christi, Texas, will also be presented and

compared to an existing conventional flexible pavement design at the same highway. The major conclusions of this chapter are itemized as follows:

- An inverted pavement is a structure composed of an asphalt layer placed on top of a well-compacted unbound granular base layer, which lies over a stabilized granular subbase layer that is, typically, cement treated. Since the unbound granular base layer works as a crack-mitigation medium, it contributes to the reduction of reflective cracking that is originated in the stabilized subbase layer. Moreover, the stiffnesses of both, base and subbase layers, lead to a significant reduction in the compressive stresses at the top of the subgrade; thus, eliminating subgrade rutting.
- The asphalt concrete layer (that could exhibit thicknesses ranging between 0.5 in and 2 in.) deforms as a membrane rather than a beam and its failure mechanism is evidenced through top-down cracking, which is a distresses easy to identify and treat. The asphalt layer provides a smooth ride quality and acts as a water sealer, avoiding water from penetrating into the structure. Its purpose is mainly to protect the unbound granular base layer from water infiltration.
- The unbound granular base layer is principally a structural load-carrying component that causes the orthogonal dissipation of the traffic stresses through particle to particle contact. This layer leads to a considerable reduction in tensile stresses at the interface between the asphalt layer and the unbound layer, thus significantly reducing the occurrence of reflective cracking. Additionally, the unbound granular base layer behaves as a crack-arrest medium; therefore, it also contributes to the mitigation of reflective cracking that is initiated in the cement stabilized granular subbase layer and propagated to the surface.
- The layer with the highest stiffness corresponds to the cement-stabilized granular subbase layer, which causes the upper layers to perform mostly in compression. As a consequence, the development of tensile stresses is mitigated; therefore, reflective cracking is prevented. The cement-stabilized granular subbase provides a suitable foundation during compaction and during the service life of the unbound granular base layer.
- During the construction process of an inverted pavement, the compaction of the unbound granular base layer is the most critical step. Since the stabilized subbase layer constitutes a robust platform, satisfactory density levels can be reached during the compaction of the unbound granular base layer. Inverted pavements design concept provide a promising alternative with better mechanical performance, longer service life, and reduced life cycle costs in lieu of conventional pavements.
- The mechanical behavior of inverted and conventional pavement structures constructed in segments of SH-123 at Corpus Christi, Texas, were evaluated using a multi-layer linear elastic approach with the purpose of comparing the different critical stresses and strains

developed in the structures due to variations in the stiffness properties of each particular layered system. The conventional pavement exhibited a tensile strain at the bottom of the asphalt concrete layer 44% higher than that of the inverted pavement, meaning that the latter has a better fatigue cracking performance. In addition, the conventional pavement exhibited a compressive strain at the top of the subgrade 90% higher than that of the inverted pavement, meaning that latter has a better permanent deformation performance. Finally, vertical stresses at the top of the subgrade in the conventional pavement were 41% higher than that of the inverted pavement, meaning that the dissipation of stresses in the inverted pavement is better. The superior performance of inverted pavement structures is evidenced from the results obtained from the numerical analysis, in terms of fatigue cracking and permanent deformation.

Chapter 14. Development of Draft Laboratory Test Procedure

This chapter provides details on the improvements to the current laboratory mixture design specification for the cement treated base and subgrade soils. To accomplish this objective, the research team incorporated the recommendations to Tex-120-E soil-cement testing specifications. A comparison table to highlight the departure from the current specification is also provided in this chapter. The main focus of the updates will be on four aspects: (1) specimen preparation, (2) curing, (3) moisture susceptibility tests, and (4) strength testing.

14.1 Comparison Between the Proposed and Current Specification

Specimen preparation includes two parts: the mixing of the materials and the subsequent compaction of the mixture. Current specifications consider the use of dry powder mixing. In the field, adding cement as a dry powder can potentially result in loss of stabilizer due to wind which could result in uneven distribution of cement in the layer. To overcome this issue, the proposed specification recommends adding cement as a slurry to ensure uniform distribution of the cement in the mix. Compaction of the specimens will follow the mixing of aggregates, water, and the treatment agent in the laboratory. Current specifications recommend the impact hammer for compaction, which is a traditionally used method to compact specimens in the laboratory. However, the application of compaction energy in the field differs from the impact hammer in the laboratory (differences include static pressure, vibration, and kneading actions). Thus, the proposed specification recommends the use of the gyratory compactor in lieu of impact hammer due to the superiority of this method to better simulate field compaction and to achieve more uniform void structure as evidenced in the X-ray Computed Tomography (CT) analysis.

The curing procedure for the compacted specimens is the same for both, the proposed and existing specifications. Test specimens are stored in a damp room for seven days (beginning on the day of molding) with porous stones on the top and bottom of the specimens. During curing, specimens must be protected from dripping water and after curing any free water must be removed from the surface of the specimens.

Current TxDOT laboratory testing practices use the tube suction test (TST) to characterize the affinity of unbound and treated aggregate systems to hold and transport moisture. During the TST, the moisture damage mechanism is imparted by capillary action, which does not represent full saturation states due to prolonged flooding scenarios that more frequently affect pavement structures. Therefore, the proposed specification recommends the use of the backpressure saturation test or the submergence test to quantify the loss of strength and degradation of the stiffness properties of the cement treated materials subjected to moisture infiltrations during flooding and heavy rainfall. Both procedures are incorporated in the proposed specification in lieu of the TST test.

Current specifications use the Unconfined Compressive Strength (UCS) as the sole criterion for the mixture design of cement treated materials in the laboratory. However, compressive strength is not the best means to characterize the anticipated primary mode of failure (i.e. cracking) of these materials under repeated loading. In addition to the compressive capacity of the fabricated specimens, tensile behavior of the cement treated materials in the base layers needs to be considered in the new design framework. Therefore, the Indirect Diametrical Tensile (IDT) Strength test was incorporated in the proposed specification along with the UCS test for determining the stabilizer content in cement treated materials.

14.2 Proposed Test Procedure for Cement Treated Materials Testing

The proposed test procedure for cement treated materials testing is presented in the Appendix. The content of the proposed specification has been organized following the same format and structure of existing published TxDOT specifications. Parts of the wording corresponds to current Tex-120-E, except for the updated procedures associated with specimen preparation, moisture susceptibility tests, and strength testing.

14.3 Summary of the Major Points

In this chapter, a draft laboratory test procedure for cement treated base and subgrade materials was proposed. The draft laboratory test procedure was developed based on the existing TxDOT protocol for soil-cement testing known as Tex-120-E. Important modifications were incorporated in the proposed specification with respect to specimen preparation, moisture susceptibility tests, and strength testing. In Table 14-1, the proposed specification is compared against the existing Tex-120-E specification as well as current laboratory and field practices regarding cement treated aggregate systems.

Table 14-1: Comparison of Current and Modified Laboratory Specifications for Mixture Design of Cement Treated Materials.

Criteria	Tex-120-E Current specification	Proposed Modification
Mixing	Dry powder mixing procedure is used to uniformly distribute the cement in the mix. Unfortunately, in the field, dry powder mixing can potentially cause loss of cement due to windy conditions. As a result, cement will be unevenly distributed into the layer.	Slurry mixing procedure is proposed to be used to distribute the cement in the mix. Adding cement as a slurry will result in a uniform distribution of the cement in the mix.
Compaction	The mix is compacted using the impact hammer for providing the compactive effort indicated in Tex-113-E in order to prepare 6-in. diameter by 8-in. height specimens for UCS testing. Nevertheless, the compaction energy applied in the field is different compared to the compaction energy applied in the laboratory. Differences comprise static pressure, vibration, and kneading actions.	The use of the gyratory compactor is proposed in lieu of the impact hammer to elaborate 6-in. diameter by 8-in. height specimens and 4-in. diameter by 4-in. height specimens for UCS and IDT testing, respectively. The gyratory compactor is capable of better simulating field compaction conditions. Additionally, as evidenced in the X-ray Computed Tomography (CT) analysis, a more uniform void structure is achieved with the gyratory compactor as compared to other compaction procedures including the impact hammer.
Curing	Compacted cement treated specimens are stored, with top and bottom porous stones, in a damp room for 7 days (beginning on the day of molding). A pan is placed on top of the upper porous stone to protect the specimen from dripping water. After curing any free water on the surface of the specimens must be removed using a cloth.	
Moisture Damage	The tube suction test (TST) is used to characterize the affinity of cement treated aggregate systems to hold and transport moisture. During the test, the moisture damage mechanism is imparted by capillary action, which does not represent full saturation states due to flooding and heavy rainfall that more frequently affect pavement structures in Texas.	Two moisture susceptibility procedures are proposed in lieu of the TST. The backpressure saturation test and the submergence test are recommended to quantify the loss of strength and degradation of the stiffness properties of the cement treated aggregate systems subjected to moisture infiltrations during prolonged flooding scenarios.
Strength Testing	The unconfined compressive strength (UCS) test is considered as the unique criterion for the mixture design of cement treated aggregate systems. Nevertheless, the UCS test is not the best method for characterizing cracking of cement treated materials subjected to repeated loading.	Both, the compressive and tensile behavior of cement treated materials are taken into consideration. The indirect diametrical tensile (IDT) test is considered in addition to the UCS test to determine the cement content in cement treated aggregate systems.

Chapter 15. Conclusions

This technical report summarizes three years of efforts to improve the current specification for laboratory mixture design of cement treated base and subgrade soils, as well as to develop and calibrate a new generation of fatigue performance models for analysis and design of flexible pavements with cement treated layers. This chapter provides a succinct summary of major tasks and components of the project, rationale for the proposed modifications, and key findings from laboratory testing, field observations, and post process data. The updated laboratory mixture design specification, calibrated fatigue performance model with inclusion of shrinkage properties of the mixes and IDT strength, as well as a series of new materials models for virgin and reclaimed aggregates for incorporation in TxME for Level II analysis, can potentially enhance the collective knowledge of the design of flexible pavements with cement treated foundations.

The research team initially conducted a comprehensive survey to compile current experiences of districts with cement treated base and subgrade soils. The primary motivation was to document the challenges and opportunities of using calcium-based stabilizers, current mixture design practices, strength thresholds, and unique issues such as past experience with using cementitious materials to treat high sulfate soils. This information served as the basis for the selection of the type and sources of virgin aggregate types, gradations, type of subgrade soils and reclaimed materials for inclusion in the experiment matrix. Several aggregate base materials including multiple sources of limestone aggregates, RCA, FDR, and RAP, as well as seven different clay and sandy subgrade soils with unique characteristics were incorporated in this effort to improve the generalization of the models and the framework for the laboratory mixture design of cement treated aggregates and soils. Several increments of treatment agent contents were added to the mixtures to cover a wide spectrum from light stabilization to heavily stabilized systems. The efforts were not limited to the sole use of cement in the mix. The experimental design was extended to include a dual stabilization approach to provide a comparative analysis of using combinations of cement, lime, and type C fly ash as well as polypropylene fibers to better understand the enhancement of adhesive bonds provided by reactions entailing calcium-based stabilizers on one hand, and the binding effect of structural fibers on the other.

Four curing/moisture treatment procedures were incorporated in this study to investigate the influence of moisture ingress on the mechanical performance of stabilized materials. The primary focus was to modify the back-pressure saturation test to simulate prolonged inundation scenarios, and to investigate the relevance of the submergence approach with expedited curing techniques to arrive at a practical laboratory approach for characterization of the moisture susceptibility of cement treated systems. This comprehensive laboratory effort provided the platform to narrow the focus on two alternative protocols to estimate the degradation of load bearing capacity of cement treated layers during flooding and extreme weather events. The moisture susceptibility protocols were incorporated as standalone segments in the updated mixture design specification. Considering the loss of bearing capacity due to moisture susceptibility during the design

characterization stage can particularly serve the coastal districts and areas prone to extended flooding conditions.

More than 3,000 specimens were prepared and subjected to various laboratory tests to characterize the compressive and tensile strength, resilient properties, and permanent deformation potential at different strength ratios for cement treated systems. Approximately 500 nondestructive laboratory tests/measurements such as free-free resonant column and dielectric value tests were conducted prior to performing the mechanical tests. Methylene Blue Value (MBV), pH, and calorimetry tests were performed to characterize the physio-chemical properties of subgrade soils, sulfate content, activity of clays, and moisture adsorption potential of subgrade soils. The index parameters, and materials properties were in turn used to develop a multi-dimensional soil feature database for subsequent development of materials models.

Two sets of material models, one for virgin aggregates and the other for reclaimed materials, were developed in this study to assist pavement design engineers with a starting point for Level II analysis in TxME.

The following section provides key findings and conclusions.

15.1 Key Findings and Conclusions

A summary of key findings and conclusions of the project is provided in the following.

- Current specifications consider unconfined compressive strength as the sole criterion for the mixture design of cement treated materials in the laboratory. However, the compressive strength value provides little insight on the cracking potential of cement treated materials. Based on the laboratory observations and trend analysis of the data, the compressive, tensile, and shrinkage cracking mechanisms of cement treated materials are vastly different. Despite the “presence of a correlation”, prediction of the tensile behavior and shrinkage cracking potential based on compressive testing of 7-day moist cured cylindrical specimen overlooks inherent complexity of cement treated materials. Therefore, in addition to routine compressive strength testing of the specimens, the research team incorporated IDT strength, as well as the retained strength for a harmonized and rapid turnaround mixture design process in the updated specification.
- Based on compressive laboratory testing of virgin and reclaimed materials with different blend ratios, two alternative moisture susceptibility approaches were incorporated in the modified mixture design specification. This will allow for quantifying the degradation of the stiffness properties of the cement treated materials subjected to moisture infiltration during flooding and extreme weather conditions.
- Due to the confinement applied to the cylindrical specimen in the backpressure saturation test, the volumetric analysis confirmed the capability of this approach to simulate near

full saturation states in approximately 7 hours from the onset of the test for base and subbase materials. The degree of saturation of specimens subjected to the submergence protocol were considerably lower than the backpressure saturation counterparts. A plausible explanation could be attributed to the absence of an outside stimuli, such as an all-around cell pressure as in the backpressure saturation test, to expel isolated air pockets in the micro-structure of specimens subjected to the submergence method. However, the ease of use and practicality of the submergence method makes a favorable approach for the determination of retained strength in the absence of backpressure saturation setup.

- The specimens fabricated using the gyratory compactor had higher density compared to specimens prepared using traditional impact hammer and vibratory hammer. A limited number of samples were also compacted with the Texas gyratory compactor for comparison purposes. The micro-structural analysis of specimens using X-ray CT showed the superiority of SuperPave gyratory compactor to minimize variations in the porosity of the specimen in orthogonal directions. The pore-structure analysis showed specimens compacted with the gyratory compactor were substantially more uniform compared to specimens prepared using impact and vibratory hammers. The absence of “lifts” in the gyratory compacted materials were also significant factor in the swelling tests. Based on the one dimensional swell test, and volumetric expansion analysis of the cylindrical specimens, plastic subgrade soils showed layer separation along the cross section of the specimens. The layer separations coincide with the locations of lifts along the height of the sample. The discontinuities imparted by inherent sample preparation using the impact hammer can potentially jeopardize the volumetric swelling results and uplift pressure calculations from routine laboratory tests. Therefore, this research incorporated the gyratory compactor, in lieu of the impact hammer, for specimen preparation in the laboratory.
- Analysis of aggregate breakage revealed that the particle loss and fines generation after gyratory compaction was considerably lower compared to the impact hammer. This was more pronounced for specimens with high RCA content. The disintegration of the concrete particles in the mix and fines generation resulted in an increase in surface area that could potentially change the demand for the binding agent in the mixture. Overlooking the particle crushing potential during the sample preparation phase may result in premature failure of the cement treated pavement foundation.
- Two sources of problematic soils from Bryan and Sierra Blanca were incorporated in the experiment design to investigate the relevance of dual stabilization to mitigate the swelling behavior of high PI high sulfate content soils in presence of calcium-based stabilizers. Multiple combinations of cement and type C fly ash were added to subgrade soils to investigate the role of stabilizers to improve the strength properties and volumetric stability of samples in the laboratory. The post processed laboratory results revealed that replacing a portion of the cement with fly ash is beneficial and improved the

compressive and tensile strength properties of subgrade soils. However, excessive amount of cement-fly ash blend resulted in overly rigid systems that became prone to shrinkage cracking as manifested in COTE tests. The propagation and coalescence of shrinkage cracks can significantly compromise the structural integrity, serviceability, and service life of pavement structures.

- In a separate effort, the combined role of calcium-based stabilizers and polypropylene fibers used to mitigate the swelling behavior of expansive subgrade soils were studied. The cement-fiber variants outperformed cement-fly ash variants in terms of lower expansion and lower swelling pressure. Uniform distribution of fibers under controlled conditions in the laboratory is achievable, however, due to the small amount of fiber in the mixture design, ensuring the uniformity of the fibers during field construction can pose a challenge.
- The analysis of particle geometry revealed that stabilized aggregate systems consisting of more angular and equi-dimensional crushed particles exhibited higher compressive and tensile strength properties as compared to systems having rounded particles. This underscores the significance of particle geometry on the interlocking effect and improvements in orthogonal load bearing capacity of cement treated pavement foundations.
- Parameters pertaining to the uniform distribution of the stabilizer in the mix, such as dry powder mixing compared to slurry mixing, were also analyzed in this study. Based on visual inspection during specimen preparation, slurry mixing provides more uniform coating of the aggregates in lightly cement treated systems. The compressive strength results for dry powder mixing and slurry mixing techniques were comparable, however, the tensile strength for the dry powder mixing was higher compared to the slurry mixing approach. This could be attributed to different failure mechanisms in compression and tension for cement treated materials.
- The multi-dimensional aggregate feature database based on comprehensive laboratory testing was instrumental to develop a series of material models for cement treated base and subgrade soils in this study. Based on observations during this study, improvements in strength and reduction of moisture susceptibility of aggregate systems consisting of reclaimed materials were drastically different from aggregate systems consisting of virgin aggregates. This was more pronounced for FDR materials. The divergence in compressive and tensile strength results for the FDR materials can be attributed to the dilution of the AC and granular base with fine grained subgrade soils in the process of base scarification. Therefore, two sets of materials for virgin and reclaimed materials were developed in this study to improve the accuracy of the predictions. Incorporating different moisture susceptibility tests, the diversity of aggregate sources, as well as the wide range of cement contents were contributing factors to improving the generalization of the developed models. These material models can serve the pavement design

community by providing an estimate of the tensile strength and the resilient modulus of cement stabilized materials for the analysis and design of pavement structures.

- Another focus of the study was to develop and calibrate a new generation of performance models for the estimation of the fatigue performance of cement treated layers. TxDOT in project Tx-06812 developed the modified IDT test to mitigate the systematic errors associated with 3-point bending beam test for lightly stabilized materials. Therefore, the research team adopted the splitting approach in lieu of modulus of rupture for the new generation of the fatigue performance model. Another major improvement to the model was incorporating shrinkage strain, from the COTE test, to account for the cracking potential due to overly rigid cement treated systems. The incorporation of shrinkage cracking potential in cement treated layers in the performance model can potentially mitigate widespread issues with reflective cracking distresses. Subsequent to the selection of the model, 64 pavement sections were used to calibrate the performance model. The traffic characteristics based on the deployment of Portable Weight-in-Motion (P-WIM) in energy corridors by the research team in project Tx-06965 were used in simulations to underscore the significance of the Super Heavy Loads (SHLs) in reduction of pavement service life in pavements with cement treated layers.

References

- A. M. Neville. (1966). "Properties of Concrete." J. Wiley.
- AASHTO. (2008). "Primer on Transportation and Climate Change." American Association of State Highway and Transportation Officials.
- Abdallah, I., Meshkani, A., Yuan, D., and Nazarian, S. (2005). "Design Modulus Values Using Seismic Moduli (SMART User's Manual)." TxDOT Report 0-1780-5, The University of Texas at El Paso.
- Adaska W. S., Luhr D. R. (2004). "Control of Reflective Cracking in Cement Stabilized Pavements. 5th International RILEM Conference." Limoges, France.
- Ahlvin, R. G., Turnbull, W. J., Sale, J. P., and Maxwell, A. A. (1971). "Multiple-Wheel Heavy Gear Load Pavement Tests." U.S. Army Corps of Engineers, Vicksburg, MS.
- American Coal Ash Association. (1990). "Flexible Pavement Manual." Alexandria, Virginia.
- Anderson D.A., LeHir Y.M., Marasteanu M.O., Planche J.P. and Martin D. (2001) "Evaluation of Fatigue Criteria for Asphalt Binders". Journal of Transportation Board (TRB), No. 1766, 2001, p. 48-56.
- Arabali, P., Lee, S. I., Sebesta, S., Sakhaeifar, M. S., and Lytton, R. L. (2018). "Application of Superpave Gyrotory Compactor for Laboratory Compaction of Unbound Granular Materials." International Conference on Transportation and Development (p. 359).
- Arcement, B. J., and Wright, S. G. (2001). "Evaluation of Laboratory Compaction Procedures for Specification of Densities for Compacting Fine Sands." Report No. FHWA/TX-02/1874-1, Federal Highway Administration.
- Arnold, G., and Morkel, C. (2012). "Development of Tensile Fatigue Criteria for Bound Materials." NZ Transport Agency Research Report 463.
- Arteaga, U. B. and Ashtiani, R. S. (2017) "Analysis of Cyclic Behavior of Geomaterials Using Dissipated Energy Concept." International Conference on Highway Pavements and Airfield Technology 2017, Philadelphia, Pennsylvania.
- Arulrajah, A. Mohammadinia, I. Phummiphon, S. Horpibulsuk, and W. Samingthong. (2016) "Stabilization of Recycled Demolition Aggregates by Geopolymers Comprising Calcium Carbide Residue, Fly Ash and Slag Precursors". Construction and Building Materials 114 (2016) 864–873, <http://dx.doi.org/10.1016/j.conbuildmat.2016.03.150>
- Ashtiani R., Abdallah I., Nazarian S. (2014) "Updated Testing Procedures for Long Life Heavy Duty Stabilized Bases: District Survey Results." Texas Department of Transportation Report 0-6812.
- Ashtiani, R. (2016). "Mechanistic-Empirical Design of Inverted Pavements Experience in BullRun Virginia." Presentation, Transportation Research Board (TRB), 95th Annual Meeting, Washington, DC.
- Ashtiani, R. and Little, D.N. (2007). "Acceptability Criteria for High Fines Content Aggregate Pavement Layers." Report No. ICAR/401131, International Center for Aggregate Research, College Station, TX.

- Ashtiani, R. and Rashidi, M. (2018). “Establishing Best Practices for Construction and Design of Cement Treated Materials.” Task 2: Survey of the Districts, Project No. Tx-6949, Texas Department of Transportation.
- Ashtiani, R.S. (2009). “Anisotropic Characterization and Performance Prediction of Chemically and Hydraulically Bounded Pavement Foundations.” Texas A&M University.
- Ashtiani, R.S., Little, D. N., and Masad, E. (2007). “Evaluation of the Impact of Fines on the Performance of Lightly Cement-Stabilized Aggregate Systems.” *Transportation Research Record*, 2026(1), 81-88.
- Ashtiani, R.S., Tarin, J., and Garibay, J. (2016). “Updated Testing Procedures for Long Life Heavy Duty Stabilized Bases.” Report No. TxDOT 0-6812, University of Texas at El Paso’s Center for Transportation Infrastructure Systems.
- Ashtiani, R.S., Little, D. N., and Rashidi, M. (2018). “Neural Network Based Model for Estimation of the Level of Anisotropy of Unbound Aggregate Systems.” *Transportation Geotechnics*, 15, 4-12.
- Ashtiani, R. S., Tarin, J. (2016). “Testing Procedure for Long Life Heavy Duty Stabilized Bases.” TxDOT Project Number 0-6812, FHWA/TX-06/0-5223-2.
- Ashtiani, R.S., Morovatdar, A., Licon, C., Tirado, C., Gonzales, J., and Rocha, S. (2019). “Characterization and Quantification of Traffic Load Spectra in Texas Overweight Corridors and Energy Sector Zones: Final Report.” Report No. FHWA/TX-19/0-6965-1, Texas Department of Transportation (TxDOT), Austin, TX.
- Ashtiani, R.S., Saeed, A. and Hammons, M., (2014) “Mechanistic Characterization and Performance Evaluation of Recycled Aggregate Systems”. *Journal of Materials in Civil Engineering*, 26(1).
- Ashtiani, R.S., Saeed, A. and Hammons, M., (2014). “Mechanistic Characterization and Performance Evaluation of Recycled Aggregate Systems.” *Journal of Materials in Civil Engineering*, Vol. 26, Issue 1.
- ASTM C1435/C1435M-20 (2020). “Standard Practice for Molding Roller-Compacted Concrete in Cylinder Molds Using a Vibrating Hammer.” ASTM International, West Conshohocken, PA.
- ASTM C496/C496M-11 (2004). “Standard Test Method for Splitting Tensile Strength of Cylindrical Concrete Specimens.” ASTM International, West Conshohocken, PA.
- ASTM C78/C78M-18 (2018). “Standard Test Method for Flexural Strength of Concrete (Using Simple Beam with Third-Point Loading)”. ASTM International, West Conshohocken, PA.
- ASTM C832-00 (2015). “Standard Test Method of Measuring Thermal Expansion and Creep of Refractories Under Load.” ASTM International, West Conshohocken, PA.
- ASTM D1635/D1635M-19 (2019). “Standard Test Method for Flexural Strength of Soil-Cement Using Simple Beam with Third-Point Loading.” ASTM International, West Conshohocken, PA.
- Atkinson, J. (2000). “Nonlinear Soil Stiffness in Routine Design.” *Geotechnique*, 50(5), 487-588.

- Australian Road Research Laboratory (1998). "Unpublished Correlations Between Compressive Strength and Modulus." Sydney, New South Wales, Australia, 1998.
- Austrroads. (2008). "Guide to Pavement Technology" Part 2: Pavement Structural Design.
- Avellandeda, D. D. C. (2010). "Inverted Base Pavement Structures." Doctoral Dissertation, School of Civil and Environmental Engineering, Georgia Institute of Technology, Atlanta, GA.
- Ayeldeen, M., and Kitazume, M. (2017). "Using Fiber and Liquid Polymer to Improve the Behavior of Cement-Stabilized Soft Clay." *Geotextiles and Geomembranes*, 45(6), 592-602.
- Barbu, B. G., and Scullion, T., (2006). "Repeatability and Reproducibility Study For Tube Suction Test." Texas Department of Transportation, FHWA/TX-06/5-4114-01-1.
- Barenberg, E. J. (1977). "Evaluating Stabilized Materials." National Cooperative Highway Research Program, Contract No. HR 63-4-1, Unpublished Report, 1977.
- Barker, W. R., Brabston, W. N., and Townsend, F. C. (1973). "An Investigation of the Structural Properties of Stabilized Layers in Flexible Pavement Systems." U.S. Army Corps of Engineers, Vicksburg, MS.
- Barksdale, R. D. and Todres, H. A. (1983). "A Study of Factors Affecting Crushed Stone Base Performance." School of Civil Engineering, Georgia Institute of Technology, Atlanta, GA.
- Barksdale, R.D. (1984). "Performance of Crushed Stone Base Courses." Transportation Research Record 954, Transportation Research Board, National Research Council, Washington, DC.
- Basha, E. A., Hashim, R., Mahmud, H. B., and Muntohar, A. S. (2005). "Stabilization of Residual Soil with Rice Husk Ash and Cement." *Construction and Building Materials*, 19(6), 448-453.
- Beatty, T. L., Danchetz, F. L., Jackson, D. C., Blanck, D. A., Dawood, D. A., Fay, J. M., Ford, R. A., Keough, D. S., Moulthrop, J. S., Rodriguez, L. M., Taylor, G. D., Voth, M. D., and Webb, Z. L. (2002). "Pavement Preservation Technology in France, South Africa, and Australia." Office of International Programs, Federal Highway Administration, U.S. Department of Transportation, and the American Association of State Highway and Transportation Officials, Alexandria, VA.
- Bennert, T., Papp Jr, W. J., Maher, A. and Gucunski, N. (2000). "Utilization of Construction and Demolition Debris Under Traffic-Type Loading in Base and Subbase Applications", *Transportation Research Record*, No. 1714, pp. 33-39
- Bin-Shafique, S., Gupta, S. D., Huang, J., and Rezaeimalek, S. (2017). "The Effect of Fiber Type and Size on the Strength and Ductility of Fly Ash and Fiber Stabilized Fine-Grained Soil Subbase." *Geotechnical Frontiers* 2017 (pp. 19-29).
- Bland, J. M., and Altman, D. G. (1996). "Statistics Notes: Measurement Error." *The Bmj*, 312(7047), 1654.
- Bloom E. F. (2016). "Assessing the Life Cycle Benefits of Recycled Material in Road Construction." Master of Science Thesis, University of Wisconsin–Madison.

- Bloom, E. F., Ponte, K. D., Natarajan, B. M., Ahlman, A. P., Edil, T. B., and Whited, G. (2016). "State DOT Life Cycle Benefits of Recycled Material in Road Construction." *Geo-Chicago 2016* (pp. 693-703).
- Boudreau, R., Vaughan, K., and Frost, D. (2016). "Inverted Pavements." Presentation, Transportation Research Board (TRB) Webinar, TRB Committee on Mineral Aggregates (AFP70).
- Buchanan, S. (2010). "Inverted Pavements-What, Why, and How?" AFTRE Industry Education Webinar, Aggregates Foundation for Technology, Research, and Education, Alexandria, VA.
- Buchanan, S. (2011). "Inverted Pavement Economics." Presentation. Georgia Department of Transportation (GDOT), Georgia, 2011.
- Bull, J. W. (1993). "Life Cycle Costing for Construction." Taylor & Francis, London.
- Burns, S. and Tillman, A. K. (2006). "Evaluation of the Strength of Cement-Treated Aggregate for Pavement Bases." Virginia Transportation Research Council VTRC 06-CR7.
- Button, J. W., Brock, J. D., Collins, R. (2001). "Perpetual Bituminous Pavements, Transportation Research Circular." Number 503, ISSN 0097-8515.
- Cackler, T. (2018). "Recycled Concrete Aggregate Usage in the US. Federal Highway Administration." Report No. DTFH61-12-H-00010, Washington, DC, 2018.
- Carmona, S., (2009). "Effect of Specimen Size and Loading Conditions on Indirect Tensile Test Results." *Materials Construction Journal*, Vol. 59, 294, 7-18, DOI: 10.3989/mc.2009.43307.
- Carpenter, A. C., Gardner, K. H., Fopiano, J., Benson, C. H., and Edil, T. B. (2007). "Life Cycle Based Risk Assessment of Recycled Materials in Roadway Construction." *Waste Management*, 27(10), 1458-1464.
- Carpenter, S. H., K. A. Ghuzlan, and S. Shen. (2003). "Fatigue Endurance Limit for Highway and Airport Pavements." *Transportation Research Record: Journal of the Transportation Research Board*, No. 1832, TRB, Transportation Research Board of the National Academies, Washington, D.C., 2003, pp. 131–138.
- Carpenter, S. H., K. A. Ghuzlan, and S. Shen. (2003). "Fatigue Endurance Limit for Highway and Airport Pavements." *Transportation Research Record: Journal of the Transportation Research Board*, No. 1832, TRB, Transportation Research Board of the National Academies, Washington, D.C., 2003, pp. 131–138.
- Celaya, M., M. Veisi, S. Nazarian, and A. Puppala (2012). "Accelerated Design Process of Lime-Stabilized Clays." *Geo-Frontiers 2011, Advances in Geotechnical Engineering*, GSP 211, [https://doi.org/10.1061/41165\(397\)457](https://doi.org/10.1061/41165(397)457).
- Cheng, M. Y., Prayogo, D., and Wu, Y. W. (2018). "Prediction of Permanent Deformation in Asphalt Pavements Using a novel Symbiotic Organisms Search–Least Squares Support Vector Regression." *Neural Computing and Applications*, 1-13.
- Chesner, W. H., Collins, R. J., and MacKay, M. H. (1998). "User Guidelines for Waste and By-Product Materials in Pavement Construction." Report No. FHWA-RD-97-148.

- Chester, M. V., and Horvath, A. (2009). "Environmental Assessment of Passenger Transportation Should Include Infrastructure and Supply Chains." *Environmental Research Letters*, 4(2), 1–8.
- Cho, G.C., Dodds, J., and Santamarina, J.C. (2006). "Particle Shape Effects on Packing Density, Stiffness, and Strength: Natural and Crushed Sands." *Journal of Geotechnical and Geoenvironmental Engineering*, 132 (5), 591–602.
- Chopra, T., Parida, M., Kwatra, N., and Chopra, P. (2018). "Development of Pavement Distress Deterioration Prediction Models for Urban Road Network Using Genetic Programming." *Advances in Civil Engineering*.
- Climate Discovery Website (2018), <https://climatediscovery.org/how-much-co2-reduction-how-much-does-it-cost-and-whats-it-worth-a-detailedprimer/#:~:text=At%20%2420%20per%20ton%20CO2,with%20emissions%20reductions%20efficiency%20measures.>
- Cokca, E. (2001). "Use of Class C Fly Ashes for the Stabilization of an Expansive Soil." *Journal of Geotechnical and Geoenvironmental Engineering*, 127(7), 568-573.
- Cortes D. D. and Santamarina J. C. (2013). "The LaGrange case History: Inverted Pavement System Characterization and Preliminary Numerical Analyses." *International Journal of Pavement Engineering*, 14:5, 463-471, <https://doi.org/10.1080/10298436.2012.742192>.
- Cortes, D.D. (2010). "Inverted Base Pavement Structures." Doctoral Dissertation, School of Civil and Environmental Engineering, Georgia Institute of Technology, Atlanta, GA.
- Cortes, D.D. and Santamarina, J.C. (2013). "The LaGrange Case History: Inverted Pavement System Characterization and Preliminary Numerical Analyses." *International Journal of Pavement Engineering*, 14 (5), 463–471.
- Cortes, D.D., Shin, H., and Santamarina, J.C. (2012). "Numerical Simulation of Inverted Pavement Systems." *Journal of Transportation Engineering*, 138 (12), 1507–1519.
- Cross, S., Chesner, W., Justus, H., and Kearney, E. (2011). "Life-cycle Environmental Analysis for Evaluation of Pavement Rehabilitation Options." *Transportation Research Record: Journal of the Transportation Research Board*, (2227), 43-52.
- Cusson, D., and Hoogeveen, T. (2006). "Measuring Early-Age Coefficient of Thermal Expansion in High-Performance Concrete." *International RILEM Conference on Volume Changes of Hardening Concrete: Testing and Mitigation* (pp. 321-330).
- De Beer, M. (1985). "Behaviour of Cementitious Subbase Layers in Bitumen Base Road Structures." Masters dissertation, Faculty of Engineering, University of Pretoria, Pretoria.
- De Beer, M. (1990). "Aspects of the Design and Behaviour of Road Structures Incorporating Lightly Cementitious Layers." Ph.D. dissertation, Faculty of Engineering, University of Pretoria, Pretoria
- De Beer, M. (2012). "South African G1 Base Course-Inverted Pavement." 2012 Transportation Research Board Mineral Aggregates Committee (AFP70) Meeting Presentation. 91st Annual Meeting of the Transportation Research Board. Jan. 22–26, 2012, Washington, D.C.

- Dempsey, B.J., and Thompson, M.R. (1973). "Vacuum Saturation Method for Predicting Freeze-Thaw Durability of Stabilized Materials." Transportation Engineering Series No. 6, Illinois Cooperative Highway Research Program Series No. 143. University of Illinois, Urbana Champaign.
- Du, Y., Liu, P., Tian, J., Zhang, J., and Zheng, Y. (2018). "Preliminary Investigation of the Feasibility of Using a Superpave Gyratory Compactor to Design Cement-Treated Aggregate Mixture." *Applied Sciences*, 8(6), 946.
- Eades, J. L., and Grim, R. E. (1966). "A Quick Test to Determine Lime Requirements for Lime Stabilization." *Highway Research Record*, (139).
- FHWA and EPA (1993). "Engineering and Environmental Aspects of Recycling Materials for Highway Construction." Federal Highway Administration and U.S. Environmental Protection Agency, Report No. FHWA-RD-93-008, Washington, DC.
- Ewell, M., (2004). "Mining and Quarrying Trends." USGS Minerals Yearbook. Retrieved April 4, 2006, from <http://minerals.usgs.gov/minerals/pubs/commodity/m&q/index.html>.
- Ferreira, C. (2001) "Gene Expression Programming: A New Adaptive Algorithm for solving Problems." *Complex Systems* 13 (2), 87e129.
- Ferreira, C. (2002). "Gene Expression Programming in Problem Solving." *Soft Computing and Industry*, Springer: Angra do Heroismo, Portugal, pp. 635-653.
- Ferreira, C. (2004). "Gene Expression Programming and the Evolution Of Computer Programs." *Recent Developments in Biologically Inspired Computing*; Springer: Oxford, UK, pp. 82-103.
- Ferreira, C. (2006). "Gene Expression Programming: Mathematical Modeling by an Artificial Intelligence." Springer: Bristol, UK, Volume 21.
- Flintsch, G. W., Diefenderfer, B. K., and Nunez, O. (2008). "Composite pavement systems: Synthesis of design and construction practices." Virginia Transportation Research Council, Report No. FHWA/VTRC 09-CR2, Charlottesville, Virginia.
- Franklin, J. A. and Dussealt M. B. (1989). "Rock Engineering." McGraw-Hill ,USA.
- Gambatese, J. A., and Rajendran, S. (2005). "Sustainable Roadway Construction: Energy Consumption and Material Waste Generation of Roadways." *Construction Research Congress 2005: Broadening Perspectives* (pp. 1-13).
- George, K. P. (2002). "Minimizing Cracking in Cement-treated Materials for Improved Performance." Portland Cement Association.
- Georges, T. (2007). "Falling Weight Deflectometer (FWD) Test Results: Entrance Road of the Lafarge Quarry in Morgan County, GA." Final Report, Georgia Department of Transportation (GDOT).
- Georges, T. (2009). "Falling Weight Deflectometer (FWD) Findings for Tests Conducted on Research Project in LaGrange, GA." Final Report, Georgia Department of Transportation (GDOT), Georgia, 2009.
- Ghuzlan, K. (2001). "Fatigue Damage Analysis in Asphalt Concrete Mixtures Based upon Dissipated Energy Concepts." Ph.D. Thesis, University of Illinois at Urbana–Champaign.

- Ghuzlan, K., and S. H. Carpenter. (2000). "Energy-Derived/Damage-Based Failure Criteria for Fatigue Testing." *Transportation Research Record: Journal of the Transportation Research Board*, No. 1723, TRB, National Research Council, Washington, D.C., 2000, pp. 141–149.
- Ghuzlan, K., and S. H. Carpenter. (2006). "Fatigue Damage Analysis in Asphalt Concrete Mixtures Using the Dissipated Energy Approach." *Canadian Journal of Civil Engineering*, No. 33: 890–901 (2006), DOI:10.1139/L06-032
- Gilazghi, S. T., Huang, J., Rezaeimalek, S., and Bin-Shafique, S. (2016). "Stabilizing Sulfate-Rich High Plasticity Clay with Moisture Activated Polymerization." *Engineering Geology*, 211, 171-178.
- Gnanendran, C. T., and Piratheepan, J. (2009). "Indirect diametrical Tensile Testing with Internal Displacement Measurement and Stiffness Determination." *Geotechnical Testing Journal*, 32(1), 1-10 ISSN 0149-6115.
- Gnanendran, C. T., and Piratheepan, J. (2010) "Determination of Fatigue Life of a Granular Base Material Lightly Stabilized with Slag Lime from Indirect Diametral Tensile Testing." *Journal of Transportation Engineering (ASCE)*, 136(8), 736-745.
- Goldberg, D. E. (1989). "Genetic Algorithms in Search, Optimization and Machine Learning." Addison-Wesley Longman Publishing, Boston, MA.
- Gonzalez, G. P., and Moo-Young, H. K. (2004). "Transportation Applications of Recycled Concrete Aggregate." FHWA State of the Practice National Review.
- Grau, R.W. (1973). "Evaluation of Structural Layers of Flexible Pavements." *Miscellaneous Paper, S-73-26*, Waterways Experiment Station.
- Güllü, H. (2014). "Function Finding Via Genetic Expression Programming for Strength and Elastic Properties of Clay Treated with Bottom Ash." *Engineering Applications of Artificial Intelligence*, 35, 143-157.
- Güneyli, H., and Rüßen, T. (2016). "Effect of Length-To-Diameter Ratio on The Unconfined Compressive Strength of Cohesive Soil Specimens." *Bulletin of Engineering Geology and the Environment*, 75(2), 793-806.
- Guthrie, W. S., Cooley, D. and Eggett, D. L. (2007). "Effects of Reclaimed Asphalt Pavement on Mechanical Properties of Base Materials." *Transportation Research Record*, No. 2006, pp. 44-52
- Guthrie, W. S., P. E. Ellis, and T. Scullion. (2001). "Repeatability and Reliability of the Tube Suction Test." *Transportation Research Board*, 80th Annual Meeting.
- Halsted, G. E., Luhr, D. R., and Adaska, W. S. (2006). "Guide to Cement-Treated Base (CTB)." Portland Cement Association.
- Harris, P., (2002). "Laboratory and Field Procedures for Measuring the Sulfate Content of Texas Soil." *Develop Guidelines and Procedures for Stabilization of Sulfate Soils*, Texas Transportation Institute.
- Hawkins, A.B., (1998). "Aspect of Rock Strength." *Bull. Eng. Geol. Env.* 57:17-30. DOI:10.1007/s100640050017

- Herbert, B. E., and Little, D. N., (2006). "Identification of Potential Risks Due to Sulfate-Induced Damage in Lime-Stabilized Soils Along The SH-130 Corridor."
- Hoek, E., and Brown, E.T. (1980). "Underground Excavation in Rock." Inst. Min. Metall. London: Chapman and Hall.
- Hogan, C. Michael (2010). "Abiotic factor in Encyclopedia of Earth" Monosson and Cleveland (eds.), National Council for Science and the Environment, Washington DC
- Holtz, R. D., and Kovacs, W. D. (2010). "An Introduction to Geotechnical Engineering." Pearson. ISBN 10: 0132496348.
- Horne, D., Belancio, G., Carradine Jr, S. A., Gaj, S., Hallin, J., Jackson, N., Jordan, C., Lucas, D., and Zink, R. (1997). "FHWA Study of South African Pavement and Other Highway Technologies and Practices." International technology FHWA's scanning program.
- Horvath, A. (2003). "A Life-Cycle Analysis Model and Decision-Support Tool for Selecting Recycled Versus Virgin Materials for Highway Applications." Recycled Materials Resource Center, Research Project Report No. 23, University of New Hampshire, Durham.
- Horvath, A. (2004). "PALATE: Pavement Life-Cycle Assessment Tool for Environmental and Economic Effects." Consortium of Green Design and Manufacturing, University of California. Berkeley. <http://www.ce.berkeley.edu/~horvath/palate.html>.
- Hoskins, B.E., McCullough, B.F., and Fowler, D.W. (1991). "The Development of a Long-Range Rehabilitation Plan for US-59, in District 11." Research Report No. 987-1, Center for Transportation Research, The University of Texas at Austin, Austin, TX.
- Hossain, M. S., Nair, H., Ozyildirim, H. C. (2017). "Determination of Mechanical Properties for Cement-Treated Aggregate Base." Virginia Department of Transportation. FHWA/VTRC 17-R21.
- Hosseini M. S., and Kim W. S. (2013). "Estimation of Subgrade Resilient Modulus Using Unconfined Compression Test." Transportation Research Board TRB 2013 Annual Meeting.
- Hudson W. Ronald, and Thomas W. Kennedy, (1968). "An Indirect Tensile Test for Stabilized Materials." The Texas Highway Department, Research Report Number 98-1.
- Hudson, W. R., Little, D. N., Razmi, A. M., Anderson, V., and Weissmann, A. J. (1997). "An Investigation of the Status of By-Product Fines in the United States." University of Texas at Austin, International Center for Aggregates Research.
- Hunter, D. (1988). "Lime-Induced Heave in Sulfate-Bearing Clay Soils." Journal of Geotechnical Engineering, 114(2), 150–167.
- U.S. Census Bureau (2005). "Industry General Summary 2002." 2002 Economic Census Construction Subject Series. U.S. Census Bureau, U.S. Department of Commerce.
- Isola, M., Betti, G., Marradi, A., Tebaldi, G., (2013) "Evaluation of Cement Treated Mixtures with High Percentage of Reclaimed Asphalt Pavement." Construction and Building Materials 48 (2013) 238–247, <http://dx.doi.org/10.1016/j.conbuildmat.2013.06.042>

- John, M. (1972). "The Influence of Length to Diameter Ratio on Rock Properties in Uniaxial Compression: A Contribution to Standardization in Rock Mechanic Testing." Rep S Afr CSIR No ME 1083/5.
- Johnson, V.W. (1960). "Comparative Studies of Combinations of Treated and Untreated Bases and Subbase for Flexible Pavements." Highway Research Board, Bulletin 289, National Research Council, Washington, DC.
- Jones, D., Rahim, A., Saadeh, S., Harvey, J. T. (2010). "Guidelines for the Stabilization of Subgrade Soils in California." University of California Pavement Research Center.
- Jooste, F. and Sampson, L. (2005). "The Economic Benefits of HVS Development Work on G1 Pavements." Gauteng: Lynn East, Department of Public Transport, Roads and Works.
- Kaklis, K. N., S. P. Mavrigiannakis, Z. G. Agioutantis, E. K. Steiakakis, F. K. Stathogianni, (2017). "Experimental Investigation of the Mechanical Properties of Alfas Stone." *Frattura ed Integrità Strutturale*, 40, 18-31; [https://doi: 10.3221/igf-esis.40.02](https://doi.org/10.3221/igf-esis.40.02).
- Katz, A., and Baum, H. (2006). "Effect of High Levels of Fines Content on Concrete Properties." *ACI Materials Journal*, 103(6), 474.
- Kaya, Z., Cetin, A., Cetin, B., and Aydilek, A. H. (2012). "Effect of Compaction Method on Mechanical Behavior of Graded Aggregate Base Materials." *GeoCongress 2012*, American Society of Civil Engineers.
- Kelfkens, R. W. C. (2008). "Vibratory Hammer Compaction of Bitumen Stabilized Materials." Doctoral dissertation, Stellenbosch: Stellenbosch University.
- Kennedy, T. W., and W. R. Hudson. (1973). "Tensile Properties of Subbases for Use in Rigid Pavement Design." Report No. CFHR 3-8-66-98-14F, Texas Highway Department, 1973.
- Kezhen, Y., Yin, H., Liao, H., and Huang, L. (2011). "Prediction of Resilient Modulus of Asphalt Pavement Material Using Support Vector Machine." *Road Pavement and Material Characterization, Modeling, and Maintenance* (pp. 16-23).
- Khalid, A. H. (2000). "A Comparison Between Bending and Diametral Fatigue Test for Bituminous Material." *Materials and Structures* Vol. 33 457-465.
- Khoury, N. N., and Zaman, M. M. (2007). "Environmental Effects on Durability of Aggregates Stabilized with Cementitious Materials." *Journal of Materials in Civil Engineering* (ASCE), 19(1), 41-48.
- Kim, S., Ashtiani, R., Vaughan, D., Islets, J. D. and Beadles, S. (2013). "Use of recycled concrete Materials as Aggregate Base Layer", *Sustainable and Efficient Pavements, Airfield and Highway Pavement*.
- Kim, W., Labuz, J. F. and Dai, S. (2007). "Resilient Modulus of Base Course Containing Recycled Asphalt Pavement", *Transportation Research Record*, No. 2006, pp. 27-35
- Kirk, S. J., and A. Dell'isola. (1995). "Life Cycle Costing for Design Professionals." McGraw-Hill, New York.
- Kuo S. S., Mahgoub, H. S. and Nazef, A. (2002). "Investigation of Recycled Concrete Made with Limestone Aggregate for a Base Course in Flexible Pavement", *Geomaterials*, No. 1787, pp. 99-108

- Kurda, R., de Brito, J., and Silvestre, J. D. (2019). "Concrete with High Volume of Recycled Concrete Aggregates and Fly Ash: Shrinkage Behavior Modeling." *ACI Materials Journal*, 116(1), 83-94.
- Kutay M. E., Arambula, E., Gibson, N., and Youtcheff, J. (2010). "Three-Dimensional Image Processing Methods to Identify and Characterize Aggregates in Compacted Asphalt Mixtures." *International Journal of Pavement Engineering*, 11:6, 511-528.
- Lee, J. C., Edil, T. B., Tinjum, J. M. and Benson, C. H. (2010). "Quantitative Assessment of Environmental and Economic Benefits of Recycled Materials in Highway Construction." *Transportation Research Record: Journal of the Transportation Research Board*, No. 2158, pp. 138–142. <http://dx.doi.org/10.3141/2158-17>.
- Lee, J. C., Edil, T. B., Tinjum, J. M. and Benson, C. H. (2010). "Quantitative Assessment of Environmental and Economic Benefits of Recycled Materials in Highway Construction." *Transportation Research Record: Journal of the Transportation Research Board*, No. 2158, pp. 138–142. <http://dx.doi.org/10.3141/2158-17>.
- Lee, S. I., Sebesta, S., Arabali, P., Lytton, R., and Sakhaeifar, M. (2019). "Application of Superpave Gyrotory Compactors for Flexible Base and Subgrade." Report No. FHWA/TX-17/0-6883-R1.
- Lewis, D.E., Ledford, K., Georges, T., and Jared, D. M. (2012). "Construction and Performance of Inverted Pavements in Georgia." Paper No. 12-1872, Poster Presentation in Session 639, 91st Annual Meeting of the Transportation Research Board, Washington, DC.
- Li, L., Benson, C. H., Edil, T. B., Hatipoglu, B., and Tastan, O. (2007). "Evaluation of Recycled Asphalt Pavement Material Stabilized with Fly Ash." *Soil and Material Inputs for Mechanistic-Empirical Pavement Design*, pp. 1-10.
- Li, W., Lang, L., Lin, Z., Wang, Z., and Zhang, F. (2017). "Characteristics of Dry Shrinkage and Temperature Shrinkage of Cement-Stabilized Steel Slag." *Construction and Building Materials*, 134, 540-548.
- Lim, S., Kestner, D., Zollinger, D. G., and David W., (2001) "Characterization of Crushed Concrete Materials for Paving and Non-Paving Application," Research Report TX-04/7-4954-1, Center for Transportation Research, The University of Texas at Austin, Texas, USA.
- Little, D. N., Godiwalla, A. M., Oshiro, P. Y., Tang, P. S. (2002). "Characterization of Design Properties (Compressive Strength and Resilient Modulus) of Lime, Cement, Fly Ash Stabilized Structural Recycled Concrete Base as a Function of Curing Time." Presented for the Federal Aviation Administration Airport Technology Transfer Conference.
- Little, D. N., Scullion, T., Kota, P., and Bhuiyan, J. (1994). "Identification of the Structural Benefits of Base and Subgrade Stabilization." Report 1287-2, Texas Transportation Institute, Texas A&M Univ., College Station, TX.
- Little, D. N., T. Scullion, P. B. V. S. Kota, and J. Bhuiyan. (1995). "Guidelines for Mixture Design and Thickness Design for Stabilized Bases and Subgrades." Final Report to FHWA/TX-95/1287-3F, Texas Transportation Institute.

- Lu, Y. T., Tan, T. S., and Phoon, K. K. (2012). "Accelerated Testing of Cement Treated Singapore Marine Clay Cured Under Elevated Temperature." *GeoCongress 2012: State of the Art and Practice in Geotechnical Engineering* (pp. 920-929).
- Luo, R., and J. A. Prozzi. (2008). "Development of Longitudinal Cracks on Pavement Over Shrinking Expansive Subgrade." *Transportation Research Board, 2008 Annual Meeting*.
- Tao, M., Mohammad, L.N., Nazzal, M.D., Zhang, Z., and Wu, Z. (2011). "Application of Shakedown Theory in Characterizing Traditional and Recycled Pavement Base Materials." *J. Transp. Eng.*, 136(3): 214-222
- Maalouf, M., Khoury, N., Laguros, J. G., and Kumin, H. (2012). "Support Vector Regression to Predict the Performance of Stabilized Aggregate Bases Subject to Wet-Dry Cycles." *International Journal for Numerical and Analytical Methods in Geomechanics*, 36(6), 675-696.
- Majumder, B. K., Das, A., and Pandey, B. B. (1999). "Cement Treated Marginal Aggregates for Roads." *Journal of Materials in Civil Engineering (ASCE)*, 11(3), 257-265.
- Snyder, M.B. (2016). "Concrete Pavement Recycling." *Pavement Engineering and Research Consultants (PERC), LLC, Engineering Consultant to CP Tech Center, Presentation file*.
- Mazari, M., and Rodriguez, D. D. (2016). "Prediction of Pavement Roughness Using a Hybrid Gene Expression Programming-Neural Network Technique." *Journal of Traffic and Transportation Engineering (English Edition)*, 3(5), 448-455.
- McRae, J.L., and McDaniel, A.R. (1962). "Gyratory Compaction Method for Determining Density Requirements for Subgrade and Base of Flexible Pavements." *Miscellaneous Paper No. 4-494, U.S. Army Engineer Waterways Experiment Station, CE, Vicksburg, Miss.*
- Metcalf, J.M., Romanoschi, S., Yongqi, L., and Rasoulian, M. (1998). "Construction and Comparison of Louisiana's Conventional and Alternative Base Courses under Accelerated Loading." *Interim Report 1, Phase 1, Louisiana Transportation Research Center, Baton Rouge, LA.*
- Miao, Y., Huang, Y., Zhang, Q. and Wang, L. (2016). "Effect of Temperature on Resilient Modulus and Shear Strength of Unbound Granular Materials Containing Fine RAP." *Construction and Building Materials* 124, pp. 1132-1141.
- Midgley, L., and Yeo, R. (2008). "The Development and Evaluation of Protocols for The Laboratory Characterization of Cemented Materials." *Austrroads Technical Report APT-T101-08.*
- Mindess, S., Young, J. F., and Darwin, D. (1981). "Concrete. Englewood Cliffs, NJ: Prentice-Hall.
- Mirabdolazimi, S. M., and Shafabakhsh, G. (2017). "Rutting Depth Prediction of Hot Mix Asphalts Modified with Forta Fiber Using Artificial Neural Networks and Genetic Programming Technique." *Construction and Building Materials*, 148, pp. 666-674.
- Missouri Asphalt Pavement Association (MAPA). "Recycling of Asphalt Pavement." www.moasphalt.org/facts/environmental/recycling.htm. Accessed July 25, 2010.
- Moody, E.D. (1994). "Field Investigations of Selected Strategies to Reduce Reflective Cracking in Asphalt Concrete Overlays Constructed over Existing Jointed Concrete Pavements."

- Transportation Research Record, Journal of the Transportation Research Board, 1449, 209–217.
- Morovatdar, A., Ashtiani, S. R., Licon, C., Tirado, C. (2019). “Development of a Mechanistic Approach to Quantify Pavement Damage using Axle Load Spectra from South Texas Overload Corridors.” Geo-Structural Aspects of Pavements, Railways, and Airfields Conference.
- Morovatdar, A., Ashtiani, S. R., Licon, C., Tirado, C., and Mahmoud, E. (2020). “A Novel Framework for the Quantification of Pavement Damages in the Overload Corridors.” 99th TRB Annual Meeting, Transportation Research Record (TRR): Journal of the Transportation Research Board.
- Narendra, B.S., Sivapullaiah, P.V., Suresh, S., Omkar, S.N., (2006). “Prediction of Unconfined Compressive Strength of Soft Grounds Using Computational Intelligence Techniques: A Comparative Study.” *Comput. Geotech.* 33, pp. 196–208.
- National Academies of Sciences, Engineering, and Medicine. (2009). “Recommended Practice for Stabilization of Sulfate-Rich Subgrade Soils.” Washington, DC: The National Academies Press. <https://doi.org/10.17226/22997>.
- National Oceanic and Atmospheric Administration, (2017). “NOAA Updates Texas Rainfall Frequency Values.” Infrastructure Design and Flood Risk Management <https://www.noaa.gov/media-release/noaa-updates-texas-rainfall-frequency-values>
- National Oceanic and Atmospheric Administration. (2018). “NOAA Updates Texas Rainfall Frequency Values.” U.S. Department of Commerce <https://www.noaa.gov/media-release/noaa-updates-texas-rainfall-frequency-values>
- Nazarian, S., Yuan, D., and Williams, R. R. (2003). “A simple Method for Determining Modulus of Base and Subgrade Materials.” *Resilient Modulus Testing for Pavement Components*, ASTM STP, 1437, 152-164.
- Nazemi, M., and Heidaripناه, A. (2016). “Support Vector Machine to Predict the Indirect Tensile Strength of Foamed Bitumen-Stabilised Base Course Materials.” *Road Materials and Pavement Design*, 17(3), pp. 768-778.
- Neter, J., Kutner, M. H., Nachtsheim, C. J., and Wasserman, W. (1996). “Applied Linear Statistical Models.” Vol. 4, p. 318, Chicago: Irwin.
- Pan, T., Tutumluer, E., and Anochie-Boateng, J. (2006). “Aggregate Morphology Affecting Resilient Behavior of Unbound Granular Materials.” *Transportation Research Record*, 1952 (1), 9.
- Papacostas, A. (2013). “Prediction of Flexural Strength and Breaking Strain of Cemented Materials: Laboratory Study.” *Austrroads Technical Report AP-T251-13*
- Papadopoulos, E. and Santamarina, J.C. (2014). “Optimization of Inverted Base Pavement Designs with Thin Asphalt Surfacing.” *Geo-Congress 2014 Technical Papers*. 2996-3004, American Society of Civil Engineers (ASCE), Atlanta, GA.
- Papadopoulos, E., Cortes, D.D., Santamarina, J.C. (2015) “In-situ Assessment of the Stress-dependent Stiffness of Unbound Aggregate Bases: Application in Inverted Base Pavements.” *International Journal of Pavement Engineering*, Taylor & Francis Group, UK.

- Papadopoulos, E., Santamarina J. C. (2014). "Optimization of Inverted Base Pavement Designs with Thin Asphalt Surfacing." Geo-Congress 2014 Technical Papers, GSP 234.
- Papadopoulos, E.G. (2014). "Performance of Unbound Aggregate Bases and Implications for Inverted Base Pavements." Doctoral Dissertation, Georgia Institute of Technology, Atlanta, GA.
- Papadopoulos, E.G. and Santamaria, J. C. (2017). "Inverted base pavements: construction and performance." *International Journal of Pavement Engineering*, Taylor & Francis.
- Papadopoulos, R. and Santamarina, J.C. (2016). "Analysis of inverted base pavements with thin-asphalt layers." *International Journal of Pavement Engineering*, Vol. 17, No. 7, 590–601, Taylor & Francis Group, UK.
- Park, H. I., Kweon, G. C., and Lee, S. R. (2009). "Prediction of Resilient Modulus of Granular Subgrade Soils and Subbase Materials Using Artificial Neural Network." *Road Materials and Pavement Design*, 10(3), 647-665.
- Paul, D. K., and Gnanendran, C. T. (2012) "Characterization of Lightly Stabilized Granular Base Materials by Flexural Beam Testing and Effects of Loading Rate." *Geotechnical Testing Journal*, Vol. 35, No. 5.
- Ping, W. V., Xing, G., Leonard, M., and Yang, Z. (2003). "Evaluation of Laboratory Compaction Techniques for Simulating Field Soil Compaction (Phase II)." Report No. FL/DOT/RMC/BB-890 (F).
- Ponte, K. D., Madras Natarajan, B., Ahlman, A. P., Baker, A., Elliott, E., and Edil, T.B. (2017). "Life-Cycle Benefits of Recycled Material in Highway Construction." *Transportation Research Record: Journal of the Transportation Research Board*, No. 2628, pp. 1–11. <http://dx.doi.org/10.3141/2628-01>.
- Pronk, A.C., and Hopman, P.C. (1991). "Energy Dissipation: The Leading Factor of Fatigue." *Highway Research: Sharing the Benefits* (J. Porter, ed.), T. Telford, London.
- Prusinski, J. R., and Bhattacharja, S. (1999). "Effectiveness of Portland Cement and Lime in Stabilizing Clay Soils." *Transportation Research Record*, 1652(1), pp. 215-227.
- Punthutaecha, K., Puppala, A. J., Vanapalli, S. K., and Inyang, H. (2006). "Volume Change Behaviors of Expansive Soils Stabilized with Recycled Ashes and Fibers." *Journal of materials in Civil Engineering*, 18(2), pp. 295-306.
- Puppala, A. J., Hoyos, L. R., and Potturi, A. K. (2011). "Resilient Moduli Response of Moderately Cement-Treated Reclaimed Asphalt Pavement Aggregates." *Journal of Materials in Civil Engineering (ASCE)*, 23(7), pp. 990-998.
- Puppala, A., and Musenda, C. (2000). "Effects of Fiber Reinforcement on Strength and Volume Change in Expansive Soils." *Transportation Research Record: Journal of the Transportation Research Board*, (1736), 134-140.
- Puppala, J., Hoyos, L. R., and Potturi, A. K. (2011) "Resilient Moduli Response of Moderately Cement-Treated Reclaimed Asphalt Pavement Aggregates." *Journal of Materials in Civil Engineering*, Vol. 23, No. 7, July 1

- Rao, S. M., and Shivananda, P. (2005). "Role of Curing Temperature in Progress of Lime-Soil Reactions." *Geotechnical & Geological Engineering*, 23(1), 79.
- Rashidi, M. And Ashtiani, S. R. (2018). "Characterization of the Moisture Susceptibility of Cement-Stabilized Base Materials Using the Tube Suction Test." ASCE's International Conference on Transportation & Development.
- Rashidi, M., and Ashtiani, R. S. (2018). "Performance Evaluation of the Cement Stabilized Reclaimed Materials for Use in Pavement Foundations." International Conference on Transportation and Development (p. 140).
- Rashidi, M., and Ashtiani, R. S. (2018). "Characterization of the Moisture Susceptibility of Cement-Stabilized Base Materials Using the Tube Suction Test." International Conference on Transportation and Development 2018: Airfield and Highway Pavements (pp. 153-164). Reston, VA: American Society of Civil Engineers.
- Rashidi, M., Ashtiani, R. S., Si, J., Izzo, R. P., & McDaniel, M. (2018). "A Practical Approach for the Estimation of Strength and Resilient Properties of Cementitious Materials." *Transportation Research Record*, 2672(52), pp. 152-163.
- Rashidi, M., Saghafi, M., and Takhtfiroozeh, H. (2018). "Genetic Programming Model for Estimation of Settlement in Earth Dams." *International Journal of Geotechnical Engineering*, pp. 1-10.
- Rasoulilian, M. (2004). "Stone Interlayer Pavements (Inverted Pavements)." Presentation, Louisiana Pavement Conference, Baton Rouge, LA.
- Rasoulilian, M., Becnel, B., and Keel, G. (2000). "Stone Interlayer Pavement Design." *Transportation Research Record 1709*, Transportation Research Board, National Research Council, Washington, DC.
- Robinette, C., and Epps J. (2010). "Energy, Emissions, Material Conservation, and Prices Associated with Construction, Rehabilitation, and Material Alternatives for Flexible Pavement." *Transportation Research Record: Journal of the Transportation Research Board*, No. 2179, pp. 10–22. <http://dx.doi.org/10.3141/2179-02>
- Rocco, C., Guinea, G.V., Planas, J., and Elices, M. (1999). "Size Effect and Boundary Conditions in the Brazilian Test: Experimental Verification." *Materials and Structures*, Vol. 32, pp. 210-217.
- Rowe, G.M. (1994). "Performance of Asphalt Mixtures in the Trapezoidal Fatigue Test." *Association of Asphalt Paving Technologists*, Vol. 62, 1993, pp. 344–384. *Fatigue Response of Asphalt-Aggregate Mixes. SHRP A-404. Strategic Highway Research Program*, TRB, National Research Council, Washington, D.C.
- Mindess, S., and Young, J.F. (1981) "Concrete." Prentice-Hall.
- Sadati, S., da Silva, L.E.B., Wunsch, I.I., Donald, C., and Khayat, K.H. (2019). "Artificial Intelligence to Investigate Modulus of Elasticity of Recycled Aggregate Concrete." *ACI Materials Journal*, 116 (1).
- Sadrossadat, E., Heidaripناه, A., and Osouli, S. (2016). "Prediction of the Resilient Modulus of Flexible Pavement Subgrade Soils Using Adaptive Neuro-Fuzzy Inference Systems." *Construction and Building Materials*, 123, 235-247.

- Santhanam, M., Cohen, M. D., and Olek, J. (2002). "Mechanism of Sulfate Attack: A Fresh Look.", Part 1: Summary of experimental results, *Cement and Concrete Research*, 32(6), 915-921.
- Scullion, T., and T. Saarenketo. (1997). "Using Suction and Dielectric Measurements as Performance Indicators for Aggregate Base Materials." *Transportation Research Record* 1577, TRB, National Research Council, Washington, D.C., pp. 37– 44.
- Scullion, T., S. Guthrie, and S. Sebesta. (2003). "Field Performance and Design Recommendations for Full Depth Recycling in Texas." Report No. FHWA/TX-03/4182-1, Texas Department of Transportation.
- Scullion, T., Sebesta, S., Estakhri, C., Harris, P., Shon, C., Harvey O., and Rose-Harvey, K. (2012) "Full-Depth Reclamation: New Test Procedures and Recommended Updates to Specifications." Texas Transportation Institute FHWA/TX-11/0-6271-2.
- Scullion, T., Sebesta, S., Estakhri, C., Harris, P., Shon, C., Harvey O., and Rose-Harvey, K. (2012). "Full-Depth Reclamation: New Test Procedures and Recommended Updates to Specifications." Texas Transportation Institute, Report No. FHWA/TX-11/0-6271-2.
- Sebesta, S., and Scullion, S. (2004). "Effectiveness of Minimizing Reflective Cracking in Cement-Treated Bases by Microcracking." Texas Department of Transportation, Report No. FHWA/TX-05/0-4502-1
- Sebesta, S., Liu, W., and Harris, P. (2009). "Improving Lab Compaction Specifications for Flexible Bases within the Texas DOT." Publication FHWA/TX-09/0-5135-3, Texas Department of Transportation, Austin, TX.
- Shen, S., and S. H. Carpenter. (2005). "Application of the Dissipated Energy Concept in Fatigue Endurance Limit Testing." *Transportation Research Record: Journal of the Transportation Research Board*, No. 1929, TRB, National Research Council, Washington, D.C., pp. 165– 173.
- Shen, S., and S. H. Carpenter. (2007). "Dissipated Energy Concepts for HMA Performance." Federal Aviation Administration, Technical Report of Research, COE Report No. 29
- Shen, S., Gordon D. Airey, Carpenter, S.H., and Huang, H. (2006). "A Dissipated Energy Approach to Fatigue Evaluation." *Road Materials and Pavement Design*, 7:1, 47-69, DOI: 10.1080/14680629.2006.9690026
- Si, Z. (2008). "Forensic Investigation of Pavement Premature Failure due to Soil Sulfate-Induced Heave." *Journal of Geotechnical and Geoenvironmental Engineering*, Vol. 134, No. 8. DOI: 10.1061/(ASCE)1090-0241(2008)134:8(1201).
- Si, Z., and Herrera, C.H. (2007). "Laboratory and Field Evaluation of Base Stabilization Using Cement Kiln Dust." *Transportation Research Record*, 1989(1), 42-49.
- Simons, B. (2016). "I-25 Inverted Pavement Project." Presentation, Transportation Research Board (TRB), 95th Annual Meeting, Washington, DC.
- Smith, G. N. (1986). "Probability and Statistics in Civil Engineering." London: Collins.
- Soares, D., de Brit, J., Ferreira, J., and Pacheco, J. (2014) "Use of Coarse Recycled Aggregates from Precast Concrete Rejects: Mechanical and Durability Performance." *Construction and Building Materials* Vol. 71, pp. 263–272.

<http://dx.doi.org/10.1016/j.conbuildmat.2014.08.034>

- Sobhan, K., and Das, B. M. (2007). "Durability of Soil–Cements Against Fatigue Fracture." *Journal of Materials in Civil Engineering (ASCE)*, 19(1), 26-32.
- Sobhan, K., and Krizek, R. J. (1998). "Resilient Properties and Fatigue Damage in Stabilized Recycled Aggregate Base Course Material." *Transportation Research Record 1611*, Transportation Research Board, Washington, DC, 98-0157, 28–36.
- Sobhan, K., and Das, B.M. (2007). "Durability of Soil–Cements Against Fatigue Fracture." *J. Mater. Civ. Eng.*, 19(1): pp. 26-32.
- Socolow, R.H., and Pacala, S.W. (2006). "A Plan to Keep Carbon in Check." *Scientific American*, pp. 50–57.
- South African Roads Board (SARB). (1998). "Pavements Constructed with Processed (Graded) Crushed Stone (Aggregate) Bases on Stabilized Subbases." Video Script, SARB, 1998.
- Stavridakis, E.I. (2005). "Evaluation of Engineering and Cement–Stabilization Parameters of Clayey–Sand Mixtures Under Soaked Conditions." *Geotechnical & Geological Engineering*, 23(6), pp. 635-655.
- Stocker, P.T. (1975). "Diffusion and Diffuse Cementation in Lime and Cement Stabilized Clayey Soils-Chemical Aspects." *Australian Road Research*, Vol. 5, No. 9, pp. 6–47.
- Sullivan, J. (1996). "Pavement Recycling Executive Summary and Report." Federal Highway Administration, Report No. FHWA-SA-95-060, Washington, DC.
- Syed, I.M., and Scullion, T. (2001). "Performance Evaluation of Recycled and Stabilized Bases in Texas." *Transportation Research Record 1757*, pp.14-21.
- Syed, I., Scullion, T., and Randolph, R. B. (1999). "Tube Suction Test for Evaluating Aggregate Base Materials in Frost- and Moisture-Susceptible Environments." *Transportation Research Record*, Paper No. 00-1147.
- Taha, R., Al-Harthy, A., Al-Shamsi, K., and Al-Zubeidi, M. (2002). "Cement Stabilization of Reclaimed Asphalt Pavement Aggregate for Road Bases and Subbases." *Journal of Materials in Civil Engineering*, 14(3), pp. 239-245.
- Taha, R., Ali, G., Basma, A., and Al-Turk, O. (1999). "Evaluation of Reclaimed Asphalt Pavement Aggregate in Road Bases and Subbases." *Transportation Research Record*, 1652(1), pp. 264-269.
- Terrel, R. G., Cox, B. R., Stokoe II, K. H., Allen, J. J., and Lewis, D. (2003). "Field Evaluation of the Stiffness of Unbound Aggregate Base Layers in Inverted Flexible Pavements." *Transportation Research Board: Journal of the Transportation Research Board*, No. 1837, Transportation Research Board of the National Academies, Washington, DC.
- Texas 2030 Committee. (2009). "Texas Transportation Needs Summary." Executive Summary.
- Texas Department of Transportation (TxDOT). (2014). "Standard Specifications for Construction and Maintenance of Highways, Streets, and Bridges." Texas Department of Transportation, Subgrade Treatments and Base, Item 247.
- Texas Department of Transportation (2002). "Test Procedure for Soil-Lime Testing." Tex-121-E Protocol.

- Texas Department of Transportation (2005). "Determining Sulfate Content Soils - Colorimetric Method." Tex-145-E Protocol.
- Texas Department of Transportation (2011). "Test Procedure for Using Suction and Dielectric Measurements as Performance Indicators for Aggregate Base Materials." Tex-144 Protocol.
- Texas Department of Transportation (1999). "Calculating the Plasticity Index of Soils." Tex-106-E Protocol.
- Texas Department of Transportation (1999). "Determining Liquid Limits of Soils." Tex-104-E Protocol.
- Texas Department of Transportation (1999). "Determining Plastic Limit of Soils." Tex-105-E Protocol.
- Texas Department of Transportation (1999). "Particle Size Analysis of Soils." Tex-110-E Protocol.
- Texas Department of Transportation (2013). "Test Procedure for Soil-Cement Testing." Tex-120-E Protocol.
- Texas Department of Transportation (2016). "Test Procedure for Particle Size Analysis of Soils." Tex-110-E Protocol.
- Texas Department of Transportation (2016). "Test Procedure for Laboratory Compaction Characteristics and Moisture Density Relationship of Subgrade Soils." Tex-114-E Protocol.
- Theyse, H.L., M. De Beer, and Rust, F.C. (1996). "Overview of South African Mechanistic Pavement Design Method." Transportation Research Record 1539, pp. 6-17.
- Thogersen, F., Busch C., and Henrichsen, A. (2005). "Mechanistic Design of Semi-rigid Pavement: An Incremental Approach." Transportation Research Board.
- Thompson, M.R., and Dempsey, B.J. (1969) "Autogenous Healing of Lime-Soil Mixtures." Highway Research Record No. 263, National Research Council, Washington D.C.
- Tirado, C., Rios-Gomes, K.Y., Fathi, A., Mazari, M., and Nazarian, S. (2017). "Simulation of Light Weight Deflectometer Measurements Considering Nonlinear Behavior of Geomaterials." Transportation Research Record: Journal of the Transportation Research Board, No. 2641, Washington, D.C., 2017, pp. 58-65, <http://doi.org/10.3141/2641-08>.
- Titi, H., Rasoulia, M., Martinez, M., Becnel, B., and Keel, G. (2003). "Long-Term Performance of Stone Interlayer Pavement." Journal of Transportation Engineering, Vol. 129, No. 2, pp. 118–126. American Society of Civil Engineers (ASCE).
- Toohey, N.M.; Mooney, M.A. and Bearce, R.G. (2013). "Relationship Between Resilient Modulus and Unconfined Compressive Strength for Lime-Stabilized Soils." Journal of Geotechnical and Environmental Engineering (ASCE), 139 (11).
- TRH (1985) "Guidelines for Road Construction Materials." TRH 14, Technical Recommendation for Highways (TRH), Department of Transport, Pretoria, South Africa.
- Tuncay, E. and Hasancebi, N. (2009). "The Effect of Length to Diameter Ratio of Test Specimens on the Uniaxial Compressive Strength of Rock." Bull Eng Geol Environ, No. 68: 491. <https://doi:10.1007/s10064-009-0227-9>

- Turk N, and Dearman W.R. (1986). "A Correction Equation on The Influence of Length-To-Diameter Ratio on the Uniaxial Compressive Strength of Rocks." *Eng Geol*, 22:293–300 [https://doi.org/10.1016/0013-7952\(86\)90030-X](https://doi.org/10.1016/0013-7952(86)90030-X)
- Tutumluer, E. (2013). "Practices for Unbound Aggregate Pavement Layers." National Cooperative Highway Research Program, NCHRP Synthesis 445, Transportation Research Board (TRB), Washington, DC.
- Tutumluer, E. and Barksdale, R. D. (1995). "Inverted Pavement Response and Performance." *Transportation Research Record* 1482, Transportation Research Board, National Research Council, Washington, DC.
- Tutumluer, E., and U. Seyhan. (1999). "Laboratory Determination of Anisotropic Aggregate Resilient Moduli Using an Innovative Test Device." *Transportation Research Record: Journal of the Transportation Research Board*, No. 1687, TRB, National Research Council, Washington, D.C., pp. 13–21.
- U.S. EPA. (2015). "Sources of Greenhouse Gas Emissions." Retrieved October 11, 2018, from <https://www3.epa.gov/climatechange/ghgemissions/sources/transportation.html>
- Vapnik, V., Golowich, S. E., and Smola, A. J. (1997). "Support Vector Method for Function Approximation, Regression Estimation and Signal Processing." *Advances in Neural Information Processing Systems*, pp. 281-287.
- Vasudev, D. (2007). "Performance Studies on Rigid Pavement Sections Built on Stabilized Sulfate Soils." Master Thesis, University of Texas at Arlington.
- Vaughan, K. (2014). "Inverted Pavements." Presentation, Vulcan Materials Company, Southeastern Asphalt User/Producer Group (SEAUPG), Nashville, TN.
- Veisi, M., B. Chittoori, M. Celaya, S. Nazarian, A. J. Puppala and C. Solis. (2010). "Accelerated Stabilization Design of Subgrade Soils." The University of Texas at El Paso, Texas Department of Transportation, TX FHWA/TX 06/0-5569-1.
- Wang, D., Zentar, R., and Abriak, N. E. (2016). "Temperature-Accelerated Strength Development in Stabilized Marine Soils as Road Construction Materials." *Journal of Materials in Civil Engineering*, 29(5), 04016281.
- Weingart, R. (2012). "Inverted Base: The Virginia Experience." 2012 Transportation Research Board, Mineral Aggregates Committee (AFP 70) Meeting Presentation, 91st Annual Meeting Transportation Research Board, Washington, DC.
- Weingart, R. (2018). "Turning Pavement Design Upside Down." Kent Seminar Lecture, Department of Civil and Environmental Engineering, University of Illinois at Urbana-Champaign.
- Wen H., and Edil T. (2014). "Characterization of Cementitiously Stabilized Layers for Use in Pavement Design and Analysis." NCHRP Project 04-36.
- Wen, H., Martono, W., Edil, T., Clyne, T. R., and Patton, R. (2010). "Field Evaluation of Recycled Pavement Materials at MNROAD." *Paving Materials and Pavement Analysis*, pp. 264-269.

- Wen, H., Muhunthan, B., Wang, J., Li, X., Edil, T., and Tinjum, J. M. (2014). "Characterization of Cementitiously Stabilized Layers for Use in Pavement Design and Analysis, Project No 4-36.
- Werkmeister, S., Dawson, A., and Wellner, F. (2004). "Pavement Design Model for Unbound Granular Materials." *J. Transp. Eng.*, 130(5), pp. 665–674.
- Wise, J. and Hudson, W.R. (1971). "An Examination of Expansive Clay Problem in Texas." Research Report Number 118-5.
- Xiao, F., and Amirkhanian, S. N. (2009). "Artificial Neural Network Approach to Estimating Stiffness Behavior of rubberized Asphalt Concrete Containing Reclaimed Asphalt Pavement." *Journal of Transportation Engineering*, 135(8), 580-589.
- Yan, W., Weihong, X., and Xiaotong, F. (2011). "Studies on Fatigue Behaviors of Cement Stabilized Macadam Mixture." *Emerging Technologies for Material, Design, Rehabilitation, and Inspection of Roadway Pavements, Geotechnical Special Publication No. 218 ASCE.*
- Yeo, R. (2008). "The Development and Evaluation of Protocols for the Laboratory Characterization of Cemented Materials." Report No. AP-T101/08.
- Yimsiri, S. and Soga, K. (2002). "Application of Micromechanics Model to Study Anisotropy of Soils at Small Strains." *Soils and Foundations*, 42 (5), pp. 15–26.
- Yuan, D., Nazarian, S., Hoyos, L.R., and Puppala, A. J. (2010). "Cement Treated Rap Mixes for Roadway Bases." Report No. FHWA/TX-10/0-6084-1.
- Yuan, D., Nazarian, S., Hoyos, L.R., and Puppala, A.J. (2011). "Evaluation and Mix Design of Cement-Treated Base Materials with High Content of Reclaimed Asphalt Pavement." *Transportation Research Record*, 2212(1), pp. 110-119.
- Zhang, Z, and M. Tao (2008). "Durability of Cement Stabilized Low Plasticity Soils." *Journal of Geotechnical and Geoenvironmental Engineering*, Vol. 134, Issue 2.
- Zhen, FU and Yong-en, C. (2005). "Numerical Analysis on the Influence of Rock Specimen Size on Crack Stress Field." *Acta Seismological Sinica*, Vol. 18, No.3, pp. 322-330.
- Zube, E., C. G. Gates, E. C. Shirley, and H. A. Munday. (1969). "Service Performance of Cement treated Base as Used in Composite Pavements." *Highway Research Record* 291, pp. 57-69.

Appendix A. Draft Laboratory Test Procedure

Test Procedure for

CEMENT TREATED MATERIALS TESTING

TxDOT Designation: Tex-120-E

Effective Date: TBD



1. SCOPE

- 1.1. This method consists of five parts.
 - 1.1.1. Part I determines the unconfined compressive strength of compacted cement treated material specimens after seven days curing (using 6 x 8 in. mold).
 - 1.1.2. Part II determines the indirect tensile strength of compacted cement treated material specimens after seven days of curing (using 4 x 4 in. mold).
 - 1.1.3. Part III determines the minimum percent cement needed for a cement treated material based on the laboratory results.
 - 1.1.4. Part IV pertains to the characterization of the moisture susceptibility of cement treated material specimens using either backpressure saturation or submergence methods.
 - 1.1.5. Part V applies to cement treated materials sampled from the roadway during construction.
- 1.2. The values given in parentheses (if provided) are not standard and may not be exact mathematical conversions. Use each system of units separately. Combining values from the two systems may result in nonconformance with the standard.

2. APPARATUS

- 2.1. As outlined in test methods:
 - Tex-101-E
 - Tex-113-E
 - Tex-117-E.

- 2.1. *Compression testing machine*, with capacity of 267 kN (60,000 lb.), capable of applying a compressive load at a controlled deformation rate of 2 in. per min, meeting the requirements of ASTM D 1633.
- 2.2. *Triaxial screw jack press* (Tex-117-E), used when anticipated strengths are not in excess of 2758 kPa (400 psi).
- 2.3. *Loading Strips*; consists of 0.75 x 0.75 x 5.50 in. rectangular steel strips. Machine the area in contact with the specimen to conform to the curvature of the specimen.
- 2.4. *Backpressure Saturation Test Components*; consists of a confining chamber, membrane, top cap assembly, locking screw, graduated cylinder, pressure cap and line, drainage valve, two pressure gauges, and a pressure source.
- 2.5. *Submergence Test Components*; consists of standard 5-gallon bucket, standard oven, and thermometer.
- 2.6. *Forced Draft Temperature Chamber or Heating Oven*, capable of maintaining $140 \pm 2^{\circ}\text{F}$ ($60 \pm 1^{\circ}\text{C}$).

3. MATERIALS

- 3.1. *Hydraulic (Portland) cement*
- 3.2. *Distilled water.*

4. PREPARING SPECIMEN

- 4.1. Select approximately 150 kg (330 lb.) of material to treat with cement in accordance with Tex-101-E, Part II.

PART I—COMPRESSIVE STRENGTH TEST METHODS (LABORATORY MIXED)

5. PROCEDURE

- 5.1. Determine the optimum moisture content and maximum density for a cement treated material containing 6% cement in accordance with Tex-113-E. The amount of cement added is a percentage based on the dry mass of the soil.
- 5.2. Recombine the sizes prepared in accordance with Tex-101-E, Part II, to make three

individual specimens and add the optimum moisture content, from Tex-113-E, to each specimen.

5.3. Thoroughly mix the materials using slurry mixing procedure. To ensure the uniform distribution of the cement in the mix, create a slurry by mixing dry cement powder with water for approximately 2 min. Then, mix the cement slurry with soil or aggregate blend until the mixture has uniform color.

5.3.1. Adjust the percent molding water content according to 5.3.2 as the percent cement is increased or decreased in the mixture. Do this in order to mold close to optimum moisture content without running a new M/D curve for each percentage of cement.

Note 1—A new M/D curve for each percentage of cement may be performed, if desired.

5.3.2. Use the following equation to vary the molding water:

$$\% \text{ molding water} = \% \text{ optimum moisture from M/D curve} + 0.25 (\% \text{ cement increase})$$

Where:

% cement increase = difference in cement content between curve and other cement contents.

5.4. Cover the mixture to prevent loss of moisture by evaporation. Allow the wetted mixture to stand for at least 12 hours before compaction. When the plasticity index (PI) is less than 12, the standing time may be reduced to not less than three hours. Split or referee mixture should stand the full term.

5.4.1. Prior to compaction, replace any evaporated water and thoroughly mix each mixture.

5.4.2. Add the cement slurry uniformly and mix thoroughly.

5.5. Compact the specimen with a diameter of 6 in. and a height of 8 in. using gyratory compactor (gyration rate of 30 gyration/min, angle of gyration of 1.25°, compaction pressure of 85 psi (600 kPa), and number of gyrations of 120).

5.6. Using the moisture contents outlined in 5.3.1 and 5.3.2, mold three specimens to complete the full set as outlined in 5.6.1 for cement treated subgrade soils and 5.6.2 for cement treated base and subbase materials.

5.6.1. For subgrade soils, use 3%, 5%, and 7% cement contents.

- 5.6.2. For base and subbase aggregates, use 2%, 4%, and 6% cement contents.
- 5.6.3. If necessary, level the top surface of each specimen and carefully center over a porous stone and remove specimen from mold by means of a small press. Subsequently, record the weight and dimensions of the specimens.
- 5.6.4. Place a card on each specimen showing the laboratory identification number and the percent of cement.

Note 2—In calculating the actual dry density of laboratory mixed cement treated material specimens, the dry mass of material is the total mass of oven dry soil or aggregate blend in the specimen plus the mass of cement. The amount of moisture should be the mass of hygroscopic moisture in the cement treated material plus the amount of water added based on the dry mass of the soil or aggregate blend plus cement.

Determine moisture content and density of road-mixed and wetted materials, and cement treated material cores from the oven dried masses.

- 5.7. Store test specimens the same day as molded, with top and bottom porous stones, in the damp room for seven days. Do not subject specimen to capillary wetting or a surcharge. Do not use a triaxial cell. Place a pan on top of the top porous stone to protect the specimen from dripping water.
- 5.8. Remove test specimens from the damp room after seven days and use a cloth to remove any free water on the surface of the specimens.
- 5.9. Test specimens in compression at 0 kPa (0 psi) lateral confinement in accordance with Tex-117-E, Section 5.19 when using an automated load frame, or Section 5.20 when using a screw jack press.

6. TEST REPORT

- 6.1. Report molding moisture to the nearest 0.1%
- 6.2. Report dry density to the nearest 1 kg/m³ (0.1 pcf).
- 6.3. Report unconfined compressive strength to the nearest whole kPa (psi) for each cement content tested.

PART II—INDIRECT TENSILE STRENGTH TEST METHODS (LABORATORY MIXED)

7. PROCEDURE

- 7.1. Recombine the material prepared in accordance with Tex-101-E, Part II, to make three individual specimens, and add the optimum moisture content according to sections 5.3.1 and 5.3.2.
- 7.2. Remove any particles greater than 1 ½ inches to avoid bedding errors.
- 7.3. Uniformly mix the soil or aggregate blend and cement slurry according to section 5.3.
- 7.4. Compact the specimen with a diameter of 4 in. and a height of 4 in. using gyratory compactor (gyration rate of 30 gyration/min, angle of gyration of 1.25°, compaction pressure of 85 psi (600 kPa), and number of gyrations of 120).
- 7.5. Using the moisture contents outlined in 5.3.1 and 5.3.2, mold three specimens to complete the full set as outlined in 5.6.1 for cement treated subgrade soils and 5.6.2 for cement treated base and subbase materials.
- 7.6. Place a card on each specimen showing the laboratory identification number and the percent of cement.
- 7.7. Store test specimens the same day as molded, with top and bottom porous stones, in the damp room for seven days. Do not subject specimen to capillary wetting or a surcharge. Do not use a triaxial cell. Place a pan on top of the top porous stone to protect the specimen from dripping water.
- 7.8. Remove test specimens from the damp room after seven days and use a cloth to remove any free water on the surface of the specimens.
- 7.9. Draw diametral lines on each end of the specimen using a suitable device that will ensure that they are in the same axial plane.
- 7.10. Determine the diameter of the test specimen to the nearest 0.005 in. by averaging three diameters measured near the ends, the middle of the specimen, and lying in the plane containing the lines marked on the two ends. Determine the length of the specimen to the nearest 0.005 in. by averaging at least two length measurements taken in the plane

containing the lines marked on the two ends.

- 7.11. Place the specimen onto the lower loading strip. Slowly lower the top loading strip to bring it into light contact with the specimen. Ensure that the loading strip is parallel and centered at the vertical diametrical plane as shown in Figure 1.
- 7.12. Apply a vertical compressive ramp load to maintain deformation rate of 0.04 in/min (1 mm/min) until the maximum load is reached. Record the maximum applied load indicated by the testing machine at failure. Note the type of failure and the appearance of the specimen.

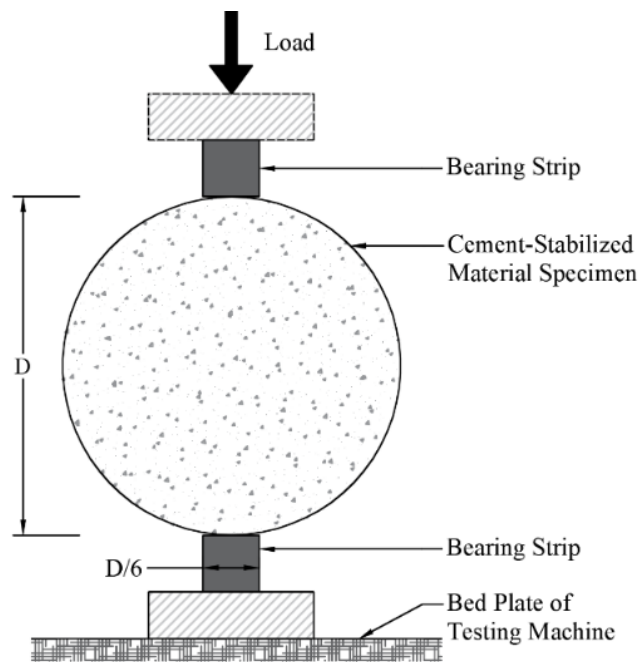


Figure 1–Schematic Representation of the Indirect Tensile Strength Test Setup.

8. TEST REPORT

- 8.1. Report molding moisture to the nearest 0.1%.
- 8.2. Report dry density to the nearest 1 kg/m^3 (0.1 pcf).
- 8.3. Calculate and report indirect tensile strength to the nearest whole kPa (psi) for each specimen using the following equation:

$$S_t = \frac{2 \times P}{\pi \times t \times D}$$

Where:

S_t = IDT strength, kPa (psi)

P = maximum load, N (lb)

t = specimen height, mm (in)

D = specimen diameter, mm (in)

PART III—DETERMINATION OF THE REQUIRED CEMENT CONTENT BASED ON THE LABORATORY RESULTS

9. DETERMINE THE REQUIRED AMOUNT OF TREATMENT AGENT

- 9.1. The required application rate of cement in the mixture is the percentage for which the minimum required strength criteria are met.
- 9.2. Figure 2 provides an example for the selection of the required cement content for laboratory mixture design of cement treated base layers.

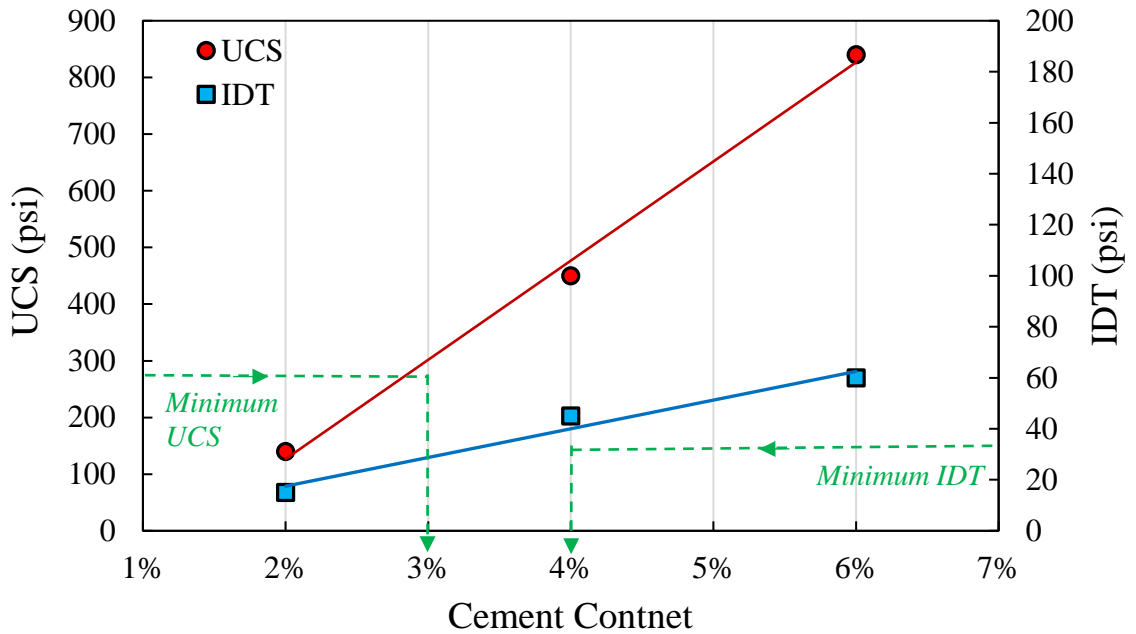


Figure 2—Determination of the Minimum Percent Cement for a Cement Treated Material. (The data used in this example was selected for illustration purposes only).

PART IV–LABORATORY CHARACTERIZATION OF THE MOISTURE SUSCEPTIBILITY OF CEMENT TREATED MATERIALS

10. BACKPRESSURE SATURATION PROCEDURE

- 10.1. Recombine the materials prepared in accordance with Tex-101-E, Part II, to make three individual specimens, add the optimum moisture content from Tex-113-E, to each specimen set as outlined in 5.6.1 for cement treated subgrade soils and 5.6.2 for cement treated base and subbase materials. The determination of cement content is based on sections 5.3.1 and 5.3.2 in Part I.
- 10.2. Uniformly mix the material and cement slurry according to section 5.3.
- 10.3. Remove particles greater than 1 ½ inches to avoid bedding errors.
- 10.4. Compact the specimen using gyratory compactor (gyration rate of 30 gyration/min, angle of gyration of 1.25°, compaction pressure of 85 psi (600 kPa), number of gyrations 120).
- 10.5. Place a card on each specimen showing the laboratory identification number and the percent of cement.
- 10.6. Store the specimens after demolding in the 140 °F (60 °C) forced draft oven for 24 hours.
- 10.7. Place test specimens in a rubber membrane sleeve for subsequent installation in the backpressure test equipment.
- 10.8. Place the test specimen on top of a porous stone, centered on the pedestal as shown in Figure 3.
- 10.9. Place a filter paper between the bottom porous stones and specimen to prevent clogging the porous stone.
- 10.10. Place a porous stone and a filter paper on top of the specimen.
- 10.11. Place the cell securely around the O-ring in the base pedestal.
- 10.12. Place the upper cap and graduated cylinder assembly on top of top porous stone and clamp tightly to hold the specimen assembly together.
- 10.13. Evacuate the air between the membrane and the cell in the acrylic confining chamber retrofitted with a membrane.

- 10.14. Apply 10 ± 0.5 psi (70 ± 3.5 kPa) confining pressure with the pump incorporated in the base assembly. Maintain the pressure throughout the tests using the pump if the system loses pressure.
- 10.15. Fill the graduated cylinder with water, retrofit with the plastic pressure cap.
- 10.16. Secure the top of the graduated cylinder with the pressure cap and apply the backpressure at top of the graduated cylinder. This pressure should be less than the confining pressure to prevent water from migrating through the side of the specimen and to prevent internal damage to the specimen. Apply a backpressure of 5 psi (35 kPa) for cement treated base materials and 3 psi (28-20 kPa) for cement treated subgrade soils.
- 10.17. Allow 48 hours to release the pressure cap from the top of the graduated cylinder and to remove all remaining water from the cylinder. Release pressure from the confining chamber. Remove the cap assemblies, upper cap and specimen from the setup shown in Figure 3.

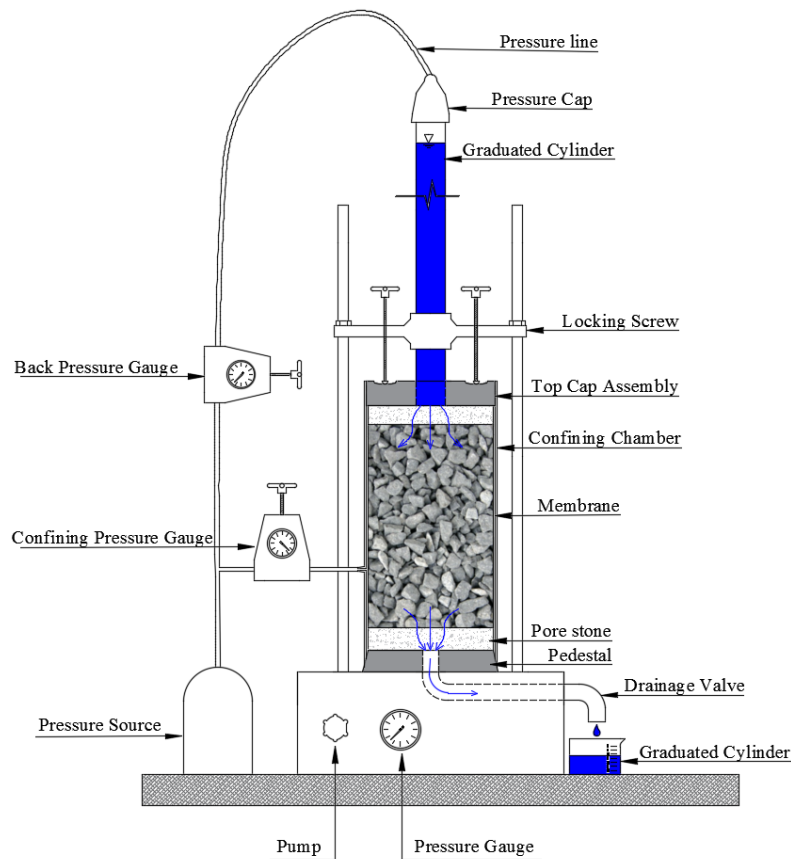


Figure 3—Schematic Diagram of Backpressure Saturation Test.

11. SUBMERGENCE PROCEDURE

- 11.1. Recombine the materials prepared in accordance with Tex-101-E, Part II, to make three individual specimens, add the optimum moisture content from Tex-113-E, to each specimen set as outlined in 5.6.1 for cement treated subgrade soils and 5.6.2 for cement treated base and subbase materials. The determination of cement content is based on sections 5.3.1 and 5.3.2 in Part I.
- 11.2. Uniformly mix the material and cement slurry according to section 5.3.
- 11.3. Remove particles greater than 1 ½ inches to avoid bedding errors.
- 11.4. Compact the specimen using gyratory compactor (gyration rate of 30 gyration/min, angle of gyration of 1.25°, compaction pressure of 85 psi (600 kPa), number of gyrations 120).
- 11.5. Place a card on each specimen showing the laboratory identification number and the percent of cement.
- 11.6. Store test specimens after demolding in the 140 °F (60 °C) forced draft oven for 24 hours.
- 11.7. Place two porous stones on top and bottom of the specimen.
- 11.8. Place test specimens, including both porous stones in a rubber membrane sleeve in order to prevent from specimen disintegration during the submergence process as shown in Figure 4.
- 11.9. Fill a standard plastic or metal 5-gallon bucket with distilled water up to 2 inches above the porous stone as shown in Figure 4.
- 11.10. Submerge specimens in 70 °F water for 24 hours.
- 11.11. After test specimens are submerged for 24 hours in the distilled water, remove the rubber membrane and upper porous stone, and then measure the weight of the specimen to calculate total absorbed water using Equation 14-3:

$$\omega_a = \frac{W_f}{\left(\frac{W_i}{1 + \omega_i}\right)} - 1$$

Where:

ω_a = total absorbed water content of specimen (%)

W_f = final total weight (lb)

ω_i = initial moisture content of specimen (%)

W_i = initial total weight of specimen, lb.

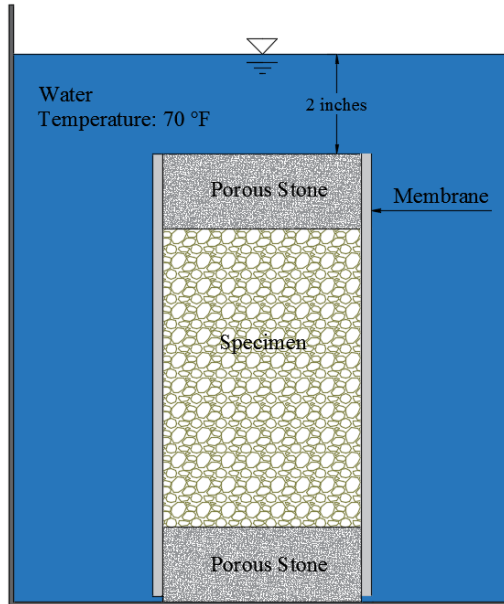


Figure 4–Schematic Diagram of Submergence Test

- 11.12. Submergence procedure can be used to characterize the moisture susceptibility of cement treated specimens in the absence of backpressure test equipment.

12. TEST REPORT

- 12.1. After completion of either backpressure saturation or submergence moisture susceptibility procedures, perform the unconfined compressive strength test according to Part I, and the indirect tensile strength test according to Part II of this specification.
- 12.2. Report the unconfined compressive strength and indirect tensile strength after moisture susceptibility procedures.
- 12.3. Calculate and report the retained compressive strength ratio using the following equation:

$$\text{Retained Compressive Strength Ratio} = \frac{\text{UCS for specimen subjected to moisture susceptibility test}}{\text{UCS for 7 day moist - cured specimen}}$$

The UCS values are the average test results from three specimens.

- 12.4. Calculate and report the retained tensile strength ratio using the following equation:

$$\text{Retained Tensile Strength Ratio} = \frac{\text{IDT for specimen subjected to moisture susceptibility test}}{\text{IDT for 7 day moist - cured specimen}}$$

The IDT strength values are the average test results from three specimens.

PART V– COMPACTION TESTING OF ROAD MIXED MATERIAL

13. PROCEDURE

- 13.1. Obtain materials for moisture/density curve just prior to the start of compaction operations on the roadway.
- 13.2. Screen cement stabilized materials taken from the roadway during construction over a 6.3 mm (1/4 in.) sieve at field moisture content, without drying.
- 13.2.1. Mix each of these two sizes, plus 6.3 mm (1/4 in.) and minus 6.3 mm (1/4 in.), for uniformity and weigh.
- 13.2.2. Cover each size fraction to maintain field moisture.
- 13.3. Recombine and mold one specimen at the field moisture condition and estimated mass to produce specimen compacted using Tex-113-E compactive effort. Molding should be accomplished using the same equipment and compactive effort as in Part I.
- 13.3.1. Adjust mass, if necessary, and weigh out not less than two additional specimens at the field moisture content for compaction. Molding moisture can be adjusted in each specimen by adding or removing moisture uniformly as needed.
- 13.3.2. Compact cement stabilized material in the laboratory in approximately the same timeframe as on the road. Sample of cement stabilized material from the road mix should not be prepared by oven drying.

Note 5—To determine the moisture-density relationship of fine-grained materials with less than 20% retained on the 6.3 mm (1/4 in.) sieve and 100% passing the 9.5 mm (3/8 in.) sieve, the engineer may elect to use a mold with approximate dimensions of 101.6 mm (4.0 in.) in diameter by 152.4 mm (6.0 in.) in height. The number of blows must be calculated

when changing mold size to maintain a compactive effort of 1100 kN-m /m³ (13.26 ft-lb/in.³).

Note 6—The contractor should be provided an initial optimum moisture based on preliminary laboratory tests.

- 13.4. Store test specimens the same day as molded, with top and bottom porous stones, in the damp room for seven days. Do not subject specimen to capillary wetting or a surcharge. Do not use a triaxial cell. Place a pan on top of the top porous stone to protect the specimen from dripping water.
- 13.5. Remove test specimens from the damp room after seven days and use a cloth to remove any free water on the surface of the specimens
- 13.6. Test specimens in compression at 0 kPa (0 psi) lateral confinement in accordance with Tex-117-E, Section 5.19 when using an automated load frame, or Section 5.20 when using a screw jack press.

14. TEST REPORT

- 14.1. Report density to the nearest 1 kg/m³ (0.1 pcf).
- 14.2. Report moisture content to the nearest 0.1%.
- 14.3. Report unconfined compressive strength to the nearest whole kPa (psi).

15. ARCHIVED VERSIONS

- 15.1. Archived versions are available.